



UNIVERSITÀ DEGLI STUDI DI MILANO
FACOLTÀ DI SCIENZE E TECNOLOGIE

Doctorate School in Chemical Science - XXVI Cycle

**Chemical approaches for improving drug
delivery of known anticancer compounds**

PhD Thesis of
Stella BORRELLI
R09025

Tutor: Prof. Daniele Passarella
Coordinator: Prof. Emanuela Licandro

Academic Year: 2013/2014

Ai miei genitori

**I can guess you guys are not ready for that yet...
but your kids are gonna love it!**

(Marty McFly, Back to the future)

Table of contents

Section 1: Nanoparticle delivery systems	13
Carrier systems for drug delivery	15
Introduction	15
Nanoparticles	16
Mechanisms for cellular targeting	19
Passive targeting: EPR effect.....	19
Active targeting	20
Nanoparticle uptake by tissues ^[5]	22
Nanoparticle clearance from the body and long-circulating nanoparticles (Stealth®)	25
Squalene	29
Chemical structure and physico-chemical properties.....	29
Squalene emulsion-based adjuvants for vaccine delivery	31
Squalene as a potential protective and preventive agent in cancer treatment	32
Squalene’s protective effects against other diseases	33
Squalene as a drug carrier	34
Squalenoylation of gemcitabine	36
Squalenoylation of siRNA.....	38
Squalenoylation of penicillin.....	40
Squalenoylation of paclitaxel.....	41
Improvement of the squalenoylation platform.....	43
Self-immolative linkers	45
Summary	48
Section 2: Disulfide-containing drug-squalene conjugates	49
Disulfide-containing dimers of anticancer compounds	51
Aim of the work	54

Our targets: tubulin-interacting compounds	56
Paclitaxel	56
Epothilone A.....	60
Podophyllotoxin	65
Tubulins and microtubules.....	66
Interaction with microtubules	68
Our targets: Topoisomerase I inhibitors	70
Camptothecin	70
Interaction with Topoisomerase I	72
Synthetic strategy	74
Nanoparticles formation and characterization	77
Preparation	77
Characterization:.....	78
Stability assessment of drug-squalene conjugates and NAs	80
Self-aggregation behavior of nanoassemblies	83
Biological evaluation	84
<i>In vitro</i> activity.....	84
Microtubule bundle formation (immunofluorescence).....	85
<i>In vivo</i> activity	88
Our targets: Cancer Stem Cells (CSCs) and their inhibitors	90
Introduction	90
Stem Cells.....	91
Stem cells and cancer	93
Hedgehog Signaling Pathway: a new biological target for the design of new anticancer compounds	94
Cyclopamine.....	97
Squalene-based derivatives.....	102
Release of cyclopamine	105
Biological evaluation	106

Summary	107
Section 3: Plasmin-activated tripeptidyl squalene derivatives	109
Introduction	111
Proteases	111
Plasmin	113
Plasmin-activated prodrugs	115
Aim of the work	118
Synthetic strategy	119
Nanoparticle formation and characterization	124
Incubation with plasmin	125
Biological evaluation	126
Summary	127
Section 4: Heterogeneous fluorescent nanoparticles: FITC- squalene conjugates	129
Introduction	131
Fluorescence spectroscopy	132
Fluorescein 5(6)-isothiocyanate derivatives	133
Fluorescent delivery systems	135
Aim of the work	138
Synthetic strategy	139
Fluorescent nanoparticles	140
Fluorescence emission	142
<i>In live</i> evaluation	146
Section 5: Summary	149
Summary and future perspectives	151

Section 6: Experimental Procedures	153
Chemistry	155
General	155
Biology	202
Stability of conjugates 8-11a in serum.....	202
Cell culture and fluorescence microscopy.....	203
Cytotoxicity assay (MCF-7 cell line).....	204
Cytotoxicity assay (A549 cell line)	205
Cell cultures and live cell imaging.....	206
Bibliography	207

List of abbreviations

AFM	atomic force microscopy
BBB	blood-brain barrier
CAC	critical aggregation concentration
CPT	camptothecin
CSC	cancer stem cell
CYP	cyclopamine
DHA	docosahexaenoic acid
DMAP	dimethylaminopyridine
DTC	deacetyl thiocolchicine
DTT	dithiothreitol
EDC.HCl	ethyl(dimethylaminopropyl)carbodiimide hydrochloride
EPO	epothilone A
FITC	fluorescein 5(6)-isothiocyanate
Gem	gemcitabine
GSH	glutathione
Hh	hedgehog
mAB	monoclonal antibody
MLV	multilamellar vesicle
MT	microtubule
MTD	maximum tolerated dose
NA	nanoassembly
NBS	N-bromosuccinimide
NMR	nuclear magnetic resonance
NP	nanoparticle
PEG	poly(ethylene glycol)
PLA	polylactide
PLGA	poly(-lactide-co-glicolide)
PNG	penicillin G
PODO	podophyllotoxin
Ptch-1	patched receptor
PTX	paclitaxel
QELS	quasi-elastic light scattering
SAR	structure-activity relationship
SLN	solid lipid nanoparticles
Smo	smoothed protein
TFA	trifluoroacetic acid
TOP I	topoisomerase I

Section 1: Nanoparticle delivery systems

Carrier systems for drug delivery

Introduction

In the past decades a significant advancement has been made in our understanding of cancer biology. Anyway, cancer still remain one of the major causes of death in the world, and one of the main reasons for this is our inability to selectively deliver therapeutics at their own sites of action without affecting healthy tissues^[1].

Moreover, in order for an active compound to show its biological activity, it is necessary to reach the therapeutic concentration inside the cell: this is possible only if the molecule is able to pass through biological barriers.

Many drug candidates have little effect because of a poor barrier permeation, a poor pharmacokinetic profile or because they are substrates for efflux proteins^[2].

Most of the drug which can cross cell membranes and physiological barriers are both small and lipid-soluble molecules, according to the Lipinski's rule-of-five. However, most drug candidates lack this physicochemical characteristics.

Some approaches have been developed to enable drugs to cross membranes:

- ✚ modifying the structure to increase the permeability by passive diffusion (e.g., prodrug approaches improving drug lipophilicity or with chemical delivery systems);
- ✚ blocking efflux transport systems;
- ✚ prodrug approach consisting in the conjugation of a drug to a vector, which is a ligand of a transporter or a receptor on the surface of the barrier;
- ✚ nanotechnology-based systems: colloidal drug carriers that permit the ideally targeted delivery of drugs dissolved, entrapped, encapsulated inside the core or adsorbed or chemically conjugated to their surface.

All these requirements can be well satisfied by biocompatible and biodegradable nanoparticles^[3].

Nanoparticles

Following the IUPAC definition, we can define a nanoparticle as:

"a particle of any shape with dimensions in the 1×10^{-9} and 1×10^{-7} m range. [...] *Note 2:* The basis of the 100-nm limit is the fact that novel properties that differentiate particles from the bulk *material* typically develop at a critical length scale of under 100 nm. *Note 3:* Because other phenomena (transparency or turbidity, ultrafiltration, stable dispersion, etc.) that extend the upper limit are occasionally considered, the use of the prefix *nano* is accepted for dimensions smaller than 500 nm"^[4].

Many kinds of nanoparticles are currently used in biomedical research and drug discovery^[5]:

- ✚ *Inorganic nanoparticles:* their core can be composed of silica, alumina, metals, metal oxides, metal sulfides and they vary in size, shape and porosity. Inorganic nanoparticles may be engineered to evade the reticuloendothelial system by varying size and surface composition; moreover, they may be porous, thus providing a physical encasement to protect a molecule by degradation.
- ✚ *Polymeric nanoparticles:* they are typically composed by a polymer, such as poly(ethylene glycol) (PEG), polylactic acid, polyglycolic acid, poly(methylmethacrylate), poly (butyl)cyanoacrylate, polylactide (PLA) and poly(-lactide-co-glycolide) (PLGA)^{[6][7][8]}. These polymers can be formulated to encapsulate several classes of therapeutic agents. They also show a good potential for surface modifications: in fact, since nanoparticles come into direct contact with cellular membranes, their surface

properties may determine the mechanism of internalization and intracellular localization.

- ✚ Solid lipid nanoparticles: they are lipid-based colloidal carriers, initially designed as an alternative to liposomes. In fact, they are more stable in biological systems due to their relatively rigid core, consisting of hydrophobic lipids that are solid at room and body temperature, surrounded by a monolayer of phospholipids. These aggregates are further stabilized by high levels of surfactants, that contribute to the release profile of the drug.
- ✚ Liposomes: they are concentric bilayered vesicles with an aqueous nucleus surrounded by a phospholipid membrane. Thanks to their amphiphilic nature, their ease of surface modification and their good biocompatibility they constitute a promising solution for increasing the circulating half-life of proteins and peptides. Liposomes can be designed to adhere to cellular membranes to deliver a drug but, unfortunately, they suffer for a low biological stability.
- ✚ Nanocrystals: they are aggregates of molecules that can be combined into a crystalline form in which the drug is surrounded by a thin coating of surfactant. One of the most important applications of these systems is as quantum dots for biological imaging.
This kind of formulation allows to increase the bioavailability of poorly soluble drugs, but has as a drawback a limited stability of nanocrystals and the fact that crystallization is required and some therapeutics are not easily crystallized.
- ✚ Nanotubes: self-assembling sheets of atoms arranged in tubes, with large internal volumes and an external surface that can be easily functionalized. The most popular version involves the use of soluble fullerene derivatives. Even if potentially promising,

human tolerance and toxicity of these compounds still remains unknown.

- ✚ Dendrimers: polymeric-based macromolecules formed from monomeric or oligomeric units such that each layer doubles or triples the number of peripheral groups. They generally have a symmetrical structure, with the possibility to create an isolated "active site" core area through chemical functionalization. Thus, water-soluble dendrimers may be designed with internal hydrophobicity, suitable for the incorporation of a hydrophobic drug.

Mechanisms for cellular targeting

Passive targeting: EPR effect

Most solid tumors possess some characteristics that are not observed in healthy tissues such as:

- ✚ an extensive angiogenesis (hypervasculation);
- ✚ abnormal gaps between the blood vessel cells: in fact, normal vasculature is impermeable to molecules larger than 2-4 nm, while tumor tissues are permeable to molecules with a diameter up to 600 nm;
- ✚ a poor lymphatic drainage system, that results in a decreased clearance of the nanocarriers from the tumor site;
- ✚ expression of a great number of permeability mediators.

These characteristics result in what is known as *enhanced permeability and retention (EPR) effect*. This effect allows nanoparticles to extravasate and accumulate in the tumor tissues and it is also known as *passive tumor targeting*^{[8][9]} (Figure 1).

Thus, passive targeting can selectively deliver anticancer drugs formulated as nanoparticles to the tumor tissue, exploiting the EPR effect. However, the drug needs then to be internalized from the tumor interstitium into the tumor cell to exhibit its biological activity.

Active targeting

Active targeting of nanoparticles is obtained by attaching a component to the nanocarrier structure that recognizes a target within the tumor-affected organ, tissue, cell or intracellular organelle, that results in a preferential accumulation of nanoparticles. Long circulating times will allow for effective transport of nanoparticles to the tumor site through the EPR effect and the targeting molecule can increase endocytosis.

Since the surface of the nanoparticle interacts with the target, the ligand should be in sufficient quantity to allow multipoint binding at the tumor site.

In addition, after administration the ligand should be not easily degraded nor have any immunogenic effect. The ligand should also be easily internalized into the tumor cell and then the drug should be easily released.

After the releasing of the drug, the ligand should be readily hydrolyzed and cleared from the body without causing any toxicity.

Here two examples of active targeting systems:

Ligand-Receptor Targeting

This kind of targeting is usually achieved by incorporating a molecule that binds a receptor, uniquely expressed or overexpressed on the tumor cell surface, in a specific manner.

This targeting mechanism via receptor-mediated endocytosis has been shown to result in an efficient drug uptake in many human cancers^{[10][11]}.

Antibody-Antigen Targeting

This strategy consists in using a monoclonal antibody (mAb) to selectively deliver a drug to a tumor cell. In particular, mAbs bind to antigens selectively expressed on the surface of the tumor cell. After this, the mAb gets absorbed into the cell via receptor-mediated endocytosis, thus taking the drug into the targeted cell. It is of fundamental importance the presence of a trigger moiety in order to initiate the cleavage of the drug^[12].

It is important to underline that the active targeting process cannot be separated from the passive one, because it occurs only after passive accumulation in tumors.

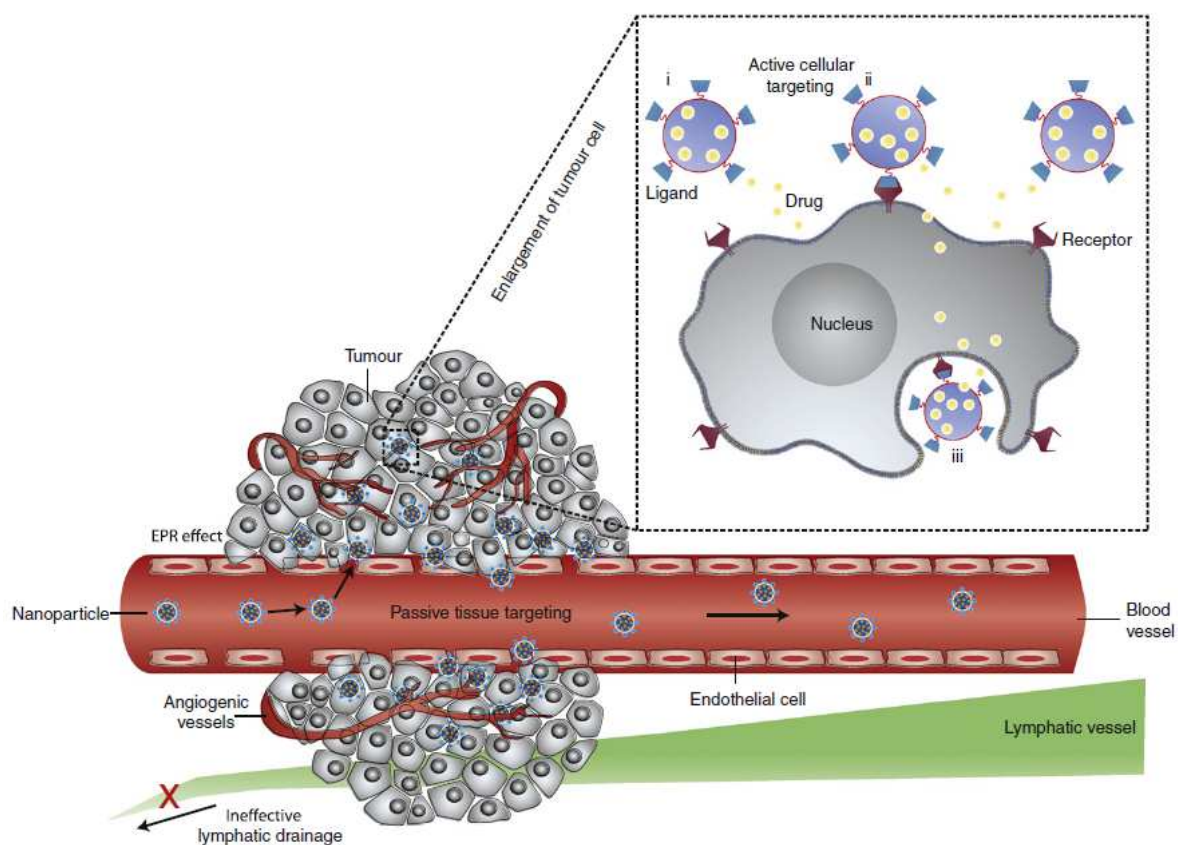


Figure 1: Active and passive targeting

Nanoparticle uptake by tissues^{[5][13]}

A succession of several membrane layers provide an obstacle for therapeutic agents attempting to target the intracellular environment. During this process compound is lost due to ineffective partition across biological membranes.

The extent of partition across a membrane is directly related to the polarity of a molecule: non polar or lipophilic molecules easily bypass this obstacle , generally by diffusion.

One interesting feature of nanoparticles is that they are able to mask a therapeutic agent from its biological environment, thus limiting the influence of a compound's physical properties on intracellular drug concentration.

Nanoparticles are ingested by cells through a mechanism called *endocytosis*, that includes three subtypes (Figure 2):

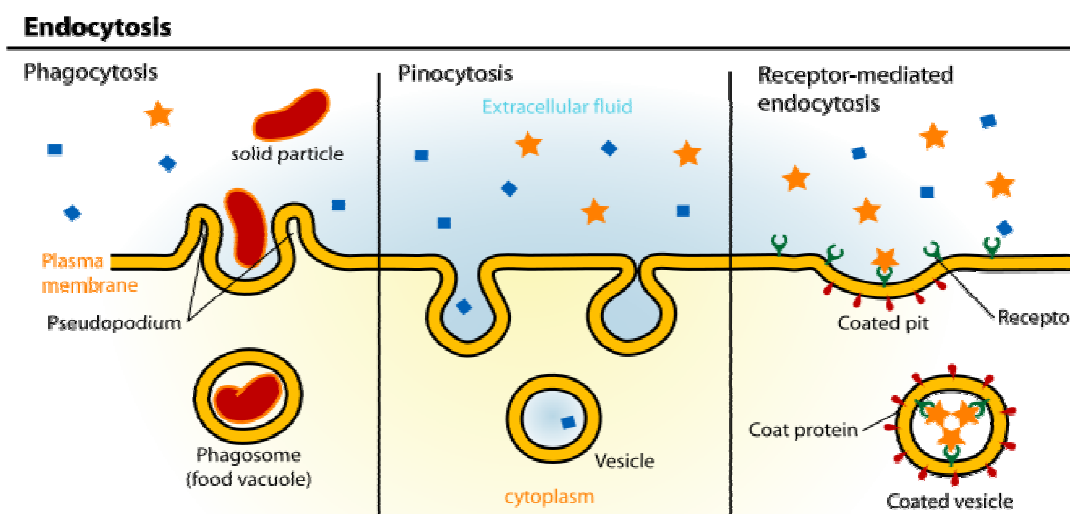


Figure 2: Endocytosis

- ✚ *Phagocytosis:* it involves the ingestion of materials with a diameter up to 10 μm and can be accomplished by few cell types of the RES system, such as macrophages, neutrophils and dendritic cells.
- ✚ *Pinocytosis:* ingestion of sub-micron material. It can be accomplished by virtually all types of cells.

✚ *Receptor-mediated endocytosis*: the cellular membrane is dotted with many receptors which, upon extracellular binding to their respective ligands, transduce a signal to the intracellular space. This signal can initiate a variety of cellular events, like for example the internalization of the ligand and its appended nanoparticle by endocytosis.

The most typical receptor-mediated endocytosis pathways are the clathrin- and caveolae-mediated one^[14].

Receptor-dependent clathrin-mediated endocytosis (CME)

Clathrin is a three-leg structure called triskelion. More triskelions assemble in a polyhedral lattice just on the cytosolic surface of the cell membrane, which deform the membrane into a coated pit of ~150 nm.

As the clathrin lattice formation continues, the pit becomes deeper and deeper until the final fission of the vesicle mediated by GTPase dynamin, forming the clathrin-coated vesicle. Later uncoating of the vesicle allows the recycling of clathrin units.

This vesicle delivers its cargo to "early endosomes", that then mature into "late endosomes" which generate a harsh environment that causes the degradation of the internalized material (Figure 3B).

Caveolae-mediated endocytosis

Although CME is the predominant endocytosis mechanism, alternative pathways have been recently identified, and among them the caveolae-mediated one is the most relevant.

Caveolae are flask-shaped membrane cavities having a size typically in the range of 50-80 nm. They are lined by caveolin and enriched with cholesterol and sphingolipids.

After binding to the cell surface, particles move along the plasma membrane to caveolae cavities, that then undergo the membrane fission

thus generating caveolae vesicles, that follow a cellular pathway similar to that of clathrin-coated ones (Figure 3C).

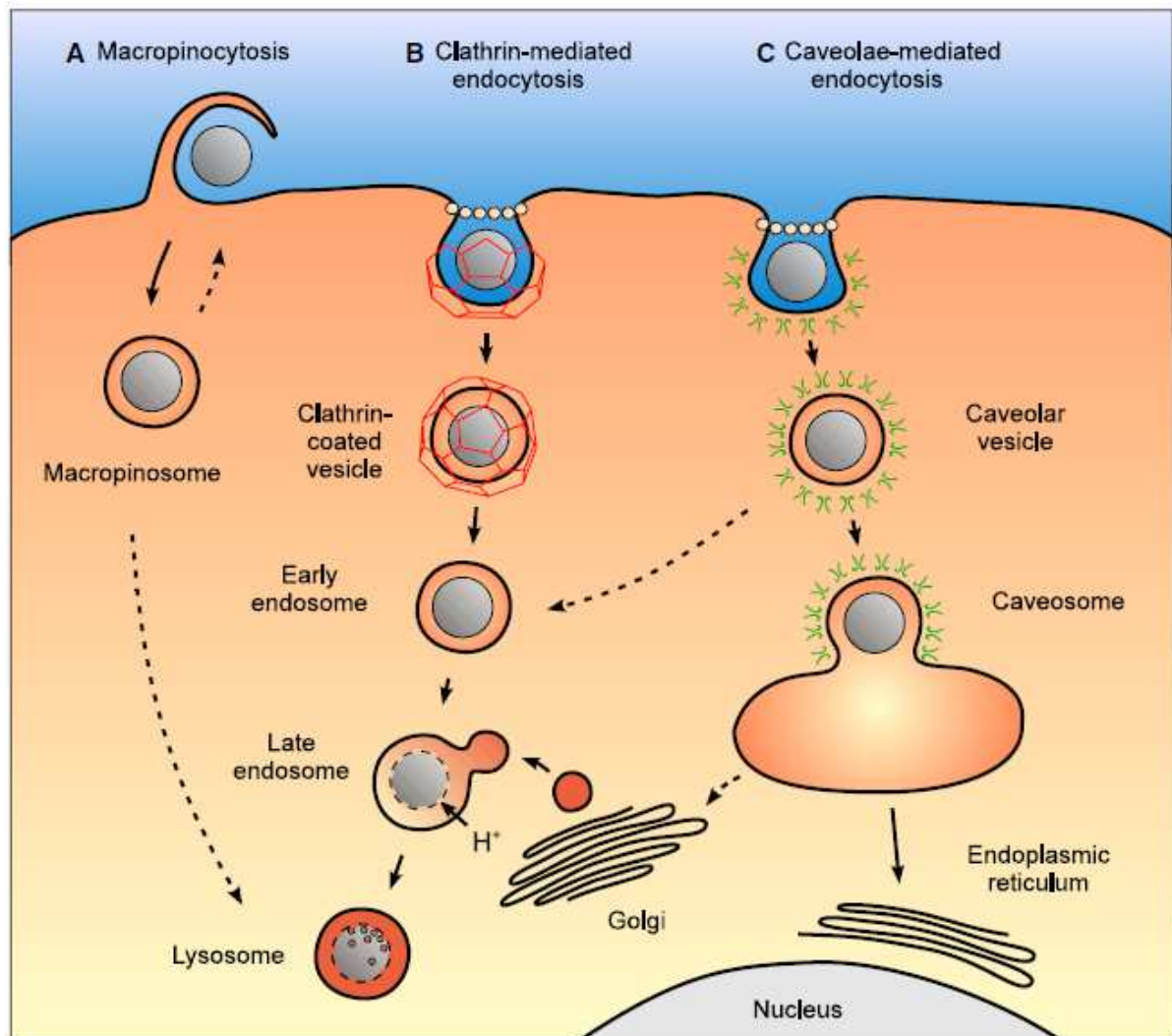


Figure 3: Clathrin- and Caveolae-mediated endocytosis pathways

Nanoparticle clearance from the body and long-circulating nanoparticles (Stealth®)

Upon intravenous injection to mice and rats, nanoparticles are rapidly cleared from the blood stream by the reticuloendothelial system (RES). In particular Kupffer cells are the major liver site for cell accumulation of nanoparticles: these phagocytic cells cannot directly identify nanoparticles themselves, but rather recognize specific opsonin proteins bound to the surface of the particle.

The process by which a foreign organism or particle is covered by opsonin proteins, thus becoming more visible to phagocytic cells is called *opsonization*. Opsonins are thought to come into contact with particles typically by random Brownian motion. Once sufficiently close to the particle, several attractive forces (including van der Waals, electrostatic and others) lead to the binding of opsonins to the surface.

After opsonization, phagocytosis can occur, which is the engulfing and eventual destruction or removal of foreign materials from the blood stream. If particles are not biodegradable, they can accumulate, leading to toxicity and other side effects.

The third and last step in the clearance process is the ingestion of foreign materials by phagocytes. This step typically involves the endocytosis of the particle and then the secretion, by phagocytes, of enzymes and factors that destroy the particle.

Most non-biodegradable particles cannot be degraded by this process and, depending on their size and weight, they will be removed by the renal system or sequestered and stored in one of the RES organs.

Since the initial opsonization step is so critical for the clearance process, most research in the area of stealth drug delivery has been focused on trying to stop or block this step.

As general rule, the opsonization of hydrophobic particles, as compared to hydrophilic particles, has been shown to occur more quickly due to enhanced adsorbability of blood serum proteins on these surfaces^[15].

Therefore, one widely used method to slow opsonization is the use of surface adsorbed or grafted shielding groups which can block the electrostatic and hydrophobic interactions that help opsonins binding.

Generally, these groups are long hydrophilic polymer chains and non-ionic surfactants, such as polysaccharides, polyacrylamide, PEG and PEG-containing copolymers^{[16][17][18]}.

Recently^[19] Pignatello and coworkers described stealth solid lipid nanoparticles (SLNs) formed by amphiphilic conjugates of m PEG2000 and mPEG5000 carboxylic acids with a lipoamino acid as lipid anchor (mPEG-C-LAA18, Figure 4):

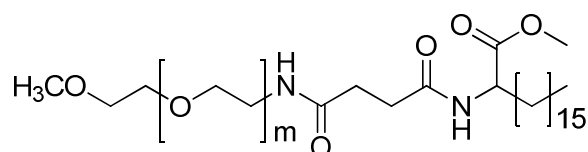


Figure 4: mPEG₂₀₀₀C-LAA18 (m=44) and mPEG₅₀₀₀C-LAA18 (m=96)

These conjugates produced uniformly dispersed SLN systems, with a mean diameter in the range of 250-270 nm. Incubation with macrophages of SLNs at different concentrations of mPEG-C-LAA18 shown that increasing the PEG derivative concentration also the ability to reduce the cell uptake was increased. At 3% molar concentration of PEG, until the second hour of incubation all nanoparticles were able to circumvent the cellular uptake (Figure 5a) while, after 4 h, the systems started to be recognized and phagocytized (Figure 5b).

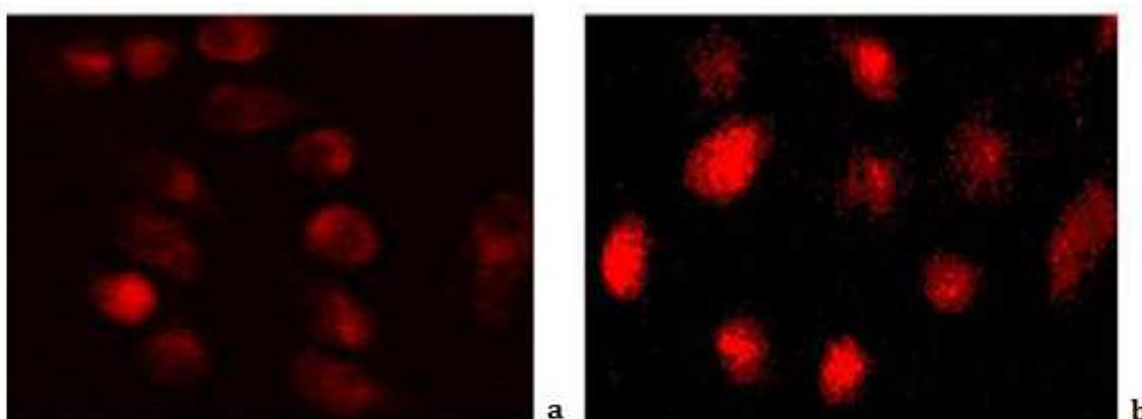


Figure 5: Fluorescent microscopy pictures of J-774 macrophages culture incubated with mPEG5000C-LAA18 after 2 h (Panel A) and 4h (Panel B)

Yeo and coworkers described^[20] the use of low molecular-weight chitosan (LMWC) as an alternative stealth coating, responsive to the pH of tumor cells.

Chitosan is a linear copolymer of glucosamine and N-acetylglucosamine, obtained by partial (>50%) N-deacetylation of chitin, the second most abundant natural polymer. The primary amines provide chitosan with a unique pKa of 6.5, which matches the weakly acidic pH of tumor tissues. In the acidity of the extracellular matrix of solid tumors, chitosan is protonated and can adhere to cells via electrostatic interactions with glycocalyx on the cell membrane.

LMWCs with various molecular weights (MWs) were covalently conjugated to poly(lactic-co-glycolic acid) (PLGA). The derivatives were formulated as nanoparticles and then loaded with paclitaxel (PTX).

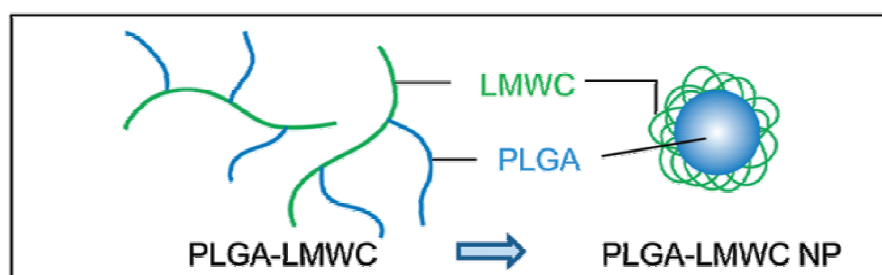


Figure 6: PLGA-LMWC nanoparticles

When incubated with J774A.1 macrophages, PLGA-LMWC_{2-4k} NP effectively avoided the uptake, whereas PLGA* NP was readily taken up by them.

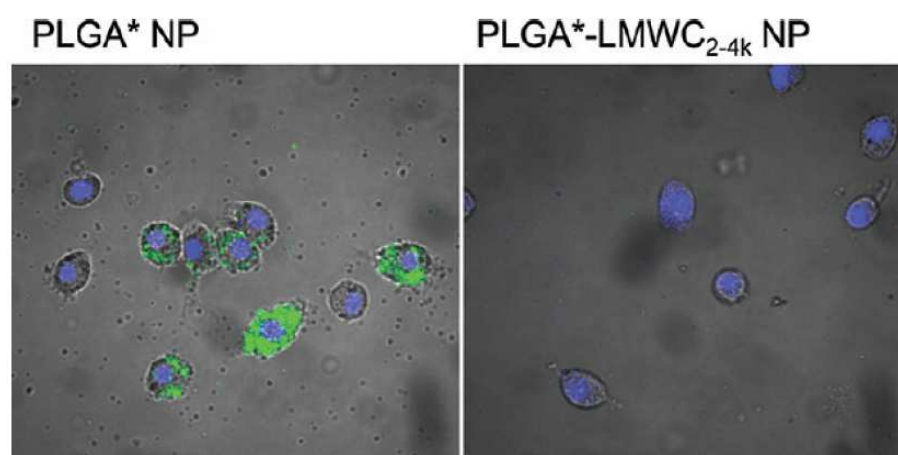


Figure 7 J774A.1 macrophages incubated with PLGA* NPs or PLGA*-LMWC_{2-4k} NPs for 3 h at pH 7.4. Overlaid images of NP (green), nuclei (blue), and transmission images

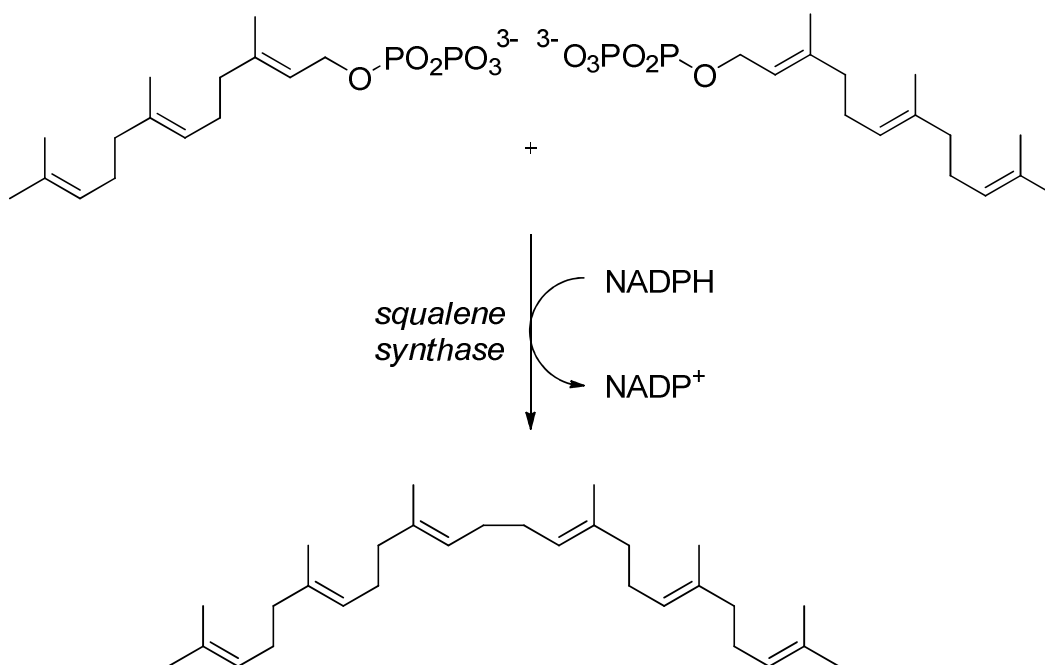
Furthermore, PLGA-LMWC_{4-6.5k} mP showed greater reduction in protein adsorption than PLGALMWC_{2-4k}. The difference may be explained by the greater coverage of the surface by LMWC_{4-6.5k}, given the LMWC content.

Squalene

Chemical structure and physico-chemical properties

Squalene is an acyclic triterpene of formula $C_{30}H_{50}$ so named because of its occurrence in shark liver oil. However it is widely distributed in nature, with very significant amounts in olive oil and olive leaves.

Squalene contains two farnesol moieties joined in a tail-to-tail fashion by the enzyme *squalene synthase*, obtaining a structure in which 6 double bonds, 10 methylenes and 8 methyl groups are symmetrically distributed respect to the C12-C13 bond (Scheme 1):



Scheme 1: Squalene biosynthesis

Even if squalene is a free-flowing oil at room temperature, crystals have been obtained at low temperature and subjected to X-ray diffraction analysis^[21].

The molecular structure displayed a symmetrical and stretched conformation: this result contrasted with the highly coiled conformation proposed to explain the terminal selectivity observed in the course of the oxidation of squalene by NBS in THF containing water^[22]. Based on NMR and molecular calculation studies^{[23][24]} it has been proposed that

in a solvent of low polarity squalene would exist for the most part in an uncoiled fully extended state, with all of the double bonds equally vulnerable to attack by an oxidizing agent.

On the other hand, in a more polar medium squalene would assume a more highly coiled, compact conformation: in this case, the internal double bonds in the coiled conformation might be sterically shielded and thus chemically less reactive, whereas the terminal olefinic links remain exposed (Figure 8).

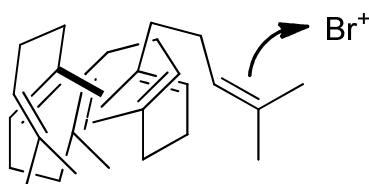


Figure 8: Compact conformation of squalene in highly polar solvents

This kind of folding maximizes the intramolecular lipophilic interactions and minimizes the contacts with the solvent, which is less lipophilic than squalene itself (oil drop effect)^[23].

Squalene emulsion-based adjuvants for vaccine delivery

Squalene is frequently used in the preparation of stable emulsions as either the main ingredient or secondary oil^{[25][26]}.

The high stability of squalene containing emulsions to its highly hydrophobic character: in fact, being almost insoluble in water, the diffusion from a small oil droplet to a larger one through the aqueous medium (Ostwald ripening, Figure 9) is very unlikely. For this reason squalene can be used in combination with other oils to reduce their tendency for Ostwald ripening and increase emulsion stability.

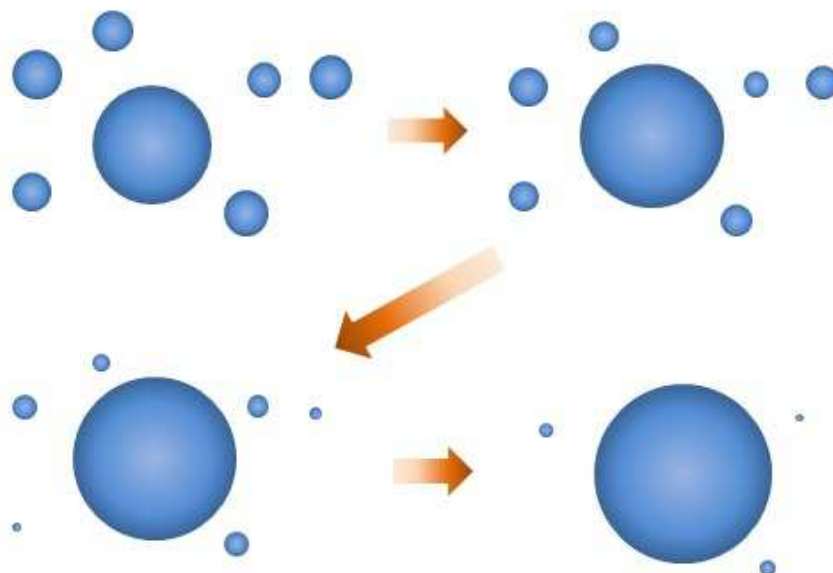


Figure 9: Schematic representation of Ostwald ripening

Squalene emulsions have been used for various applications, especially as immunological adjuvant in the delivery of vaccines, that is as substance employed to increase or to modulate the potency of the immune response while remaining non-toxic and safe for the host^[27].

Squalene as a potential protective and preventive agent in cancer treatment

Although squalene by itself is a weak inhibitor, it has been shown to prevent or arrest tumor growth in conjunction with anticancer drugs in various experimental tumor models^[28]. Many studies demonstrated that squalene is a potential chemopreventive agent, especially for breast, pancreatic, colon carcinomas, and similar tumors associated with ras oncogene mutations^[29].

In general, squalene likely protects against carcinogenesis by the following mechanisms:

- ✚ inhibition of Ras oncoprotein farnesylation as well as restricting the conversion of HMG CoA to mevalonate, which is necessary for DNA synthesis and cell proliferation, by indirectly inhibiting HMG CoA reductase via negative feedback regulation of endogenous cholesterol synthesis;
- ✚ modulating biosynthesis and function of xenobiotic metabolizing enzymes, thus altering the metabolic activation of carcinogens;
- ✚ acting as a free radical scavenger^[28].

Squalene as an emulsion has been reported to contribute either directly or indirectly to the treatment of cancer through a potentiation effect on co-administered anticancer agents^{[30][31]}.

Moreover squalene has been shown to display selective cytoprotective activity, protecting normal but not tumor cells from chemotherapeutic toxicity: for instance, squalene protected normal bone marrow colony forming units, but not neuroblastoma tumor cells, from cisplatin and other anticancer drug-induced toxicity^[32].

Squalene's protective effects against other diseases

Shark liver oil, a source of squalene and alkylglycerol, is reputed to provide protection against bacterial and fungal infections, especially when administered to patients suffering from atopic dermatitis caused by xerosis and skin lesions^[33]. Squalene alone is also believed to protect the skin from ultraviolet radiation-induced damage because a high percentage of squalene (about 12%) is secreted in sebum^[34]. This natural triterpene accumulates in high concentrations in the skin, where it plays a vital role in quenching free radical oxygen (oxygen singlets), thus preventing harmful effects of lipid peroxidation.

Furthermore, squalene and phenolic compounds in olive oil have been shown to provide considerable protection against coronary heart disease and aging^[35].

Squalene as a drug carrier

Drug carriers offer various advantages to passenger therapeutics: they allow administration of poorly soluble compounds, protect drugs from undesirable plasmatic metabolism, improve half-life, modify biodistribution, reduce toxicity, and facilitate drug targeting^{[36][37]}.

Lipids have gained significant attention for the purposes of drug delivery for a wide variety of reasons including biocompatibility, inertness, nontoxicity, and ability to fuse with cell membranes or to transport biologically active compounds through them.

Squalene has so far been used as a drug carrier in either emulsions or squalene-drug conjugates. For instance, a squalene emulsion stabilized by phosphatidylethanolamine or poloxamer 188 was shown to prolong *in vitro* release of a morphine prodrug^[38].

Administered intravenously *in vivo*, these prodrug-loaded squalene emulsion formulations exhibited prolonged analgesic activity in rats. Similar emulsions have been successfully employed to deliver lipophilic ester prodrugs of nalbuphine (a κ -opioid receptor agonist with a short halflife)^[39].

The concept of lipid-drug conjugates has gained considerable attention in recent years^{[40][41]}. Various lipid-drug conjugates have now reached Phase I/II clinical trials, such as a docosahexaenoic acid conjugate of paclitaxel (Taxoprexin, Protarga Inc., USA)^[42], an elaidic acid conjugate of cytarabine (Elacyt, Clavis Pharma, Norway)^[43], and a cardiolipin conjugate of gemcitabine (Neopharm Inc, USA)^[44]. The lipid-drug conjugates are usually obtained by covalent coupling of the drug to biocompatible lipid moieties. In some cases, these bioconjugates have been shown to improve pharmacokinetics, decrease toxicity, and increase the therapeutic index of the associated drugs.

Squalene nanoparticles

In this context, it has been disclosed by Couvreur and coworkers^[45] that the covalent linkage of squalene to hydrophilic drug molecules led to the formation of amphiphilic bioconjugates that self-assembled in water without the need of any surfactant.

Squalenoylation is an original technology platform for generating more potent anticancer nanometer-scale medicines. This concept is to chemically link a terpenoid to a biologically active drug molecule in order to create a bioconjugate, which can self-aggregate as nanoassemblies in water without the need of any other transporter material and without any surface active-agent, which, from a toxicological point of view, would be a major advantage for intravenous administration^[46].

This concept was firstly demonstrated with the nucleoside anticancer agent gemcitabine (2,2'-difluorodeoxycytidine).

Squalenoylation of gemcitabine

Gemcitabine (2',2'-difluorodeoxyribofuranosylcytosine) is an anticancer nucleoside analogue active against a wide variety of solid tumors, including colon, lung, pancreatic, breast, bladder and ovarian cancers. However, following intravenous administration, this drug is rapidly inactivated by enzymatic deamination and displays a short biological half-life, thus necessitating the administration of high doses that lead to unwanted side effects^[47].

The gemcitabine squalene bioconjugate (SqGem, Figure 10) overcomes the above drawbacks by self-aggregating in water as nanoassemblies (with a diameter in the range of 100-300 nm)^[45].

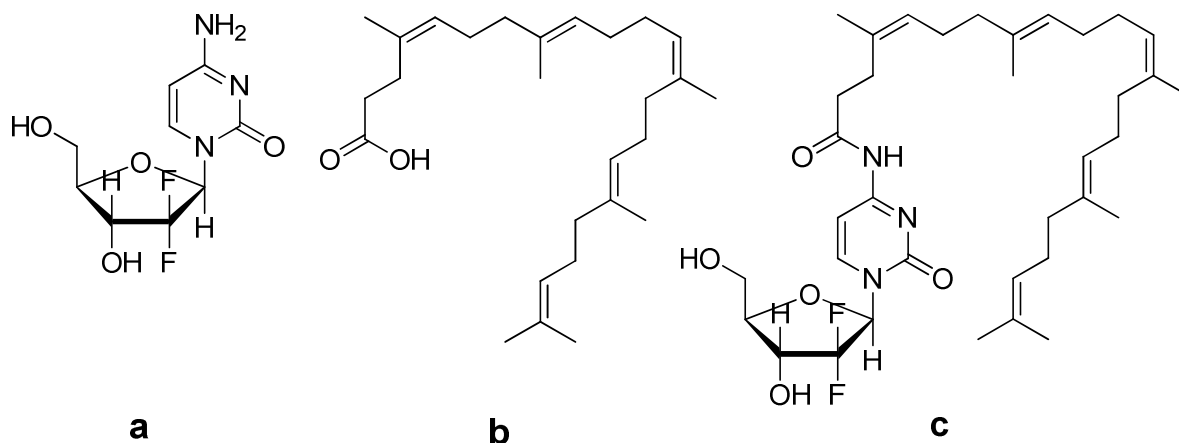


Figure 10: a) Gemcitabine (Gem); b) 1,1',2-trisnorsqualenic acid; c) 4-(N)-trisnorsqualenoyl gemcitabine (Gem-Sq)

The ability of squalene to form nanoassemblies when linked with gemcitabine was explained both by the amphiphilic character of the bioconjugate, the squalene corresponding to the lipophilic moiety, whereas the gemcitabine represented the hydrophilic part of the molecule, and, of course, by the capability of squalene itself to form spontaneously nanoassemblies in polar medium.

The anticancer activity of Gem-Sq nanoparticles was evaluated *in vitro* on the MCF-7 and KB3-1 cancer cell lines and showed that Gem-Sq aggregates were about 6- to 8-fold more cytotoxic than gemcitabine itself. When Gem-Sq NP were separated from the cells by inserts with a pore size smaller than the particle diameter, the aggregates maintained

their cytotoxicity after 72 h incubation: that means that, even when physically separated from the cells they were able to deliver the active drug. This observation suggests that the aggregate form of Gem-Sq (i.e. nanoassemblies) is in equilibrium with Gem-Sq as individual molecules, the latter being responsible for the cytotoxicity observed.

The anticancer efficacy of Gem-Sq NP was also determined after oral administration to F344 Fischer rats, finding that Gem-Sq NP were able to prolong the survival time of rats more than the free drug.

Squalenoylation of siRNA

Small interfering RNAs (siRNAs) are one of the emerging therapies for the papillary thyroid carcinoma (PTC), usually associated with a somatic mutation of the RET proto-oncogene (RET/PTC1) that encodes for a membrane tyrosine kinase receptor not expressed in healthy cells. Recently, a siRNA specific for RET/PTC1 oncogene has been discovered^[48], and this constitutes a very promising and specific therapeutic strategy, because RET/PTC1 is present only in tumor cells. However, in vivo delivery of siRNAs is a key challenge, due to the poor stability in biological systems and the low intracellular penetration because of their highly hydrophilic and anionic character^[49].

Couvreur and coworkers prepared^[50] a siRNA-squalene derivative (siRNA-Sq, Figure 11) with the aim of protecting siRNA from degradation and of improving the cell delivery by increasing the overall lipophilicity.

It is known that the modification of the 5'-hydroxyl groups of the siRNA strand can hamper the siRNA function, thus the authors linked squalene at the 3'-end of the 21-mer sense strand siRNA:

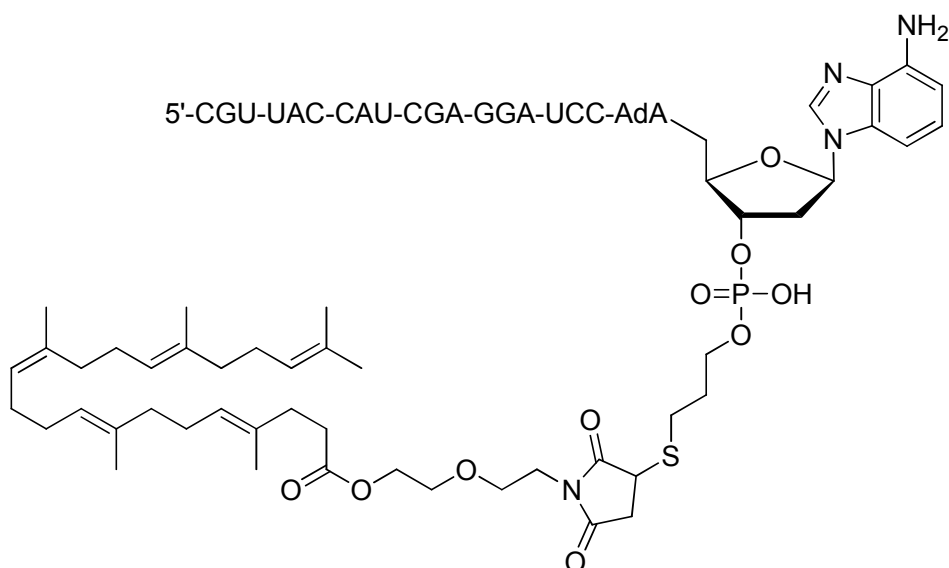


Figure 11: Couvreur's siRNA-squalene conjugate

By a real time quantitative reverse transcription PCR (qRT-PCR) it was found that the RET/PTC1 oncogene was down-regulated and the

RET/PTC1 protein expression was decreased. Anyway, the cytotoxicity evaluation of RET/PTC1 siRNA-Sq NPs in the same model (BHP 10-3 cell line) didn't show any cell growth inhibition.

Noteworthy, a preliminary in vivo evaluation showed that siRNA-Sq NPs were able to significantly reduce the tumor size, whereas the control siRNA didn't show any statistical difference respect to the control saline.

Squalenoylation of penicillin

Beta-lactams are one of the most important class of antibiotics. They can be used to treat infections caused by a variety of pathogens, but they suffer from a low intracellular uptake due to their weakly acidic character. One of the strategies to overcome this problem was the use of nanoparticulate carriers^[51], such as antibiotic-loaded liposomes^[52] and polyalkylcyanoacrylate nanoparticles^[53]. However, the drug loading was poor, thus necessitating the administration of a high amount of nanoparticles that in some cases resulted in side effects.

In order to overcome this limitations, Couvreur and coworkers prepared two amphiphilic squalene derivatives of penicillin G (PNG) containing a pH-sensitive or pH-insensitive bond^[54] (Figure 12):

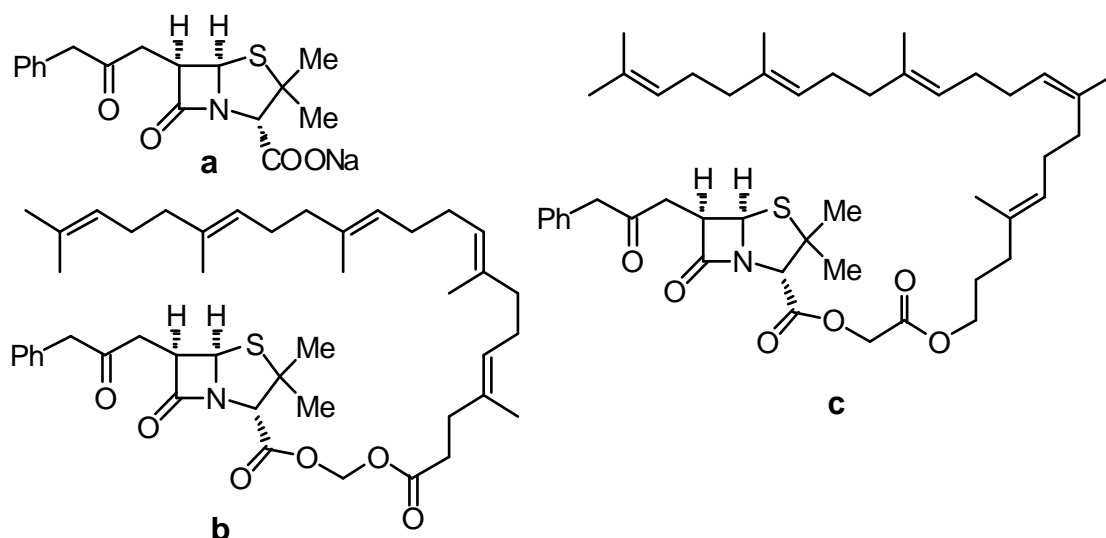


Figure 12: Penicillin G (PNG) and Couvreur's squalene-PNG conjugates

These bioconjugates were able to spontaneously self-assemble in water as NPs, yielding impressive antibiotic loading (44%); they also proved to induce fast and significant killing of *S. aureus*-infected J774 cells.

Biological membranes are permeable only to the uncharged form of antibiotics, thus PNG, being negatively charged at physiological pH (in fact it's a weak acid), cannot diffuse inside infected cells. On the other hand, squalenoylated PNG-loaded nanoparticles enter into the cells through endocytic pathways and accumulate in acidic late endosomes, where their pH-sensitivity triggers the release of free PNG.

Squalenoylation of paclitaxel

In 2010 Dosio^[55] and coworkers described the preparation of a small collection of conjugates (Figure 13) in which a paclitaxel (PTX) molecule was covalently linked to a squalene tail using different linkers:

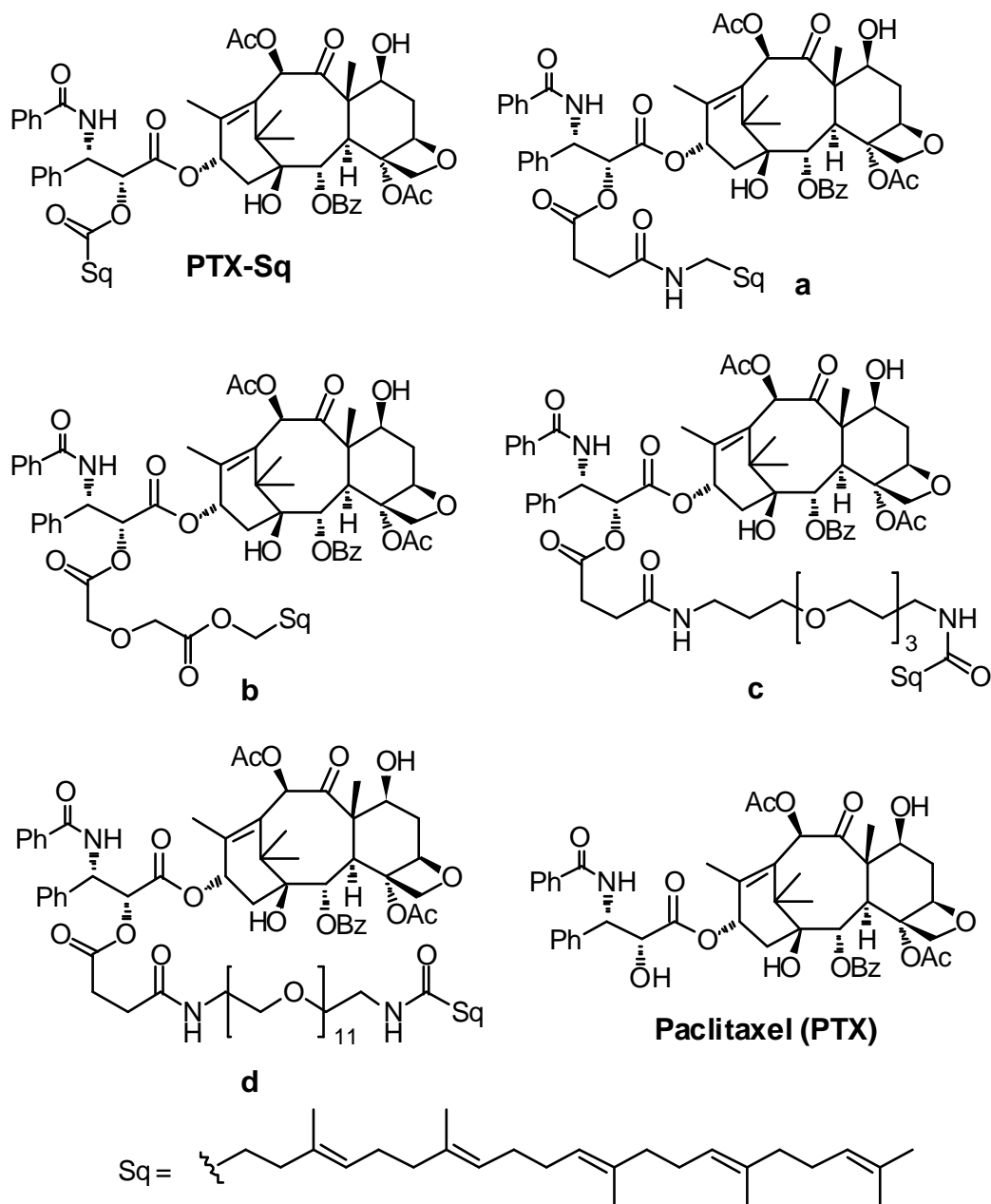


Figure 13: Dosio's collection of paclitaxel-squalene conjugates

All these compounds were able to self-assemble in water, leading to stable nanoparticle suspensions, with a PTX loading in the range of 45-69%.

This was *a priori* unexpected with regard to the dramatic lipophilicity and absence of amphiphilicity of the conjugates.

In vitro cytotoxicity was evaluated in M109 murine lung carcinoma cell lines, and the results are summarized in Table 1:

Compound	IC ₅₀ (nm)
PTX	9.0±2.65
PTX-Sq	175.0±5.51
a	365.0±5.3
b	490.0±4.58
c	6450.0±7.0
d	16500.0±7.81

Table 1: IC₅₀ (nm) of Dosio's PTX-squalene conjugates

Even if these compounds showed to possess a cytotoxic activity, they still remain less active than their parent drug, and also unsatisfactory results were obtained from the *in vivo* evaluation. This decrease in the activity could be due to an incomplete release of the drug, because of the covalent bond between the two moieties. In fact, it is well known that the hydroxyl group at the 2'- position has a significant relevance for the biological activity of paclitaxel.

Castelli and coworkers investigated also the possibility to incorporate compound **a** into dimyristoylphosphatidylcholine (DMPC) multilamellar vesicles (MLV)^[56]. MLV were prepared empty and loaded with **a** and paclitaxel as a comparison and analyzed by differential scanning calorimetry experiments, that can reveal the effect caused by insertion of "stranger" molecules inside the vesicles by the variations in thermotropic parameters, such as transition temperature (T_m) and enthalpy change (ΔH), usually dependent on the amount of compound interacting with MLV.

PTX-Sq resulted much more able to interact with MLV than paclitaxel and remained inside them. This is probably due to its increased lipophilicity and, thus, affinity for phospholipid bilayers.

Improvement of the squalenoylation platform

On the base of the results obtained for compound PTX-Sq, Couvreur and coworkers prepared a small collection of its analogues, in which paclitaxel and squalene units were connected together by six different 1,4-*cis,cis*-pentadiene units^[57] (Figure 14).

This idea came from another analogue of paclitaxel: docosahexaenoic-acid-paclitaxel (DHA-PTX, Taxoprexin). This is a very promising slow-release conjugate that reached the phase III clinical trial for the treatment of metastatic malignant melanoma and, even if DHA and squalene moieties are very similar, DHA-PTX is much more active than PTX-SQ.

Since the major difference between these two lipophilic moieties seemed to be the absence of methylene groups, the authors decided to intercalate a spacer between PTX and squalene tail, not to disrupt the self-organizing properties of the resulting conjugates.

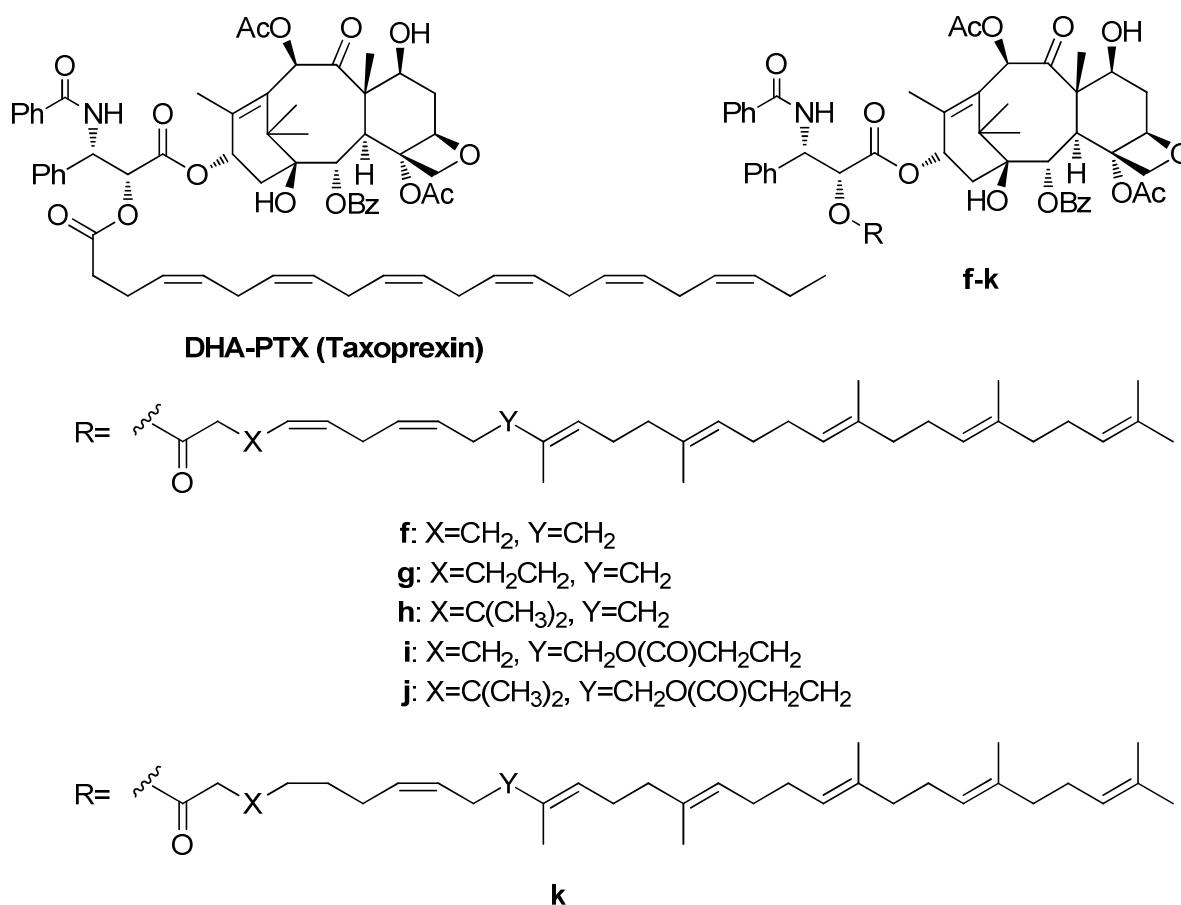


Figure 14: Analogues of compound PTX-Sq

In vitro biological evaluation showed that these compounds displayed notable cytotoxicity on several tumor cell lines, compounds **1f** and **1g** being the most promising ones.

For **f** and **g** also in vivo activity was evaluated but unfortunately, while being better tolerated (MTD for PTX-Cremofor EL: 10 mg/kg, MTD for **f**, **g**: 32 mg/kg), they resulted less active than PTX-Cremophor EL.

Self-immolative linkers

The squalenoylation platform enlightens how the covalent linkage between a squalene molecule and a drug unit can modulate the physical properties of the latter, improving its cellular uptake. It can happen that the derivative thus obtained shows a good biological activity, but in most of the cases it results lowered because a functional group necessary for the activity of the drug unit is involved in the linkage.

In these cases a good strategy could be to connect the two portions in a cleavable way (Figure 15a) or by attaching a triggering moiety that, upon specific conditions or in the presence of specific enzymes, is able to start a cascade that ends with release of the drug (Figure 15b). In the latter case, the linker forms a scissible bond with a protecting group and a stable bond with the drug unit, that becomes labile upon removal of the protecting group, resulting in a rapid disassembly of the three components (self-immolative elimination)^[58].

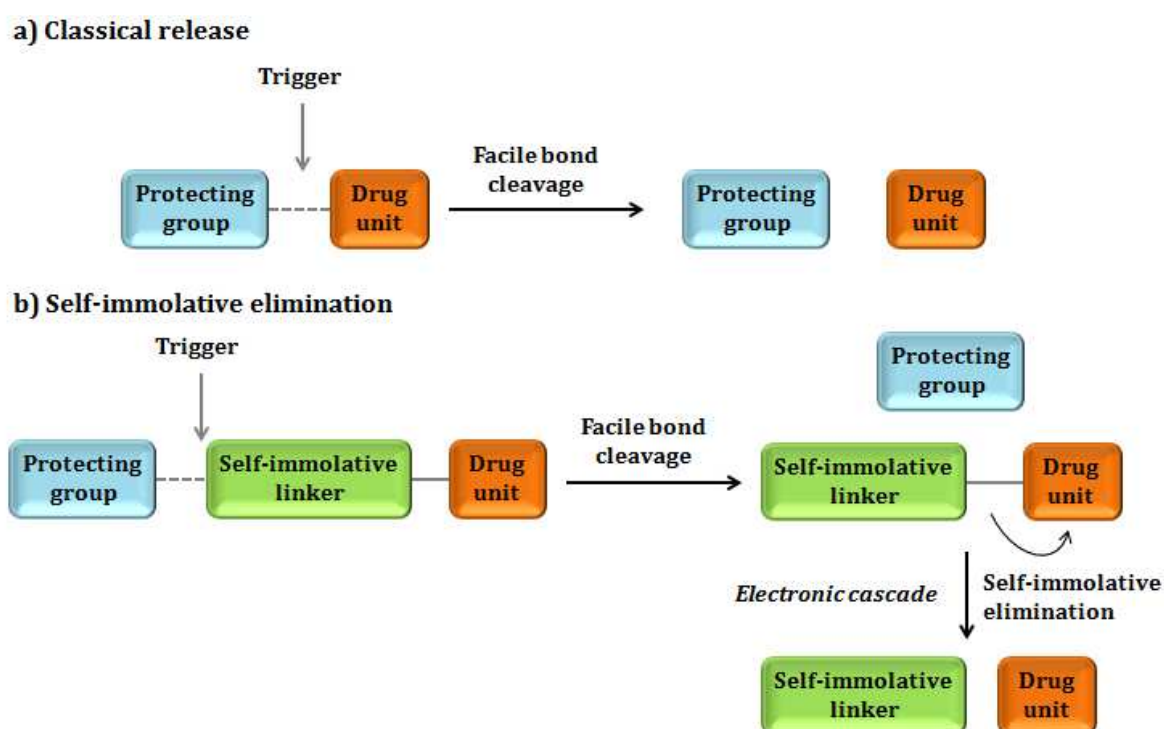


Figure 15: Different approaches for drug release

Some examples of self-immolative linkers including their mechanism of drug release are summarized in Table 2^[59]:

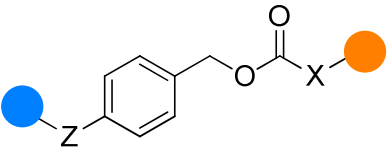
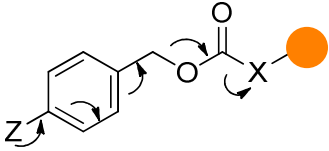
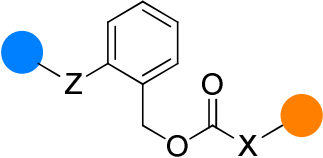
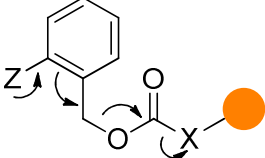
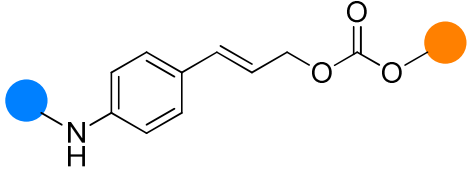
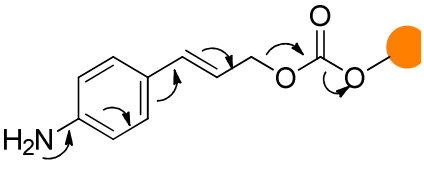
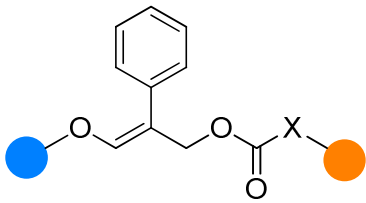
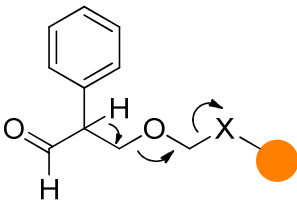
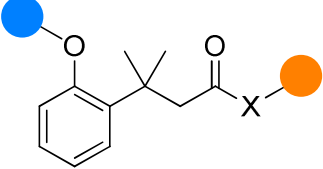
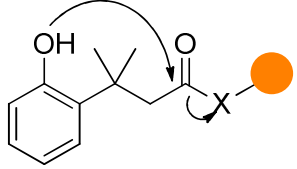
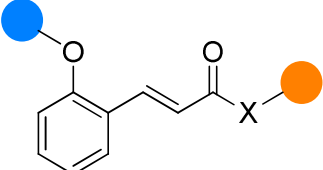
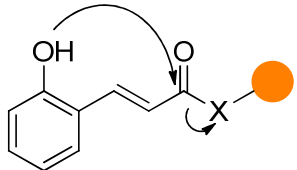
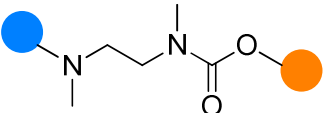
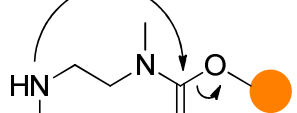


Linker	Reaction type	Release mechanism
	1,6-benzyl elimination	
	1,4-benzyl elimination	
	1,8-elimination	
	β -elimination	
	Cyclization (lactonization)	
	Cyclization (lactonization)	
	Cyclization	

Table 2: Self-immolative linkers and their mechanism of drug release;  = Protecting group;  = Drug unit; X, Z = O, NH

The evolution of self-immolative linker technology has led to self-immolative systems capable of amplified release, such as dendrimers (Figure 16a) and polymers (Figure 16b).

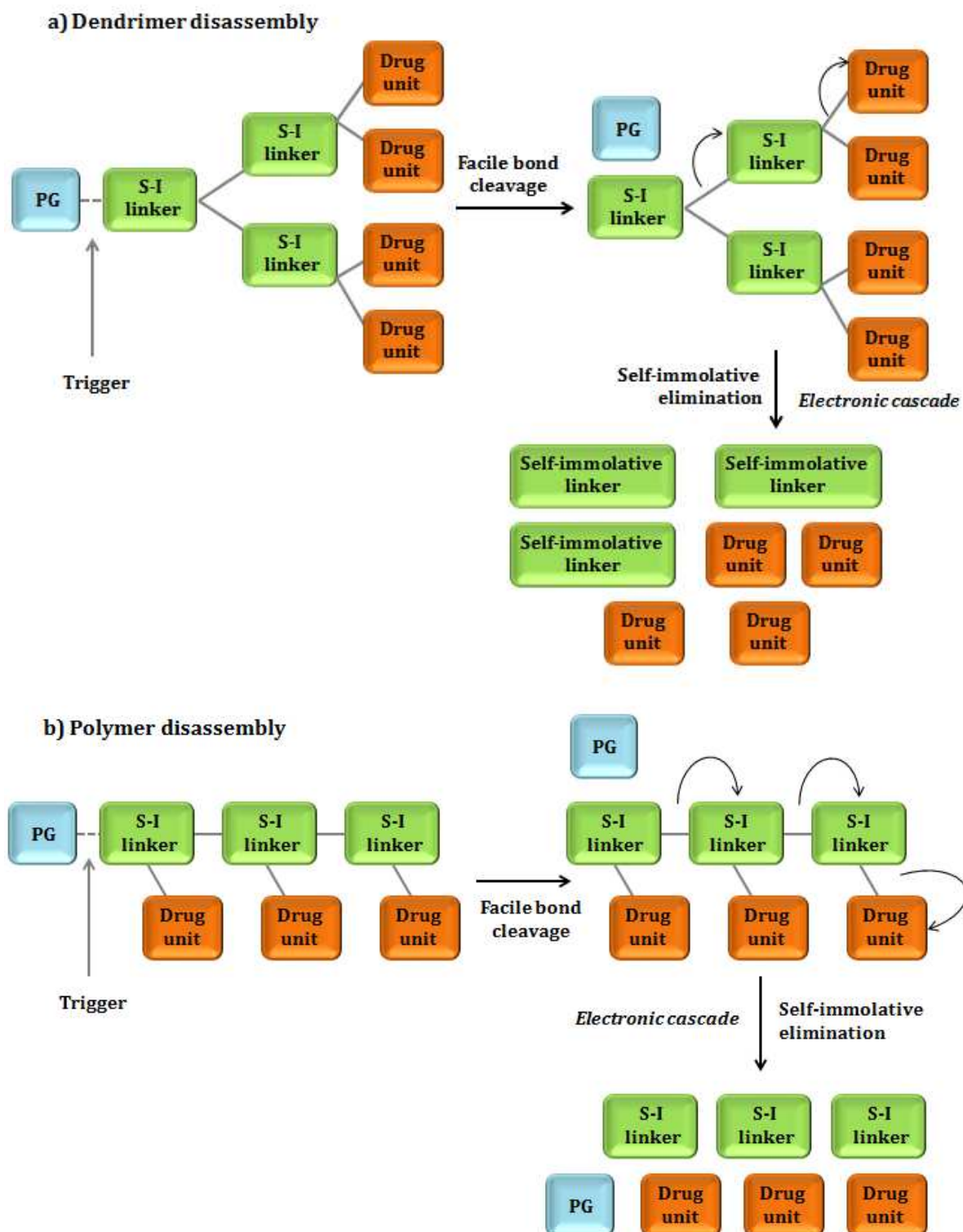


Figure 16: Dendrimer and polymer disassembly

Summary

On the base of these examples we can conclude that squalenylation of active molecules results in the possibility to overcome some of the problems connected to a low water solubility of hydrophobic drugs, such as paclitaxel.

Furthermore, squalene derivatives are more lipophilic than "free" compounds, and so the attachment of a squalene tail to hydrophilic molecules, such as gemcitabine, can improve the penetration through phospholipidic membranes.

Anyway, it can happen that, in order to show a higher activity, the parent drug needs to be released from the squalene conjugate. This can be accomplished by the action of specific enzymes or by the presence of labile moieties that are cleaved in specific conditions (pH, temperature etc^[7]).

For these reasons the preparation of drug-releasing squalene derivatives could be a good strategy for improving the delivery of drugs.

Section 2: Disulfide-containing Squalene conjugates

Disulfide-containing dimers of anticancer compounds

In the last years our research group investigated the possibility to improve the biological activity of anticancer compounds by modifying their structures in order to overcome some drawbacks associated to this molecule, such as low water solubility, low physiological stability etc.

In particular we used different strategies:

- ✚ Modifications based on modeling studies^{[60][61][62][63]};
- ✚ Substitution of precise portions of the molecule with bioisosteric ones^{[64][65][66]};
- ✚ Preparation of dimers, with possible applications to target-guided synthesis^{[67][68][69][70][71]}.

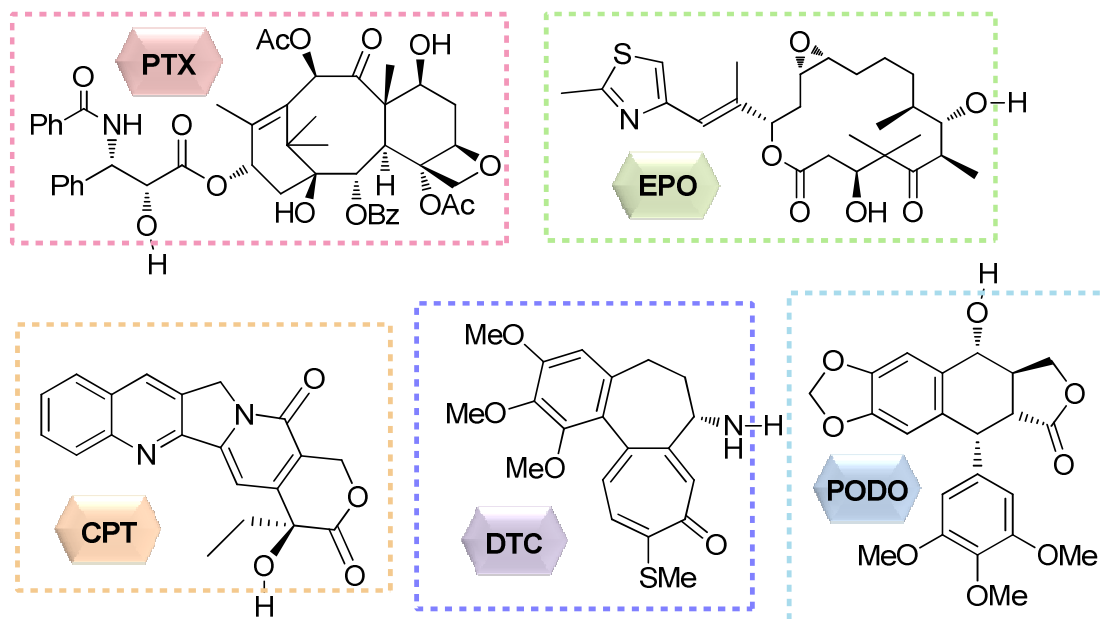
Among them, the preparation of dimers (Figure 17) offers some advantages concerning the possibility to obtain a better stability, a higher quantity of compound that reaches the intracellular environment and to exploit all the aspects related to the nature of the linker used to connect the two drugs units. For example, it is possible to use linkers with polar substituents, in order to improve the water solubility or to introduce labile functional groups that can be cleaved in specific conditions related to the tumor environment.

For these reasons we prepared different classes of homo- and heterodimeric compounds using different disulfide-containing linkers and different anticancer compounds (Figure 18 and Figure 18).



Figure 17: General structure of homo- and heterodimeric derivatives of anticancer compounds

Drugs:



Linkers:

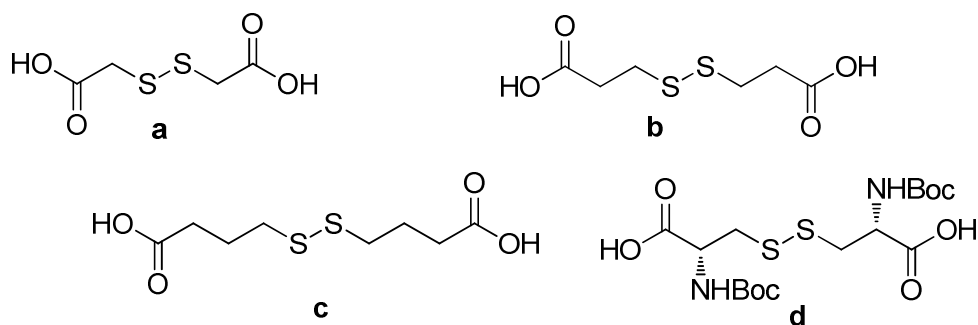
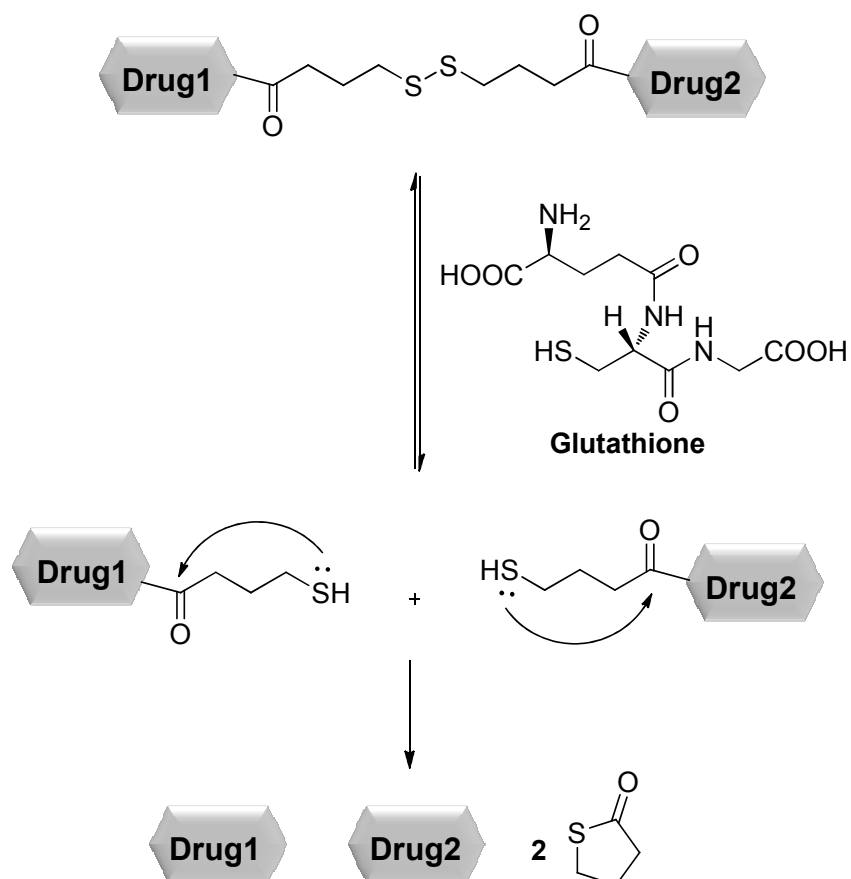


Figure 18: Drugs and linkers used for the preparation of our conjugates

In fact, it is well established that in many kinds of tumor a high concentration of glutathione (GSH) is present inside cells (1mM instead of micromolar extracellular concentration) and that GSH is able to reduce disulfide bonds.

So we hypothesized that, after reduction of the disulfide bond, our conjugates could be able to release the drugs, following, for example in the case of linker **c**, the closure of the thiolactone ring:



Scheme 2: Reduction of disulfide bond by GSH

Interestingly, these conjugates were able to release the parent drugs after incubation with GSH. They showed also to possess a biological activity, even if lower than the corresponding free drugs.

We also applied the so-called *target-guided synthesis* approach^[71] to verify the ability of tubulin, when incubated with different S-S containing DTC-PODO dimeric compounds, to select by itself the building blocks that will lead to the more stabilized (and so more active) conjugate: ESI-FT-ICR-MS analyses revealed that the conjugate most stabilized by non-covalent interactions with the target was compound DTC-2 (Figure 19).

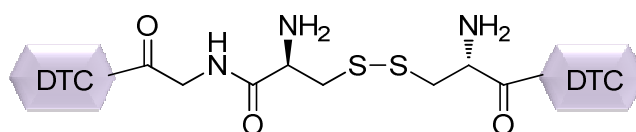


Figure 19: Structure of compound DTC-2

Aim of the work

On the base of our experience in the preparation of bivalent compounds in which two drug units are linked by a labile spacer able to release the active compound, we decided to go into the possibility of connecting two different compounds (a drug and a squalene tail) by a linker containing a disulfide bond (Figure 20).

In this purpose, we started a collaboration with Professor F. Dosio (Università degli Studi di Torino, *Dipartimento di Scienza e Tecnologia del Farmaco*) in order to prepare a small collection of conjugates (Figure 20) and to verify their ability to form nanoassemblies, thanks to the presence of squalene moiety, and to release the active drug inside the cells. In fact, this kind of compounds may undergo a disulfide exchange reaction in the intracellular environment thus releasing the active drug.

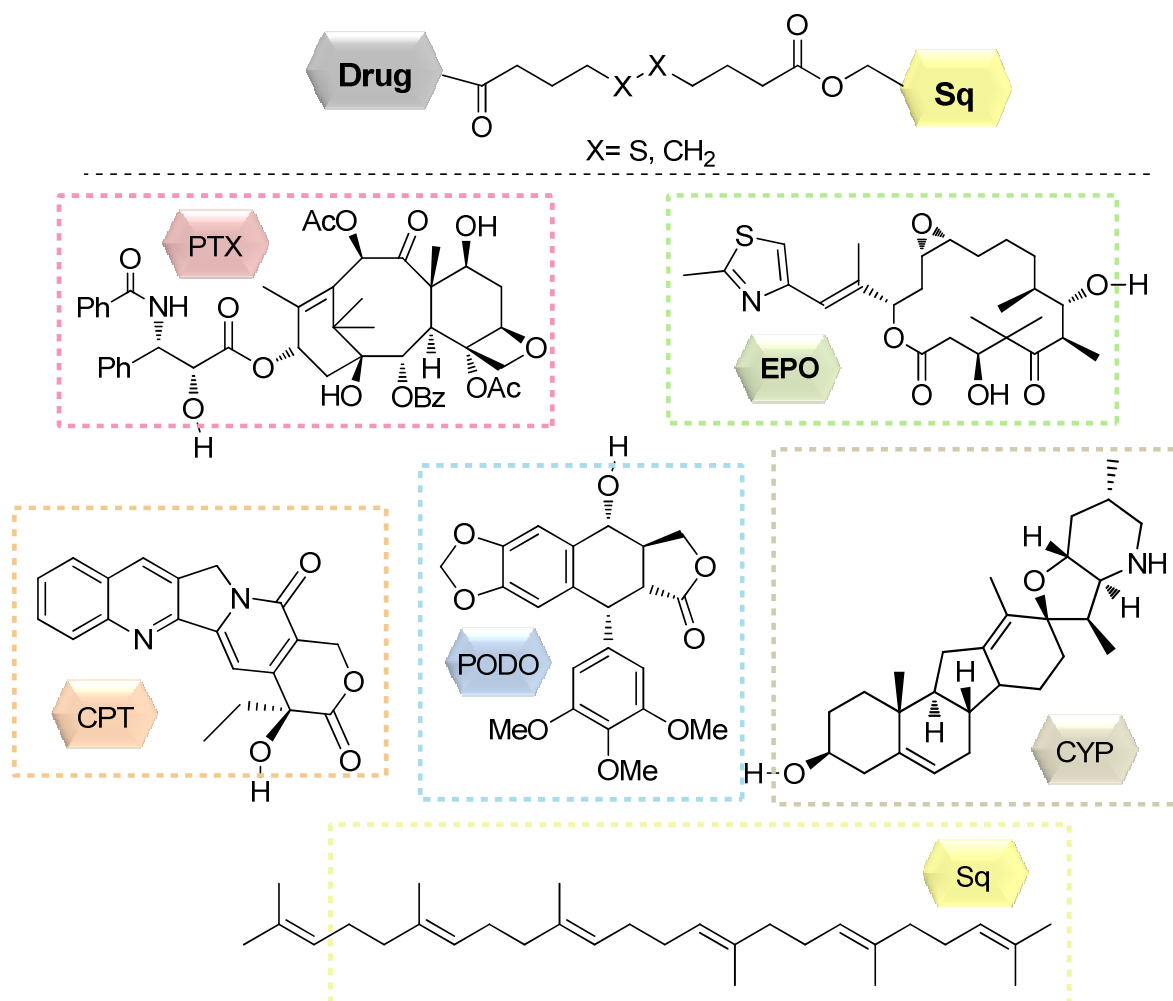


Figure 20: General structure of our drug-squalene conjugates, structure of drugs we used and squalene

As active compounds we chose paclitaxel, podophyllotoxin, epothilone A, camptothecin and cyclopamine. In order to better elucidate the importance of the presence of the disulfide bond, we also prepared the corresponding derivatives in which the sulfur atoms were replaced by two methylene groups.

Our targets: tubulin-interacting compounds

Paclitaxel

Paclitaxel was first isolated in 1971 from the Western Yew *Taxus Brevifolia* by Wani, Wall and coworkers, who established its structure by X-ray crystallographic methods^[72] (Figure 21).

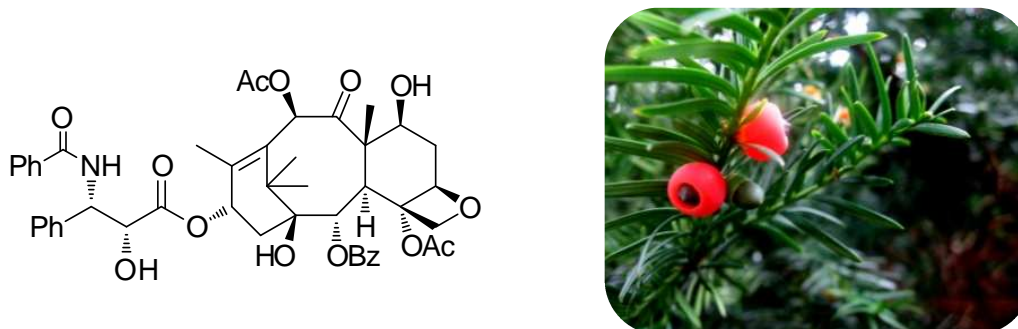


Figure 21: Paclitaxel and *Taxus Brevifolia*

Different from most anticancer drugs, PTX acts as a microtubule-stabilizing drug, which inhibits cellular growth by preventing cytoskeletal microtubule depolymerization to free tubulin and disrupting the balance between polymerization and depolymerization, and thus leads to cessation of the cell cycle with arrest at the G2/M phase^[73].

Despite its promising cytotoxic activity, many limitations in its clinical use are related to its low water solubility. For this reason paclitaxel is usually formulated in adjuvant Cremophor EL, that anyway has been reported to cause serious side effects, including hypersensitivity reactions, nephrotoxicity, cardiotoxicity and neurotoxicity ^[74]. Furthermore, significant side effects are also induced due to paclitaxel nonspecific, indiscriminate biodistribution in the body after administration.

Therefore, many kinds of PTX analogues have been prepared^[75], on the base of SAR studies, in order to improve water solubility while maintaining the activity, such as:

✚ *7-PEG carbamates and carbonates*: poly(ethylene glycol) (PEG) is known to enhance water solubility and reduce immunogenicity of high molecular weight protein adducts. Greenwald and coworkers reported^{[76][77]} the synthesis of PEG-paclitaxel conjugated (Figure 22) in which the PEG portion and the drug unit were linked together via a carbamate or a carbonate functionality at the 7 position (not essential for the biological activity):

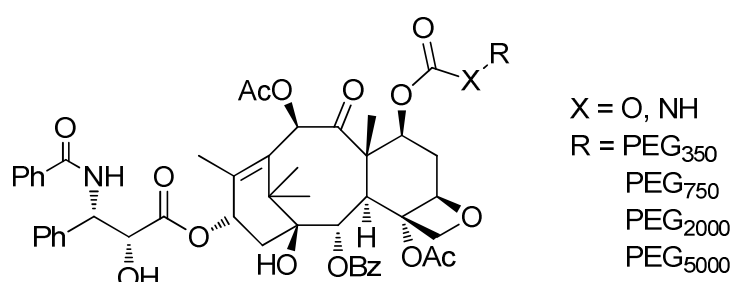


Figure 22: 7-PEG carbamate and carbonate derivatives of PTX

These compounds resulted approximately 30000 times more soluble than paclitaxel.

✚ *2'-derivatives containing base-labile moieties*: Nicolaou and coworkers^[78] prepared a small collection of paclitaxel analogues in which the 2'-hydroxyl group was functionalized with different groups having the following characteristics: ability to initiate their own cleavage thus generating paclitaxel in situ, ability to increase the water solubility and lability in basic conditions, as showed in Figure 23 (in fact some drug-resistant tumor cells have a basic microenvironment):

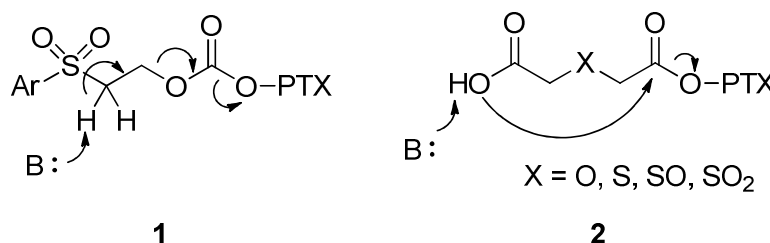


Figure 23: Base-labile drug-releasing PTX derivatives

Both the two classes showed an improvement in the water solubility, the one of class two being higher. When tested against a broad range of cancer cell lines, these compounds showed an activity comparable to that of paclitaxel. Furthermore, paclitaxel was isolated from the aqueous medium of the cell cultures, proving the *in vitro* release of the active drug.

- + *Reductively activated disulfide prodrugs:* Vrudhula and coworkers prepared a series of unsymmetrical paclitaxel prodrugs^[79] derived from 2,2-dimethyl-4-mercaptobutyric acid which contain polar moieties as part of the disulfide residue for increased hydrophilicity (Figure 24).

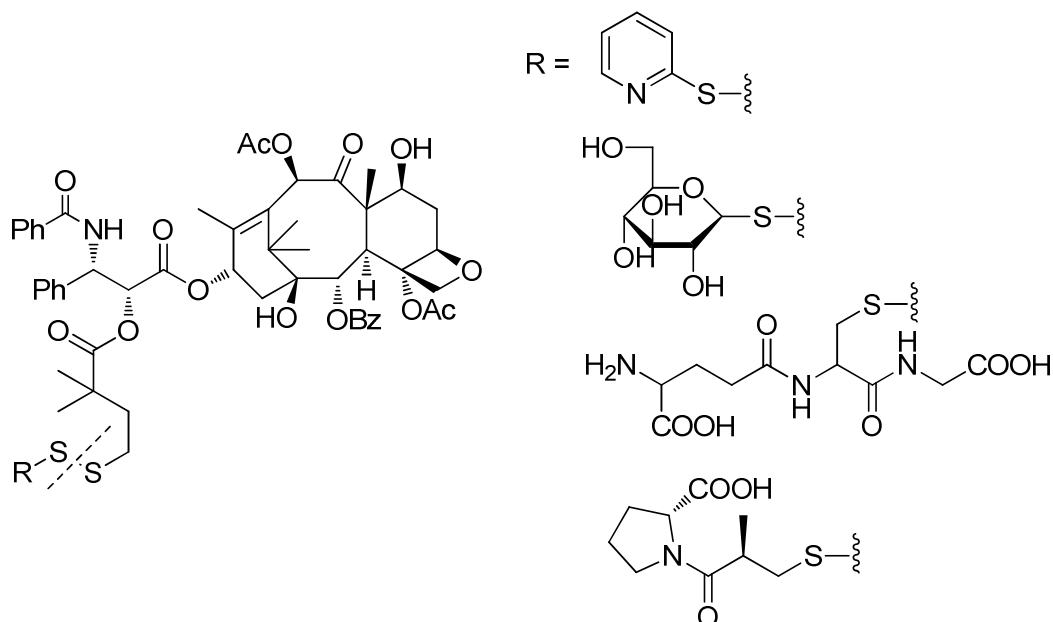


Figure 24: Reductively activated PTX derivatives

These compounds were able to be activated in the presence of dithiothreitol (DTT) and possess a good cytotoxic activity, even if slightly lower than paclitaxel.

Different approaches, obtained from SAR studies, for the preparation of paclitaxel analogues can be summarized as in Figure 25^{[80][81]}:

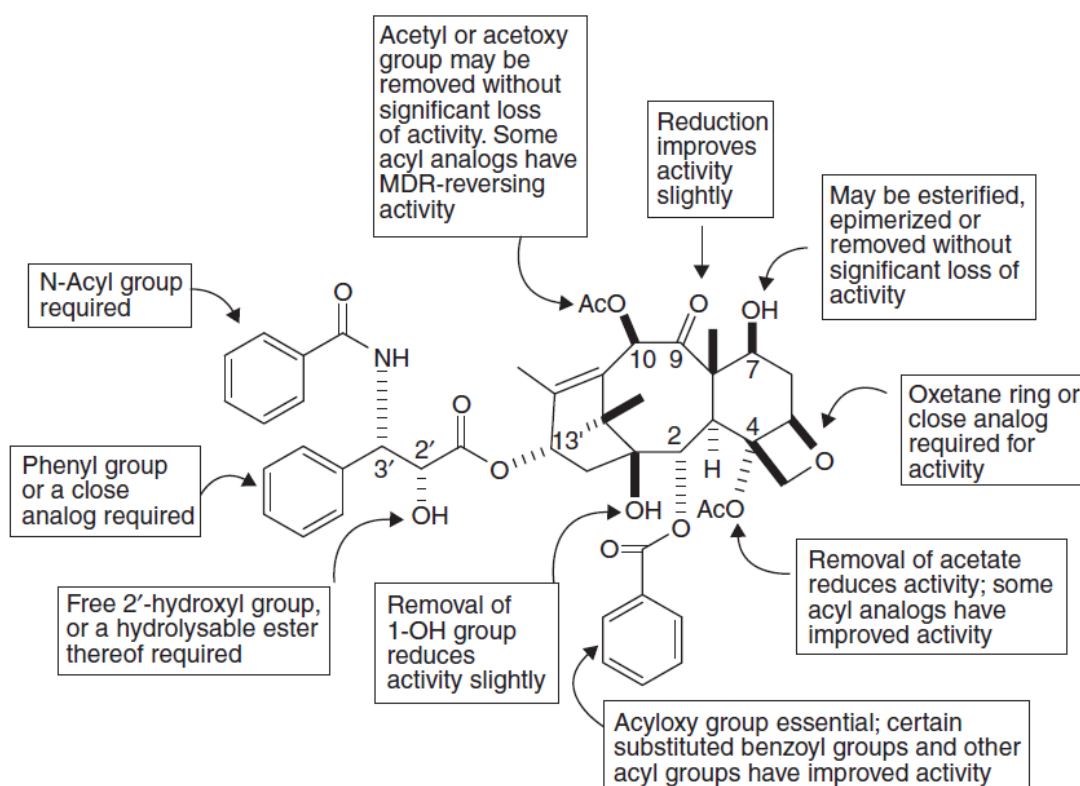


Figure 25: SAR studies for paclitaxel

Another strategy is to find a different formulation to avoid the use of Cremophor EL, and also in this direction many efforts have been made and some good results have been obtained, such as those related to albumin-bound paclitaxel (Abraxane®)^{[82][83]84}.

Epothilone A

The epothilones are a new class of natural cytotoxic compounds first isolated by Gerhard Höfle of the National Biotechnology Research Institute in Braunschweig, Germany from a cultured strain of the myxobacterium *Sorangium cellulosum* in the late 1980s [85][86]. The chief components of the fermentation process are epothilone A and B, with epothilone C and D found in smaller amounts. Trace amounts of other epothilones are also detected (Figure 26).

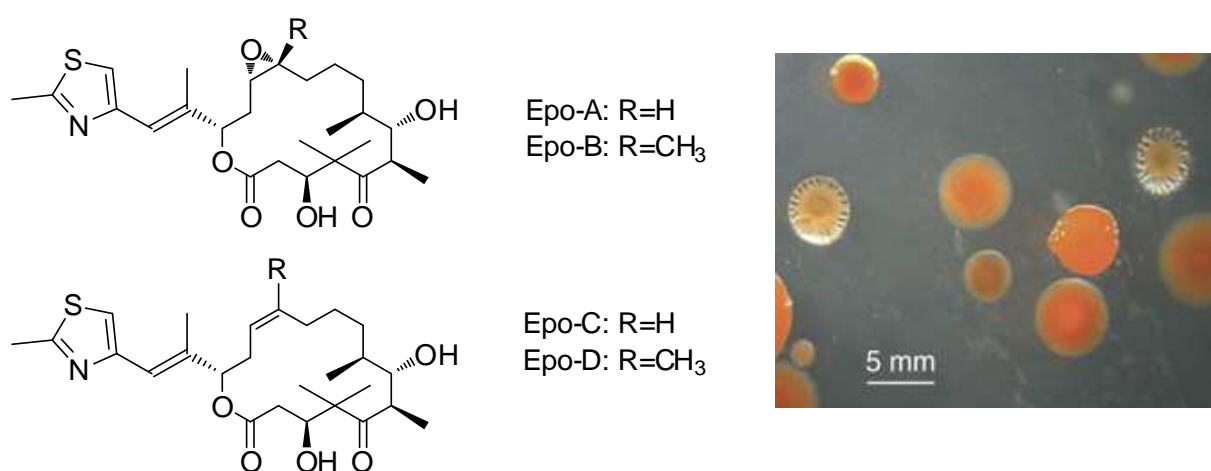
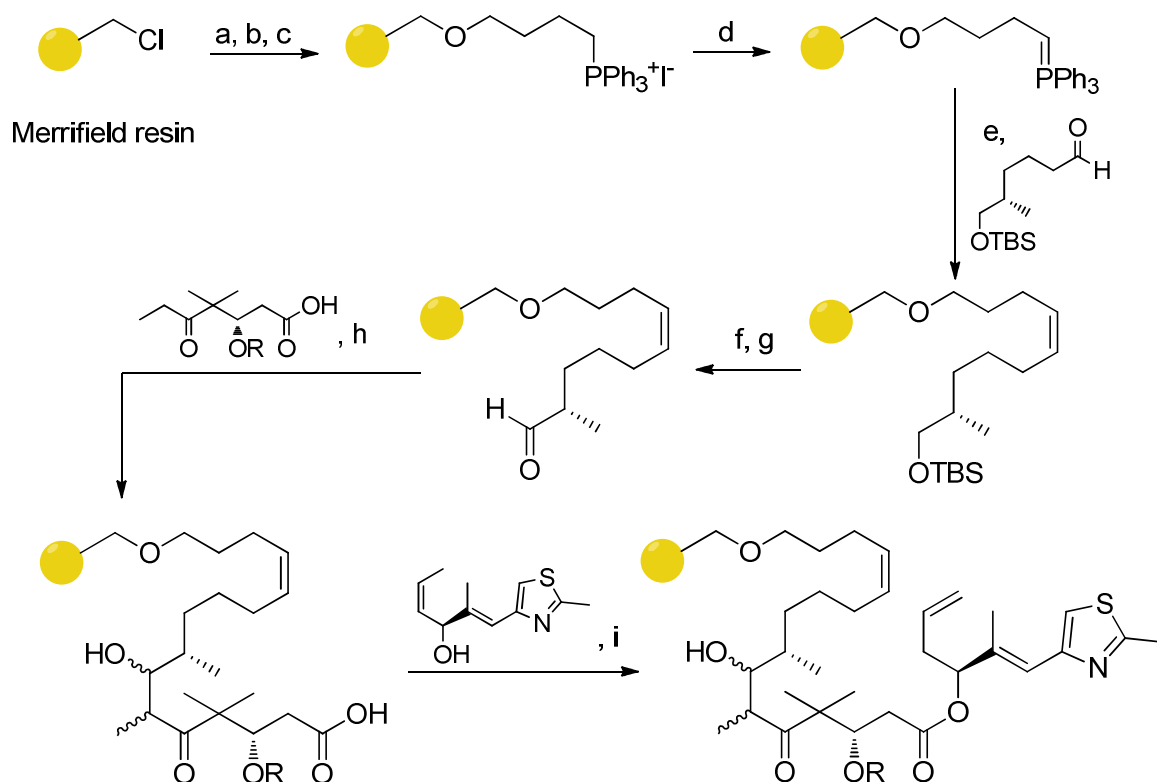


Figure 26: Epothilones and *Sorangium Cellulosum*

The structures of epothilones A and B include a 16-membered macrocyclic lactone that differs only in the presence of a hydrogen or methyl group, while epothilones C and D lack of the epoxide ring.

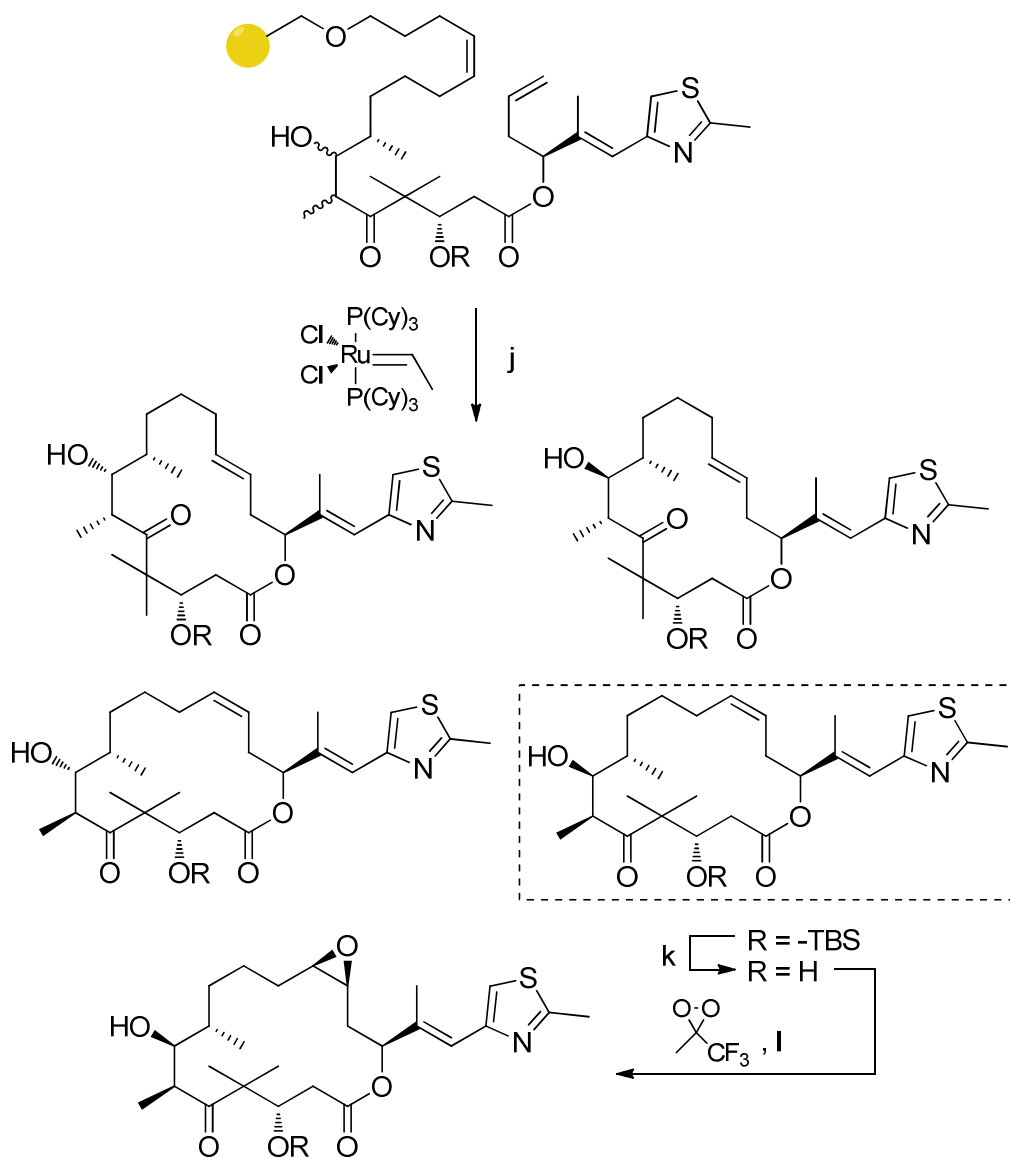
Although the epothilones can already be made by fermentation, several research groups have reported methods for their total synthesis [87].

One example is the solid-phase synthesis of epothilone A proposed by Nicolaou and coworkers in 1997 (Scheme 3)[88]:



Scheme 3: First steps of Nicolaou's synthesis of epothilone A. Reaction conditions: a) 1,4-butanediol, NaH, n-Bu₄NI, DMF, 25°C, 12h; b) PPh₃, I₂, imidazole, CH₂Cl₂, 25°C, 3h; c) PPh₃, 90°C, 12h; d) NaHMDS, THF/DMSO, 25°C, 12h; e) THF, 0°C, 3h; f) HF-py, THF, 25°C, 12h; g) (COCl)₂, DMSO, Et₃N, from -78°C to 25 °C; h) LDA, THF, from -78°C to -40°C, 1h, then ZnCl₂, THF, from -78°C to -40°C, 2h; i) DCC, DMAP, 25°C, 15h.

In the last steps of the synthesis a ring-closing metathesis leads to the formation of four different products that need to be separated by chromatography (Scheme 4):



Scheme 4: Final steps of epothilone A synthesis. Reaction conditions: j) CH_2Cl_2 , 25°C , 48h; k) 20% TFA, CH_2Cl_2 ; l) 0°C , 2h.

Epothilones, like paclitaxel, induce tubulins to form microtubules at low temperatures and without guanosine triphosphate or microtubule-associated proteins [89].

Epothilones exhibit kinetics similar to those of paclitaxel in inducing tubulin polymerization into microtubules in vitro (filtration, light scattering, sedimentation, and electron microscopy) and in producing enhanced microtubule stability and bundling in cultured cells. Furthermore, these 16-membered macrolides are competitive inhibitors

of paclitaxel binding, exhibiting a 50% inhibitory concentration almost identical to that of paclitaxel in displacement competition assays.

Epothilone A has been shown to be 2000 to 5000 times more active than paclitaxel *in vitro* against *P*-glycoprotein- expressing MDR tumors and cell lines as well as tumors resistant to the taxanes based on tubulin mutations.

Unfortunately, epothilones showed to be unstable in mouse plasma, resulting in metabolites with a mass 18 units higher than the parent drugs, and it was subsequently demonstrated that administration of the esterase inhibitor bis(4-nitrophenyl)-phosphate produced an active result in the A2780 ovarian carcinoma tumor model.

For these reasons many efforts have been made in order to synthesize epothilone analogues with the goal of improving metabolic stability.

Ixabepilone

Ixabepilone is the lactam analogue of epothilone B (Figure 27). It showed to be able to maintain the beneficial *in vitro* properties of the parent epothilones and, furthermore, *in vivo* studies proved ixabepilone to be stable to hydrolysis on incubation in both mouse and human sera.

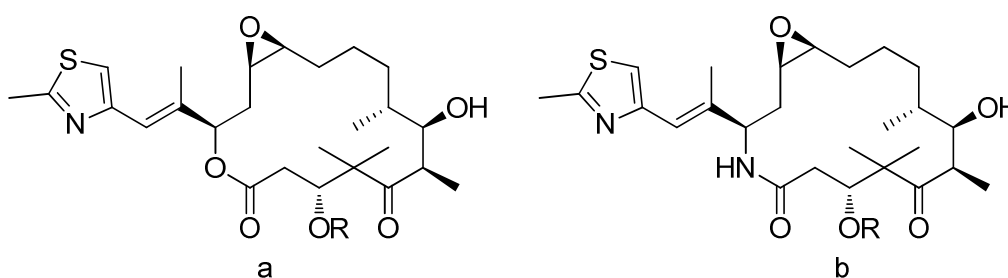


Figure 27: Epothilone B and Ixabepilone

Pharmacokinetic analyses of this compound delivered as an i.v. bolus in mice showed rapid systemic clearance and extensive tissue distribution, with a terminal half-life of 3 h. The protein binding was 87% and 85% in mouse and human plasma, respectively, indicating the presence of substantial free drug in each species.

Ixabepilone possess a potent tubulin polymerization activity, similar to that of epothilone A or epothilone B and 2-fold lower than paclitaxel, and a highly potent cytotoxicity across a broad panel of tumor cells, with a median IC₅₀ value of 2.9 nmol/L^[90].

Ixabepilone was mechanistically confirmed to block cells in the mitotic phase of the cell division cycle. Moreover, the concentration needed to arrest cells in mitosis corresponded well to the concentration required to kill cells over the same treatment duration.

Importantly, a comparison of the cytotoxicity of ixabepilone and paclitaxel in cell lines with different mechanisms of drug resistance indicated that, like the natural product epothilones, the lactam retained sensitivity toward paclitaxel-resistant lines driven by drug efflux pumps as well as tubulin mutations.

Podophyllotoxin

Podophyllotoxin^[91] is a naturally occurring aryl tetralin lactone isolated from the genera *Podophyllum*. Due to its high toxicity, this compound is currently used only as local antiviral agent: in fact, it was found unsuitable for clinical use as an anticancer agent due to its toxic side effects. However, its semi-synthetic derivative etoposide is an important anticancer drug due to a mechanism of action based on the inhibition of the enzyme topoisomerase II.

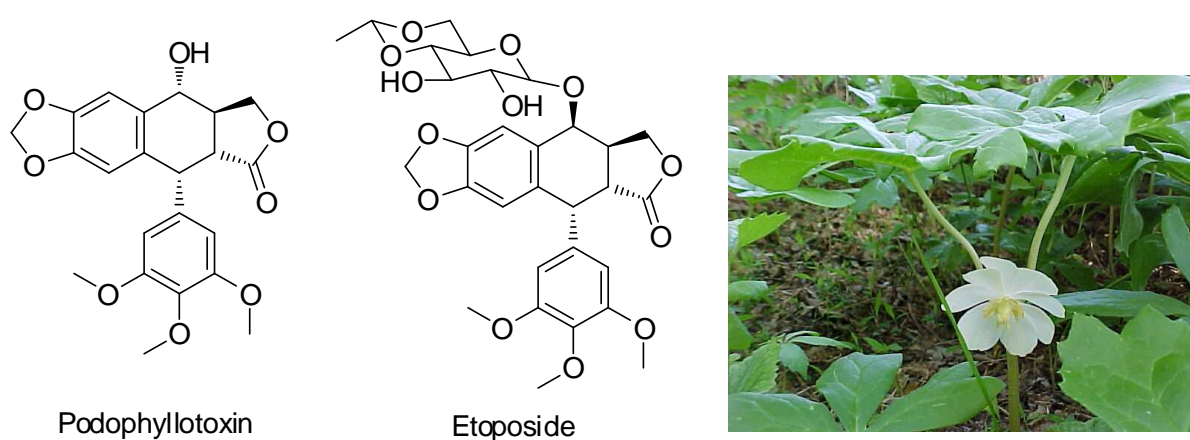


Figure 28: Podophyllotoxin, Etoposide and *Podophyllum Peltatum*

Podophyllotoxin is able to inhibit the formation of the mitotic spindle: this microtubule disruption causes the cell cycle arrest at the G2/M phase and subsequently induces apoptosis^[92].

In general, the binding behaviour of podophyllotoxin results in the partial unfolding of the secondary structure of β -tubulin at the carboxy terminus and prevents polymerization^[93].

Semi-synthetic podophyllotoxin derivatives, such as etoposide, are recognized as clinically useful drugs against various cancers, including small-cell lung cancer, testicular carcinoma, lymphoma and Kaposi's sarcoma^[94]. Even if these derivatives possess a superior pharmacological profile and broader therapeutic uses, the major drawback is the low water solubility that, for example in the case of etoposide, can cause severe allergic reactions.

Tubulins and microtubules

Tubulin is a heterodimeric protein composed of globular α and β tubulin subunits arranged in a polar head-to-tail fashion and represents the monomeric building block of microtubules, which are one of the fundamental structural components of cytoskeleton in all eukaryotic cells.

Microtubules (MTs, Figure 29) are involved in such diverse cellular processes as cell division, locomotion and intracellular transport and they are dynamic polar structures.

In vertebrate cells the centrosome acts as the major site of MT nucleation by lowering the critical concentration of tubulin required for polymerization and anchoring the minus ends of the resultant MTs.

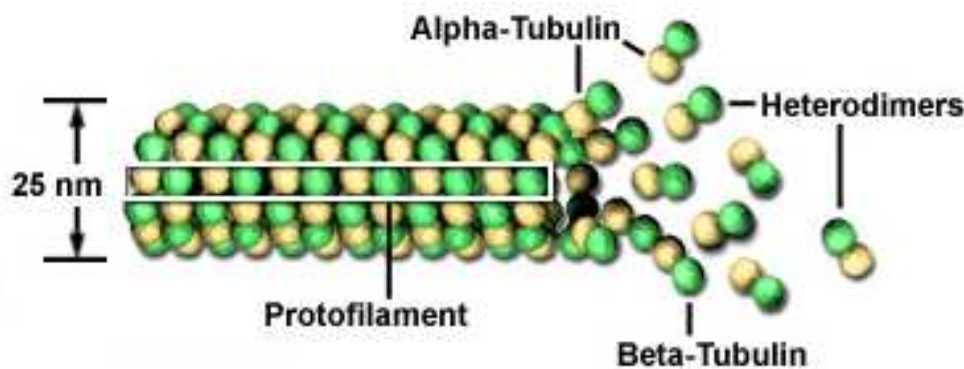


Figure 29: Tubulins and microtubules

Fully assembled microtubules are long hollow cylinders ~25 nm in diameter composed of laterally associated tubulin protofilaments. The number of protofilaments per microtubule can range from 10 to 18.

Microtubule-targeting drugs

Drugs that target the MT can be classified into two main groups based on their mechanism of action (Figure 30):

- ✚ MT-destabilizing agents (MDAs), such as podophyllotoxin and Vinca alkaloids, promote depolymerization and prevent polymerization of tubulin;
- ✚ MT-stabilizing agents (MSAs), such as epothilones and taxanes, promote polymerization of tubulin and stabilize the polymer, preventing depolymerization.

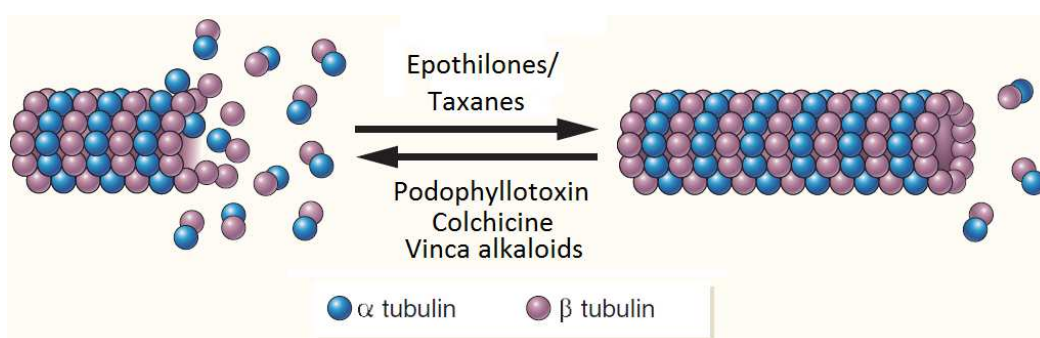


Figure 30: Microtubules stabilizing and destabilizing drugs

The exact mechanism of mitotic arrest and consequent apoptosis induced by an MSA is still not fully understood. It is however widely accepted that their antimitotic action occurs through interference with the spindle dynamics within the cell. Affected cells fail to pass mitotic checkpoints and arrest at the G₂/M phase of the cell cycle (Figure 31). G₂/M block is the hallmark of MSAs. Cells blocked in G₂/M subsequently undergo cell death. MTs are also required for endothelial cell migration, and thus some MT-targeting agents are able to inhibit angiogenesis as well as mitosis, inhibiting vascularization of tumors.

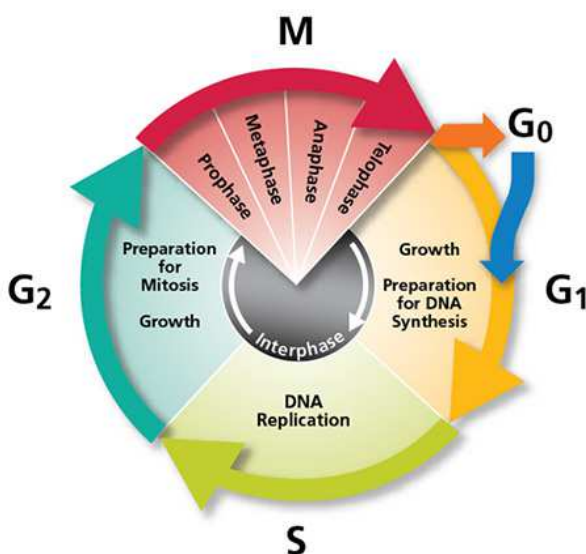


Figure 31: Phases of the cell cycle

Interaction with microtubules

Paclitaxel is a microtubule-stabilizing agent that acts by binding to β -tubulin in assembled microtubules. The 2'-hydroxyl group is an absolute requirement for activity because it forms a persistent hydrogen bond with D26 within the binding site. Substituent at the 3'-position function to orient the 2'-OH group for a productive hydrogen bond interaction with the protein^{[95][96]}(Figure 32).

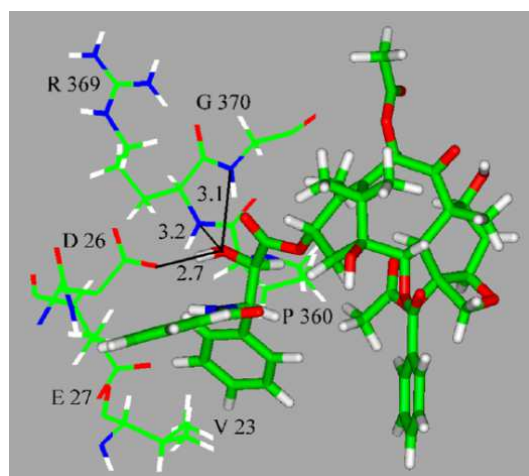


Figure 32: Binding mode of paclitaxel

Epothilone A competitively inhibits the binding of paclitaxel to tubulin, suggesting that the two types of compounds share a common or overlapping binding site (Figure 33).

Anyway, even if Epo-A and PTX overlap in their occupation of a rather expansive common binding site on tubulin, each ligand exploits the binding pocket in a unique and qualitatively independent manner^[97].

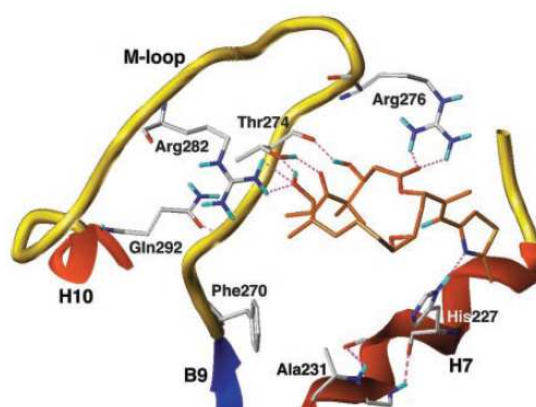


Figure 33: Binding mode of Epothilone A

Podophyllotoxin From the crystal structure of the tubulin-podophyllotoxin complex, it was observed that a threonine residue (Thr179) is present in close proximity with the 4 ϵ -hydroxy group of ring D of podophyllotoxin (Figure 5). The measured distance (approximately 3.4 Å) ensures a strong possibility of the interaction between the

carbonyl oxygen of Thr179 with the 4-hydroxy group of ring D on podophyllotoxin^[98] (Figure 34).

Podophyllotoxin competes for the colchicine-binding site on tubulin. This podophyllotoxin-mediated competitive inhibition of colchicine binding has been ascribed to the fact that both compounds possess a trimethoxy phenyl ring.

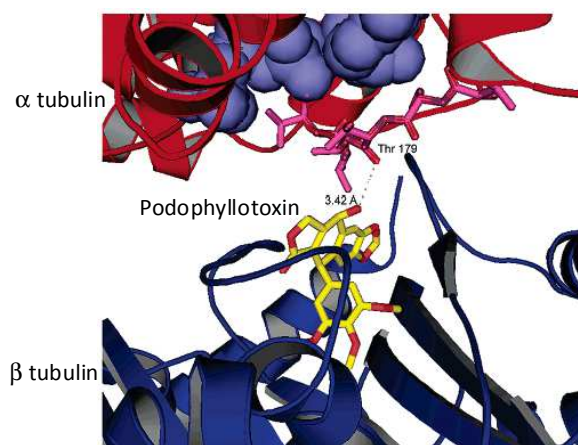


Figure 34: Binding mode of podophyllotoxin

Our targets: Topoisomerase I inhibitors

Camptothecin

Camptothecin (CPT) is a pentacyclic alkaloid isolated in 1958 from *Camptotheca Acuminata*^[99] (Figure 35) that acts as a selective inhibitor of the nuclear enzyme Topoisomerase I (TOP I).

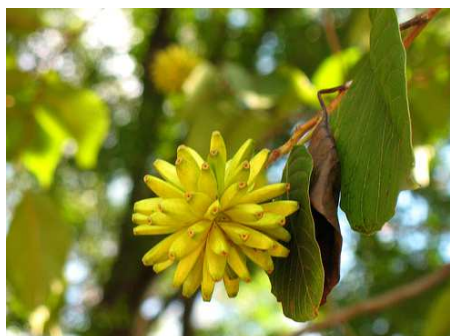
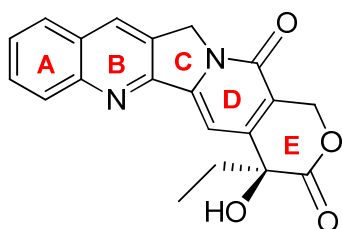
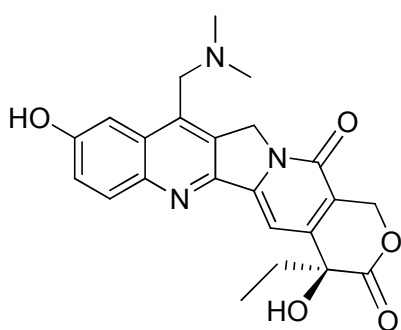


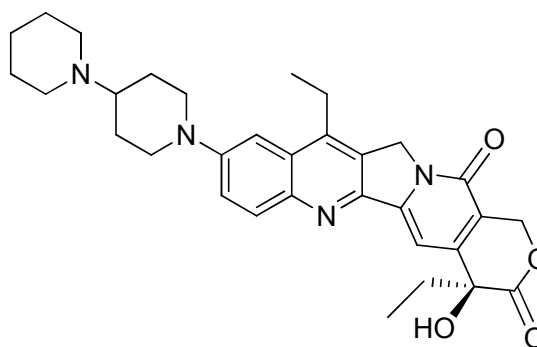
Figure 35: Camptothecina and *Camptotheca Acuminata*

Unfortunately, therapeutic application of unmodified CPT is hindered by very low water solubility in aqueous medium, high toxicity and rapid inactivation through lactone hydrolysis in vivo.

To overcome the solubility and stability issues, various derivatives have been developed. Although a number of small and large molecule compounds are currently in clinical trials, only two CPT derivatives, irinotecan and topotecan, are approved for clinical use (Figure 36)^[100].



Topotecan



Irinotecan

Figure 36: Structures of camptothecin analogues

Irinotecan is currently used for metastatic colorectal cancer, while topotecan has been approved for ovarian cancer, cervical cancer and small-cell lung cancer.

These derivatives employ tertiary amine cations to improve solubility and subsequently improve lactone stability.

Substituted camptothecins

To summarize the SAR studies, the A and B rings are the most tolerant to modification with substitutions at positions 7, 9, 10, and 11 improving or retaining activity^[101]. Interestingly, von Hoff has provided evidence that substitutions that increase hydrogen bonding at the 7-position improve binding to TOP I, thus increasing activity over CPT^[102]. On the other hand, altering the C and D rings or substituting positions 12 and 14 inactivates the molecules.

Finally, the E-ring lactone is necessary for activity by binding to TOP I: Hydrolysis or removal of the lactone leads to loss of all activity. The equilibrium between the closed, active lactone and the open, inactive carboxylate form is influenced by both the affinity of the carboxylate for human serum albumin and the local pH *in vivo* (Figure 37).

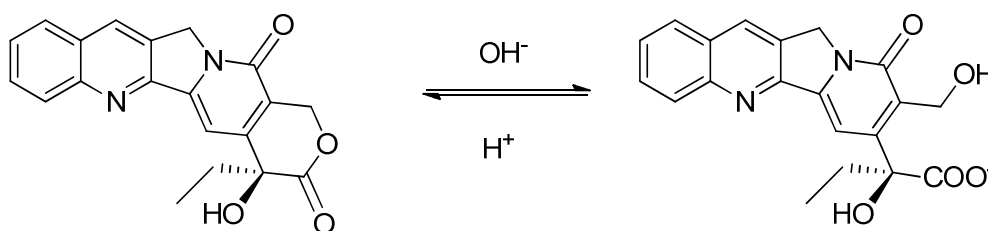


Figure 37: Lactone hydrolysis

Since it's the site where binding to TOP I occurs, the E ring tolerates only minor modifications without dramatic, negative effects. For example, enlargement of the ring to form the beta-hydroxy lactone improves stability and drug activity. Interestingly, modification of the C20 hydroxyl group through alkylation or acylation has been shown to stabilize the lactone^[70]. Acylation is the favored method for linking CPT covalently to macromolecules.

In addition, different kinds of CPT formulations have been prepared in order to accomplish CPT delivery to tumor cells by passive targeting, including micelles^[103], liposomes^[104], chitosan nanoparticles^[105] and hydrogels^[106].

Interaction with Topoisomerase I

CPTs gained much interest in the late 1980s when the molecular target was identified: DNA topoisomerase I (TOP I) is believed to be the single point of biological activity^[107].

Topoisomerase I acts clamping around DNA, nicking it, and forming a covalent bond between the active-site tyrosine and the 3' end of the DNA upstream of the cut, while hydroxylcapping the 5' end of the downstream DNA (Figure 38). After this enzymatic step, supercoils are relaxed by rotation of the DNA duplex downstream of the cut around the intact strand; the drive to rotate is provided by the energy stored in the supercoils and the number of full rotations of the downstream DNA equals the number of supercoils that are eliminated. Subsequently, the DNA backbone is religated, and the protein releases the DNA.



Figure 38: TOP1-DNA "cleavable complex"

The intermediate in TOP1-linked DNA breakage is referred to as a "cleavable complex", because it is readily reversible to a noncovalent enzyme-DNA complex before or after topoisomerization of the DNA. Experimental studies^[108] suggest interaction of CPT with both the enzyme and the DNA, forming a ternary complex that stabilizes the transesterification intermediate.

Modeling studies^[109] suggest that the interaction of CPT with DNA and top1 involves pseudointercalation between the base pairs of DNA flanking the top1 cleavage site. The protein backbone of TOP I extends toward the major groove of DNA. The camptothecin molecule is oriented with the E ring near the DNA break, and the concave portion of the drug molecule faces the DNA major groove^{[110][111]}.

Upon binding to TOP I, CPT prevents religation and causes apoptosis (Figure 39).

Interestingly, CPT exhibits little or no binding to either DNA or TOP I alone.

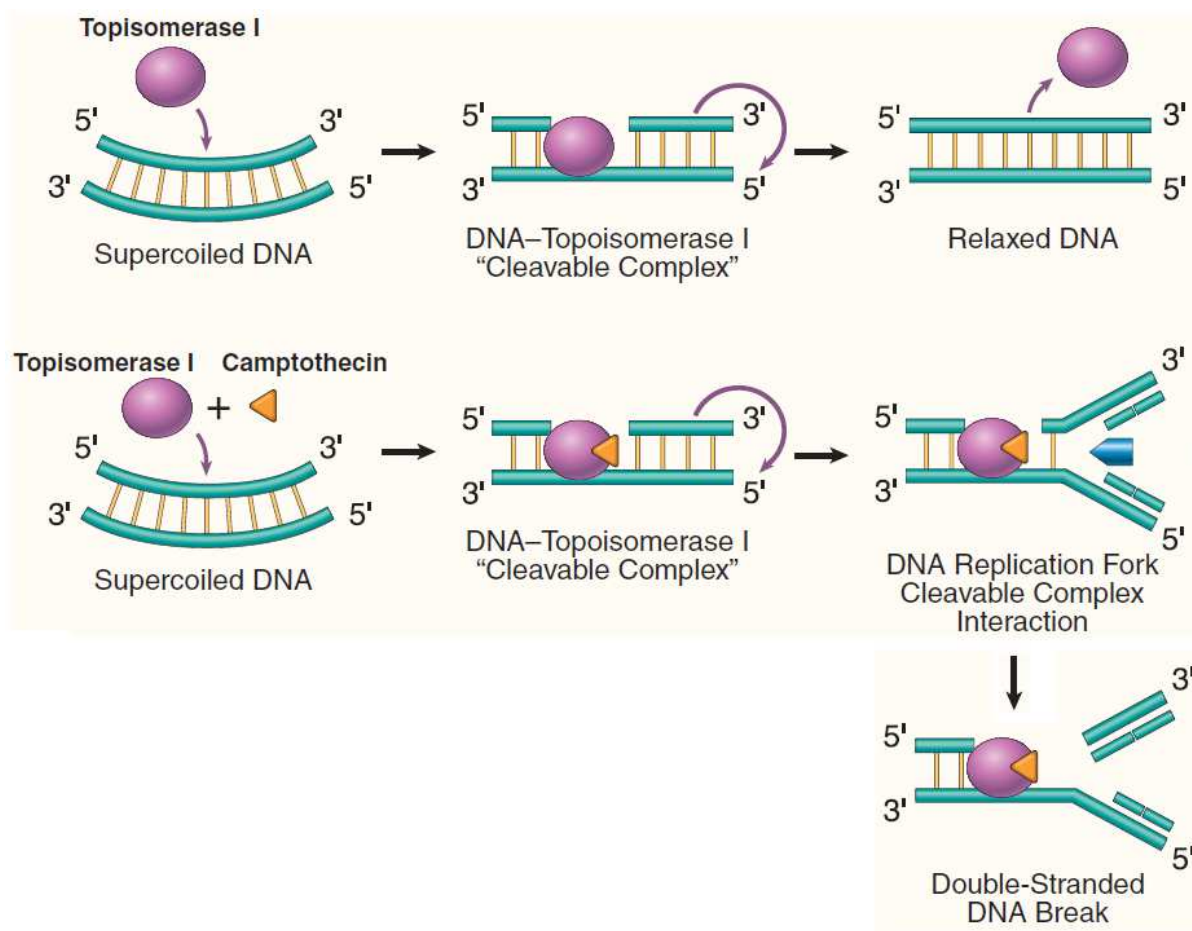


Figure 39: Binding of CPT to TOP1-DNA "cleavable complex"

Synthetic strategy

As depicted in Figure 40, two disconnections have been individuated, in the correspondence to the ester bonds, obtainable via two condensation reactions from a compound containing two carboxylic groups and two different alcohols:

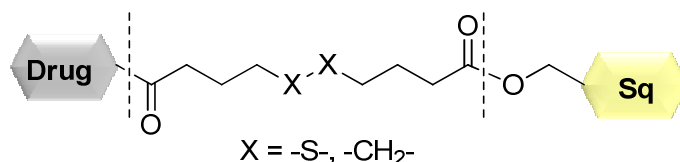


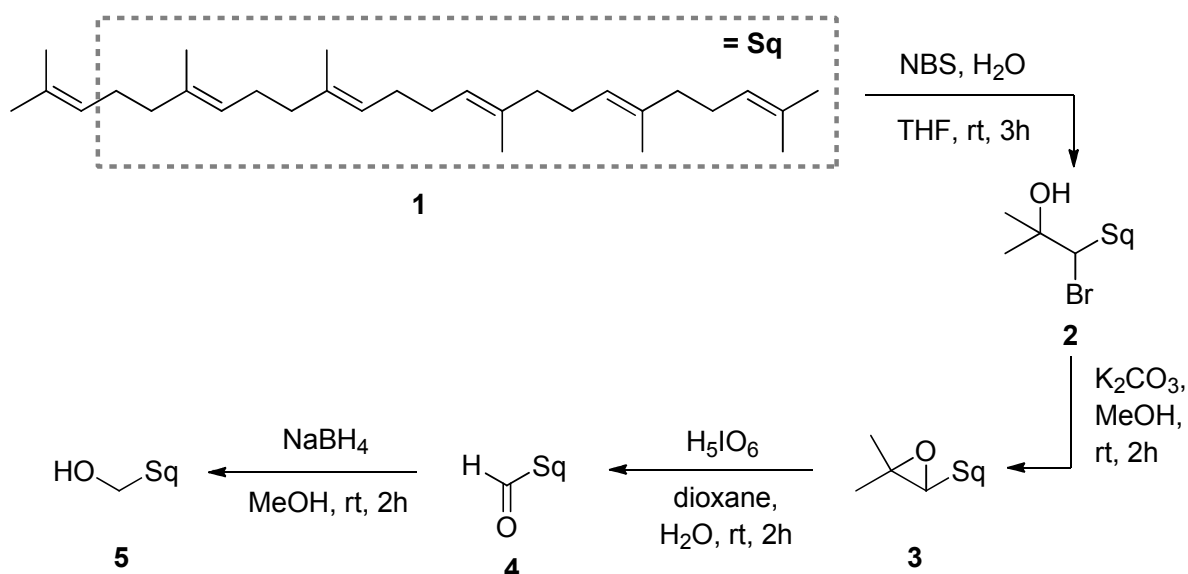
Figure 40: General structure of our drug-squalene conjugates

In order to minimize the loss of active drug due to the not high yields of this kind of reactions, we decided to firstly effect the coupling between the spacer and the squalene portion and, in the end, to attach the drug unit.

For this reason we started from the preparation of 1,1',2'-tris-nor-squalene alcohol **5**.

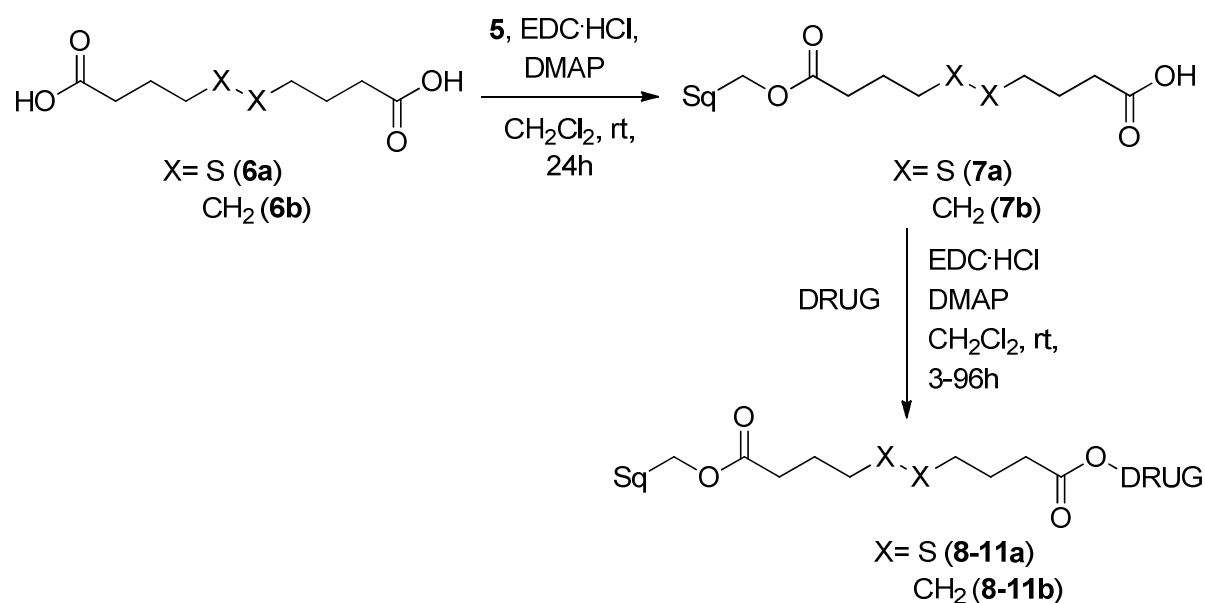
The first step consists in the preparation of the terminal monobromohydrine of squalene (**1**), that means to differentiate the six non-conjugated double bonds, approximately equivalent. As already mentioned, this is possible because in very polar solvents squalene assumes a compact conformation in which just one of the terminal double bonds is available to react.

The monobromohydrine **2** is then transformed in the corresponding epoxide **3** by treatment with K_2CO_3 in MeOH. After an oxidative opening of **3** with H_5IO_6 to give aldehyde **4** and consequent reduction with $NaBH_4$, the final 1,1',2'-tris-nor-squalene alcohol **5** is obtained, with an overall yield of 69% over four steps (Scheme 5).



Scheme 5: Synthesis of 1,1',2-tris-nor-squalene alcohol **5**

The final compounds have been prepared performing two consecutive condensations using EDC·HCl/DMAP as activating system in CH₂Cl₂ at room temperature for 3-96h (Scheme 6):



Scheme 6: Synthesis of drug-squalene conjugates **8-11**

Using this pathway and starting from two different dicarboxylic acids **6a**, **6b** (dithiodibutyric and sebacic acid) we were able to prepare a small collection of compounds (Figure 41):

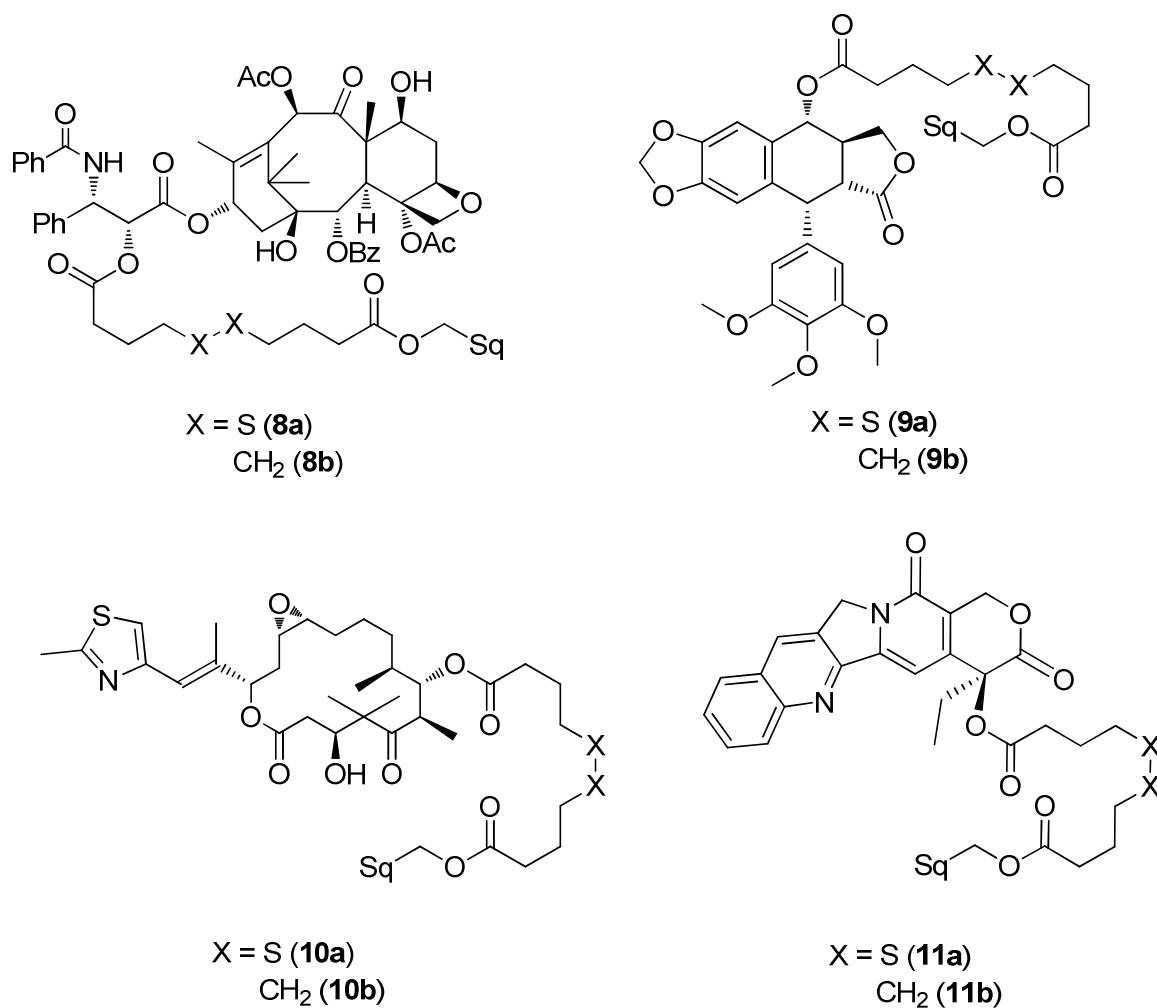


Figure 41: Structures of drug-squalene conjugates **8-11**

Reaction times and yields for compounds **8-11** are summarized in Table 3:

Compound	Reaction Time (h)	Yield (%)
8a	22	65
8b	24	40
9a	24	48
9b	18	31
10a	31	31
10b	96	19
11a	72	32
11b	48	28

Table 3: Reaction times and yields for the preparation of compounds **8-11**

Nanoparticles formation and characterization

Preparation

In order to allow the formation of nanoassemblies, the *solvent displacement method* was applied.

In a typical procedure, 4 mg of the conjugate were dissolved in 1 ml of EtOH, the solution was added dropwise to 2 ml of MilliQ water and then the organic solvent was removed under reduced pressure, with subsequent formation of a nanoaggregate suspension at a final concentration of 2 mg/ml (Figure 42).

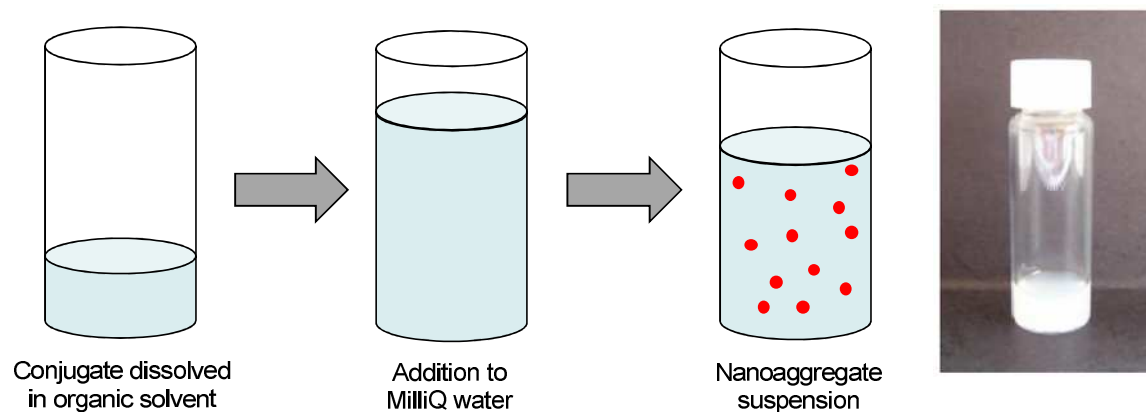


Figure 42: Typical preparation of a nanoparticle suspension

All the compounds were able to self-assemble in water and the suspensions were characterized to determine the mean diameter, the polydispersity index and the Z-potential.

Characterization

- ✚ Dimensional analysis: mean diameter and dimensional homogeneity (polydispersity index) of nanoassemblies were determined with quasi-elastic light scattering (QELS) experiments, at a fixed angle of 90°, using a 90 Plus Particle Size Analyzer (Brookhaven Instrument, Co.).
- ✚ Z-potential measurement: nanoassemblies surface charge was evaluated by measuring Z-potential, a parameter that controls electrostatic repulsion between adjacent particles, thus influencing the stability of the colloidal system. At low Z-potential values attractive forces prevail, while at high values repulsive forces prevail. In general it can be affirmed that colloidal systems are stable when their Z-potential assumes values between +30mV and -30mV. To determine the electrophoretic mobility, the NAs samples were diluted with 0.1 mM KCl and placed in the electrophoretic cell, where an electric field of 15.24 V/cm was established. Each sample was analyzed in triplicate. The zeta potential values were calculated using the Smolochowski equation. The results we obtained are summarized in

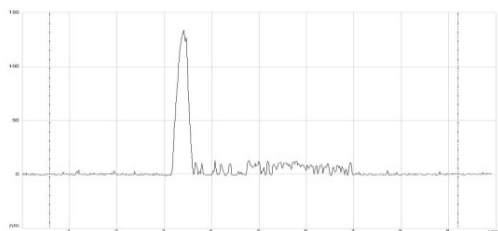
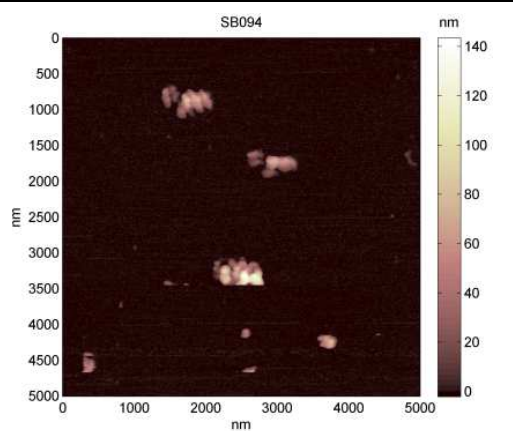
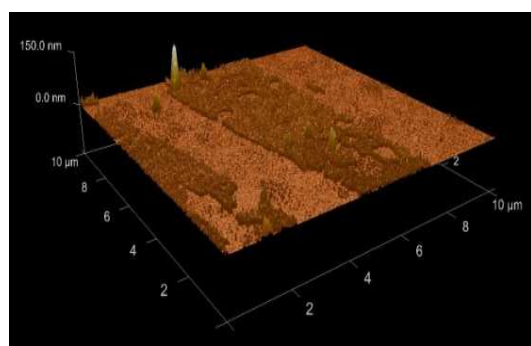
Table 4:

Compound	Mean Diameter (nm)	Polydispersity Index	Z potential (mV)
8a	103.2±0.7	0.052	-37.56
8b	107.0±0.1	0.049	-20.78
9a	184.3±2.4	0.063	-11.42
9b	179.6±1.1	0.048	-28.47
10a	161.6±6.8	0.090	-56.37
10b	124.1±2.5	0.131	-25.39
11a	195.2±6.8	0.083	-41.02
11b	154.8±7.0	0.279	-39.14

Table 4: Mean diameter, polydispersity index and Z potential of nanosuspensions of compounds **8-11**

✚ Atomic Force Microscopy (AFM): to better elucidate the morphology of our suspensions we submitted a sample of **8a** (considered as reference compound for our collection of conjugates) and a sample of PTX-Sq as a comparison to an Atomic Force Microscopy (AFM) analysis. Compound **8a** forms nanoassemblies with a softer and less shaped structure, respect to PTX-Sq. This could mean that **8a** nanosuspension is less stable that PTX-Sq one and, as a consequence, drug release inside the cell could be favoured.

a)



b)

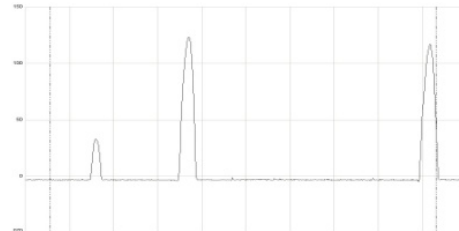
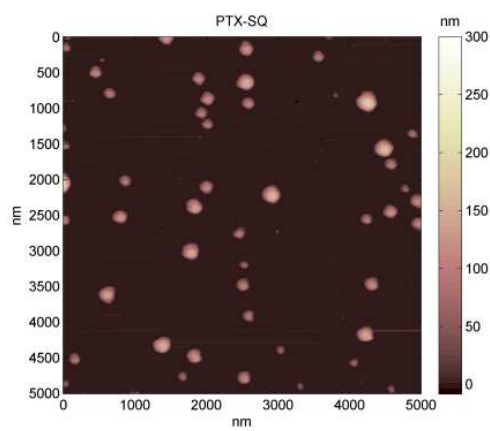
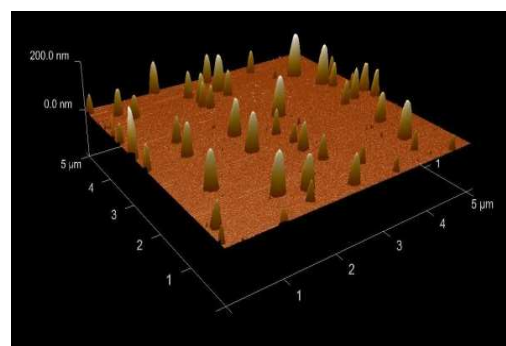


Figure 43: AFM analyses of 8a (a) and PTX-SQ (b)

Stability assessment of drug-squalene conjugates and NAs

Stability of the conjugates

Dithiothreitol (DTT)

To define the stability of disulfide bonds we used the method described by Satyam, with slight modifications^[112]. Each drug-squalene conjugate was dissolved in acetonitrile or ethanol/acetonitrile mixture to obtain a 1 mg/ml solution (0.5 ml) and then 10 μ l of 0.2 M borate buffer (pH 9), 50 μ l of water and 20 μ l of a 16 mM solution of DTT in acetonitrile were added. The vials were capped and kept at room temperature under N₂ atmosphere, with occasional shaking by hand. For comparison the same solutions without DTT were prepared. Samples (20 μ l) were spiked and analyzed by HPLC at various time points. For evaluating the release of drugs from the conjugates we monitored the disappearance of the major peak related to the pure compound (Figure 44).

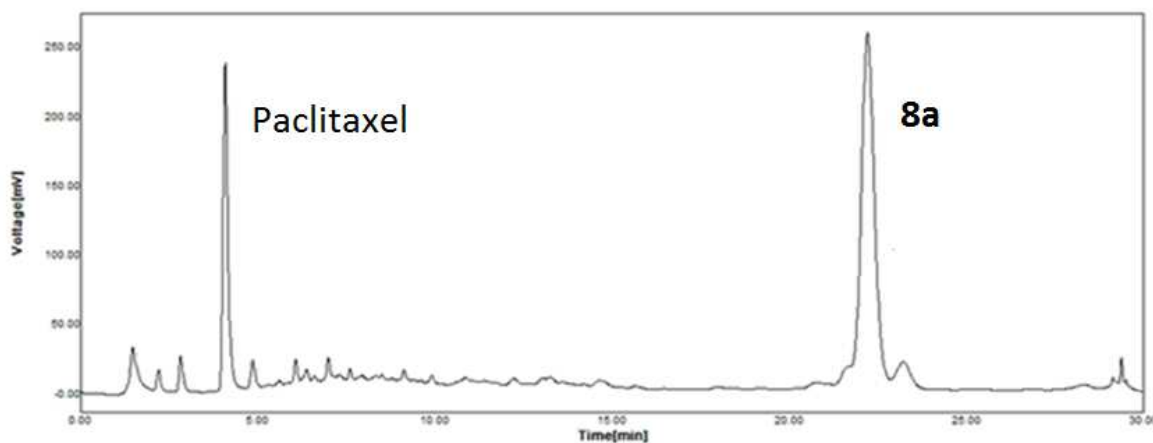


Figure 44: HPLC analysis for compound **8a** after 1h incubation with DTT

Podophillotoxin derivative **9a** was unstable and a rapid degradation due to basic environment appeared.

The same analyses were carried on also for compounds **8-11b**: both the buffer alone and DTT did not influenced the stability of the conjugates.

Glutathione (GSH):

In order to verify the stability of conjugates **8-11a** in the presence of GSH we applied the same procedure we used for other disulfide-containing compounds^{[69][70]}.

Typical procedure: a solution of GSH (0.0058 mmol) in H₂O (0.300 ml) was added to a solution of the drug-squalene conjugate (0.0058 mmol) in MeOH (3 ml) and the reaction mixture was stirred at room temperature for 24 hours. A sample of the reaction mixture was submitted to an ESI-MS spectrometry analysis in order to detect the presence of one or more of the possible products, and possibly the free drug (Figure 45).

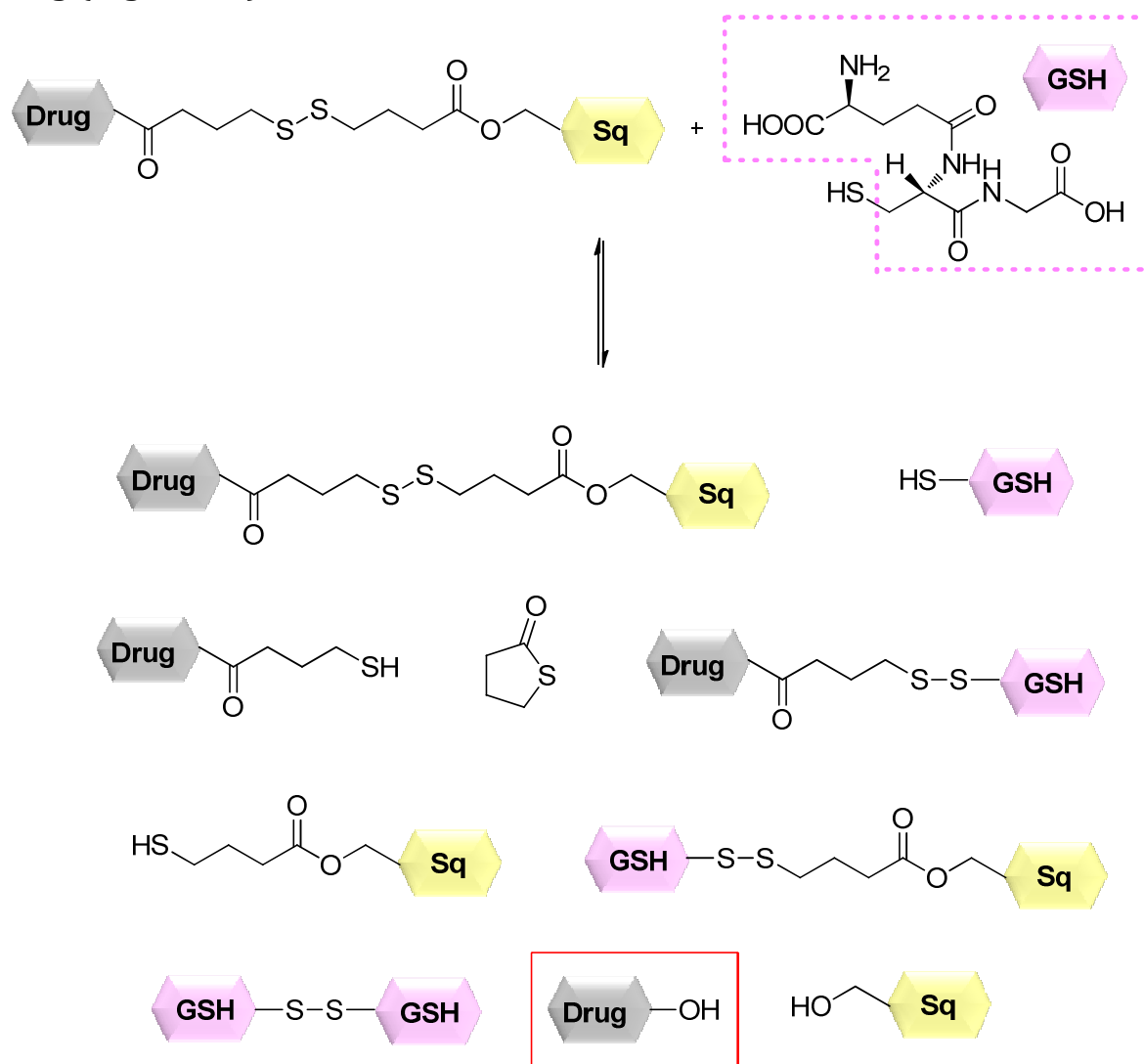


Figure 45: Possible products of the reaction of **8-11a** with GSH

As showed by ESI-MS analyses, compounds **8-11a** were able to release the parent drugs over a 24 hours incubation with GSH.

The same analyses were carried on also for compounds **8-11b** and, as expected, incubation with GSH didn't affect the stability of the conjugates.

Stability of nanosuspensions

Dithiothreitol (DTT):

The same proportions of buffer and DTT (dissolved in water) used to prove the stability of our conjugates were used to analyze also the stability of nanosuspensions. Samples at different times were diluted with acetonitrile (50 μ l) just before HPLC injection.

All the NAs appeared stable when treated with DTT in borate buffer, with a very slow release of drug during the first two days. NAs size measurements during incubation did not present significant differences.

Glutathione (GSH):

Nanosuspensions (1 mg/ml) were incubated with GSH (final concentration : 10 mM) at 37°C, sampling the size of NAs after different times (0, 1, 6, 24, 48, 78 h).

For compounds **8a**, **10a**, **11a** a progressive slight increase of size was evident but only for nanosuspension of compound **9a** the size became dramatically increased and precipitation occurred.

Serum:

Furthermore nanosuspensions of compounds **8-11a** were incubated in serum at 37°C for 48 hours, then samples were analyzed by HPLC. Compound **8a** was the most stable while significant release occurred for **9a** and **11a** derivatives (around 48-42% released).

Self-aggregation behavior of nanoassemblies

The physical stability of the squalene-drug NAs was assessed in water. All the nanosuspensions were found to be remarkably stable at 5°C over a three-month period without any significant size modification.

This unique ability of squalene-derivatives to form NAs in water was further confirmed by the critical aggregation concentration (CAC) measurement.

The critical aggregation concentration test (CAC) was performed by steady state fluorescence spectra using a described procedure^[55]. Briefly, samples of nanosuspensions in water, with concentrations ranging from 0.1 µg/L to 0.5 g/L were incubated with a constant pyrene concentration of 0.6 µM for 12h at room temperature under stirring.

Fluorescence emission spectra were recorded from 360 to 550 nm, using 343 nm excitation wave length. In the emission spectra of unstacked pyrene, the intensity ratio of the first band (I_{373}) to the third band (I_{384}) was analyzed as a function of NAs concentration. CAC values were determined from the intersection of the tangent to the curve at the inflection with the horizontal tangent through the points at low concentration.

It has to be noted that the observed CAC values were higher than compound **16** but still lower than those of polymeric micelles used for drug delivery purposes (5-10 mg/L)^[113].

Compound	CAC (mg/l)	Mean diameter (nm)	Mean diameter after 3 months (nm)
8a	1.5	103.2	106.5
8b	1.1	107.0	110.5
9a	0.7	184.3	215.3
9b	0.5	179.6	210.5
10a	0.6	161.6	191.1
10b	nd	124.1	142.9
11a	nd	195.2	210.2
11b	nd	154.8	172.4
PTX-Sq	0.2	173.5	181.1

Table 5: CAC values and mean diameters of nanosuspensions after three months since their preparation

Biological evaluation

In vitro activity

The cytotoxicity of squalene conjugates (NAs) was evaluated using MCF-7 cell line (human breast cancer) by incubation for 48 h (Table 6). In order to check the release ability by reducing agent the same experiments were carried out after NAs treatment with DTT (10 mM).

Comparison of the dose-response curves obtained for each drug and squalene conjugates NAs revealed that the conjugation to squalene decreased the cytotoxicity toward MCF-7 cell line for each compound (Table 6).

Whereas MCF7 seems very sensitive to single drug (in nano and sub-nanomolar range), the various squalene conjugates exhibited different IC₅₀ values. There is not a direct correlation between cytotoxicity of free drug and conjugates, indeed the paclitaxel derivative **8a** appeared 100 times much toxic than the **9a**, when the podophillotoxin is the most active free drug. In a scale of activity we can place **8a** > **9a** > **10a** > **11a**.

The ability of a more efficient release of toxic moiety appeared evident comparing the disulfide linked and alkyl chain derivatives. These latter were active at very high concentrations ranging from 1 to 100 micromolar. When incubated with DTT, NAs of compounds **8a**, **9a**, **11a** allowed a better release of the active molecule as detected by a 10-fold increase of activity. In particular compound **8a** reached an activity closer to free paclitaxel. As expected, treatment with DTT did not significantly changed the activity of NAs made by compounds without the disulfide bond (**8b**, **9b**, **11b**) or native drugs.

The cytotoxicity of our conjugates was also evaluated on A549 cell line, even if this case our compounds resulted less active (Table 6).

Compound	MCF-7		A549
	IC50 (μM)	IC50 after treatment with DTT (μM)	
Paclitaxel	0.004	0.005	0.05
8a	0.06	0.003	0.34
8b	1.2	1.5	nd
PTX-Sq	9	8.7	-
Podophyllotoxin	0.0001	0.0004	0.06
9a	0.4	0.06	7.6
9b	105	110	6.2
Epothilone A	0.0009	0.0008	>5
10a	1	0.5	>5
10b	40	45	>5
Camptothecin	0.0005	0.0003	0.49
11a	8	0.8	>5
11b	10	20	>5

Table 6: IC50 values (μM) of squalene conjugates and naïve compounds against MCF-7 and A549 cell lines

Microtubule bundle formation (immunofluorescence)

In order to confirm the anti-microtubule effect of squalene bioconjugates, we investigated microtubule structure and distribution in A549 cell line exposed 1h to 200 $\mu\text{g}/\text{ml}$ of the conjugates or to equal concentration of parent compounds. Microscopy analyses revealed that control cells are spread with a well-organized microtubular network, whereas treated cells are shrinking, with no obvious differences following incubation with naïve compounds and squalene conjugates (Figure 46). As expected, paclitaxel and epothilone-A induced microtubule bundling; on the other hand, podophyllotoxin completely disrupts microtubules.

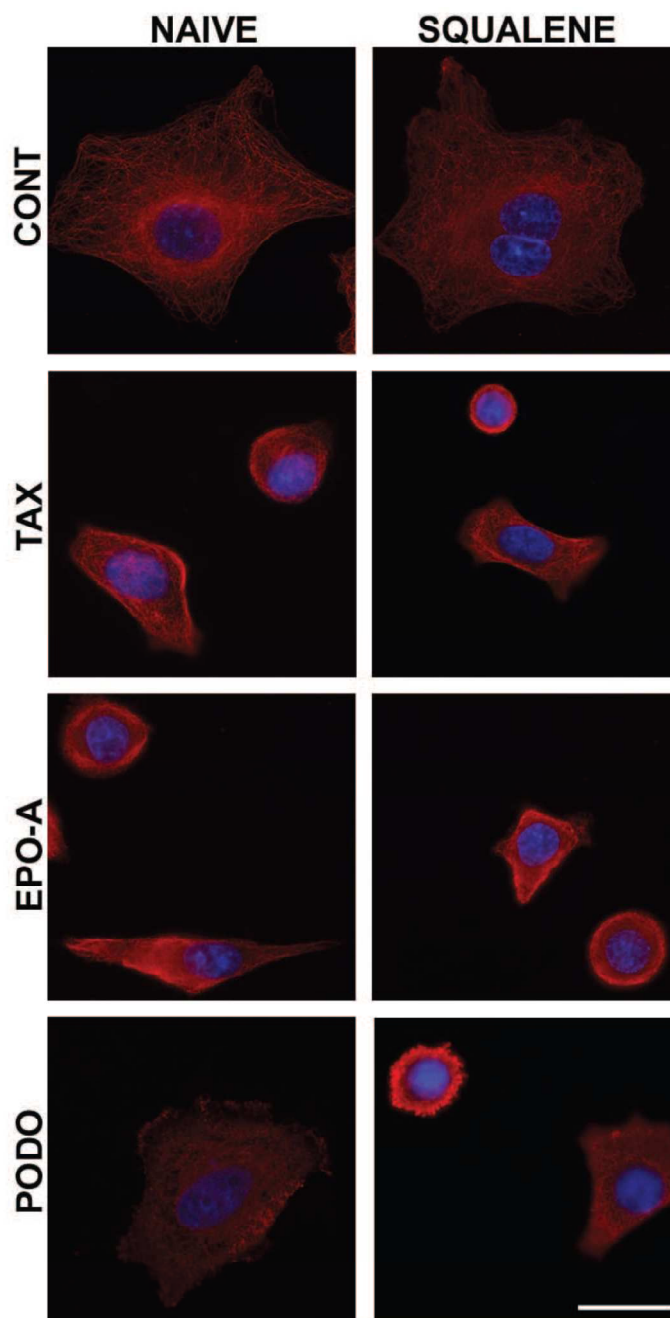


Figure 46: Microtubule network (α -TUB staining, red) and nuclei (DAPI, blue) of A549 cells not loaded (CONT) or incubated 1h with naïve compounds (naïve) or squalene conjugate (squalene) taxol (TAX) epothilone-A (EPO-A) and podophyllotoxin (PODO).
Scale bar = 20 μ m

To verify that the observed effects were due to intracellular action of the squalene conjugates, at least for paclitaxel and its derivatives, we verified if they had retained the ability to cross the cell membrane.

In this purpose, we removed unassembled tubulin, using previously described procedures^[114] with minor modifications. With more detail, to avoid the administration of further taxol, we used a microtubule-

optimized PEM buffer (85 mM PIPES, pH 6.94, 10 mM EGTA, 1 mM MgCl₂, 2 M glycerol, 1 mM phenylmethylsulfonyl fluoride, 0.1 mM leupeptin, 1 μM pepstatin, 2 μg/ml aprotinin). After fixation and permeabilization, cells were double immunostained using a polyclonal anti-taxol antibody (abcam, Cambridge, UK) 1:1000 in PBS for 1 h at 37°C and then a monoclonal anti- α -tubulin antibody. Afterward we used a mix of secondary antibodies, goat anti-mouse Alexa Fluor568 and donkey anti-rabbit Alexa Fluor488 (Life Technologies Italia, Monza, Italy).

As showed in Figure 47, both naïve paclitaxel and its squalene conjugate enter into the A549 cells and stain microtubule bundles.

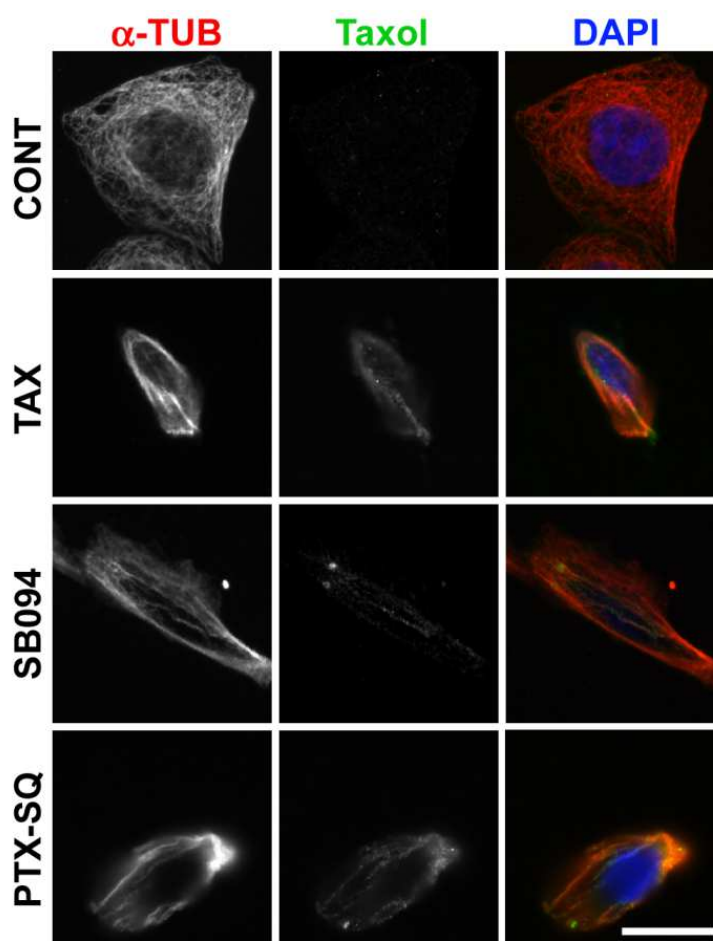


Figure 47: Microtubule network (α -TUB, red), microtubule-binded taxol (TAX, green) and nuclei (DAPI, blue) of A549 cells not loaded (CONT) or incubated 1h with naïve paclitaxel (TAX) or squalene bioconugated taxanes (**8a** and PTX-SQ). Scale bar = 20 μ m

In vivo activity

The obtained results pointed out compound **8a** as the most interesting obtained conjugate compound on the base of its stability, releasable capacity and cytotoxicity. We then planned to evaluate its behaviour *in vivo*.

To this aim MDA-MB-231 tumor-bearing mice were randomized when their tumor masses were about 350 to 400 mg to receive **8a** at the doses of 34 mg/Kg (23.6 mmol/Kg). Treatment was compared with the use of taxol (20 mg/Kg, 23.4 mmol/Kg). The results (Figure 48) show that **8a** is not toxic (body weight is not affected by the treatment) and unfortunately it is not active in fact the tumor growth seems to be affected only after 40 days from the first treatment.

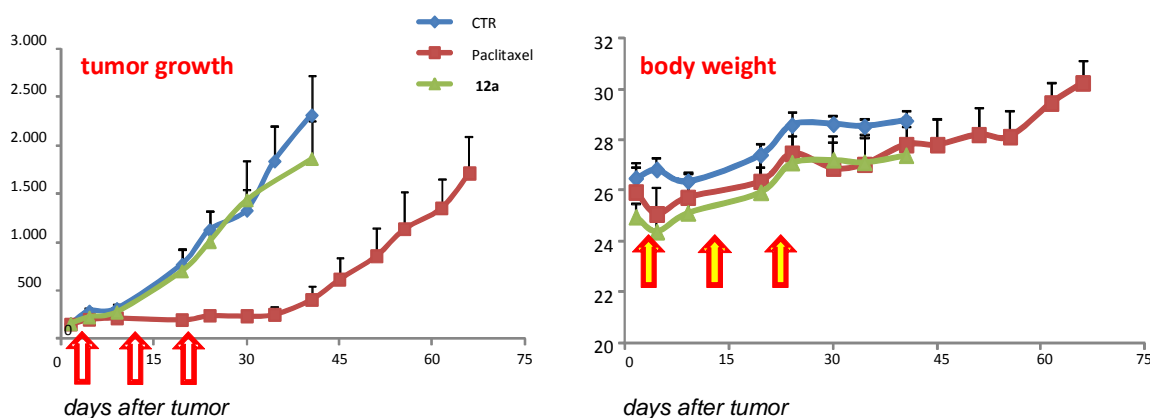


Figure 48: Influence on tumor growth and body weight of the treatment (once each 7 days for 21 days) with **8a** (NAs) and comparison with the treatment with paclitaxel. Doses at 20 mg /Kg (paclitaxel equivalent)

The unpleasant result moved us to investigate the efficacy of paclitaxel release by **8a** after the *in vivo* administration. We evaluated paclitaxel plasma and tumor levels. We selected 3 time points (1, 4 and 24 hours) after an intravenous dose of 20 mg/Kg paclitaxel (23.4 mmol/Kg) and compared with 34 mg/Kg (23.6 mmol/Kg) of **8a**.

Figure 49 shows that after 4 h the level of paclitaxel in plasma is very low. This could be comparable with the situation of treatment with paclitaxel and could suggest a slow release of the drug, but the data regarding the level of paclitaxel in the tumor is whispering that release is not efficient *in vivo*. We investigated the level of paclitaxel in the liver and also in this case we detected a very low amount of drug.

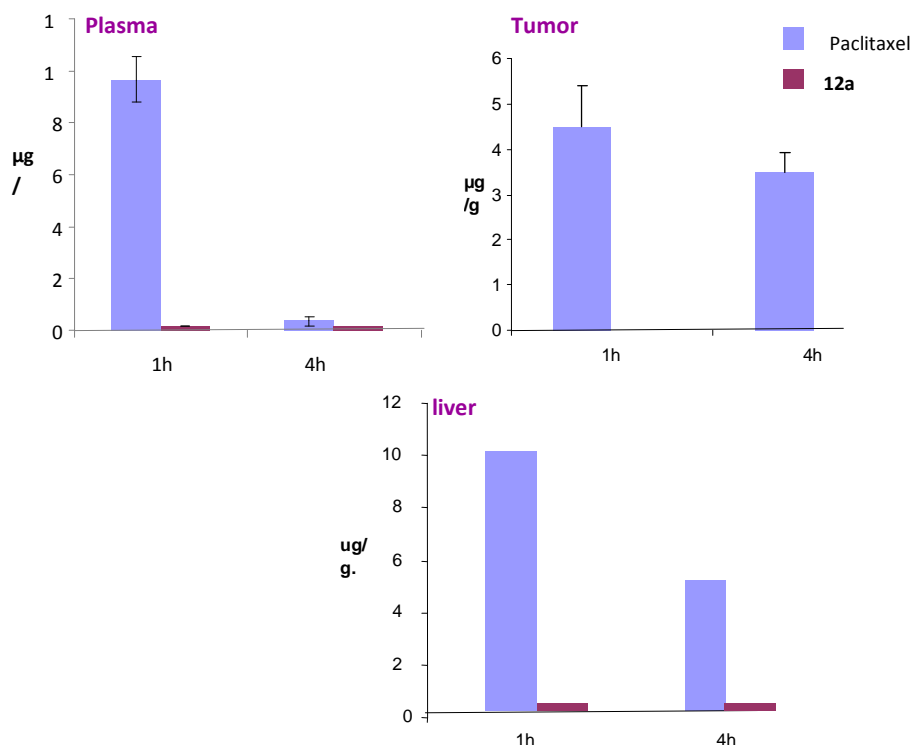


Figure 49: Paclitaxel plasma, tumor and liver levels in MDA-MB-231 tumor-bearing mice after treatment (once each 7 days for 21 days) with **8a** (NAs) and paclitaxel. Doses at 20 mg /Kg (paclitaxel equivalent)

Further studies in order to determine the amount of compound **8a** in other organs are currently under investigation in the laboratories of Dr. Damia (*Istituto Mario Negri, Milano*).

Our targets: Cancer Stem Cells (CSCs) and their inhibitors

Introduction

The different organs in human organism are constituted by tissues with mature and specialized cells and its specific stem cells. Even if stem cells represent only a small fraction of cells that constitute each tissues, they are the only cells able to self-renew. The organ-specific stem cells have specific properties in order to maintain the tissue integrity and they have a fundamental importance due to their ability to undergo self-renewal and differentiation into a variety of mature cells.

Malignant neoplasias are believed to result from sequential mutations that can occur as a consequence of progressive genetic instability and/or environmental factors.

The cancer stem cells (CSCs) hypothesis postulates that normal stem cells may be the origin of cancer, and that a specific subset of cancer cells with stem cells characteristics can give rise to a hierarchy of proliferative and differentiated bulk of tumor cells that result in tumor initiation, progression and recurrence. In fact specific CSC markers have recently been identified showing a similar expression also in normal stem cells of the same organ. Furthermore, when xenografted in immunodeficient mice, CSCs have been shown to possess the ability to give rise to new tumors.

Additional confirmations that stem cells can play a role in carcinogenesis are the homologies between normal adult stem cells and cancer cells. Besides self-renewal capacity, these characteristics include the production of differentiated cells, activation of antiapoptotic pathways, induction of angiogenesis, resistance to apoptosis and drugs and the ability to migrate and propagate. Differently from normal adult stem cells, that remain constant in number, CSCs can increase as the tumor grow and originate a progeny that can be both locally invasive and/or colonize distant sites.

Stem Cells

Despite the variety of cells in adult tissues, all cells derive from a single egg after fertilization of an ovule by a spermatozoid. Egg fertilization results in the creation of totipotent stem cells, precursors of all tissues of embryo. After approximately four days these totipotent stem cells undergo several mitotic divisions to form identical cells and, after this point, they tend to gradually lose their high proliferative potential and begin to specialize, until they become nullipotent (Figure 50).

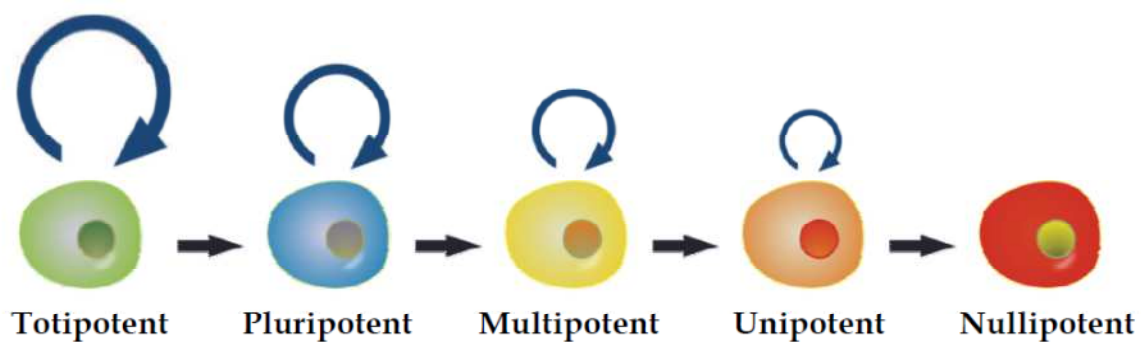


Figure 50: Stem cells plasticity

In most adult tissues there are pools of progenitor cells that are able to multiply and differentiate into specialized tissues of origin and, at the same time, to maintain a reserve of undifferentiated cells. These adult progenitor cells are defined *somatic stem cells*.

Due to its remarkable regeneration capacity, the liver is probably the best example of a tissue with stem cells and differentiated cells.

Stem cells can divide in two different ways (Figure 51):

- ✚ symmetrically: two daughter cells share the same stem cell feature. It occurs when their number (stem cell pool) needs to be expanded, such as during embryonic development and after tissue injury.
- ✚ asymmetrically: one of the progeny remain undifferentiated, replenishing the pool of stem cells, while the other daughter cell can proliferate and differentiate into specialized cells to generate new tissue mass.

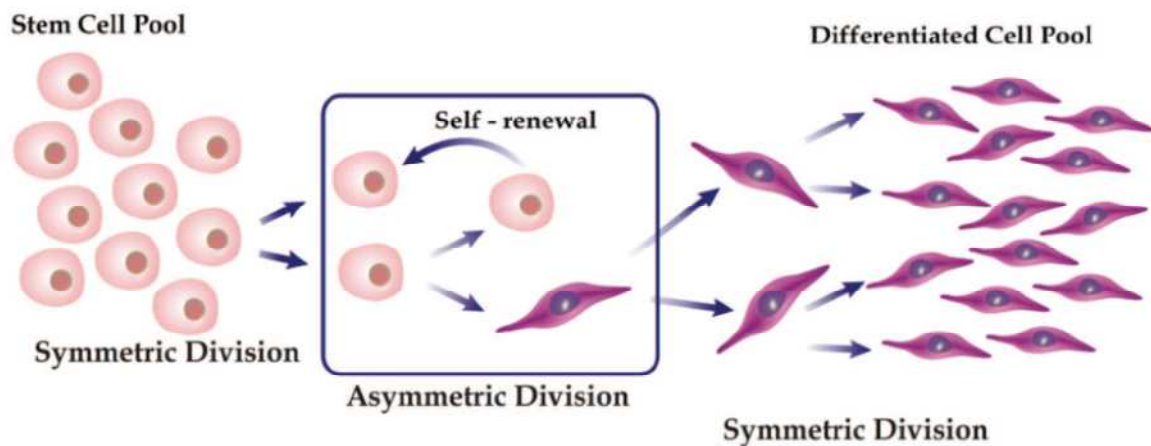


Figure 51: Stem cells symmetrical and asymmetrical division

In summary, stem cells differ from other cells in the body because they have four major properties:

- ✚ they are undifferentiated and unspecialized;
- ✚ they are able to multiply for long periods while remaining undifferentiated;
- ✚ they are capable of differentiating into specialized cells of a particular tissue;
- ✚ they can be serially transplanted.

The combination of these properties is called "stemness".

Stem cells and cancer

Normal adult multipotent stem cells are usually able to self-renew, producing at least one progeny cell with a similar developmental capacity and many evidences indicate that this cell population, through initial genetic or epigenetic alterations, can become responsible for the development of several tumors through a progressive establishment of a CSC population.

The CSCs model suggests that tumor progression, metastasis and recurrence after therapy can be driven by a rare subset of tumor cells that have the capacity to self-renew, while the bulk of the tumor doesn't have this capacity.

For these reasons the deregulation of the self-renewal process may be a key event in carcinogenesis, and while self-renewal can drive tumorigenesis, the differentiation process may contribute to tumor phenotypic heterogeneity.

CSCs as targets for cancer treatment

It is well known that several cancers are peculiarly resistant to conventional radio- and chemotherapy that typically kill the majority of cancer cells. This clinical response may reflect the targeting of the bulk of non-stem cell population.

On the other hand, there are several specific key intracellular signaling pathways implicated in CSCs self-renewal and proliferation processes that appear to be promising therapeutic targets.

An ideal therapeutic strategy might be to sensitize CSCs to chemo- and radiotherapy by inhibiting their stem properties and then by promoting a direct cytotoxicity. Since the CSCs population is driven by embryonic signaling pathways, the targeting of these pathways could result in a better outcome of the therapy: in this direction, many drugs for the inhibition of embryonic signaling pathways are currently under development.

Hedgehog Signaling Pathway: a new biological target for the design of new anticancer compounds

Some of the most characterized signaling pathways controlling self-renewal and differentiation in adult stem cells, such as Wnt/b-catenin, Hedgehog, Notch and TGF- β /BMP pathways are frequently modulated in cancer by epigenetic mechanisms.

Hedgehog (Hh) is a key signaling pathway for the regulation of embryonic development and tissue repair, mainly through the control of stem and progenitor cells (e.g. neural stem cells) and for the control of a number of genes involved in cell fate determination and stemness features. When hyperactivated by genetic and/or epigenetic alterations, Hh pathway promotes tumorigenesis in several tissues by subverting the regulation of stemness-determining genes overexpressed in that type of cancer.

Normal Hh signaling

Binding of Hh to its receptor Patched (Ptch-1) activates the transmembrane protein Smoothed (Smo), which subsequently activates the Gli family of transcription factors, leading to activation of target genes (Figure 52):

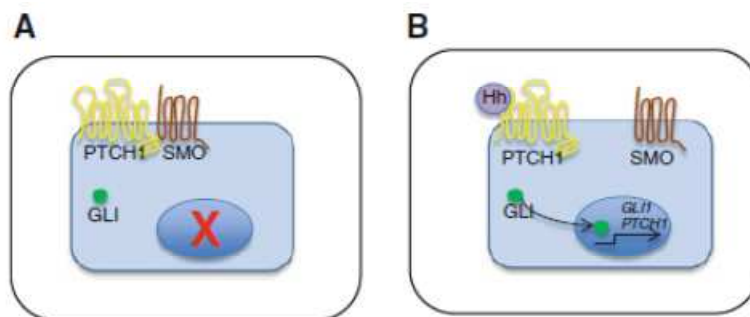


Figure 52: Normal Hedgehog signaling pathway

Hedgehog signaling in cancer

Aberrant Hh signaling occurs in some cases because of a ligand-independent activation of SMO due to a mutation in PTCH1 or in SMO (Figure 53a), but it generally happens through ligand-dependent mechanisms (Figure 53b,c). Increased Hh ligand expression leads to increased Hh signaling in the activated target cell. This can theoretically occur through either an autocrine mechanism (Figure 53b) where the malignant cells both secrete and respond to Hh ligand, or through a paracrine mechanism (Figure 53c) where the secreting cell and recipient target cell are different. Even if the autocrine mechanism has been reported for multiple tumor types, the currently overall favored mechanism is the paracrine model, based partly on evidence that tumor cells do not appear to respond to Hh ligand themselves^[115].

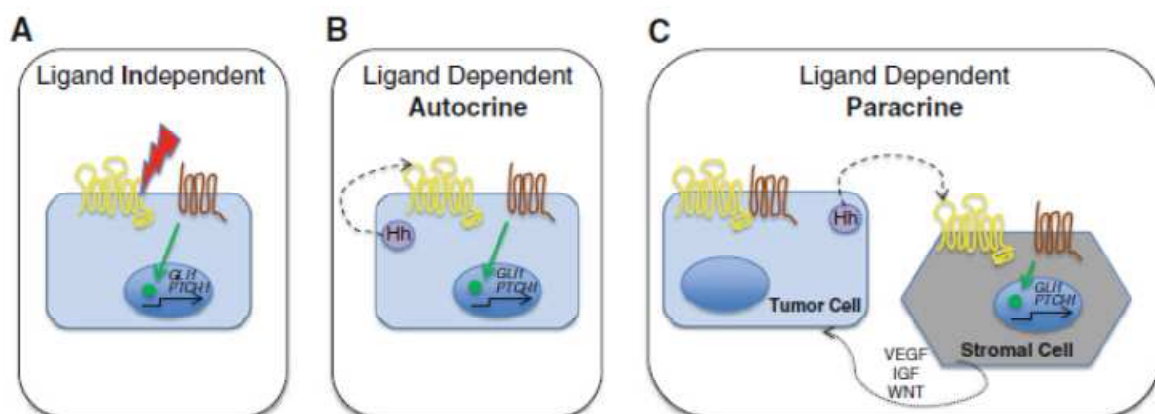


Figure 53: Hedgehog signaling in cancer

One proposed explanation has been that tumor cells lack the primary cilium necessary for canonical Hh signaling through PTCH1 and SMO.

Hedgehog inhibitors

On the base of the acquired knowledge concerning the signaling steps of the Hh signaling pathway, it is possible to identify different potential ways to inhibit this pathway in cancer. To date, the best-characterized approach is to target the SMO receptor with small molecule inhibitors, and many of such inhibitors are under clinical trial investigation.

Alternatively, preventing SMO from converting from the inactive to the active form should also achieve the same result.

The limitation with these two approaches is that they will fail if activation occurs by alteration of the signaling pathway downstream of SMO.

Drugs that can interfere with the Hh signaling pathway downstream of SMO are therefore also of potential therapeutic benefit.

Cyclopamine

The *Veratrum* alkaloid known as cyclopamine was the first agent that was found capable of disrupting the Hh signaling pathway^[116].

Cyclopamine belongs to the family of jervine alkaloids, which constitute the majority of *Veratrum* secondary metabolites. The association of *Veratrum Californicum* to sheep congenital deformities during the 1950s raised the possibility that jervine alkaloids could be potent teratogens. Later studies confirmed that jervine and cyclopamine given during gestation can directly induce cephalic defects in lambs, including cyclopia.



Figure 54: *Veratrum Californicum*

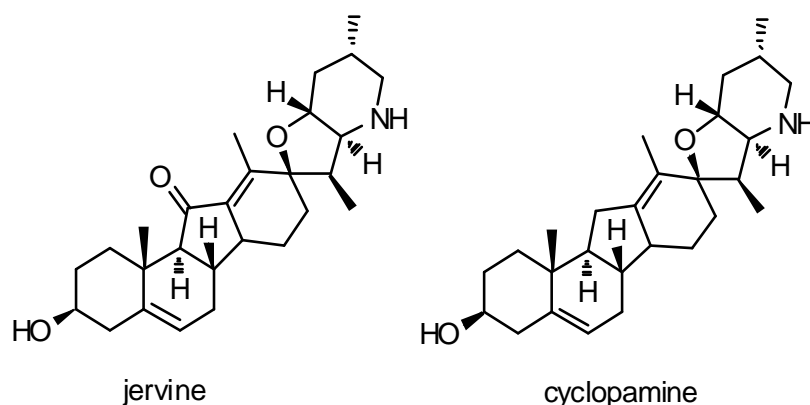


Figure 55: Structure of jervine and cyclopamine

Cyclopamine^[117] was shown to be a potent antagonist of the Hh pathway, directly acting on the protein Smo, and has been shown to have antitumor activity in several xenograft models.

Despite the attractive pharmacological profile of cyclopamine, its use as a systemic treatment may be limited by its poor aqueous solubility (~5µg/ml) and stability in acid. In fact, cyclopamine readily converts to

veratramine as a result of an acid-catalyzed opening of the spiro-tetrahydrofuran E ring followed by rapid aromatization of the D ring (Figure 56). Veratramine, while not acting as Hh antagonist, has been shown to interact with several other receptors and cause hemolysis.

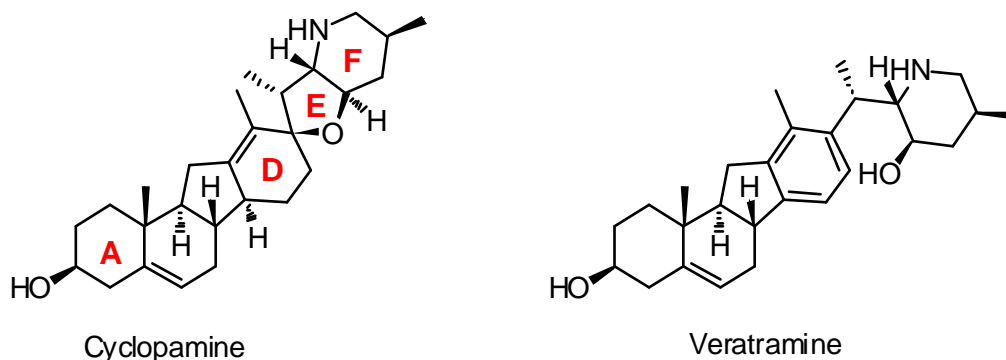


Figure 56: Structure of cyclopamine and veratramine

In order to obtain more stable and soluble hedgehog inhibitors, many efforts have been made for the preparation of cyclopamine analogues^{[118][119]}.

✚ *Glycosidic derivatives:* it is well known that sugars attached to small molecule-based drugs can dramatically influence pharmacodynamics and pharmacokinetics^{[120][121]}. Recent studies revealed a set of nonmetabolic sugars able to improve the anticancer activity of a range of scaffolds^{[122][123][124]}. This set includes both D- and L- enantiomers of aldopentoses, D-glucurono-6,3-lactone and D-threose.

Goff and Thorson reported the preparation of cyclopamine neoglycosides containing both metabolic and nonmetabolic sugars^[125] (Figure 57).

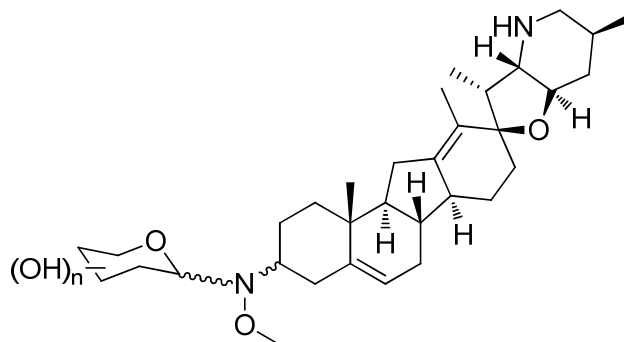


Figure 57: General structure of neoglycosidic derivatives of cyclopamine

Both the kinds of sugars were able to increase the solubility of cyclopamine, but those containing non metabolic sugars induced a higher inhibition of cancer cell growth than the other ones.

✚ *Peptide-containing prodrugs*: cyclopamine selectively inhibits the Hedgehog pathway. This pathway is highly activated in the cancer stem cell population, but it is also active in somatic stem cells, and this results in toxicity of cyclopamine towards non-cancerous stem cells. In order to reduce this toxicity, one strategy could be to obtain a targeted delivery of cyclopamine to its site of action.

In 2008^[126] Khan and coworkers described a "prodrug" of cyclopamine in which the active agent was coupled to a peptide carrier that is a substrate for a prostate tissue-specific serine protease: prostate-specific antigen (PSA). PSA is expressed in a high level only in prostate cells, while in the blood circulation is present only in an inactive form.

This kind of inactive prodrug should be non-toxic in the circulation and in PSA-negative tissues, but should become active when processed proteolytically by PSA. In this context, the authors prepared two "prodrugs" containing two different peptidic sequences (Figure 58). These derivatives were able to release cyclopamine when incubated in presence of PSA and possessed biological activity compared to the one of cyclopamine.

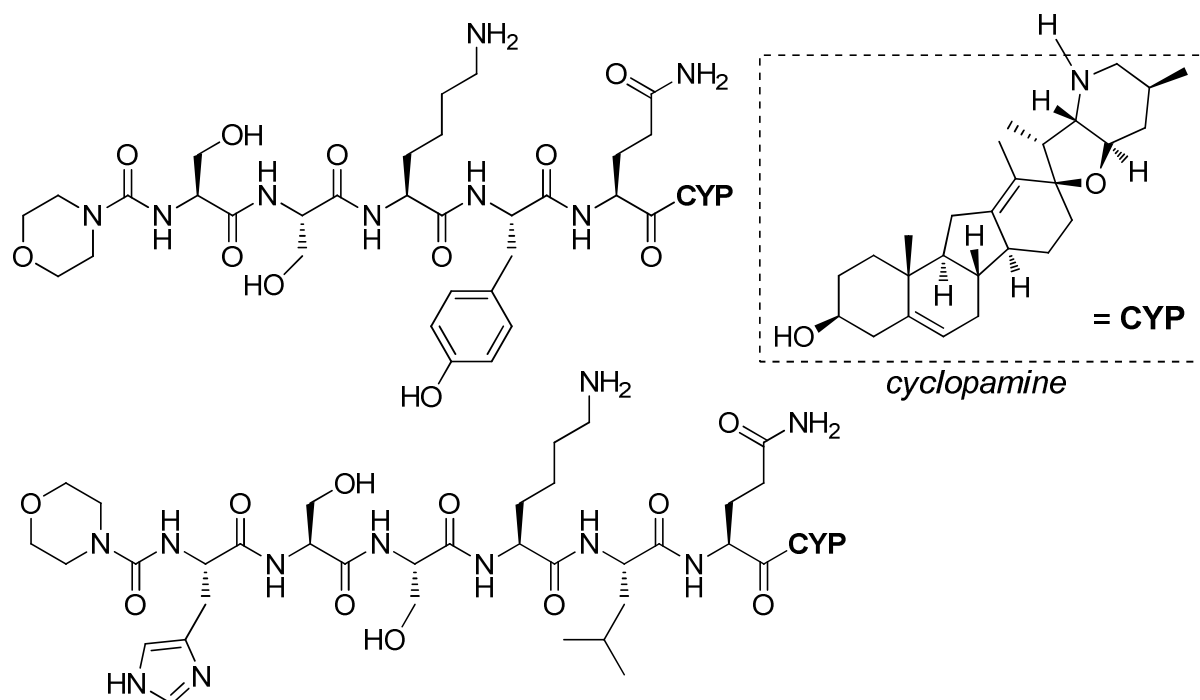


Figure 58: Peptidic derivatives of cyclopamine

+ *Multiple-drug micelles:* Kwon and coworkers recently^[127] described the preparation of poly(ethylene glycol)-*block*-poly(ϵ -caprolactone) (PEG-*b*-PCL) micelles loaded with cyclopamine (CYP), Paclitaxel (PTX) and Gossypol (GSP) (Figure 59). Gossypol is a polyphenolic compound able to inhibit anti-apoptotic proteins, such as Bcl-2, Bcl-x_L and Mcl-1. The interesting aspect of this delivery system is that all three anticancer drugs are poorly water-soluble and PEG-*b*-PCL micelles can deliver all three together.

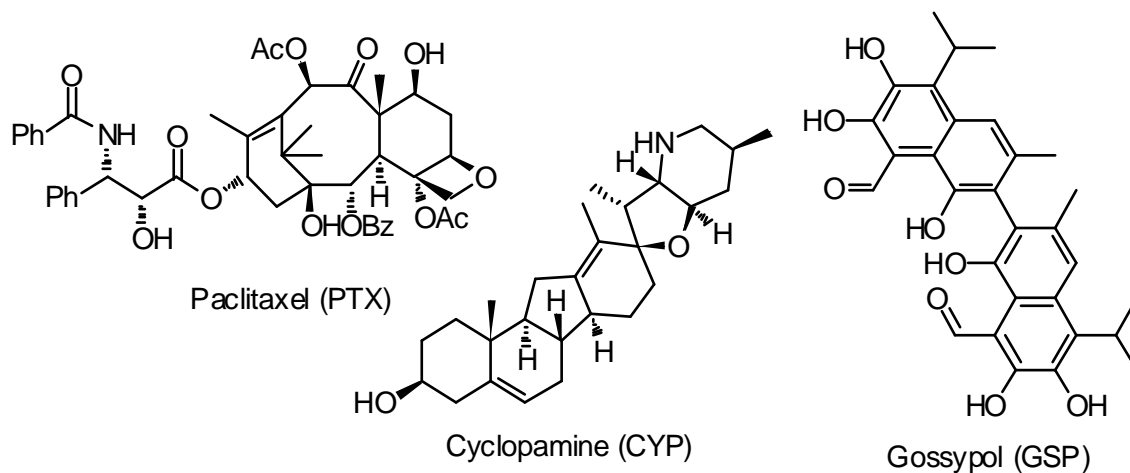


Figure 59: Structure of paclitaxel, cyclopamine and gossypol

PEG-b-PCL micelles containing only PTX (30mg/Kg) were effective in delaying tumor progression during drug treatment, but after termination of the treatment the tumor started to regrow.

On the other hand, 3-drug PEG-b-PCL micelles with PTX, CYP and GSP at 30, 30, 30 mg/kg also prevented tumor progression but, after the second treatment, were able to stop the regrowth for about two weeks. Even if this kind of delivery system gives some benefits, most of all concerning the toxicity of the vehicle, micelles shown to be quite unstable: in fact, part of the three drugs precipitated over a 24 h period. For this reason, the obtainment of stable micelles (or, in general, of assemblies) is one of the most important features to gain for this kind of treatment to be effective.

Squalene-based derivatives

In order to overcome the problems connected to the instability and low water solubility of cyclopamine, we envisioned the possibility to prepare two squalene-cyclopamine conjugates, following the same strategy previously described for paclitaxel, podophyllotoxin, epothilone A and camptotecin (Figure 60):

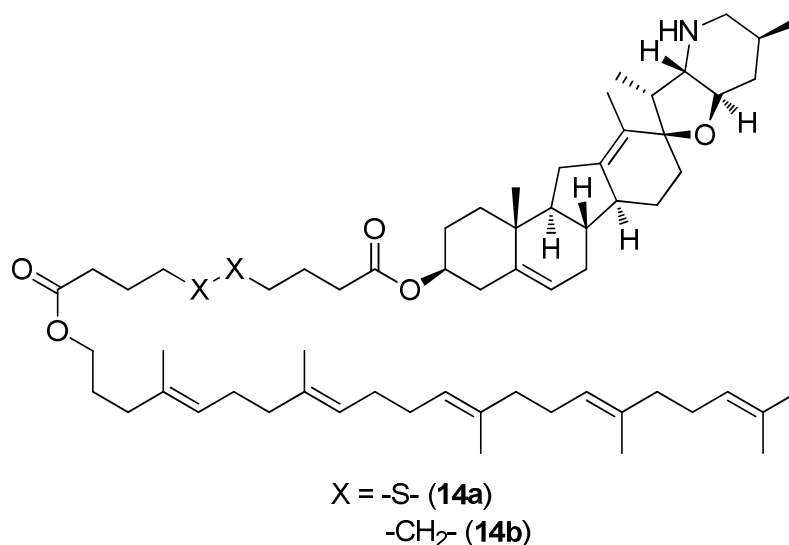
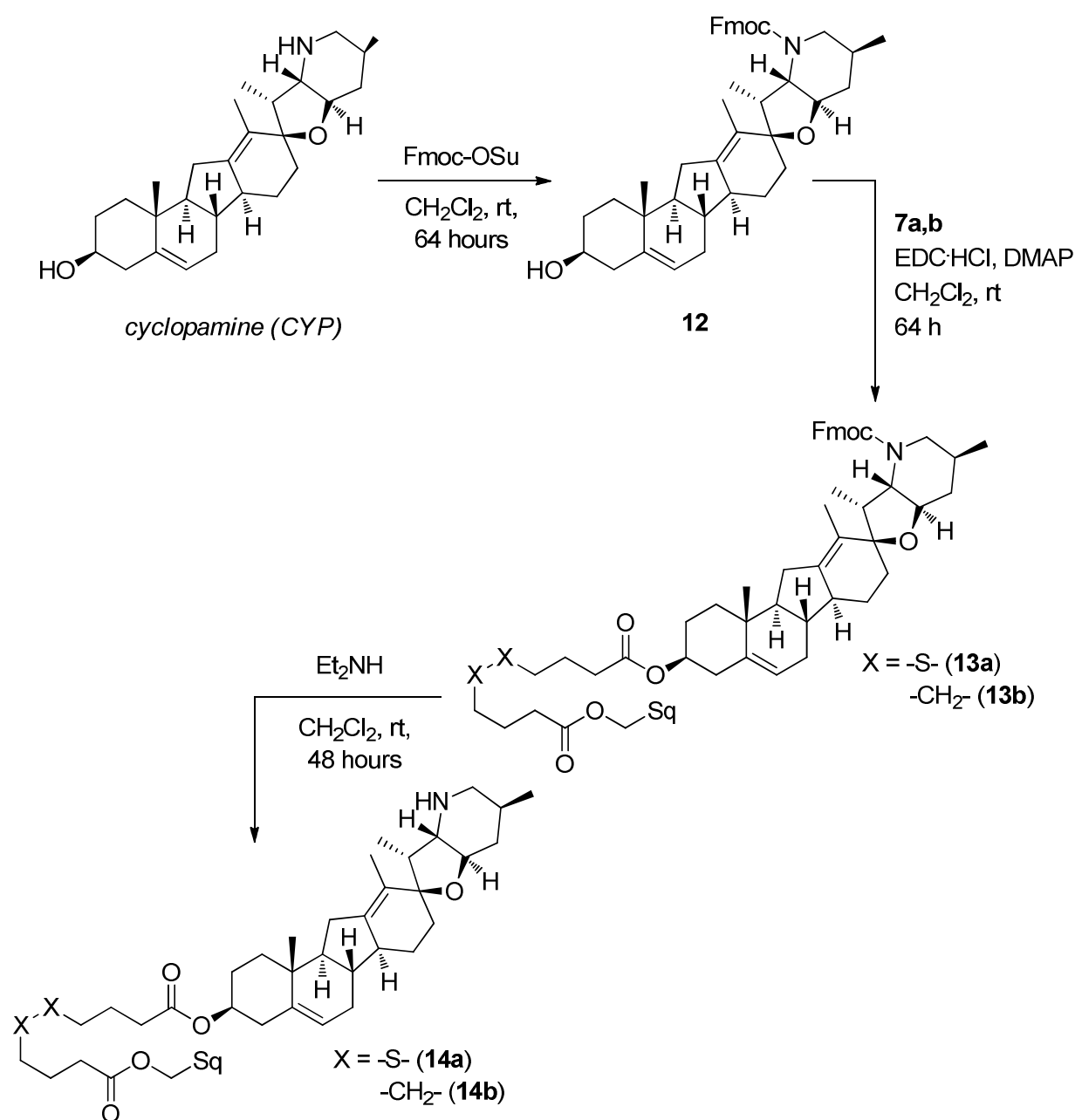


Figure 60: Structure of squalene-cyclopamine conjugates **14a-b**

This kind of conjugates should be able to self-assemble in water, thanks to the squalene tail, and, due to the EPR effect, to reach in a more selective way tumor tissues.

As already described, once the nanoaggregates reach the tumor site, they could be internalized and then, in the presence of glutathione, the disulfide containing compound **14a** should release cyclopamine.

The derivatives were prepared following the pathway described in Scheme 7:



Scheme 7: Synthesis of cyclopamine-squalene conjugates

In order to allow the hydroxy group to react as a nucleophile, we protected piperidine nitrogen with a Fmoc group, following a procedure described by Tremblay and coworkers^[117]. N-Fmoc-protected cyclopamine was then coupled to **7a-b**, prepared as already described using EDC·HCl/DMAP as activating system. In the end, the protecting group was removed by treatment with Et₂NH in CH₂Cl₂. The final compounds were characterized by ¹H- and ¹³C-NMR and ESI-MS spectra.

Formulation as nanoparticles

Preparation: in order to allow the formation of nanoassemblies, the solvent displacement method was applied.

In a typical procedure, 4 mg of the conjugate were dissolved in 1 ml of EtOH, the solution was added dropwise to 2 ml of MilliQ water and then the organic solvent was removed under reduced pressure, with subsequent formation of a nanoaggregate suspension at a final concentration of 2 mg/ml.

Both the two compounds were able to self-assemble and the two suspensions were characterized to determine the mean diameter, the polydispersity index and the Z-potential.

Characterization:

✚ Dimensional analysis: mean diameter and dimensional homogeneity (polydispersity index) of nanoassemblies were determined with quasi-elastic light scattering (QELS) experiments, at a fixed angle of 90°, using a 90 Plus Particle Size Analyzer (Brookhaven Instrument, Co.)

The results we obtained are summarized in Table 7:

Compound	Mean Diameter (nm)	Polydispersity Index
14a	105.6	0.063
14b	109.3	0.249

Table 7: Mean diameter and polydispersity index for compounds **14a, b**

✚ Z-potential measurement: Unfortunately, we weren't able to obtain a precise measure of Z-potential values, in fact repeating the measurements we obtained values very different one from the other. This can be due to malfunctioning of the instrument or to intrinsic properties of the suspensions. In any case, the measurements are currently being repeating in our laboratories.

Release of cyclopamine

In order to verify the stability of conjugates **14a**, **b** in the presence of GSH we applied the same procedure we used for other disulfide-containing compounds^{[69][70]}.

A solution of GSH (0.0058 mmol) in H₂O (0.300 ml) was added to a solution of the **14a** (0.0058 mmol) in MeOH (3 ml) and the reaction mixture was stirred at room temperature for 24 hours. A sample of the reaction mixture was submitted to an ESI-MS spectrometry analysis in order to detect the presence of one or more of the possible products, and possibly free cyclopamine (Figure 45).

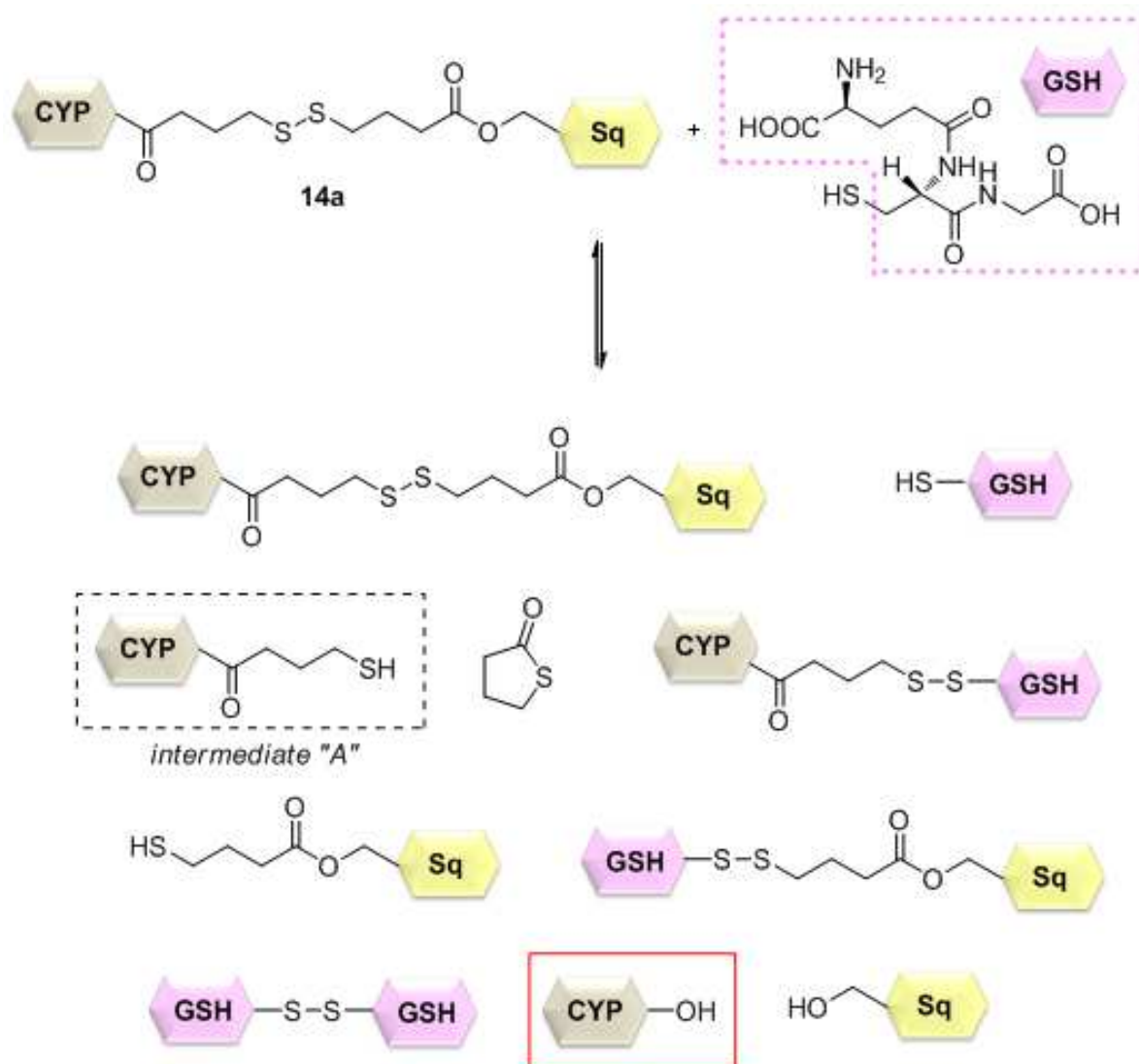


Figure 61: Possible products of the reaction of **14a** with GSH

As a comparison, we effected the same reaction also with compound **14b**.

As showed by ESI-MS analyses, in both the cases the peak of free cyclopamine (m/z: 412) was detected, while only for compound **14a** we found also the peak of intermediate "A" (m/z: 513).

This means that GSH could be involved in the release of cyclopamine from **14a**, thus exploiting the presence of the disulfide bond; on the other hand, the presence in both the cases of cyclopamine could be due to a low stability of our conjugates in solution or to a fragmentation of the molecular ion.

In order to better elucidate the stability and releasing issues of our conjugates, all these aspects are currently under investigation in our laboratories.

Biological evaluation

A preliminary biological evaluation of the in vitro cytotoxicity of compounds **14a** and **14b** is currently under investigation in the laboratories of Prof. P. Sotiropoulou (*Université Libre de Bruxelles*).

Summary

The results obtained with compounds **8-11a** and **14a** enlightened as an efficient release of parent drugs from conjugates can greatly improve the biological activity. In fact compound **8a** possesses a cytotoxicity almost comparable to that of free paclitaxel.

Using different kind of cleavable linkers it is possible to prepare a variety of conjugates, able to release drugs in different specific conditions, thus exploiting some intrinsic peculiarity of tumors.

Thus, we decided to take into consideration also different linkers and mechanisms for a tumor-targeted drug release.

Section 3: Plasmin-activated tripeptidyl squalene derivatives

Introduction

A persistent problem in cancer chemotherapy is the low therapeutic index of most anticancer drugs. An approach to overcome this problem is to design anticancer "prodrugs" which are inactive until locally activated by some tumor-associated enzyme^[75].

Tumors that contain a high level of some specific enzyme could convert the prodrug into the pharmacologically active drug in the vicinity of the tumor^{[128][129]}. In this purpose proteases, a number of which, such as plasmin, are known to participate and collaborate in tumor invasion and metastasis, are one of the most useful family of enzymes.

Proteases

Proteases are enzymes that perform proteolysis, thus effecting protein catabolism by hydrolysis of peptidic bonds. Proteases are currently classified into six groups:

- ✚ Serine proteases;
- ✚ Threonine proteases;
- ✚ Cysteine proteases;
- ✚ Aspartate proteases;
- ✚ Glutamic acid proteases;
- ✚ Metalloproteases.

Serine proteases

In particular, serine proteases use a serine residue as a nucleophile to attack the carbonyl group of a peptidic bond, that thus is cleaved.

On the base of their structure they can be further divided in two groups:

- ✚ Chymotrypsin-like serine proteases, then subdivided in chymotrypsin-, trypsin- and elastase-like;
- ✚ Subtilisin-like serine proteases.

The family of trypsin-like serine proteases contains more than 70 members, involved in many physiological and pathological processes. Although all of them cleave their substrates after the basic amino acids arginine or lysine, there are big differences in their substrates specificities: in fact, some of them are highly specific towards very few natural substrates, while others can hydrolyze a variety of substrates.

Functions of proteases

Proteases are thought to play a primary role in the dissolution of the extracellular matrix that is necessary for the passage of migrating cells through tissue barriers in a diversity of biological processes. The migration and invasion of cells in physiological situations, such as embryo morphogenesis, angiogenesis, wound healing and other processes involving tissue destruction and remodelling, is of limited extent and duration and therefore must be subject to strict regulation to initiate, localize, and terminate the proteolytic activity. The same proteolytic enzyme systems are also thought to contribute to the invasive properties and metastatic potential of malignant tumor cells. Among the proteases involved in these processes, plasmin and its generation by plasminogen activators plays a key role.

Plasmin

The plasmin system is recognized to play a key role in tumor invasion and metastasis by its matrix degrading activity and its involvement in tumor growth factor activation and angiogenesis [130]. In fact, active plasmin catalyzed the breakdown of extracellular matrix proteins and, thus, contributes to migration, invasion and metastasis of tumor cells [131].

In the body plasmin is predominantly present in its inactive pro-enzyme form plasminogen. Active plasmin is formed locally at or near the surface of tumor cells by urokinase-type plasminogen activators (u-PA), produced by cancer and/or stroma cells [132].

Plasmin activity is kept localized because cell-bound urokinase can activate cell-bound plasminogen into active plasmin, which stays cell-bound. Active urokinase and active plasmin do not occur in the blood circulation because they are rapidly inhibited by PAI-1 and α_2 -antiplasmin respectively.

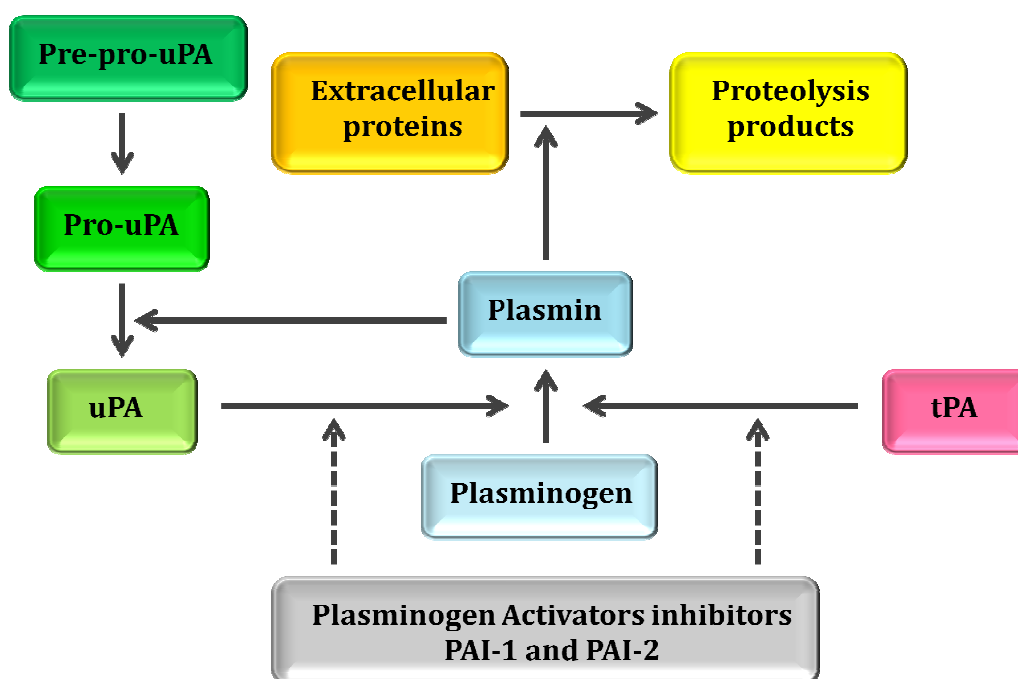


Figure 62: Schematic illustration of the formation of plasmin from plasminogen and proteolysis of plasmin substrates

Many tumor cell lines have significantly higher u-PA level than that of their normal counterparts^[133] and u-PA was shown to be correlated with invasive behavior and to be strong prognostic factors for reduced survival and increased relapse in many types of tumors^[134].

Thus, plasmin is a very promising enzyme for exploitation in a tumor-specific prodrug approach because the proteolytically active form is localized at the tumor level. Moreover, it is possible to design highly specific substrates for plasmin incorporating a short peptide sequence that can be selectively cleaved by plasmin.

Plasmin-activated prodrugs

The first prodrugs designed for specific activation by plasmin were reported by Katzenellenbogen and his coworkers in the beginning of '80s^{[135][136][137]}. In the beginning they prepared two classes of "prodrugs", coupling two anticancer agents to a tripeptidic sequence, with the aim of obtaining inactive peptidyl derivatives selectively activated by plasmin in the proximity of tumor cells. In this purpose, they chose as anticancer agents acivicin and phenylenediamine mustard:

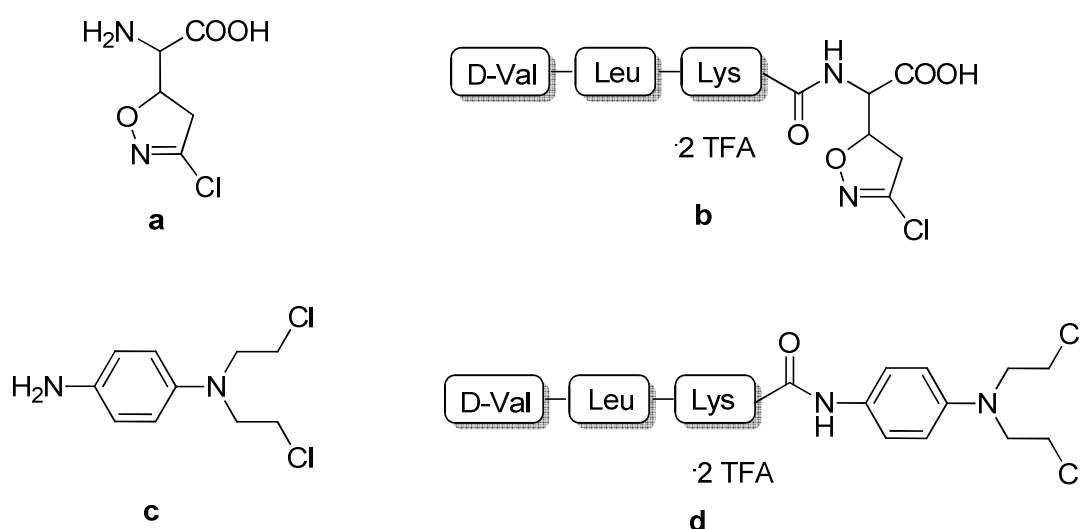


Figure 63: Acivicin (**a**) and its peptidyl derivative (**b**); phenylenediamine mustard (**c**) and its peptidyl derivative (**d**)

Interestingly, these compounds showed a 5- to 7-fold increase in selectivity compared to the free drugs and the addition to the cell medium of a plasmin inhibitor (*p*-nitrophenyl *p'*-guanidinobenzoate) dramatically reduced the activity (dose for 50% effect increased 9-fold)^{[135][136]}. On the base of the evidences obtained for compounds **b** and **d**, the authors decided to prepare the same peptidyl derivative of doxorubicin^[137].

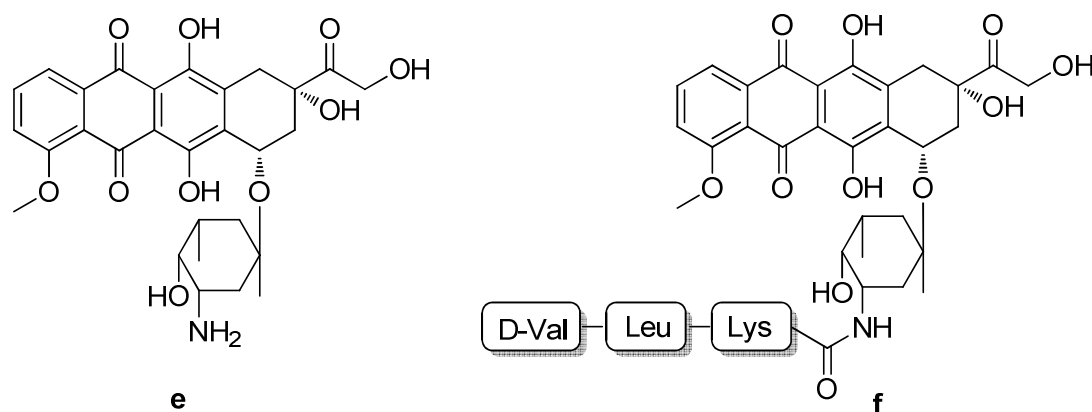


Figure 64: Doxorubicin (e) and its peptidyl derivative (f)

Despite an increase in the *in vitro* selectivity compared to the free drug and a decrease in the *in vivo* toxicity, this compound showed a poor potency, thus limiting its utility. The authors hypothesized that this could be due to a steric hindrance limiting the cleavage by plasmin, and that this could be overcome by inserting a spacer between the peptide and the drug moiety^{[138][139]}.

For this reason they prepare a small collection of conjugates, using different spacers and drugs (Figure 65).

Noteworthy, the incorporation of self-immolative 1,6-elimination spacers in plasmin activated prodrugs resulted in an increased enzymatic activation rates (up to 10-fold higher) due to a facilitated proteolytic cleavage.

In particular these prodrugs, while showing a decrease in the cytotoxicity in different normal cell lines, gave promising results when tested in cell cultures transfected with wildtype u-PA. In fact, they showed the same cytotoxic effect than the free drug, indicating a complete conversion of the prodrug by plasmin. Furthermore, the addition of the plasmin inhibitor trasylol, which had no effect on free drugs treated cells, drastically increased the ID_{50} values in the u-PA transfected cells^{[140][141][142]}.

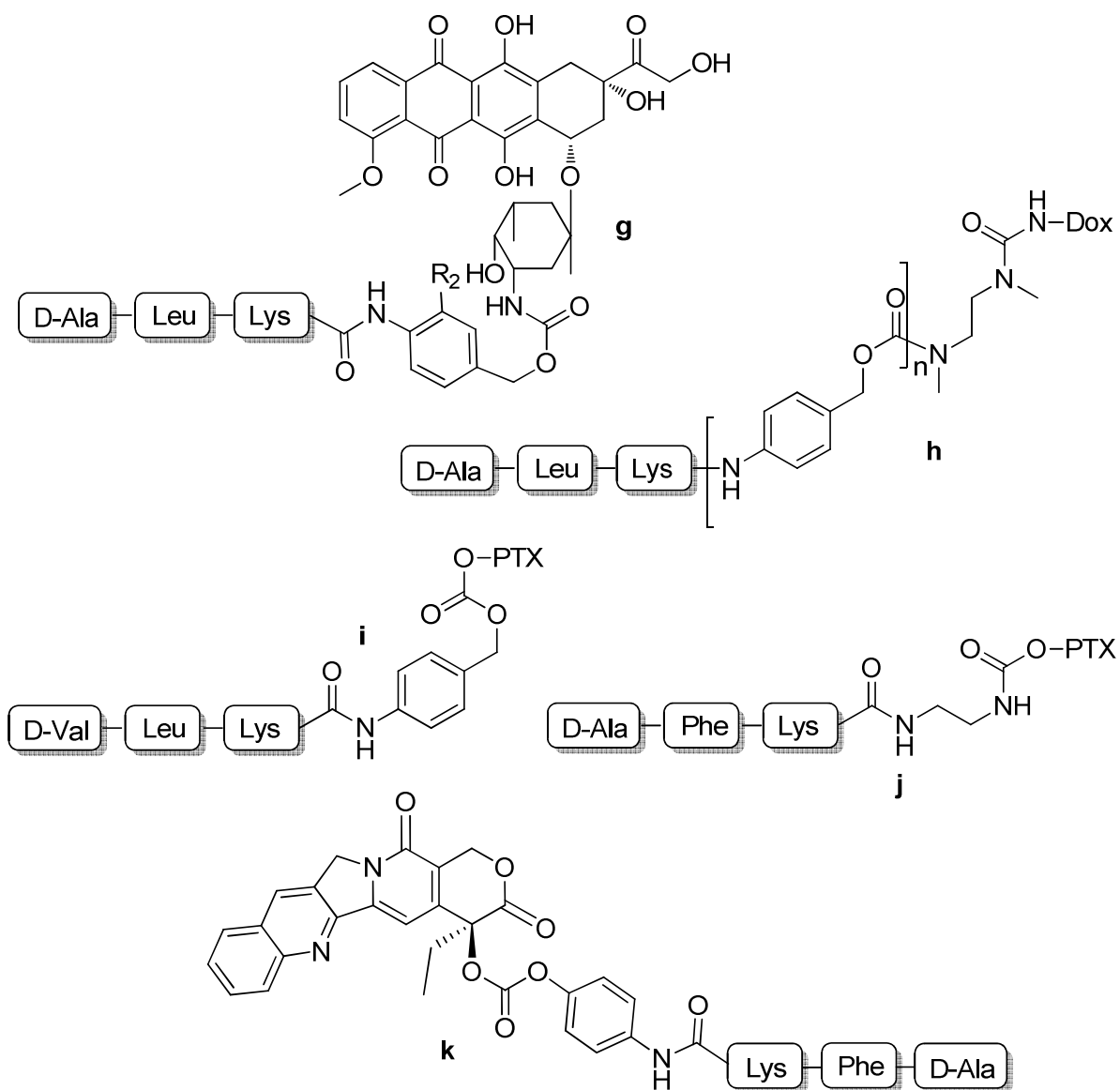


Figure 65: Doxorubicin (**g**, **h**), paclitaxel (**i**, **j**) and camptothecin (**k**) peptidyl derivatives containing a spacer

Aim of the work

On the base of the results obtained for disulfide-containing squalene derivatives and taking into account the interesting applications of plasmin in the activation of prodrugs by cleavage of a tripeptidic sequence, we envisioned the possibility of preparing a "2nd generation" collection of drug-releasing squalene conjugates (Figure 66):

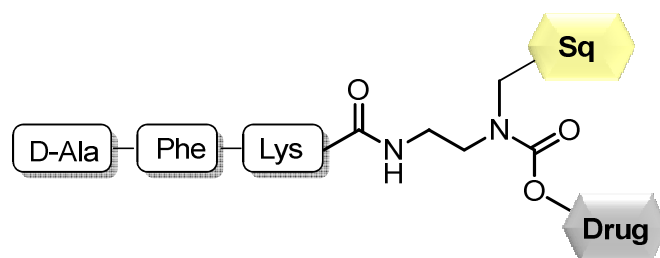
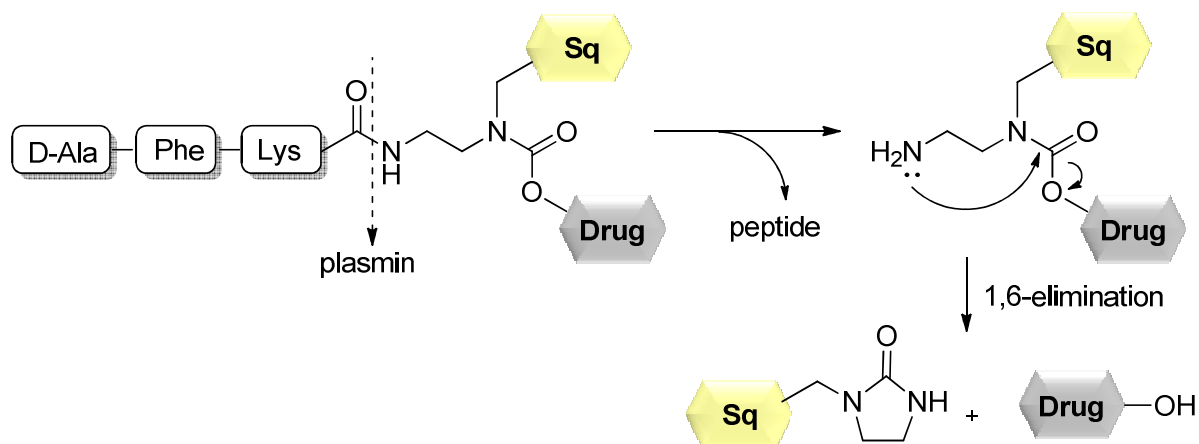


Figure 66: Tripeptidyl drug-squalene conjugates

These compounds contain a D-Ala-Phe-Lys sequence that is a substrate for the protease activity of plasmin and acts like a trigger: in fact, after a 1,6-elimination of the spacer, free drugs could be released (Scheme 8):



Scheme 8: Release of the drug unit from our tripeptidyl squalene conjugates

We individuated four different portions, deriving from three main disconnections: the peptide, the 1,6-elimination spacer, the squalene moiety and the active drug (Figure 67).

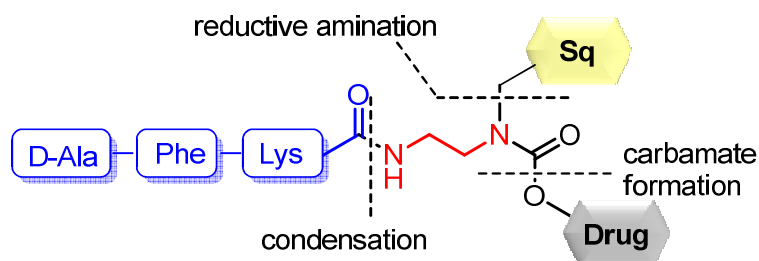
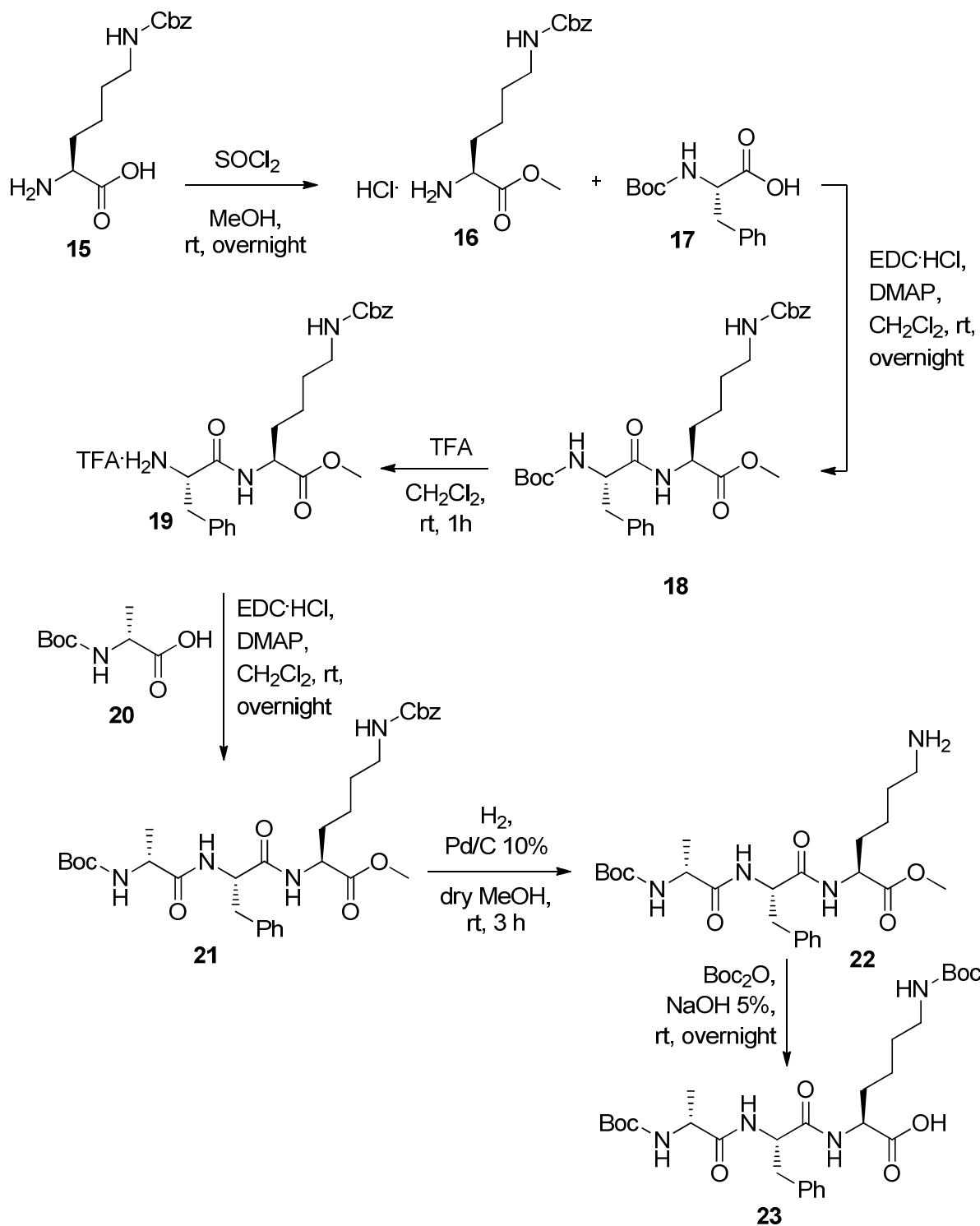


Figure 67: Retrosynthetic analysis

Synthetic strategy

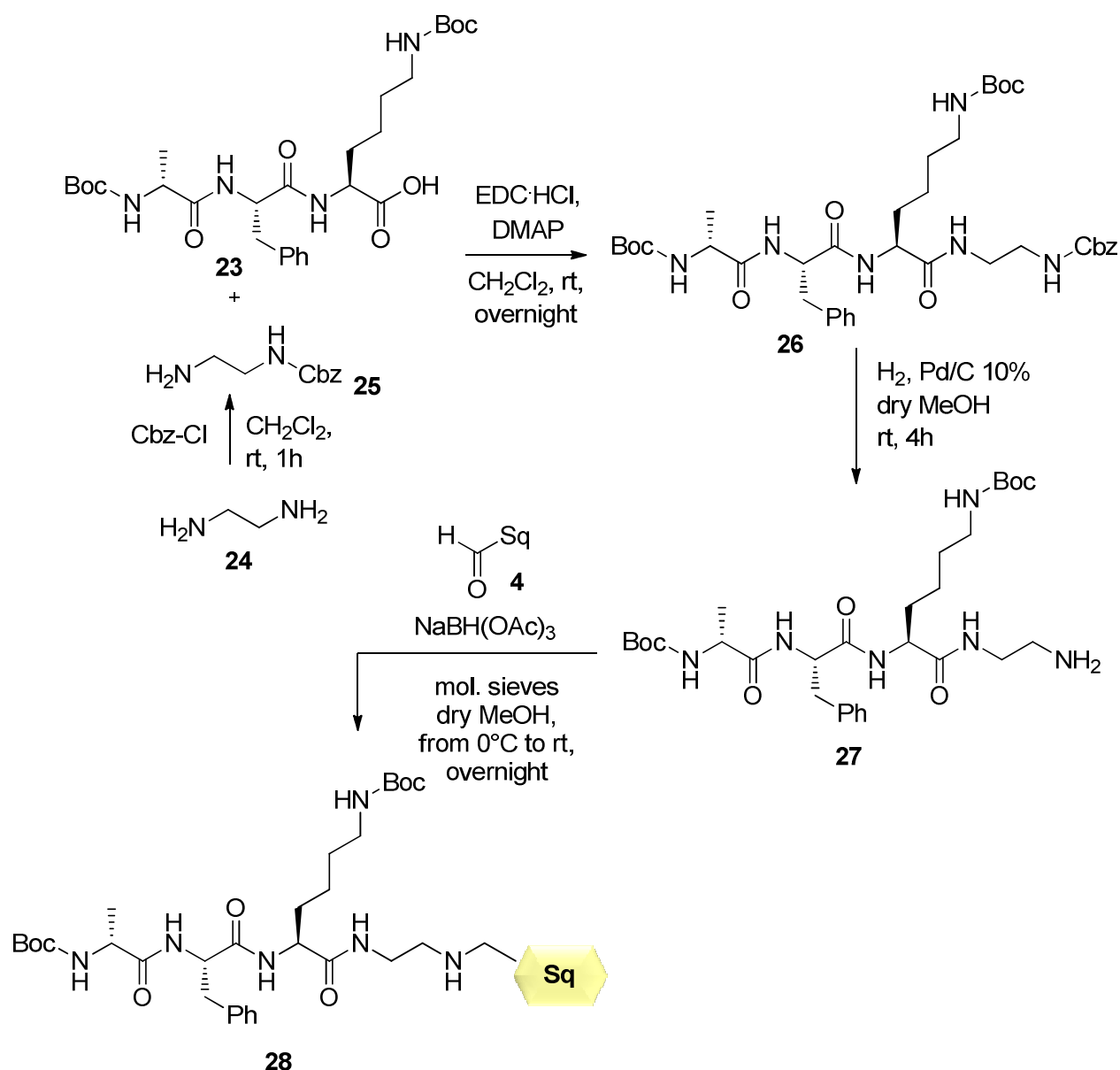
The synthetic pathway we followed for the preparation of the tripeptidyl portion is summarized in Scheme 9.

*N*_ε-Z-L-lysine methylester hydrochloride, obtained by treatment of *N*_ε-Z-L-lysine with SOCl₂ in MeOH, was coupled to *N*-Boc-L-phenylalanine using EDC·HCl/DMAP as activating system. Dipeptide **18** was then N-deprotected with TFA in CH₂Cl₂ affording **19** that was coupled to *N*-Boc-D-alanine in the presence, also in this case, of EDC·HCl/DMAP. The carbobenzyloxyl moiety was then cleaved by hydrogenation involving Pd/C 10% weight as a catalyst. In the end, the reaction of the tripeptidyl intermediate **22** with Boc₂O and NaOH 5% led to the formation, after pH adjustment to 5, of the desired compound **23**.



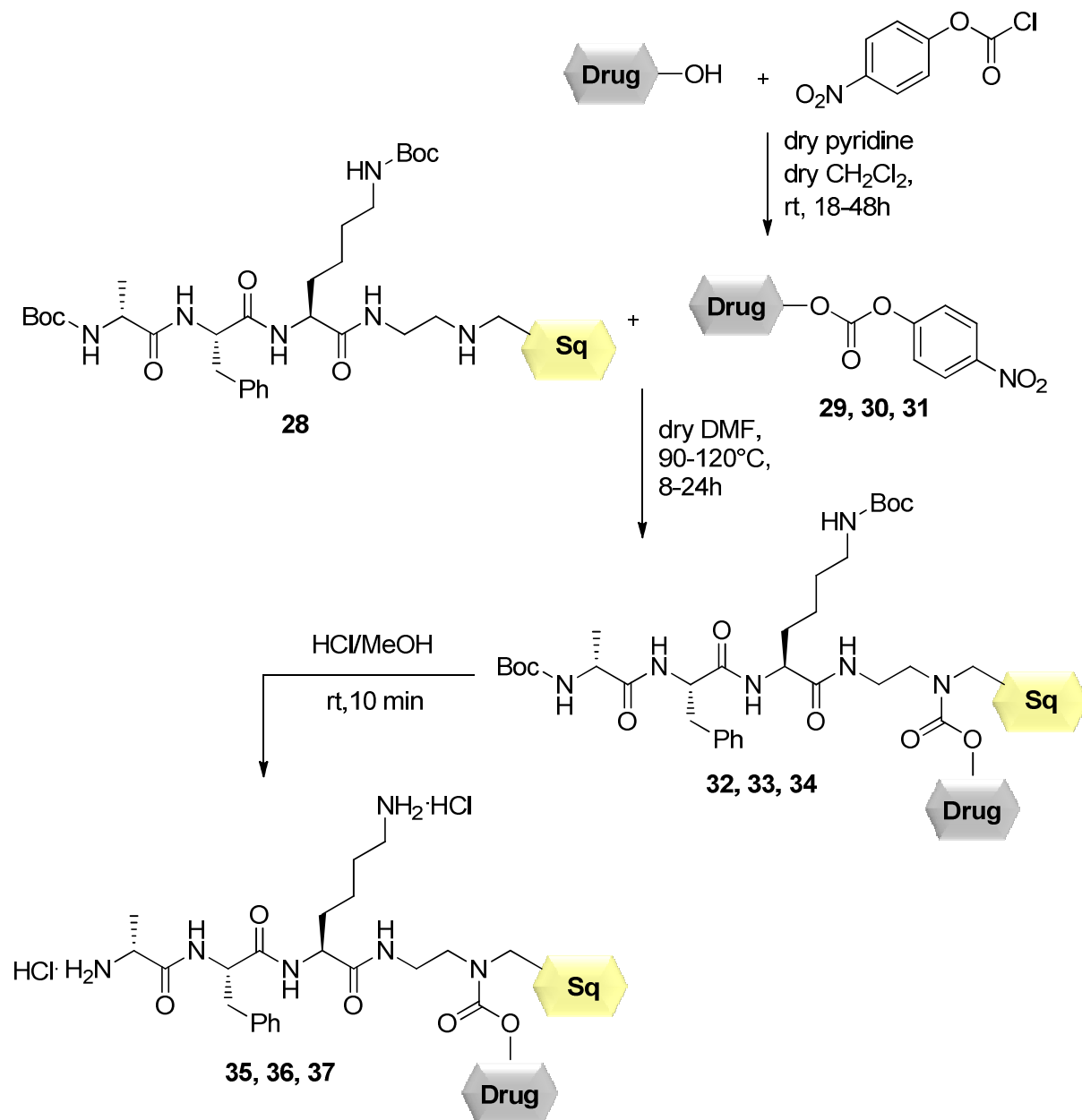
Scheme 9: Synthesis of compound **23**

Once the tripeptidyl portion was obtained, it was coupled to the ethylenediamine mono-Cbz-protected spacer **25**, and then the Cbz protecting group was cleaved by catalytic hydrogenation. Compound **27** underwent a reductive amination with **4** with $\text{NaBH}(\text{OAc})_3$, leading to intermediate **28**. Since **27** is a primary amine, it was necessary to use an excess of it respect to the aldehyde (molar ratio: 3:1), in order to minimize the amount of the product deriving from a double alkylation (Scheme 10).



Scheme 10: Synthesis of compound **28**

Compound **28** was then used for the synthesis of three tripeptidyl drug-squalene conjugates following the pathway depicted in Scheme 11. In detail, compound **28** reacts with a molecule of drug previously activated by *p*-nitrophenyl-chloroformate (**29-31**). After carbamates formation, the Boc moieties are cleaved by treatment with a saturated solution of HCl in MeOH, thus obtaining the desired products **35-37**.



Scheme 11: Synthesis of tripeptidyl drug-squalene conjugates **35-37**

On the base of the poor stability of epothilone A-derived disulfide containing squalene conjugates described in Section 2, we decided to prepare only three final conjugates, using paclitaxel, podophyllotoxin and camptothecin as active drugs (Figure 68).

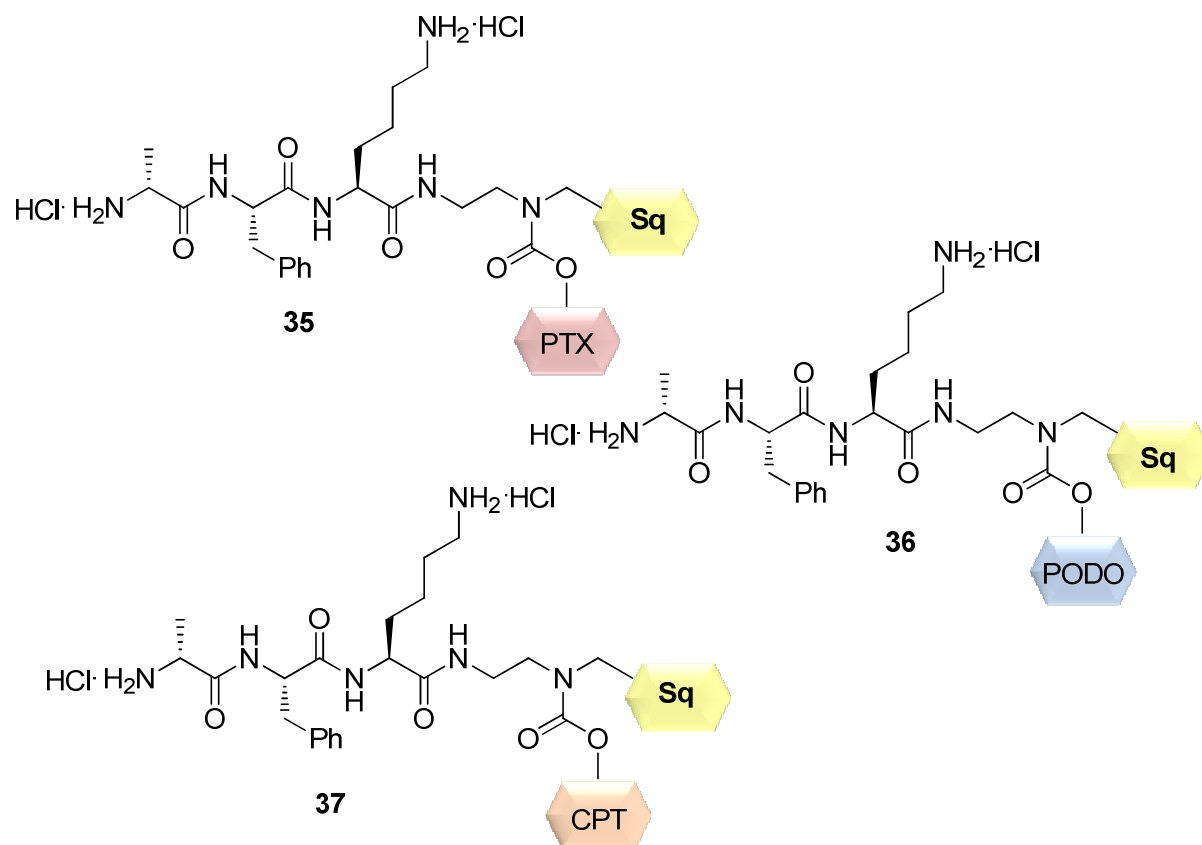


Figure 68: Structure of compounds 35-37

Nanoparticle formation and characterization

Compounds **35-37** have been formulated using the same protocol than disulfide-containing conjugates (see Section 2).

Interestingly, tripeptide-containing squalene conjugates didn't show the ability to self-assemble in water, but they resulted completely soluble in an aqueous medium. This was totally unexpected, since all the compounds containing a squalene tail prepared until now, even those containing a polar counterpart, were able to nanoprecipitate.

As an explanation, we hypothesized that the presence of a polar tripeptidic chain containing two hydrochloride amino groups led to a dramatic increase in the water solubility, so that the lipophilic squalene tail wasn't able to allow the formation of nanoassemblies.

This could be overcome by eliminating the two hydrochloric acid molecules, but the small quantities of conjugates we were handling didn't allow us to.

Furthermore, since the nature of the aqueous medium influences the nanoprecipitation process, it could be possible that, using different buffer solutions, the optimal conditions for the formation of nanoassemblies could be found.

All these aspects are currently under investigation in our laboratories.

Incubation with plasmin

In order to verify the ability of compounds **35-37** to release the corresponding parent drug, we incubated **35-37** with human plasmin (purchased by Sigma-Aldrich) following a procedure described by de Groot^[141].

In this purpose we incubated the conjugates at a concentration of 200 μM in 0.1 M ammonium acetate buffer (pH 7.3) in the presence of 100 $\mu\text{g/ml}$ human plasmin.

As a comparison, we prepared also the same solution but without plasmin (blank).

Aliquots of 50 μL at different times were submitted to ESI-MS analysis, in order to detect the possible peak of released free drugs.

Unfortunately, the results we obtained are very difficult to explain, being very different from one conjugate to another:

- ✚ compound **35** (Paclitaxel derivative): we were able to see the peak of free paclitaxel ($m/z = 876.9$) in both the sample relative to incubation with and without plasmin;
- ✚ compound **36** (Podophyllotoxin derivative): we weren't able to detect any significant peak, probably because of a low stability of the conjugate in the buffer solution;
- ✚ compound **37** (Camptothecin derivative): we detect in both the reaction with and without plasmin peaks attributable to tripeptidyl and squalene fragmentations, but not to free camptothecin. Suspecting eventually released camptothecin was not stable in the reaction conditions, we also incubated it in the same buffer solution used for reaction with plasmin. ESI-MS analysis clearly revealed the peak of camptothecin molecular ion.

We are currently investigating other possible reaction conditions (using different buffer solutions and analysis techniques) in order to determine whether the release of free drugs actually takes place or not and to find a way to favor it.

Biological evaluation

Compounds **35-37** were submitted to a preliminary evaluation of their cytotoxicity against A549 cell lines in collaboration with Dr. Damia (*Istituto Mario Negri*, Milano). Unfortunately they displayed a low cytotoxic activity, as enlightened by the results summarized in Table 8:

Compound	IC50 (μM)
35	>5
36	>5
37	>5

Table 8: IC50 values (μM) of compounds **35-37**

Since the low biological activity could be due to a not efficient release of the active drugs *in vitro*, we are currently evaluating the possibility to firstly incubate cells with human plasmin (purchased by Sigma-Aldrich) before treatment with our conjugates, in order to favor the cleavage of the peptidiyl sequence.

Summary

The results obtained with conjugates **35-37** apparently suggest that the addition of a squalene tail to a class of compounds that have been demonstrated able to release free drug units when incubated with plasmin is not a useful approach for improving biological activity. Indeed, squalene moiety could cause a steric hindrance that doesn't allow plasmin to cleave the tripeptidyl sequence and, without an efficient release mechanism, the cytotoxicity of the conjugates results lowered respect to the parent drug.

Anyway, the tripeptidyl sequence could allow a better bioavailability of drugs (as demonstrated by the water-solubility of compounds **35-37**), while squalene could favor the passage through cell membranes, thus improving the biological profile of a drug.

For these reasons we are currently taking into consideration these issues, in order to better understand the mechanism of action of plasmin and in which conditions it could be favored.

**Section 4: Heterogeneous
fluorescent nanoparticles:
FITC-squalene conjugates**

Introduction

Besides the improvements due to attaching a squalene tail to an active drug, that thus becomes able to self-assemble in water, another interesting aspect is to study the mechanisms of cellular uptake of nanoparticles, once they are formed.

To do this, it would be necessary to label nanoparticles in some way, in order to elucidate how they interact with cell membranes.

Thus, we envisioned the possibility to prepare a fluorescent derivative of squalene able to form biocompatible fluorescent nanoparticles, for studying their mechanisms of internalization and their localization inside the cell.

An interesting feature of this system is the fact that the fluorescent is not physically adsorbed on a matrix or included in a system but is covalently linked to squalene, thus resulting in a higher stability and biocompatibility of the materials.

This kind of approach could be applied also to diagnostic purposes, for the localization of agents in live beings.

Fluorescence spectroscopy

The use of fluorescence spectroscopy allows highly sensitive measurements with instrumentation exploiting different sensing modes, like intensity, lifetime and polarization detection. In addition, the combination of those methodologies with the high spatial resolution of fluorescence microscopy has enabled the intracellular monitoring of many different species for medical and biological purposes^{[143][144][145]}.

Radioactive molecular imaging^[146], magnetic resonance imaging^{[147][148]}, and optical imaging^[149] have been recognized as powerful techniques in this field. Easy manipulation and high sensitivity make optical imaging the most widely used technique.

Fluorescent methods based on organic dyes are simple, diverse and nondestructive methodologies and their applications depend on the nature of the molecule they are bound to, thus being useful not only as diagnostics but also as therapeutics.

However, these dyes suffer from intrinsic limitations, in fact they show:

- ✚ low absorption coefficients and weak signals that normally reduce the sensitivity and response of the applications;
- ✚ poor photobleaching resistance that limits their use in long-term tracking;
- ✚ short fluorescent lifetimes^[150].

Moreover, when their application is the intracellular detection, researchers are still dealing with other drawbacks, such as the toxicity of some organic dyes, their aggregation inside tissue or cells, and their interaction with cell components that might lead to the quenching of the fluorescence.

Fluorescein 5(6)-isothiocyanate derivatives

Among fluorescent compounds, fluorescein presents a number of attractive features:

- ✚ its excitation wavelength ($\lambda = 488 \text{ nm}$) does not interfere with the absorbances of cellular proteins;
- ✚ it has been extensively used in the preparation of fluorescent sensors^{[151][152][153]};
- ✚ it is easily accessible;
- ✚ it does not require sophisticated microscopic instruments.

Our research group recently prepared^[154] a small collection of fluorescein 5(6)-isothiocyanate (FITC) derivatives containing a tubulin binder unit (deacetylthiocolchicine, paclitaxel and cephalomannine), with the aim of obtaining new fluorescent dyes that can secure a direct assay to evidence the tubulin/microtubules network both in cells and in vivo and to overcome the invasive techniques of transfection or microinjection (

Figure 69). In fact, in light of our interests concerning the biology of tubulins and their implication in cancer and neurodegenerative diseases^{[67][69][70]}, fluorescent dyes specific for tubulin for in vitro and in vivo imaging studies could be very useful.

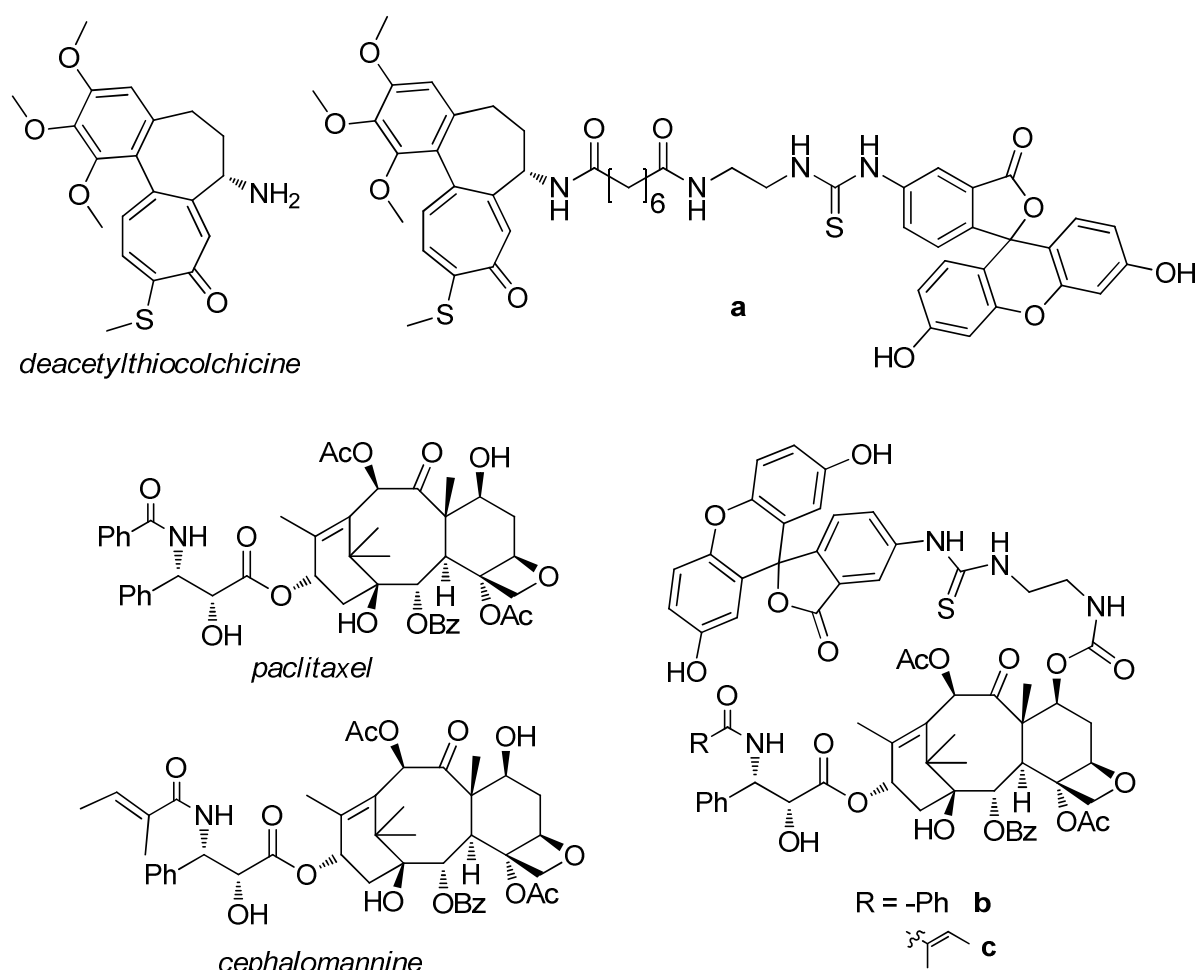


Figure 69: Structures of deacetylthiocolchicine and its fluorescent derivative **a**, paclitaxel and its fluorescent derivative **b**, cephalomannine and its fluorescent derivative **c**

Unfortunately, taxane derivatives **b** and **c** were unstable. Compound **a** was minimally able to inhibit tubulin polymerization, was cell permeable and able to bind to microtubules in a cellular context requiring a dynamic exchange between free and polymerized tubulin, thus meeting some of the demanding requirements for a new fluorescent dye that can secure a direct assay to evidence the tubulin/microtubule network in cells.

Fluorescent delivery systems

Besides the possibility of finding new fluorescent molecules, the recent advances in nanotechnology and nanomaterials have been integrated into analytical chemistry for the preparation of novel fluorescent delivery systems^[155].

In fact, nanoparticle systems can provide advantages over traditional approaches in term of sensitivity, stability, and capability for multiplexing^[156]. Instead of using single organic dye probes, these organic fluorophores have been encapsulated in a particle matrix: these particles are brighter than single dyes since one particle contains several fluorescent molecules, and they also are more photostable, since the entrapment enhances the stability and biocompatibility of the fluorophores.

The particle sizes generally range from 2 nm to several μm , even though the majority is within the nm scale. The small size of nanoparticles provides an opportunity for high signal to noise ratio response and signal amplification, therefore improving the analytical sensitivity and the response time. Importantly, their molecular size minimizes physical perturbation of living cells, and also provides high spatial resolution.

The first applications of fluorescent nanoparticles for intracellular measurements were for the labeling and imaging of cells, bacteria, cell components and tissues, for the exploring of intracellular processes^[157]. Later, other important intracellular applications were their use for diagnosis and therapeutics, especially for the recognition of cancer cells *in vivo*^[158]. Finally, during the last years, the application of fluorescent nanoparticles in the field of intracellular sensing is being examined for the real time quantification of intracellular analyte concentration^[159], which can give more insights into the chemical microenvironment on the sub-cellular level.

Recent applications of fluorescent nanoparticle delivery systems

In the last years many research groups reported the use of nanoparticle delivery systems as carriers of fluorescent dyes, such as the two following examples:

- ✚ *Bovin serum albumin nanoparticles*: Patel and coworkers described^[160] the preparation of glutathione(GSH)-containing bovin serum albumin nanoparticles (Figure 70) encapsulating, as fluorescent dye, molecules of fluorescein sodium salt.

Since GSH is among the few molecules (such as O₂, H₂O and CO₂) able to pass through the blood brain barrier (BBB), these nanoparticle were able to reach the brain, and this was confirmed by exploiting the presence of fluorescent molecules.

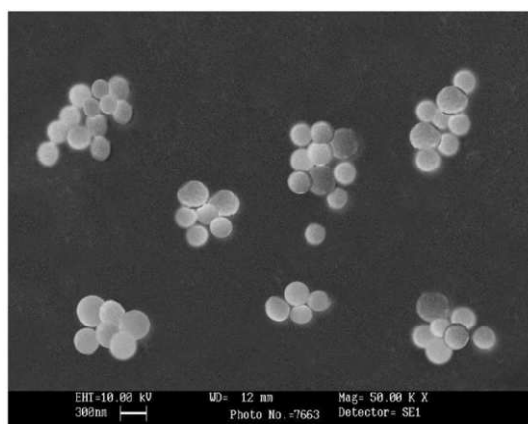


Figure 70: SEM image of glutathione-conjugated fluorescein sodium-loaded BSA nanoparticles

- ✚ *Mesoporous silica nanoparticles*: Yuan and coworkers prepared a different kind of delivery system based on mesoporous silica nanoparticles covalently bound to paclitaxel by a disulfide bond and containing FITC molecules^[161](
✚ Figure 71).

These kind of system present interesting features since: the formulation as nanoparticles allow a selective delivery to tumor tissues, the disulfide bond connecting paclitaxel to silica can be cleaved by the high concentration of GSH in some kind of tumor cells and the presence of FITC makes nanoparticles be fluorescent, thus allowing the study of the internalization mechanisms.

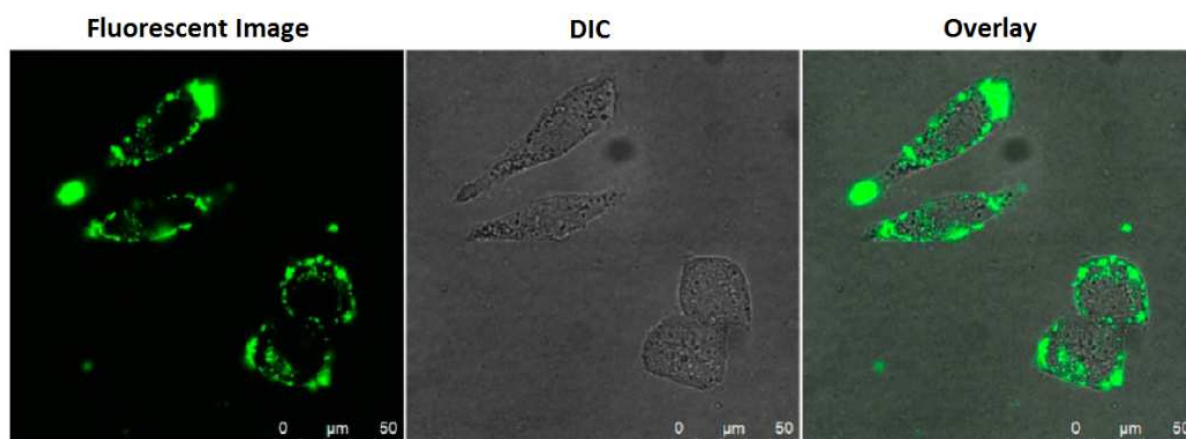


Figure 71: Confocal laser scanning microscopy (CLSM) images of HeLa cells incubated with 100 $\mu\text{g}/\text{mL}$ of the FMSN-PTX conjugate for 4 h. (Left) Spotlike green fluorescent images showing internalized FMSN-PTX conjugates. (Middle) Differential interference contrast (DIC) images. (Right) Merged image of DIC and green.

- ✚ *Ruthenium polypyridyl squalene derivatives:* with the aim of expanding the squalenylation platform (see Section 1) to include novel cell-imaging probes, Dosio and coworkers described the conjugation of the bulky complex $[\text{Ru}(\text{II}) \text{bis}(2,2'\text{-bipyridine})\text{-}\{1\text{-methyl-}2(4\text{-methylpyridin-}2\text{-yl})\text{-benzimidazole}\}](\text{PF}_6)_2$ to squalene^[162]:

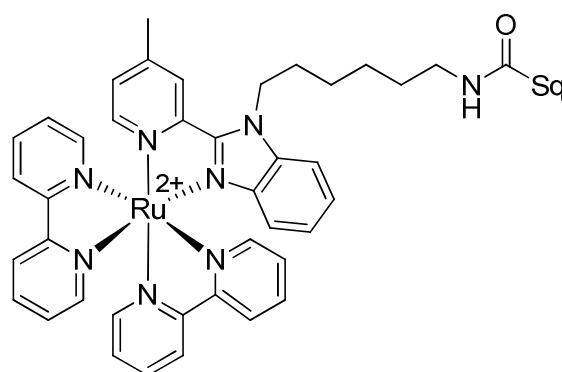


Figure 72: Dosio's $[\text{Ru}(\text{II}) \text{bis}(2,2'\text{-bipyridine})\text{-}\{1\text{-methyl-}2(4\text{-methylpyridin-}2\text{-yl})\text{-benzimidazole}\}](\text{PF}_6)_2$ - squalene conjugate

This compound was capable of self-assembling in water, underwent cellular uptake and diffusion, and didn't exercise a significant toxicity.

Aim of the work

On the base of our experience in the preparation of fluorescent tubulin binders and in the preparation of squalene-based nanoparticles, we envisioned the possibility to combine these two different approaches in order to obtain a new kind of nanoassemblies containing both a fluorescent squalene derivative and a drug-squalene conjugate to better investigate the mechanisms of internalization of drug-squalene nanoparticles.

For this preliminary study, we chose to use as squalene-drug conjugate compound **16** (PTX-Sq) and to link a FITC molecule to a squalene tail to obtain the fluorescent derivative **17** (Figure 73):

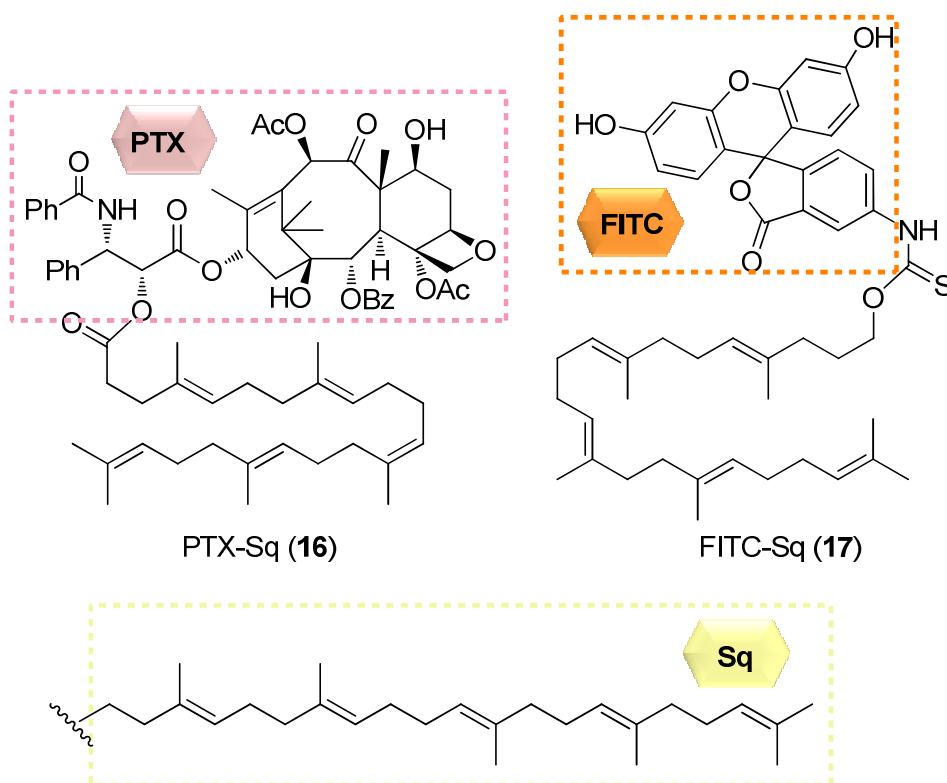
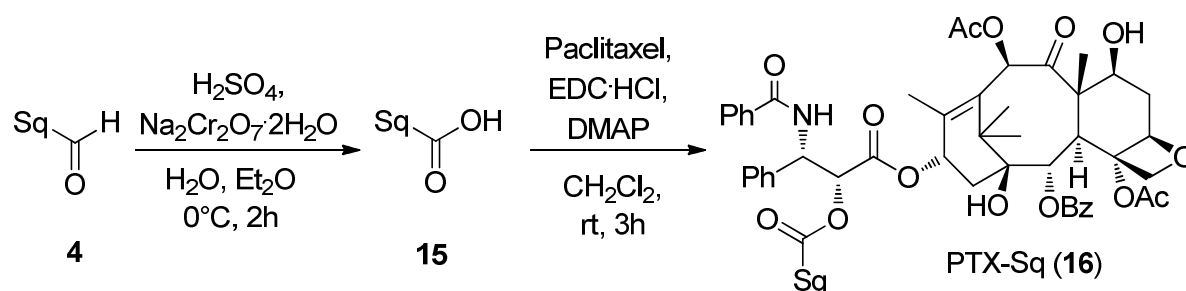


Figure 73: Structures of PTX-Sq and FITC-Sq

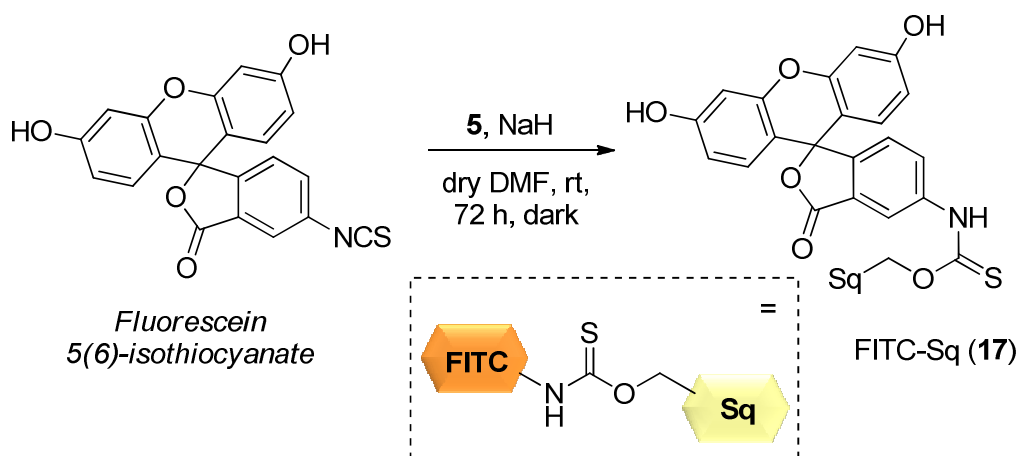
This kind of co-nanoassemblies could have all the advantages of the application of nanotechnology to optical imaging and, in addition, could exploit the biocompatibility of squalene. Furthermore, since the fluorescent dye is covalently linked to squalene, and not simply encapsulated in a polymeric matrix, the resulting co-nanoassemblies could be more stable.

Synthetic strategy

PTX-Sq was prepared following a procedure described by Dosio and coworkers^[55]. Compound **4** was oxidized to the corresponding carboxylic acid **15** by treatment with H₂SO₄/Na₂Cr₂O₇ and then condensed to paclitaxel using EDC·HCl/DMAP as activating system (Scheme 12):



Compound **17** (FITC-Sq) was prepared by reaction of fluorescein 5(6)-isothiocyanate with the anion of compound **5**, generated in situ by treatment with NaH (Scheme 13).



Fluorescent nanoparticles

In order to verify the ability of compound **17** (FITC-Sq) to form nanoassemblies and of compounds **16** and **17** to form homogeneous mixed nanoparticles, we prepared 5 different nanosuspensions applying the same procedure used for the other drug-squalene conjugates:

- A) FITC-Sq (2 mg/ml);
- B) PTX-Sq (2 mg/ml) : FITC-Sq = 10 : 1;
- C) PTX-Sq (2 mg/ml) : FITC-Sq = 20 : 1;
- D) PTX-Sq (2 mg/ml) : FITC-Sq = 30 : 1;
- E) PTX-Sq (2 mg/ml).

In the case of suspensions B, C and D, the final concentration (2 mg/ml) is referred to PTX-Sq, while the amount of FITC-Sq was calculated considering the molar ratios PTX-Sq : FITC-Sq (10:1, 20:1, 30:1).

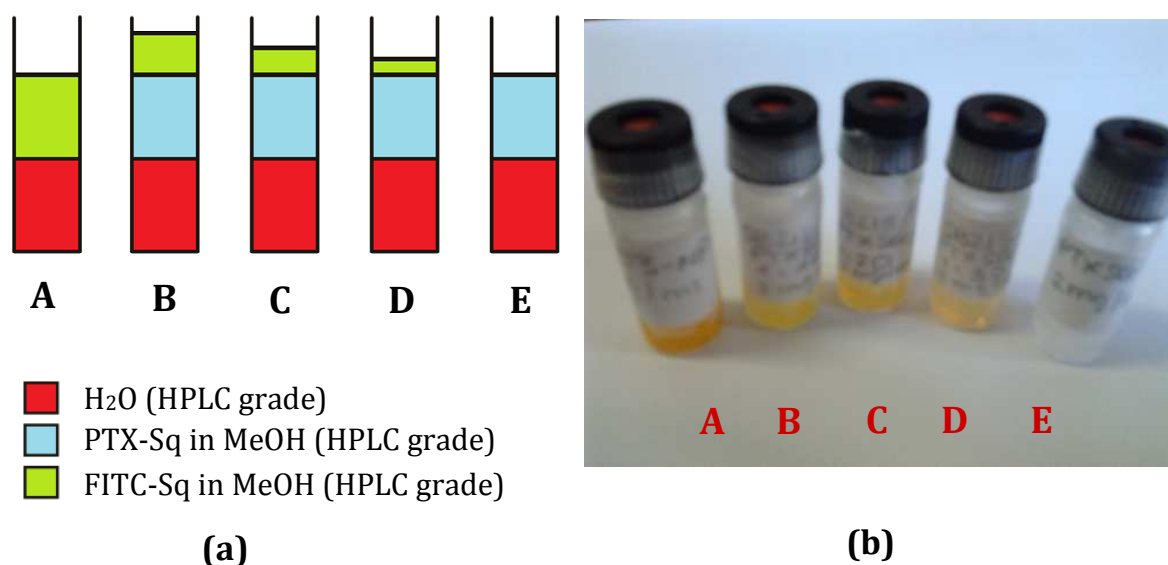


Figure 74: Schematic representation (a) and picture (b) of the five mixtures

In each case the formation of nanoassemblies was verified. The nanosuspensions were then characterized, in order to determine mean diameter, polydispersity index and Z potential. The results we obtained are summarized in Table 9.

Compound	Mean Diameter (nm)	PI	Z potential (mV)
FITC-Sq (A)	196.4	0.232	-19.91
PTX-Sq: FITC-Sq 10:1 (B)	149.4	0.147	n.d.
PTX-Sq: FITC-Sq 20:1 (C)	171.9	0.179	n.d.
PTX-Sq: FITC-Sq 30:1 (D)	225.4	0.190	n.d.
PTX-Sq (E)	231.6	0.270	n.d.

Table 9: Mean diameter, polydispersity index and Z potential of the five mixtures

Unfortunately, we weren't able to obtain a precise measure for Z potential of most of the suspensions, but values very different one from the other (all the measurements were always repeated thrice). This could be due to intrinsic factors of our nanoparticles or to a malfunctioning of the instrument we used.

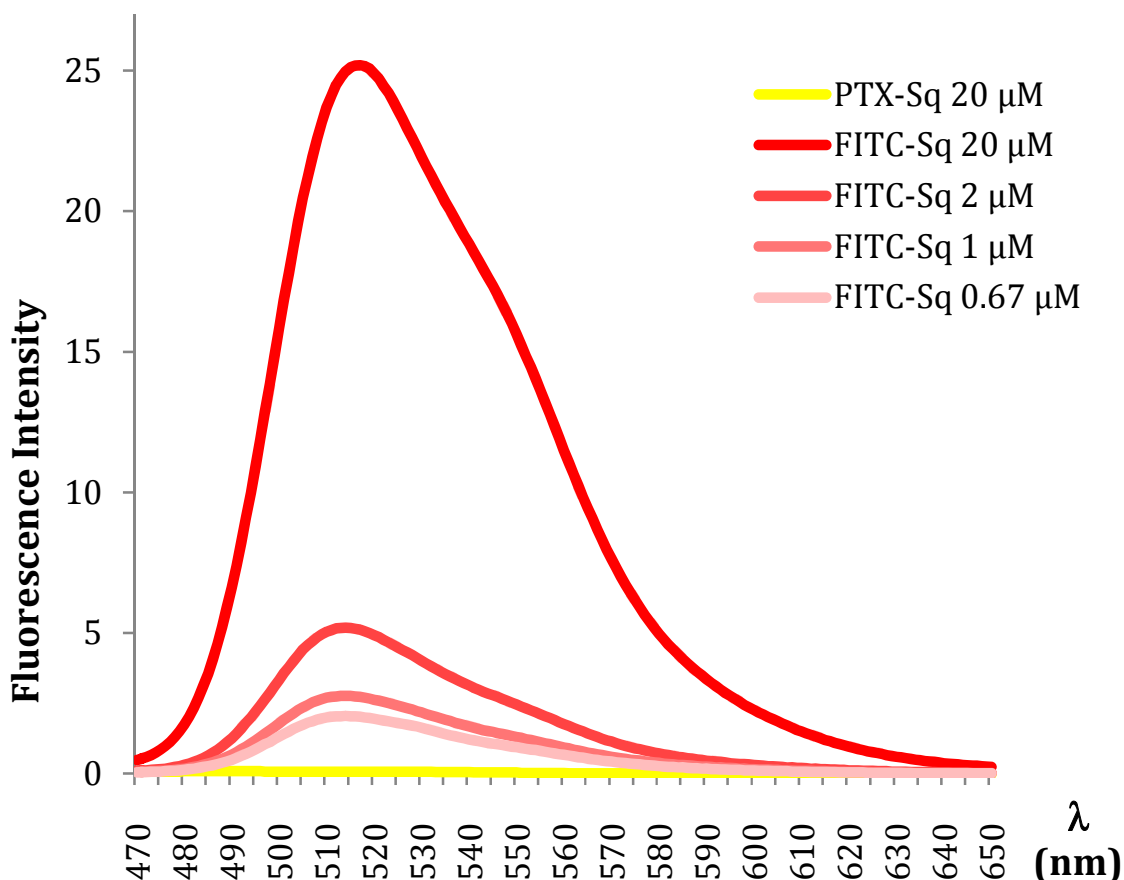
Even if the mean diameter of nanoparticles in sample B was lower than in sample A, it is possible to see that, decreasing the amount of SB213 in the mixture, the mean diameter of nanoparticles increased towards the value of sample E.

Fluorescence emission

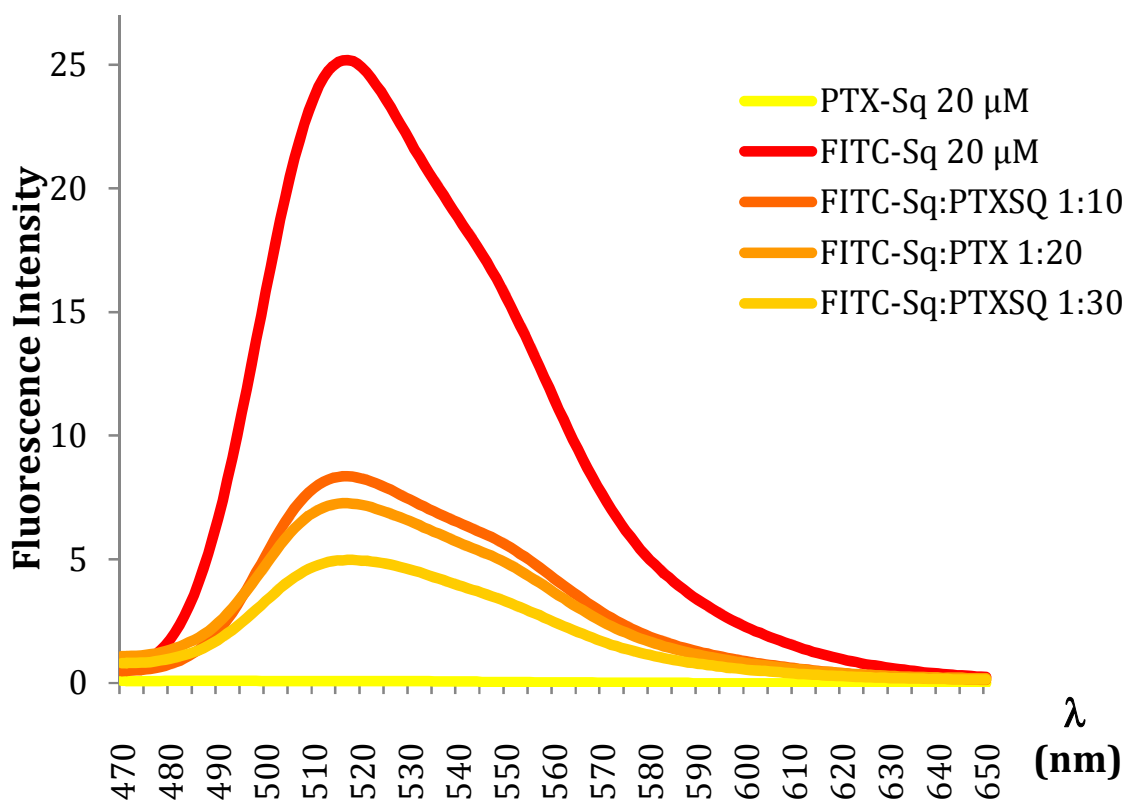
In order to verify the relationship between the amount of FITC derivative and the fluorescence emission of the mixtures and the dependence on the nature of the samples (solutions or nanosuspensions), we measured the fluorescence emission using a Spectrofluorometer FP-750 (Jasco).

For a better measurement nanoparticle samples were diluted with water (HPLC grade) and pure FITC-Sq was dissolved in MeOH (HPLC grade) in order to have the main component of the mixture at a fixed concentration. The results we obtained are summarized in the following graphs.

- ✚ *Graph A: FITC-Sq (17) at different concentrations (samples as nanoparticles). Samples with higher amounts of FITC-Sq possess a higher fluorescence emission.*

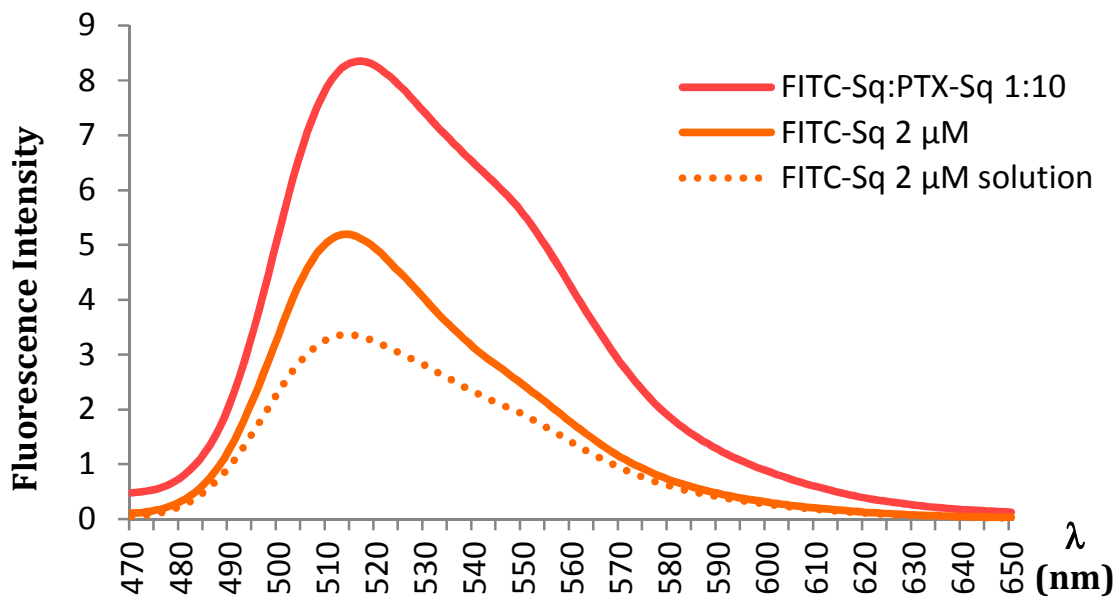


- ✚ *Graph B:* PTX-Sq at a fixed concentration (20 μM) with different amounts of FITC-Sq compared to FITC-Sq 20 μM (samples as nanoparticles). Also in this case, samples with higher amounts of FITC-Sq possess a higher fluorescence emission.

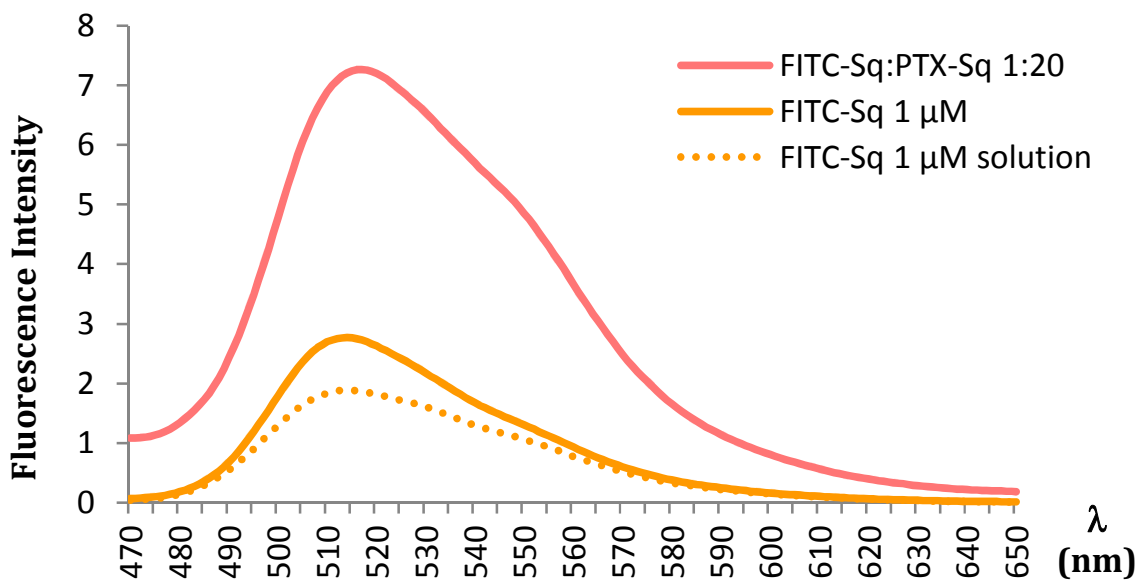


- ✚ *Graphs C, D and E:* samples with different amounts of FITC-Sq (as nanoparticles) were compared to samples containing the same amounts of FITC-Sq but in solution. Noteworthy, the samples of nanosuspensions displayed a higher emission of fluorescence than the corresponding solutions and, at each value of FITC-Sq concentration, the mixture of PTX-Sq and FITC-Sq displayed a higher emission than FITC-Sq alone. This can be explained by the fact that the more hydrophobic the environment is, the higher the emission: thus, a nanosuspension results to be a more hydrophobic environment than a methanolic solution even if the sample is diluted with water.

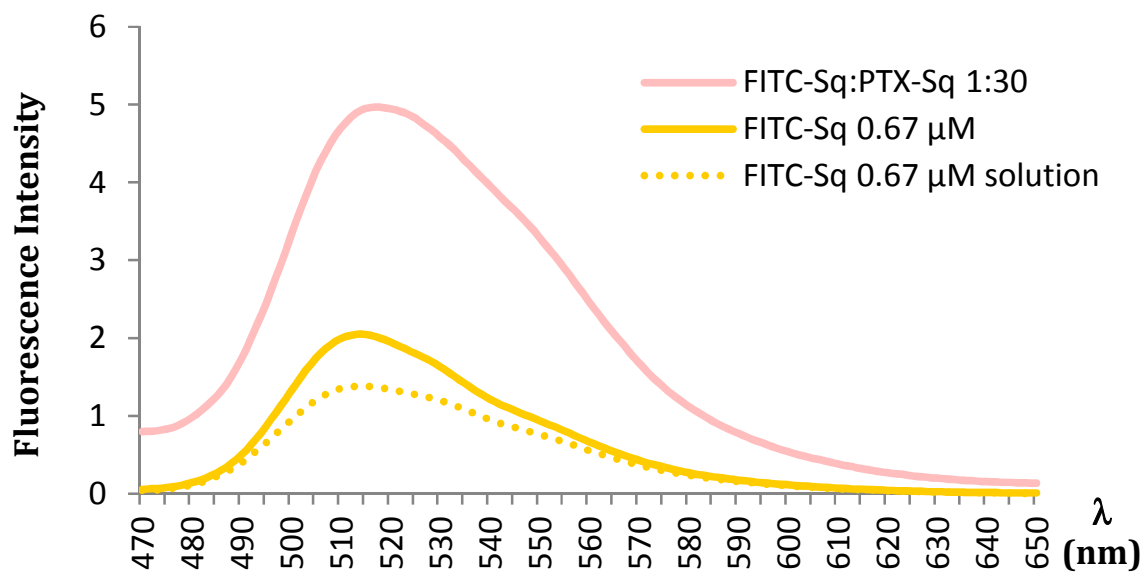
Moreover, the presence of PTX-Sq in a 10:1 ratio respect to FITC-Sq further increase the hydrophobicity of the system.



Graph A: Fixed FITC-Sq concentration: 2 μM



Graph B: Fixed FITC-Sq concentration: 1 μM



Graph C: Fixed FITC-Sq concentration: 0.67 μM

In live evaluation

To verify the ability of our nanosuspensions to cross cell membranes monitored their internalization kinetics by fluorescent microscopy experiments.

A549 cells were incubated with nanosuspensions containing both PTX-Sq and FITC-Sq at two different molar ratios (10:1 and 30:1) and then various images have been taken at different times (10, 30 and 60 min).

For these measurements nanosuspensions have been prepared applying the solvent displacement method (concentration of PTX-Sq: 2 mg/ml), then they were diluted ten times, obtaining for FITC-Sq the following concentration values:

- ✚ Mixture B (PTX-Sq/FITC-Sq 10:1): 13.8 μM
- ✚ Mixture D (PTX-Sq/FITC-Sq 30:1): 4.6 μM

As shown in Figure 75, FITC-Sq (in green) accumulates in the perinuclear region of cells incubated with samples at both the two molar ratios, whereas in the case of 30:1 mixture the signal is weaker (even still present).

Furthermore, it is also possible to recognize some intact nanoparticles (fluorescent spherical spots are evident inside cells), with mean diameters similar to those measured by QELS.

These results strongly indicate that PTX-Sq/FITC-Sq co-nanoassemblies are internalized in cultured cells.

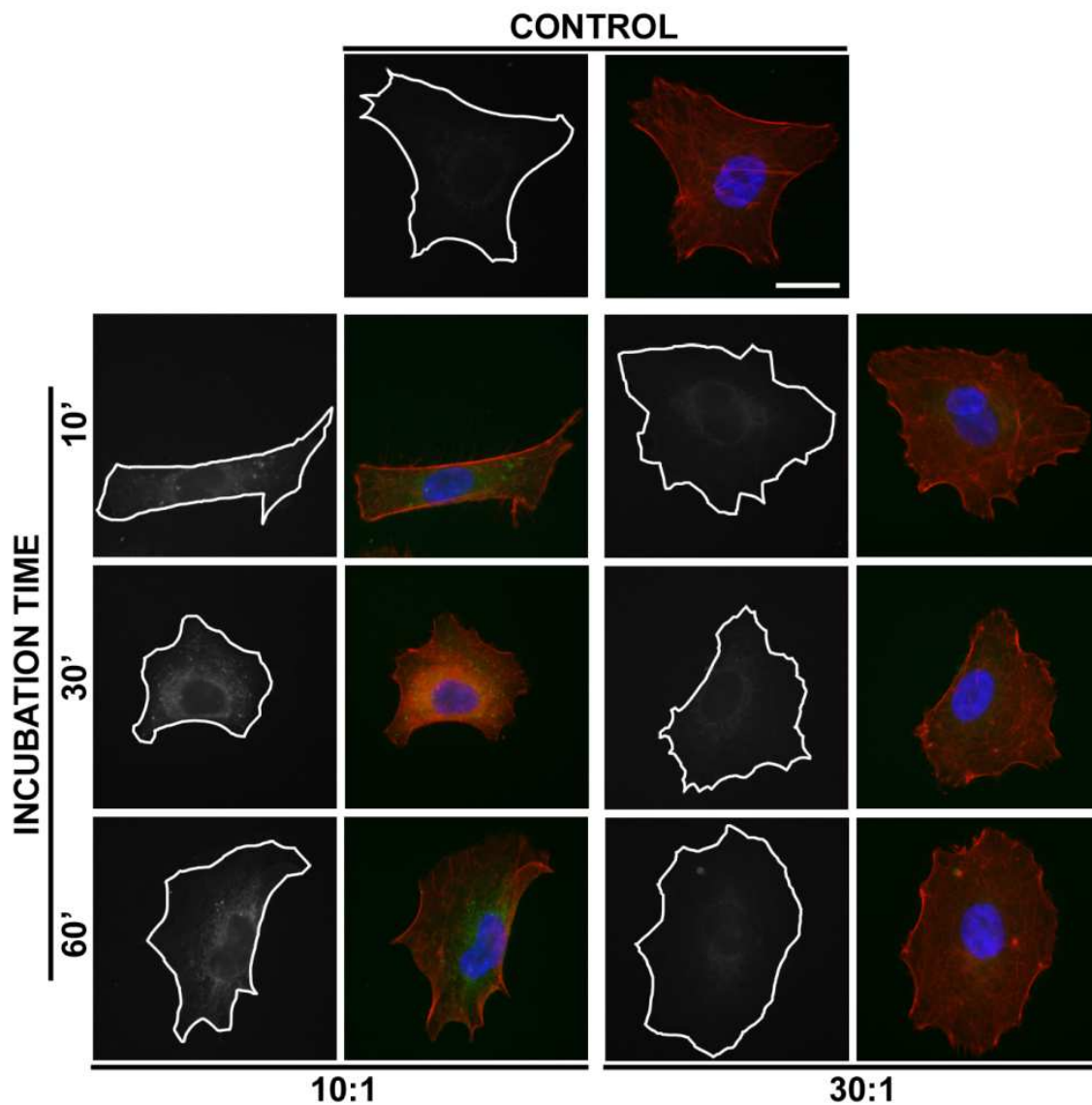


Figure 75: Right columns show actin filaments (red) and nuclei (blue), whereas white lines in the left columns mark the cell boundaries. Top row (Control) shows A549 cell that were not incubated with PTX-Sq/FITC-SQ co-nanoassemblies.

Scale bar = 20 μm .

The interaction of our nanoparticles with microtubules is currently under investigation in the laboratories of Dr. Cappelletti (Università degli Studi di Milano, *Dipartimento di Biologia*).

Section 5: Summary

Summary and future perspectives

The work effected during this three-year project confirmed the utility of squalene in modulating the biological profile of active drugs and showed how this platform can be improved by including drug-releasing linkers in squalene derivatives.

In this thesis we described two different approaches do allow drug release from squalene conjugates, but to them many others could be added by changing the mechanism of release.

Furthermore, we also illustrated the preparation and characterization of a fluorescent squalene conjugate that resulted very promising for the study of nanoparticles internalization mechanisms by fluorescence spectroscopy. This approach can be extended also to co-nanoprecipitation with other squalenoylated drugs and drug-releasing squalene conjugates, with a variety of applications.

Another interesting aspect could be the preparation of different kinds of heterogeneous squalene nanoparticles for combined chemotherapy.

All these issues will be carried on by our research group in the next months.

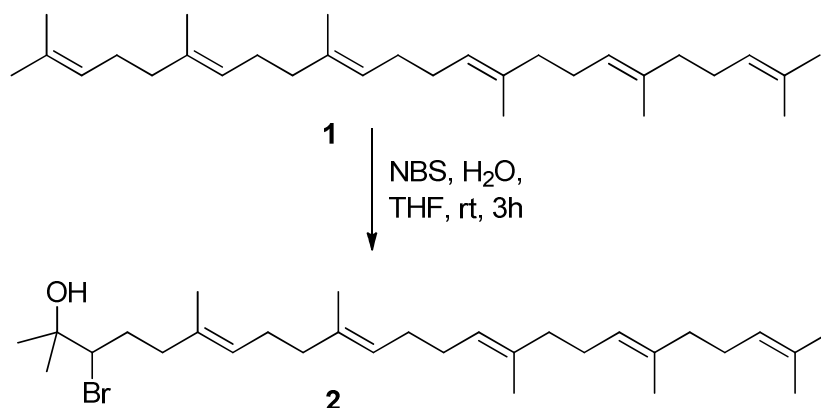
Section 6: Experimental Procedures

Chemistry

General

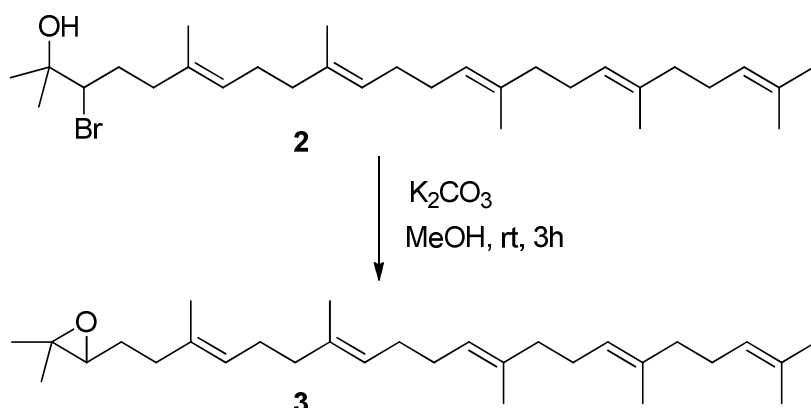
Thin-layer chromatography (TLC) was performed on Merck precoated 60F254 plates. Reactions were monitored by TLC on silica gel, with detection by Uv light ($\lambda = 254$ nm) or by charring with 1% permanganate solution. Flash chromatography was performed using Silica gel (240-400 Mesh, Merck). NMR spectra were recorded with Bruker 300 and 400 MHz spectrometers. Chemical shifts are reported in parts per million (δ) downfield from tetramethylsilane (TMS). EI mass spectra were recorded at an ionizing voltage of 6 kEv on a VG 70-70 EQ. ESI mass spectra were recorded on FT-ICR APEXII. Specific rotations were measured with a P-1030-Jasco polarimeter with 10 cm optical path cells and 1 ml capacity (Na lamp, $\lambda = 589$ nm).

Synthesis of 2



To a solution of Squalene (**1**, 4.290 g, 0.010446 mol) in THF (30 ml) H₂O (5 ml) is added and then THF dropwise to obtain a clear solution. N-bromosuccinimide (2.231 g, 0.012535 mol) is added portionwise and the reaction mixture is stirred at room temperature for 3h. The solvent is removed under reduced pressure, brine (100 ml) is added and extracted with AcOEt (5x20 ml). The organic layers are dried over Na₂SO₄ and the solvent is removed under reduced pressure. The crude is purified by flash chromatography (CH₂Cl₂:Hex 1:1) to obtain **2** as a pale-yellow oil (1.652 g, Yield: 31%).

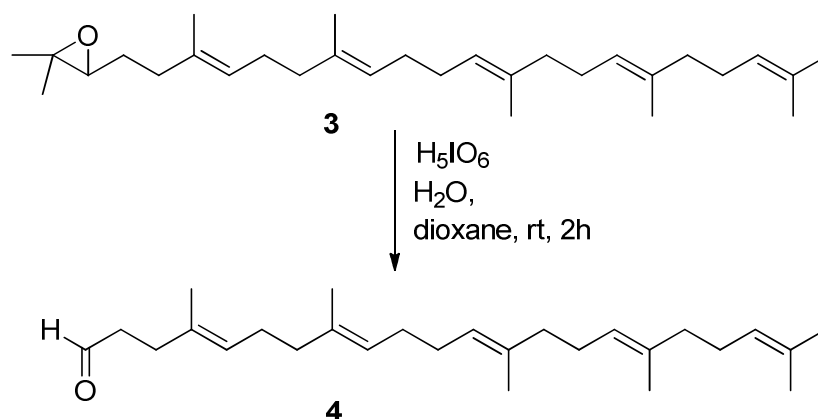
¹H-NMR (CDCl₃, 400 MHz): δ (ppm)= 5.10-5.25 (m, 5H); 4.01 (dd, J = 11.3 Hz, J = 1.9 Hz, 1H); 2.32-2.35 (m, 1H), 1.95-2.17 (m, 18H); 1.77-1.88 (m, 1H); 1.70 (s, 3H); 1.63 (bs, 15H); 1.37 (s, 3H); 1.36 (s, 3H). **¹³C-NMR** (CDCl₃, 100 MHz): δ (ppm)= 135.11; 134.89; 132.97; 131.24; 126.03; 124.47; 124.26 (3C); 72.44; 71.01; 39.73 (3C); 38.18; 32.17; 28.28 (3C); 26.68 (2C); 25.75 (3C); 17.68; 16.03 (3C); 15.85. **APCI-MS**: m/z 507.3 [M]⁺.

Synthesis of **3**

To a solution of **2** (1.652 g, 0.003258 mol) in MeOH (60 ml) K_2CO_3 (0.898 g, 0.006517 mol) is added and the reaction mixture is stirred at room temperature for 2 h, then concentrated under reduced pressure. H_2O (120 ml) is added and extracted with AcOEt (4x30 ml). The organic layers are dried over Na_2SO_4 and the solvent is removed under reduced pressure to obtain **3** as a yellow oil (1.360 g, Yield: 98%) without any further purification.

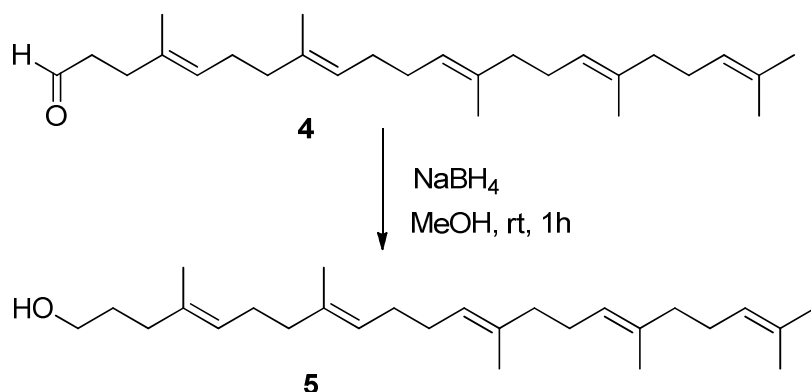
$^1\text{H-NMR}$ (CDCl_3 , 300 MHz): $\delta(\text{ppm})= 5.06\text{-}5.17$ (m, 5H); 2.69 (t, $J = 6.1$ Hz, 1H); 1.95-2.19 (m, 20H); 1.68 (s, 3H); 1.60 (s, 3H); 1.58 (bs, 12H); 1.28 (s, 3H); 1.24 (s, 3H). **$^{13}\text{C-NMR}$** (CDCl_3 , 100 MHz): $\delta(\text{ppm})= 135.06$; 134.89 (2C); 133.96; 131.18; 124.93; 124.26 (4C); 64.17; 58.27; 39.72 (3C); 36.31; 28.25 (2C); 27.46; 25.69; 24.89 (2C); 18.72; 17.67; 16.00 (3C). **APCI-MS**: m/z 427.3 $[\text{M}+1]^+$.

Synthesis of 4



To a solution of H_5IO_6 (1.379 g, 0.006058 mol) in H_2O (5 ml) a solution of **3** (1.434 g, 0.003366 mol) in dioxane (12 ml) is added and the reaction mixture is stirred at room temperature for 2h. H_2O (150 ml) is added and extracted with AcOEt (3x40 ml). the organic layers are washed with brine (100 ml) and H_2O (100 ml), then dried over Na_2SO_4 and concentrated under reduced pressure to obtain **4** as a pale yellow oil (1.111 g, Yield: 86%) without any further purification.

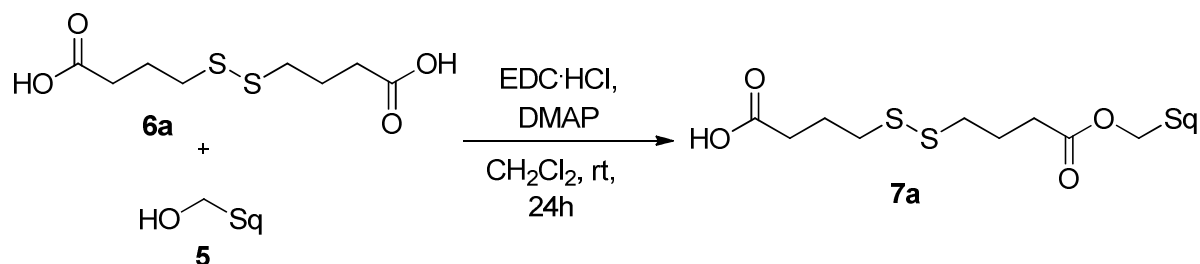
$^1\text{H-NMR}$ (CDCl_3 , 300 MHz): δ (ppm)= 9.73 (s, 1H); 5.06-5.13 (m, 5H); 2.49 (t, $J = 7.1$ Hz, 2H); 2.30 (t, $J = 7.1$ Hz, 2H); 1.97-2.10 (m, 16H); 1.67 (s, 3H); 1.55 (bs, 15H). **$^{13}\text{C-NMR}$** (CDCl_3 , 75 MHz): δ (ppm)= 202.65; 135.11; 134.88; 134.77; 132.86; 131.23; 125.41; 124.52; 124.37; 124.25 (2C); 67.06; 42.14; 39.73 (2C); 39.51; 31.83; 28.24 (2C); 26.73; 26.62; 25.68 (2C); 17.66; 16.01 (3C). **APCI-MS**: m/z 385.3 [M+1]⁺.

Synthesis of **5**

To a solution of **4** (1.111 g, 0.002893 mol) in MeOH (45 ml) NaBH₄ (0.055 g, 0.001446 mol) is added portionwise and the reaction mixture is stirred at room temperature for 1 h. HCl 1M is added to quench the unreacted NaBH₄. The solvent is removed under reduced pressure, H₂O (150 ml) is added and extracted with AcOEt (3x40 ml). The organic layers are dried over Na₂SO₄ and concentrated under reduced pressure to obtain **5** as a colorless oil (1.016 g, Yield: 91%) without any further purification.

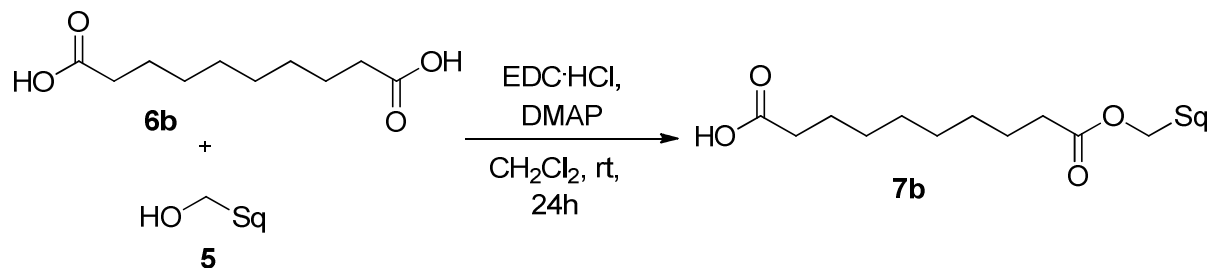
¹H-NMR (CDCl₃, 300 MHz): δ(ppm)= 5.08-5.13 (m, 5H); 3.61 (t, J = 6.3 Hz, 2H); 1.99-2.08 (m, 18H); 1.78-1.85 (m, 2H); 1.67 (s, 3H); 1.59 (s, 15H). **¹³C-NMR** (CDCl₃, 75 MHz): δ(ppm)= 135.11; 134.92 (2C); 134.54; 131.24; 125.83; 124.42 (2C); 124.26 (2C); 62.80; 39.72 (3C); 35.99; 30.73; 28.24 (2C); 26.60 (3C); 25.67 (2C); 17.66; 15.99 (3C). **APCI-MS**: m/z 387.3 [M+1]⁺.

Synthesis of 7a



To a solution of **5** (0.660 g, 0.001706 mol) in dry CH_2Cl_2 (18 ml) dithiodibutyric acid (**6a**, 0.812 g, 0.003411 mmol), EDC·HCl (0.393 g, 0.002047 mol) and DMAP (0.146 g, 0.001194 mmol) are added and the reaction mixture is stirred at room temperature for 24 h. HCl 1M (15 ml) is added and extracted with CH_2Cl_2 (5x5 ml). The organic layers are dried over Na_2SO_4 and the solvent is removed under reduced pressure. The crude is purified by flash chromatography (AcOEt/Hex) to obtain **7a** as a colorless oil (0.596 g, Yield: 58%).

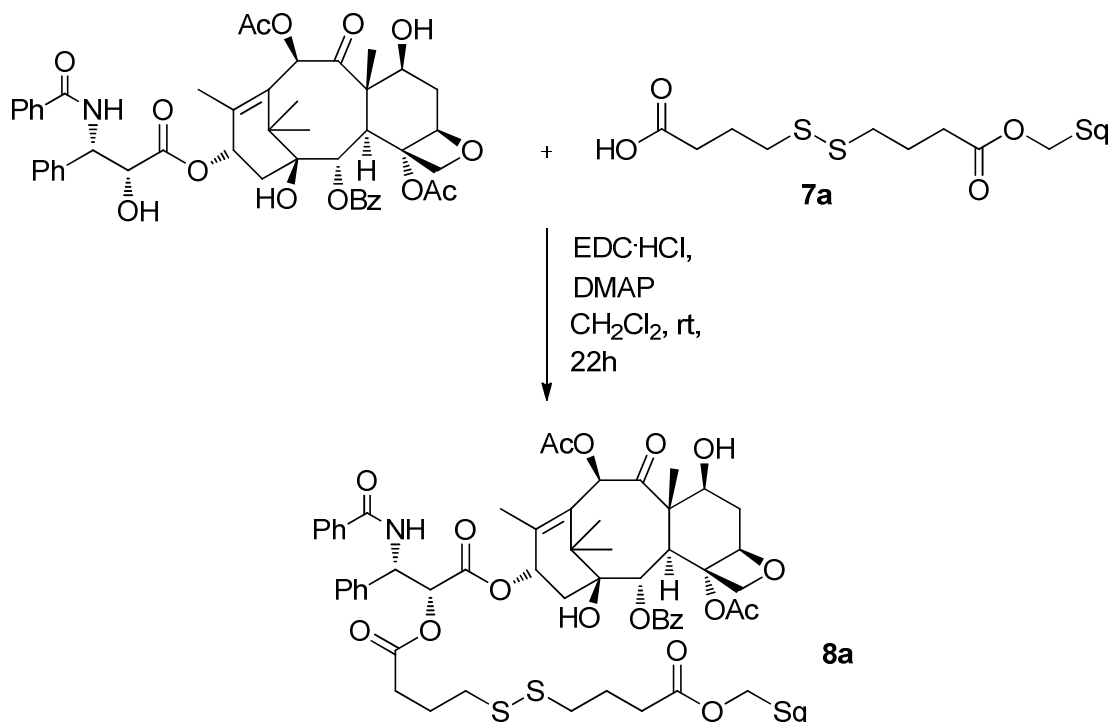
$^1\text{H-NMR}$ (CDCl_3 , 300 MHz): δ (ppm)= 5.06-5.12 (m, 5H); 4.03 (t, $J = 6.0$ Hz, 2H); 2.68-2.74 (m, 4H); 2.40-2.51 (m, 4H); 1.99-2.07 (m, 22H); 1.71-1.79 (m, 2H); 1.68 (s, 3H); 1.59 (s, 15H). **$^{13}\text{C-NMR}$** (CDCl_3 , 75 MHz): δ (ppm)= 178.0; 173.1; 135.1; 134.9; 133.6; 125.1; 124.3 (4C); 64.3; 39.7 (3C); 37.8; 37.6; 35.8; 32.6; 32.1; 28.2 (3C); 26.8; 26.7 (3C); 25.7; 24.3 (2C); 23.9; 17.7; 16.0 (3C); 15.9. **ESI-MS**: m/z 606.2 $[\text{M}-1]^+$.

Synthesis of **7b**

To a solution of **5** (0.100 g, 0.000258 mol) in dry CH₂Cl₂ (2.5 ml) sebacic acid (**6b**, 0.104 g, 0.000517 mol), EDC·HCl (0.060 g, 0.000310 mol) and DMAP (0.022 g, 0.000181 mol) are added and the reaction mixture is stirred at room temperature for 24 h. HCl 1M (15 ml) is added and extracted with CH₂Cl₂ (5x5 ml). The organic layers are dried over Na₂SO₄ and the solvent is removed under reduced pressure. The crude is purified by flash chromatography (AcOEt/Hex 1:3) to obtain **7b** as a colorless oil (0.051 g, Yield: 35%).

¹H-NMR (CDCl₃, 300 MHz): δ(ppm)= 5.06-5.13 (m, 5H); 4.02 (t, J = 9.0 Hz, 2H); 2.25-2.36 (m, 4H); 1.97-2.08 (m, 20H); 1.59-1.84 (m, 22H); 1.30 (bs, 8H). **¹³C-NMR** (CDCl₃, 75 MHz): δ(ppm)= 178.9; 173.9; 135.1; 134.9; 1337.7; 125.1; 124.3 (4C); 64.0; 39.7 (3C); 35.8; 34.3; 33.8; 29.7; 29.0 (4C); 28.2 (3C); 26.9; 26.7 (2C); 25.6; 24.9 (2C); 24.6; 17.7; 16.0 (4C). **ESI-MS**: m/z 507.3 [M-1]⁺.

Synthesis of 8a

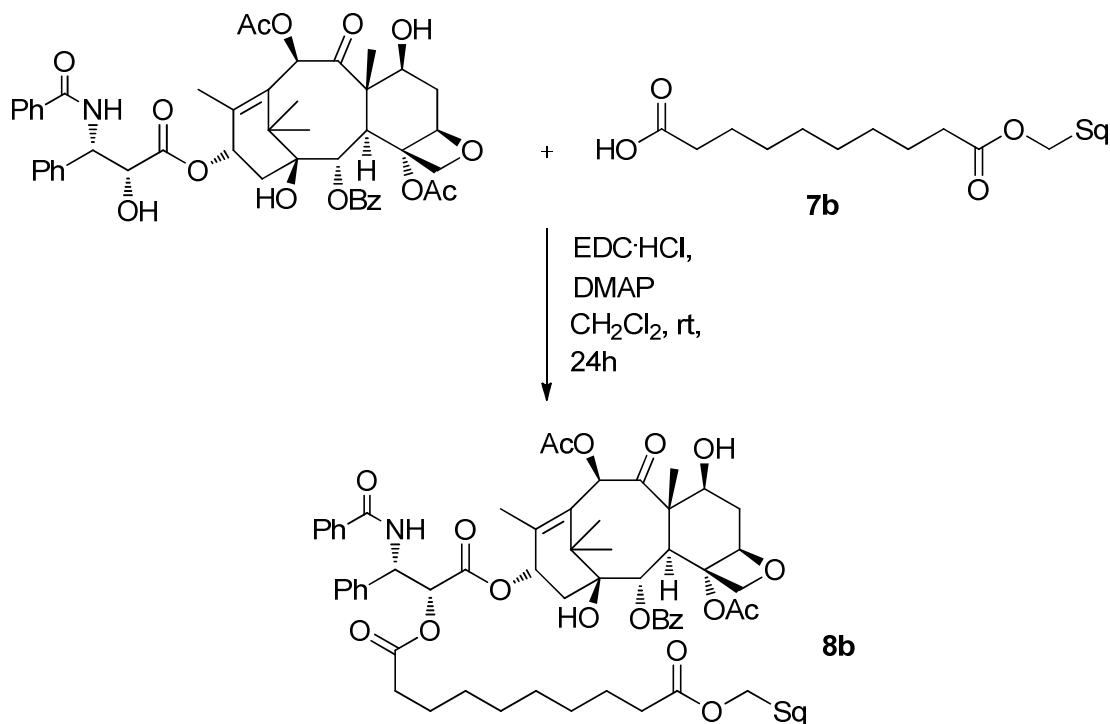


To a solution of **7a** (0.024 g, 0.000494 mol), in dry CH₂Cl₂ (2.5 ml) EDC·HCl (0.013 g, 0.000659 mol) and DMAP (0.003 g, 0.000231 mol) are added. Then paclitaxel (0.020 g, 0.000330 mol) is added and the reaction mixture is stirred at room temperature for 22h. HCl 1M (15 ml) is added and extracted with CH₂Cl₂ (5x5 ml). The organic layers are dried over Na₂SO₄ and the solvent is removed under reduced pressure. The crude is purified by flash chromatography (AcOEt/Hex from 1:2 to 1:1) to obtain **8a** as a white solid (0.025 g, Yield: 65%).

¹H-NMR (CDCl₃, 400 MHz): δ(ppm)= 8.17 (d, J = 7.1Hz, 2H); 7.77 (d, J = 7.1 Hz, 2H); 7.63 (t, J = 7.1 Hz, 1H); 7.51-7.56 (m, 3H); 7.35-7.47 (m, 10H); 6.93 (d, J = 9.3 Hz, 1H); 6.32 (s, 1H); 6.28 (t, J = 9.0 Hz, 1H); 6.00 (dd, J = 9.2 Hz, J = 3.1 Hz, 1H); 5.71 (d, J = 7.1 Hz, 1H); 5.53 (d, J = 3.1 Hz, 1H); 5.32 (s, 2H); 5.10-5.16 (m, 5H); 5.00 (d, J = 7.6 Hz, 1H); 4.50 (dd, J = 10.9 Hz, J = 6.6 Hz, 1H); 4.34 (d, J = 8.4 Hz, 1H); 4.23 (d, J = 8.4 Hz, 1H); 4.05 (t, J = 6.7 Hz, 2H); 3.84 (d, J = 7.0 Hz, 2H); 2.51-2.73 (m, 6H); 2.48 (s, 3H); 2.25 (t, J = 7.2 Hz, 2H); 2.25 (s, 3H); 2.15-2.22 (m, 2H); 1.87-2.13 (m, 20H); 1.68-1.79 (m, 8H); 1.63 (bs, 18H); 1.26 (s, 3H); 1.16 (bs, 3H).

¹³C-NMR (CDCl₃, 100 MHz, detected signals): δ(ppm)= 204.5; 173.6; 172.6; 171.9; 170.5; 168.7; 167.8; 143.5; 137.7; 135.8; 135.6; 134.4; 134.3; 133.5; 132.7; 130.9; 129.8; 129.4; 129.2; 127.8; 127.2; 125.8; 125.0; 124.9; 85.1; 81.7; 79.9; 77.1; 76.3; 75.8; 74.7; 72.8; 72.5; 65.0; 59.2; 53.4; 46.3; 43.9; 40.4; 38.4; 37.8; 36.5; 36.3; 33.3; 32.7; 29.0; 27.6; 27.5; 27.4; 26.4; 24.9; 24.6; 23.4; 22.8; 21.5; 18.3; 16.7; 16.6; 15.5. **ESI-MS** (C₈₂H₁₀₇NO₁₇S₂): m/z 1465.8 [M+Na]⁺. [α]_D²² = -46.2300 (c = 0.100, CHCl₃).

Synthesis of **8b**



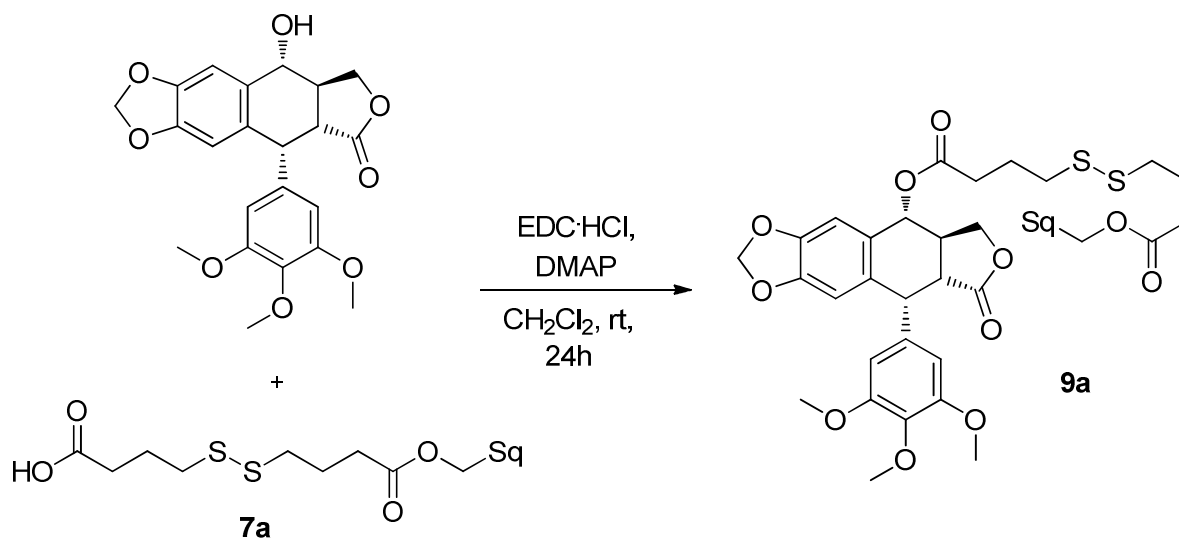
To a solution of **7b** (0.017 g, 0.000035 mol), in dry CH₂Cl₂ (1.5 ml) EDC·HCl (0.009 g, 0.000046 mol) and DMAP (0.002 g, 0.000016 mol) are added. Then paclitaxel (0.019 g, 0.000023 mol) is added and the reaction mixture is stirred at room temperature for 24h. HCl 1M (15 ml) is added and extracted with CH₂Cl₂ (5x5 ml). The organic layers are dried over Na₂SO₄ and the solvent is removed under reduced pressure. The crude is purified by flash chromatography (AcOEt/Hex from 1:2 to 1:1) to obtain **8b** as a white solid (0.013 g, Yield: 40%).

¹H-NMR (CD₃OD, 400 MHz, detected signals): δ(ppm)= 8.14 (d, J = 8.0 Hz, 2H); 7.83 (d, J = 8.0 Hz, 2H); 7.70 (t, J = 7.2 Hz, 1H); 7.44-7.63 (m, 10H); 7.29 (t, J = 7.2 Hz, 1H); 6.48 (s, 1H); 6.09 (t, J = 6.8 Hz, 1H); 5.87 (d, J = 6.4 Hz, 1H); 5.66 (d, J = 7.2 Hz, 1H); 5.11-5.16 (m, 5H); 5.02 (d, J = 8.0 Hz, 1H); 4.37 (dd, J = 11.2 Hz, J = 6.8 Hz, 1H); 4.21 (s, 2H); 4.05 (t, J = 6.8 Hz, 2H); 3.84 (d, J = 7.2 Hz, 1H); 2.43-2.50 (m, 5H); 2.30 (t, J = 8.0 Hz, 2H); 2.19 (s, 3H); 1.99-2.15 (m, 16H); 1.95 (s, 2H); 1.72-1.88 (m, 6H); 1.68 (bs, 6H); 1.63 (bs, 15H); 1.28 (bs, 8H); 1.56 (bs, 6H). **¹³C-NMR** (CD₃OD, 100 MHz, detected signals): δ(ppm)= 203.8; 174.2; 174.0;

166

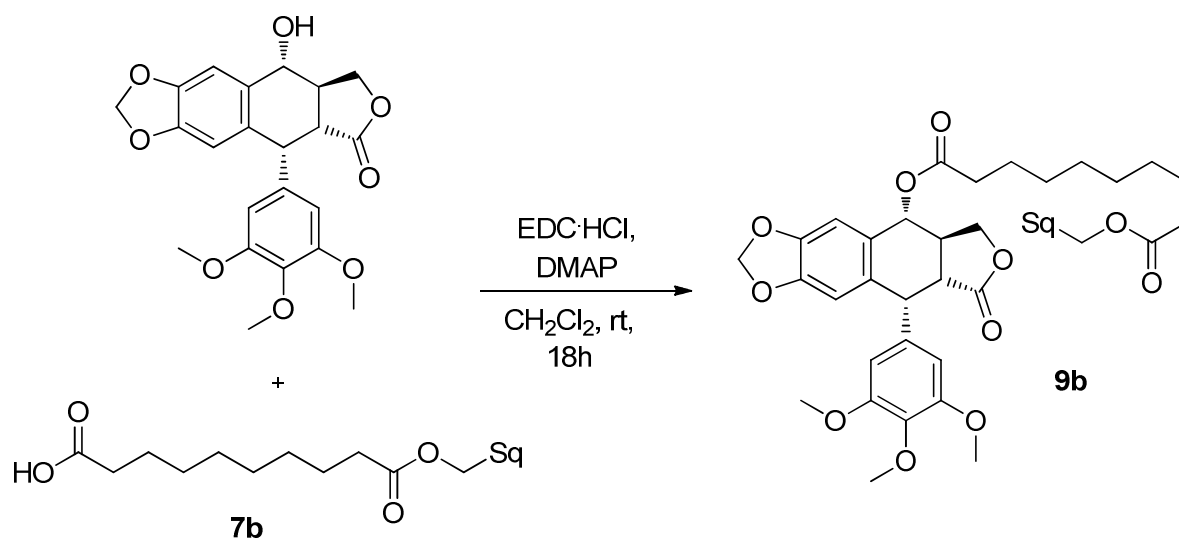
170.2; 169.9; 169.1; 166.3; 141.0; 137.0; 134.6; 134.4; 134.2; 133.5;
133.2; 131.5; 130.6; 130.0; 129.8; 128.7; 128.5; 128.3; 128.2; 127.2;
124.9; 124.3; 124.2; 124.1; 84.5; 80.9; 77.7; 76.1; 75.4; 74.9; 74.3; 71.5;
70.9; 63.6; 57.9; 53.9; 46.5; 43.2; 39.4; 39.3; 36.1; 35.5; 35.1; 33.8; 33.2;
28.7; 28.5; 27.8; 26.6; 26.5; 26.2; 26.1; 25.6; 24.7; 24.5; 21.9; 21.0; 19.4;
14.8; 14.6; 13.5; 9.0. **ESI-MS** ($C_{84}H_{111}NO_{17}$): m/z 1429.9 $[M+Na]^+$. $[\alpha]_D^{22} =$
-24.0900 ($c = 0.100$, $CHCl_3$).

Synthesis of 9a



To a solution of **7a** (0.088 g, 0.000145 mol), in dry CH₂Cl₂ (2 ml) EDC·HCl (0.042 g, 0.000219 mol) and DMAP (0.012 g, 0.000098 mol) are added. Then podophyllotoxin (0.060 g, 0.000145 mol) is added and the reaction mixture is stirred at room temperature for 24h. HCl 1M (10 ml) is added and extracted with CH₂Cl₂ (3x4 ml). The organic layers are dried over Na₂SO₄ and the solvent is removed under reduced pressure. The crude is purified by flash chromatography (CH₂Cl₂/MeOH 20:1) to obtain **9a** as a white solid (0.069 g, Yield: 48%).

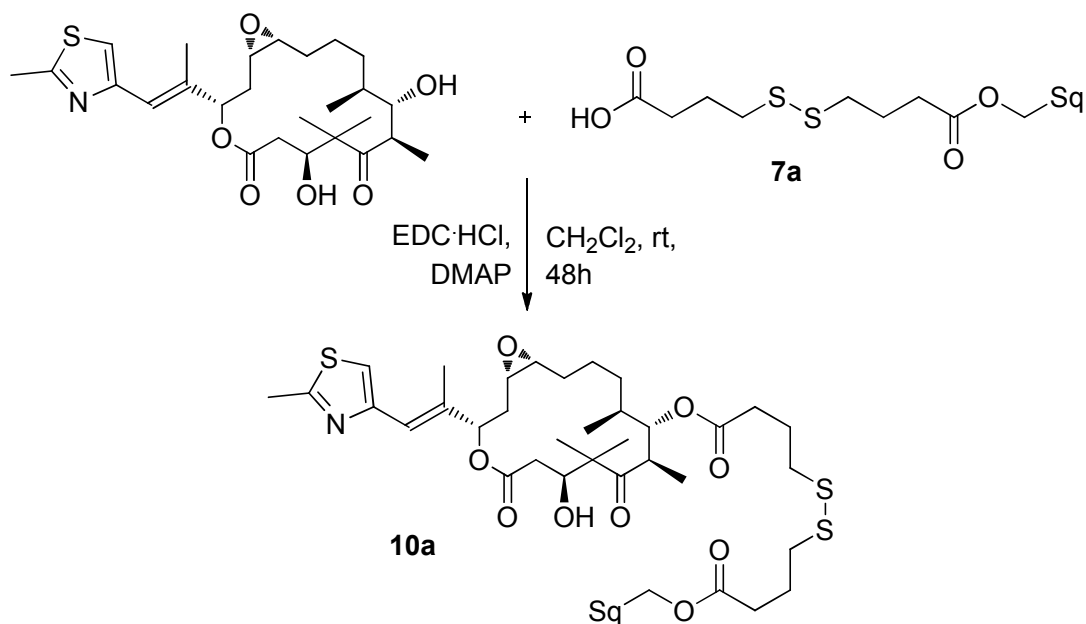
¹H-NMR (CDCl₃, 400 MHz): δ(ppm)= 6.79 (s, 1H); 6.57 (s, 1H); 6.42 (bs, 2H); 6.02 (d, J = 1.0 Hz, 1H); 6.00 (d, J = 1.0 Hz, 1H); 5.92 (dd, J = 9.0 Hz, J = 4.0 Hz, 1H); 5.10-5.17 (m, 5H); 4.63 (d, J = 4.2 Hz, 1H); 4.37-4.42 (m, 1H); 4.19-4.25 (m, 1H); 4.07 (t, J = 6.7 Hz, 2H); 3.83 (s, 3H); 3.79 (s, 6); 2.83-2.98 (m, 2H); 2.73-2.80 (m, 4H); 2.55-2.64 (m, 2H); 2.46 (t, J = 6.8 Hz, 2H); 1.95-2.28 (m, 20H); 1.74-1.80 (m, 4H); 1.70 (s, 3H); 1.65 (s, 15H). **¹³C-NMR** (CDCl₃, 100 MHz): δ(ppm)= 125.2; 124.3 (2C); 109.8; 108.3 (2C); 107.00; 101.6; 73.8; 71.3; 64.3; 60.7; 56.2; 45.6; 43.8; 39.7 (2C); 38.7; 37.8; 37.7; 35.8; 33.1; 32.6 (2C); 28.3; 26.7; 26.0; 25.2; 24.5 (2C); 24.3; 24.1 (2C); 16.0 (5C). **ESI-MS** (C₅₇H₇₈O₁₁S₂): m/z 1025.6 [M+Na]⁺. [α]_D²² = -51.607 (c = 0.100, CHCl₃).

Synthesis of **9b**

To a solution of **7b** (0.055 g, 0.000097 mol), in dry CH₂Cl₂ (1.5 ml) EDC.HCl (0.037 g, 0.000194 mol) and DMAP (0.008 g, 0.000068 mol) are added. Then podophyllotoxin (0.040 g, 0.000097 mol) is added and the reaction mixture is stirred at room temperature for 18h. HCl 1M (10 ml) is added and extracted with CH₂Cl₂ (3x4 ml). The organic layers are dried over Na₂SO₄ and the solvent is removed under reduced pressure. The crude is purified by flash chromatography (AcOEt/Hex 1:2) to obtain **9b** as a white solid (0.029 g, Yield: 31%).

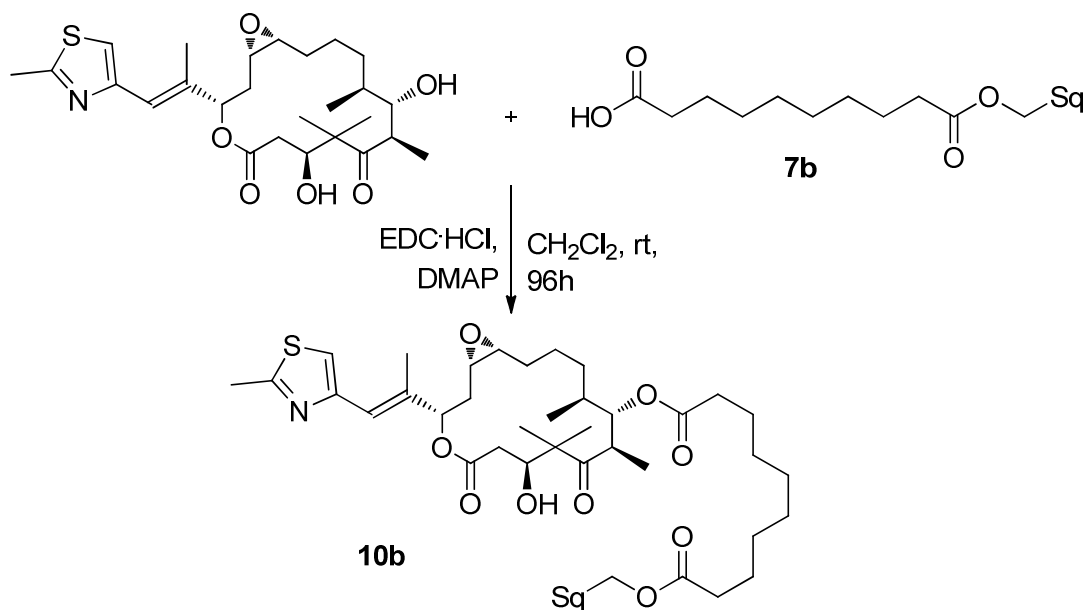
¹H-NMR (CDCl₃, 400 MHz): δ(ppm)= 6.77 (s, 1H); 6.57 (s, 1H); 6.42 (s, 2H); 6.01 (d, J = 6.5 Hz, 2H); 5.91 (d, J = 9.0 Hz, 1H); 5.11-5.21 (m, 5H); 4.63 (d, J = 4.1 Hz, 1H); 4.39 (t, J = 7.8 Hz, 1H); 4.23 (t, J = 7.8 Hz, 1H); 4.06 (t, J = 6.7 Hz, 2H); 3.84 (s, 3H); 3.77 (s, 6H); 2.96 (dd, J = 9.0 Hz, J = 4.5 Hz, 1H); 2.79-2.90 (m, 1H); 2.30-2.47 (m, 16H); 1.52-1.78 (m, 24H); 1.35 (bs, 8H). **¹³C-NMR** (CDCl₃, 100 MHz, detected signals): δ(ppm)= 152.7; 134.99; 134.87; 132.36; 131.85; 128.46; 125.09; 124.41 (2C); 124.29 (2C); 109.75; 108.20 (2C); 106.99; 101.60 (2C); 73.44 (2C); 71.40; 64.02; 60.77; 56.19 (2C); 45.64; 43.79; 39.75 (3C); 38.79; 35.81; 34.36 (2C); 29.71; 29.11 (4C); 28.28 (3C); 26.95; 26.69 (2C); 24.97 (3C). **ESI-MS** (C₅₉H₈₂O₁₁): m/z 990.6 [M+Na]⁺. [α]_D²² = -53.0800 (c = 0.100, CHCl₃).

Synthesis of 10a



To a solution of **7a** (0.024 g, 0.000494 mol), in dry CH₂Cl₂ (2.5 ml) EDC·HCl (0.013 g, 0.000659 mol) and DMAP (0.003 g, 0.000231 mol) are added. Then epothilone (0.020 g, 0.000330 mol) is added and the reaction mixture is stirred at room temperature for 48h. HCl 1M (15 ml) is added and extracted with CH₂Cl₂ (5x5 ml). The organic layers are dried over Na₂SO₄ and the solvent is removed under reduced pressure. The crude is purified by flash chromatography (AcOEt/Hex from 1:2 to 1:1) to obtain **10a** as a white solid (0.025 g, Yield: 31%).

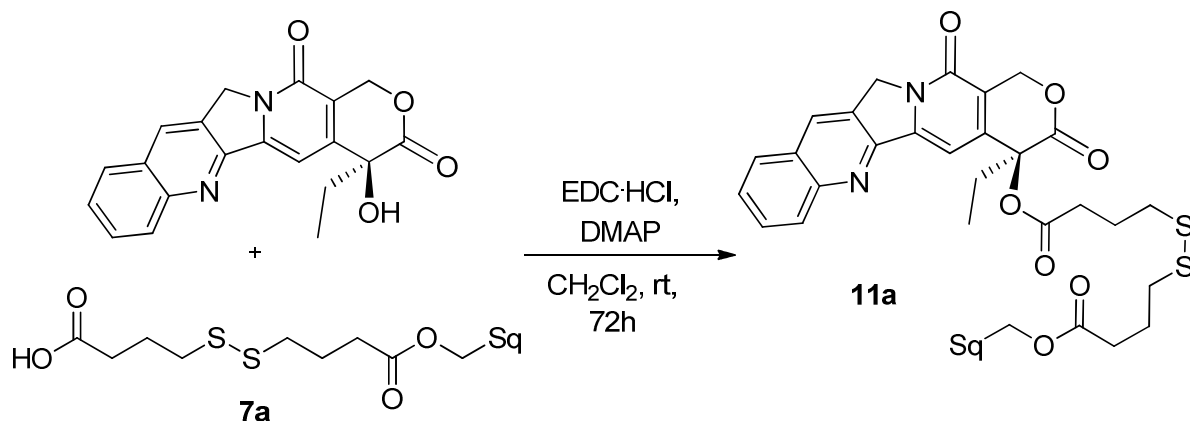
¹H-NMR (CDCl₃, 400 MHz): δ(ppm)= 7.05 (s, 1H); 6.73 (s, 1H); 5.71 (dd, J = 11.4 Hz, J = 2.4 Hz, 1H); 5.55 (d, J = 7.9 Hz, 1H); 5.46 (d, J = 6.2 Hz, 1H); 5.37 (d, J = 7.1 Hz, 1H); 5.10-5.17 (m, 5H); 4.15-4.21 (m, 1H); 4.07 (t, J = 6.7 Hz, 2H); 3.28-3.44 (m, 1H); 3.00-3.11 (m, 1H); 2.89-2.97 (m, 1H); 2.65-2.82 (m, 8H); 2.38-2.64 (m, 6H); 1.98-2.18 (m, 20H); 1.80-1.95 (m, 2H); 1.71-1.78 (m, 4H); 1.70 (s, 3H); 1.49-1.68 (m, 21H); 1.41 (s, 3H); 0.90-1.33 (m, 9H). **¹³C-NMR** (CDCl₃, 100 MHz, detected signals): δ(ppm)= 216.4; 172.9; 172.5; 170.6; 135.1; 135.0; 133.6; 125.2; 124.4; 75.8; 71.2; 64.3; 57.6; 57.3; 54.9; 54.4; 43.3; 42.5; 39.7; 38.5; 37.9; 37.6; 36.1; 35.8; 34.6; 32.7; 30.9; 29.7; 28.3; 26.9; 26.7; 25.7; 24.3; 23.9; 16.9; 16.0; 15.5. **APCI-MS** (C₆₁H₉₅NO₉S₃): m/z 1082.6 [M]⁺. [α]_D²² = -7.5200 (c = 0.100, CHCl₃).

Synthesis of **10b**

To a solution of **7b** (0.020 g, 0.000035 mol), in dry CH₂Cl₂ (2 ml) EDC·HCl (0.013 g, 0.000070 mol) and DMAP (0.003 g, 0.000025 mol) are added. Then epothilone (0.026 g, 0.0000525 mol) is added and the reaction mixture is stirred at room temperature for 96h. HCl 1M (10 ml) is added and extracted with CH₂Cl₂ (4x3 ml). The organic layers are dried over Na₂SO₄ and the solvent is removed under reduced pressure. The crude is purified by flash chromatography (AcOEt/Hex 2:3) to obtain **10b** as a white solid (0.007 g, Yield: 19%).

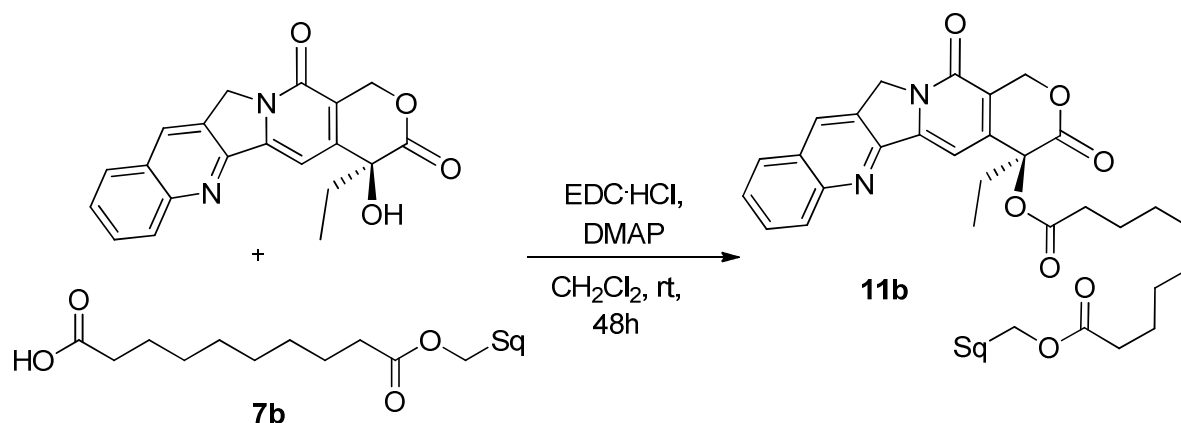
¹H-NMR (CDCl₃, 400 MHz, detected signals): δ(ppm)= 7.05 (s, 1H); 6.75 (s, 1H); 5.72 (dd, J = 11.4 Hz, J = 2.5 Hz, 1H); 5.56 (dd, J = 9.9 Hz, J = 2.2 Hz, 1H); 5.44 (m, 1H); 5.36 (d, J = 7.4 Hz, 1H); 5.10-5.14 (m, 5H); 4.20 (m, 1H); 4.05 (t, J = 6.7 Hz, 2H); 3.34-3.40 (m, 1H); 3.05-3.09 (m, 1H); 2.90-2.94 (m, 1H); 2.82 (m, 2H); 2.50-2.72 (m, 5H); 2.28-2.38 (m, 6H); 2.97-3.18 (m, 20H); 1.55-1.80 (m, 20H); 0.98-1.47 (m, 26H). **¹³C-NMR** (CDCl₃, 100 MHz, detected signals): δ(ppm)= 173.9; 173.4; 170.6; 135.1; 135.0; 133.7; 125.1; 124.4; 75.8; 70.8; 64.0; 57.7; 54.9; 43.6; 39.8; 38.8; 37.5; 36.1; 35.8; 34.4; 31.6; 29.7; 29.1; 28.3; 26.9; 26.7; 25.7; 25.1; 25.0; 24.0; 22.7; 17.5; 16.1; 15.9; 15.6. **ESI-MS** (C₆₃H₉₉NO₉S): m/z 1069.4 [M+Na]⁺. [α]_D²⁰ = -20.1800 (c = 0.100, CHCl₃).

Synthesis of 11a



To a solution of **7a** (0.023 g, 0.000038 mol), in dry CH₂Cl₂ (1.5 ml) EDC·HCl (0.015 g, 0.000076 mol) and DMAP (0.003 g, 0.000027 mol) are added. Then camptothecin (0.020 g, 0.000057 mol) is added and the reaction mixture is stirred at room temperature for 72h. HCl 1M (10 ml) is added and extracted with CH₂Cl₂ (3x4 ml). The organic layers are dried over Na₂SO₄ and the solvent is removed under reduced pressure. The crude is purified by flash chromatography (AcOEt 100%) to obtain **11a** as a yellow solid (0.012 g, Yield: 32%).

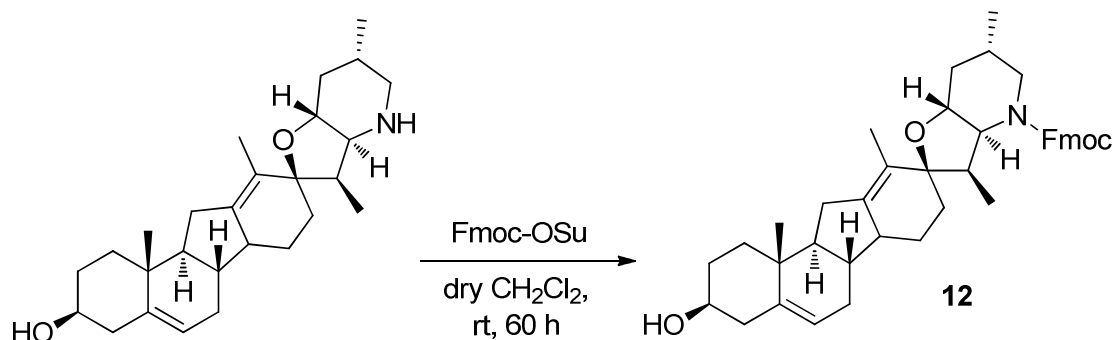
¹H-NMR (CDCl₃, 400 MHz): δ(ppm)= 8.42 (s, 1H); 8.25 (d, J = 8.0 Hz, 1H); 7.96 (d, J = 8.0 Hz, 1H); 7.86 (t, J = 8.0 Hz, 1H); 7.70 (t, J = 8.0 Hz, 1H); 7.24 (s, 1H); 5.70 (d, J = 17.2 Hz, 1H); 5.42 (d, J = 17.2 Hz, 1H); 5.31 (bs, 2H); 5.10-5.16 (m, 5H); 4.04 (t, J = 6.8 Hz, 2H); 2.61-2.76 (m, 6H); 2.40 (t, J = 7.3 Hz, 2H); 2.28- 2.33 (m, 1H); 2.15-2.20 (m, 1H); 1.98-2.09 (m, 22H); 1.62-1.76 (m, 20H); 1.00 (t, J = 7.5 Hz, 3H). **¹³C-NMR** (CDCl₃, 100 MHz): δ(ppm)= 173.6; 172.6; 168.2; 158.0; 153.0; 149.6; 147.0; 146.6; 135.8; 135.7; 134.3; 131.9; 131.4; 130.3; 129.2; 128.9; 128.7; 125.8; 125.0 (4C); 120.9; 96.6; 67.8; 64.9; 50.6; 40.4 (2C); 38.4; 37.9; 36.5; 33.3; 32.8; 32.5; 28.9 (2C); 27.6; 27.5 (2C); 26.4; 24.9; 24.6; 18.37; 16.7 (3C); 16.6; 8.3. **ESI-MS** (C₅₅H₇₂N₂O₇S₂): m/z 960.3 [M+Na]⁺. [α]_D²⁰ = -36.3200 (c = 0.100, CHCl₃).

Synthesis of **11b**

To a solution of **7b** (0.030 g, 0.000053 mol), in dry CH₂Cl₂ (1.5 ml) EDC·HCl (0.020 g, 0.000105 mol) and DMAP (0.004 g, 0.000037 mol) are added. Then camptothecin (0.027 g, 0.000079 mol) is added and the reaction mixture is stirred at room temperature for 48h. HCl 1M (10 ml) is added and extracted with CH₂Cl₂ (4x3 ml). The organic layers are dried over Na₂SO₄ and the solvent is removed under reduced pressure. The crude is purified by flash chromatography (AcOEt/Hex 1:1) to obtain **11b** as a yellow solid (0.013 g, Yield: 28%).

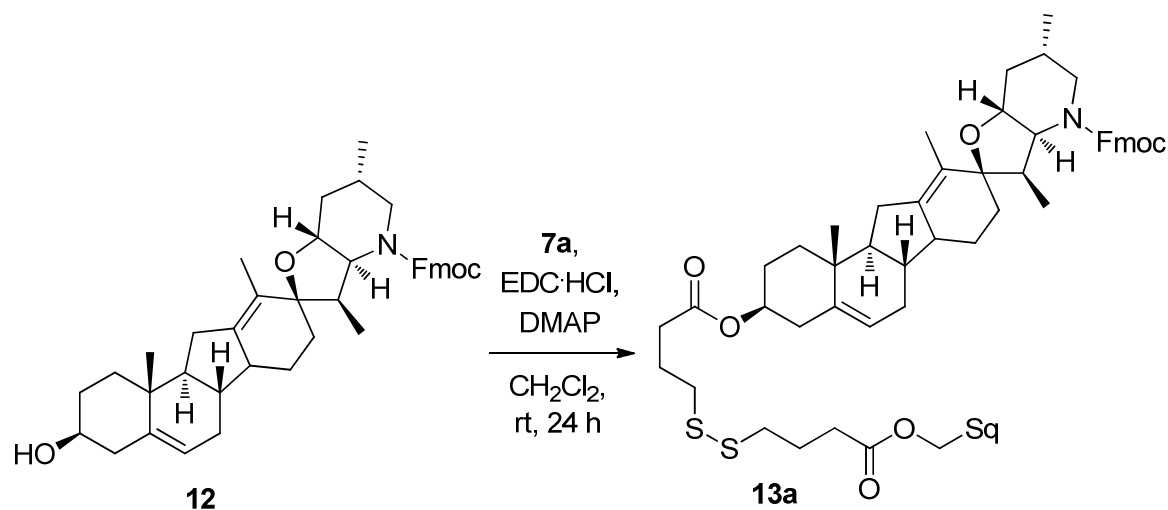
¹H-NMR (CDCl₃, 400 MHz): δ(ppm)= 8.42 (s, 1H); 8.24 (d, J = 8.0 Hz, 1H); 7.97 (d, J = 8.0 Hz, 1H); 7.86 (t, J = 8.0 Hz, 1H); 7.69 (t, J = 8.0 Hz, 1H); 7.24 (s, 1H); 5.70 (d, 16.0 Hz, 1H); 5.42 (d, J = 16.0 Hz, 1H); 5.31 (bs, 2H); 5.12-5.18 (m, 5H); 4.04(t, J = 7.5 Hz, 2H); 2.48-2.59 (m, 2H); 2.27-2.36 (m, 1H); 2.21-2.25 (m, 2H); 2.14-2.20 (m, 1H); 1.95-2.14 (m, 20H); 1.59-1.77 (m, 22H); 1.28 (bs, 8H); 1.00 (t, J = 8.1 Hz, 3H). **¹³C-NMR** (CDCl₃, 100 MHz, detected signals): δ(ppm)= 167.5; 146.0; 131.2; 130.6; 129.6; 128.5; 128.2; 128.0; 125.0; 124.4; 124.3; 120.4; 96.0; 67.1; 64.0; 49.9; 39.7; 35.8; 34.3; 33.8; 31.9; 29.7; 29.1; 29.0; 28.3; 26.9; 26.7; 25.7; 24.9; 24.6; 16.0; 7.6. **ESI-MS** (C₅₇H₇₆N₂O₇): m/z 924.2 [M+Na]⁺. [α]_D²⁰ = -21.30 00 (c = 0.175, CHCl₃).

Synthesis of 12



To a solution of cyclopamine (0.045 g, 0.000109 mol) in dry CH_2Cl_2 (2 ml) Fmoc-OSu (0.044 g, 0.000131 mol) is added and the reaction mixture is stirred at room temperature for 60 h. The solvent is then removed under reduced pressure and the crude material is purified by flash chromatography ($\text{CH}_2\text{Cl}_2/\text{MeOH}$ 10:0.05) to obtain **12** as a white solid (0.062 g, Yield: 92%).

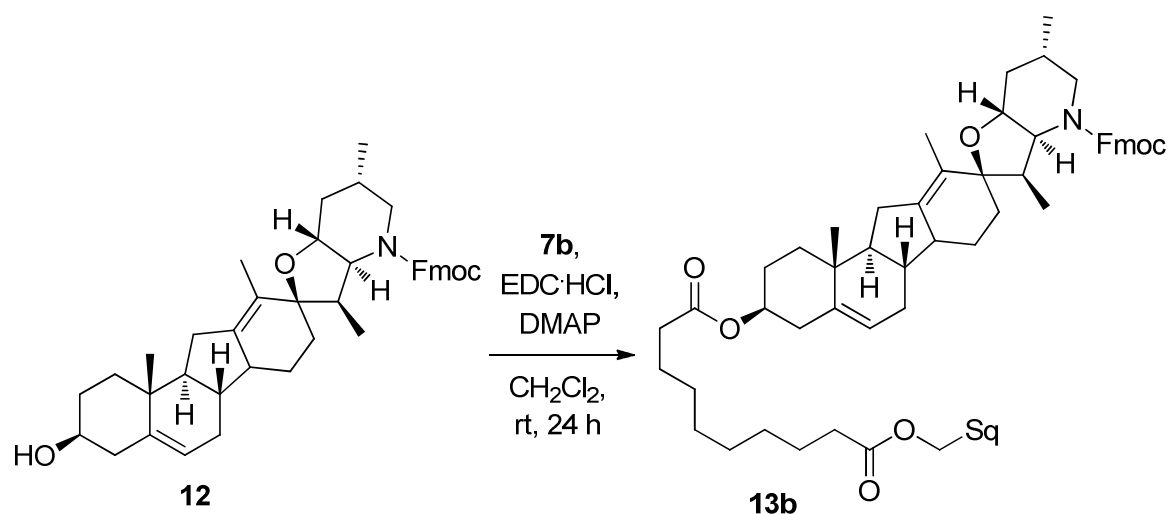
$^1\text{H-NMR}$: (CDCl_3 , 300 MHz): $\delta(\text{ppm})$ = 7.72 (dd, J = 7.2, 7.2 Hz, 2H); 7.58 (dd, J = 7.2, 2 Hz, 2H); 7.37 (dd, J = 16, 7.2 Hz, 2H); 7.30(ddd, J =14.8, 7.2, 1.2 Hz, 2H); 5.37(br d, J = 2.8 Hz, 1H); 4.68 (dd, J = 10.8, 5.2 Hz, 1H); 4.57(dd, J = 10.8, 5.6 Hz, 1H); 4.21 (dd, J = 5.2, 5.6 Hz, 1H); 3.54 (dd, J =12.8, 4.0 Hz, 2H); 3.44 (ddd, J = 11.6, 11.6, 4.0 Hz, 1H); 2.95 (dd, J = 9.6, 7.2 Hz, 1H); 2.75 (dd, J = 12.8, 8.4 Hz, 1H); 2.39-2.35 (m, 1H); 2.30-2.09 (m,5H), 1.75 (s, 3H); 1.85-1.63 (m, 5H); 1.59-1.49 (m, 1H), 1.46-1.39 (m, 4H); 1.35-1.27(m, 1H); 1.23 (ddd, J = 13.2, 3.2, 3.2 Hz, 1H); 1.02-0.88 (m, 2H); 0.93 (d, J = 6.8 Hz, 3H); 0.93 (s, 3H); 0.6 (s,3H). **$^{13}\text{C-NMR}$:** (CDCl_3 , 100 MHz): $\delta(\text{ppm})$ = 157.94; 143.97; 143.87; 142.59; 141.69; 141.45; 141.39; 127.65; 127.62; 127.09; 127.06; 126.66; 124.58; 121.79; 119.99; 119.95; 84.76; 72.63; 71.73; 66.58; 52.05; 51.05; 49.19; 47.31; 41.78; 41.57; 41.50; 38.21; 36.56; 35.22; 32.63; 31.35; 31.08; 30.89; 29.00; 28.28; 24.60; 20.26; 18.66; 13.63; 10.23. **ESI-MS:** m/z 634.67 [$\text{M}^+ \text{H}$] $^+$. $[\alpha]_{\text{D}}^{32} = -7.5462$ ($c = 0.067$, CHCl_3).

Synthesis of **13a**

To a solution of **12** (0.030 g, 0.000047 mol) in CH_2Cl_2 (1 ml) **7a** (0.029 g, 0.000047 mol), EDC·HCl (0.011 g, 0.000057 mol) and DMAP (0.005 g, 0.000040 mol) are added and the reaction mixture is stirred at room temperature for 24 h. The solvent is then removed under reduced pressure and the crude material is purified by flash chromatography (CH_2Cl_2 /Hex 8:2) to obtain **13a** as a colorless oil (0.030 g, Yield: 52%).

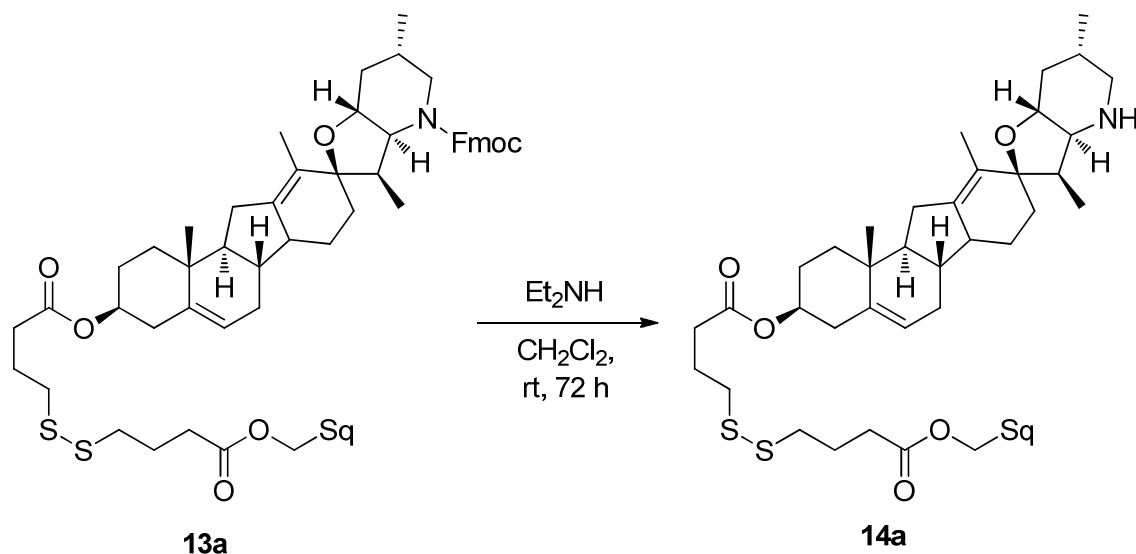
$^1\text{H-NMR}$: (CDCl_3 , 300 MHz): δ (ppm)= 7.68-7.80 (m, 2H); 7.51-7.60 (m, 2H); 7.22-7.41 (m, 4H); 5.35-5.45 (m, 1H); 5.06-5.20 (m, 5H); 4.50-4.74 (m, 2H); 4.00-4.25 (m, 4H); 3.27-3.70 (m, 2H); 2.92-2.97 (m, 1H); 2.69-2.80 (m, 4H); 2.40-2.45 (m, 4H); 0.91-2.38 (m, 74H). **ESI-MS**: m/z 1246.1 $[\text{M}+\text{Na}]^+$. $[\alpha]_{\text{D}}^{31} = -4.9062$ ($c = 0.133$, CHCl_3).

Synthesis of 13b



To a solution of **12** (0.031 g, 0.000049 mol) in CH₂Cl₂ (1 ml) **7b** (0.028 g, 0.000049 mol), EDC·HCl (0.011 g, 0.000058 mol) and DMAP (0.005 g, 0.000041 mol) are added and the reaction mixture is stirred at room temperature for 24 h. The solvent is then removed under reduced pressure and the crude material is purified by flash chromatography (CH₂Cl₂/Hex 13:7) to obtain **13b** as a colorless oil (0.027 g, Yield: 47%).

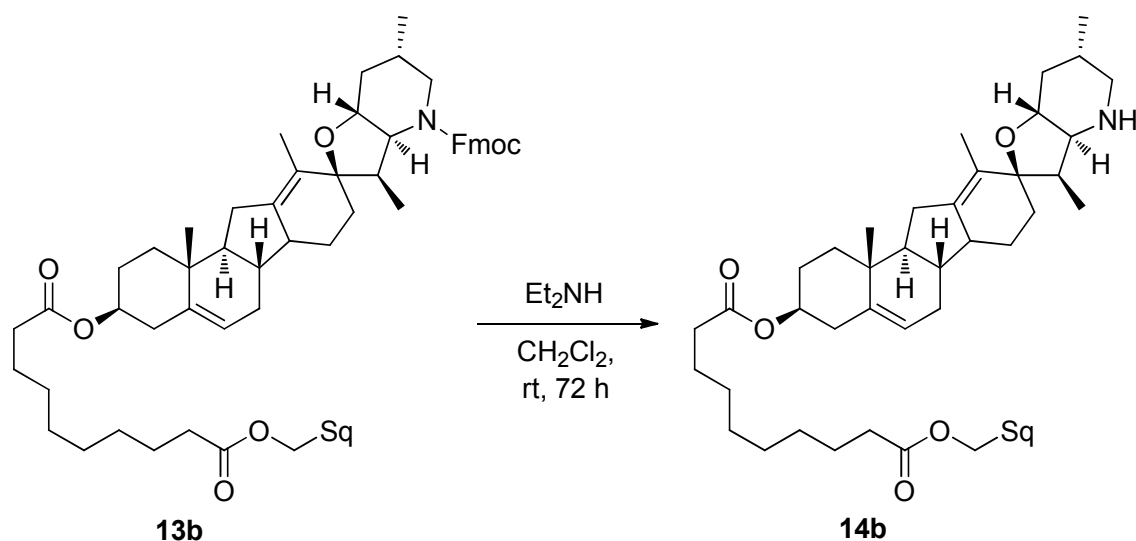
¹H-NMR: (CDCl₃, 300 MHz): δ(ppm)= 7.65-2.80 (m, 2H); 7.50-2.75 (m, 2H); 7.13-7.50 (m, 4H); 5.31-5.45 (m, 1H); 5.00-5.20 (m, 5H); 4.50 - 4.70 (m, 2H); 4.13-4.25 (m, 1H); 3.92-4.10 (m, 3H); 2.75-3.30 (m, 2H); 2.69-2.80 (m, 1H); 0.67-2.45 (m, 88H). **ESI-MS:** m/z 1209.3 [M+Na]⁺. [α]_D³¹ = -5.5589 (c = 0.133, CHCl₃).

Synthesis of **14a**

To a solution of **13a** (0.030 g, 0.000024 mol) in CH_2Cl_2 (0.6 ml) diethylamine (0.106 g, 0.001447 mol) was added and the reaction mixture was stirred at room temperature for 72 h. The volatiles were then removed under reduced pressure and the crude material was purified by flash chromatography (from 100% CH_2Cl_2 to AcOEt/MeOH 25:1) to obtain **14a** as a colorless oil (0.013 g, Yield: 52%).

$^1\text{H-NMR}$: (CDCl_3 , 300 MHz): δ (ppm)= 5.40 (m, 1H); 5.03-5.20 (m, 5H); 4.56-4.70 (m, 2H); 4.03 (t, $J = 7.1\text{Hz}$, 2H); 3.32-3.51 (m, 2H); 3.14-3.25 (m, 1H); 2.71 (t, $J = 7.1 \text{ Hz}$, 4H); 2.37-2.46 (m, 4H); 0.81-2.32 (m, 76H). **$^{13}\text{C-NMR}$** : (CDCl_3 , 75 MHz, detected signals): δ (ppm)= 172.94; 172.27; 144.25; 142.67; 140.42; 135.10; 134.45; 133.60; 126.95; 125.19; 125.12; 124.38; 124.36; 134.20; 122.78; 86.32; 84.67; 73.92; 69.82; 64.62; 64.30; 51.85; 49.05; 41.51; 39.72; 39.64; 39.59; 39.57; 38.22; 37.84; 37.63; 36.60; 35.76; 33.68; 32.96; 31.03; 29.67; 29.14; 28.90; 28.39; 28.24; 27.51; 26.84; 26.75; 26.64; 26.57; 24.29; 24.21; 24.16; 19.30; 18.55; 18.42; 17.65; 16.02; 15.85; 13.69; 13.09; 10.72. **ESI-MS**: m/z 1000.9 $[\text{M}+1]^+$. $[\alpha]_{\text{D}}^{31} = -12.0955$ ($c = 0.660$, CHCl_3).

Synthesis of 14b

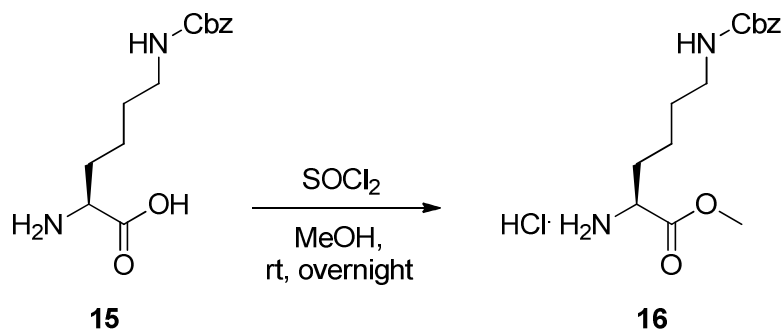


To a solution of **13b** (0.027 g, 0.000023 mol) in CH_2Cl_2 (0.6 ml) diethylamine (0.098 g, 0.001342 mol) was added and the reaction mixture was stirred at room temperature for 72 h. The volatiles were then removed under reduced pressure and the crude material was purified by flash chromatography (from 100% CH_2Cl_2 to AcOEt/MeOH 25:1) to obtain **14b** as a colorless oil (0.007 g, Yield: 29%).

$^1\text{H-NMR}$: (CDCl_3 , 300 MHz): δ (ppm)= 5.38-5.42 (m, 1H); 5.00- 5.20 (m, 5H); 4.50-4.70 (m, 2H); 4.02 (t, J = 6.4Hz, 2H); 3.25-3.40 (m, 1H); 3.11-3.19 (m, 1H); 2.68-2.79 (m, 1H); 2.48-2.62 (m, 1H); 0.80-2.45 (m, 87H).

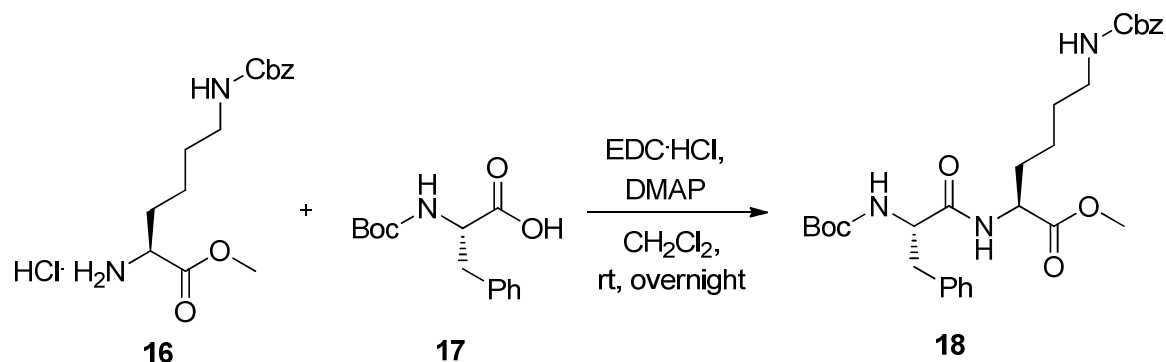
$^{13}\text{C-NMR}$: (CDCl_3 , 75 MHz, detected signals): δ (ppm)= 173.87; 173.20; 144.29; 140.51; 134.96; 133.67; 125.04; 124.37; 124.25; 122.66; 86.34; 73.54; 63.95; 51.86; 49.05; 39.71; 39.64; 35.77; 34.33; 29.06; 28.24; 26.89; 26.63; 24.96; 18.56; 18.41; 17.65; 16.00; 15.83; 13.08. **ESI-MS**: m/z 965.0 $[\text{M}+1]^+$. $[\alpha]_{\text{D}}^{31} = -17.9880$ ($c = 0.467$, CHCl_3).

Synthesis of 16



H-Lys(Z)-OH (**15**, 0.500 g, 0.001786 mol) is suspended in MeOH (17 ml). At 0°C, SOCl₂ (0.257 ml, 0.003571 mol) is added dropwise and the reaction mixture is stirred overnight at room temperature. The volatiles are then removed under reduced pressure, affording **16** as a white solid without any further purification (0.580 g, Yield: 99%).

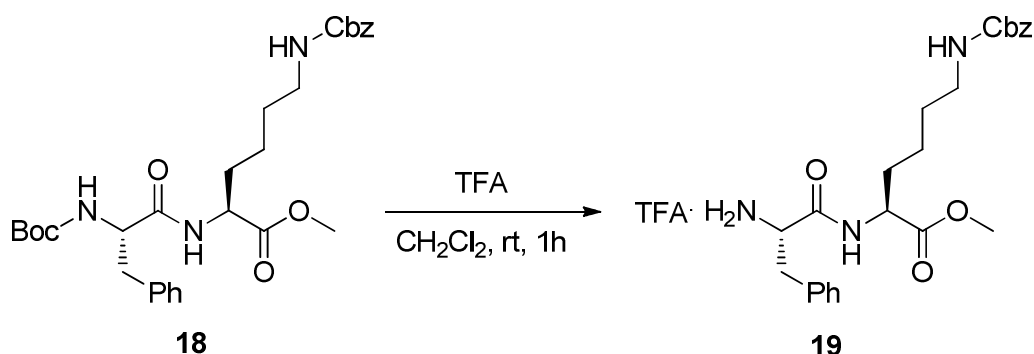
¹H-NMR (CDCl₃, 300 MHz): δ (ppm)= 8.69 (bs, 3H); 7.31 (bs, 5H); 5.50 (bs, 1H); 5.05 (s, 2H); 4.10 (bs, 1H); 3.74 (s, 3H); 3.16 (bs, 2H); 2.51 (bs, 2H); 2.02 (bs, 2H); 1.51 (bs, 2H). **¹³C-NMR** (CDCl₃, 75 MHz): δ (ppm)= 169.9; 156.7; 136.7; 128.5 (2C); 128.0 (2C); 127.9; 65.5; 53.3; 53.0; 40.3; 29.7; 28.9; 21.9. $[\alpha]_{\text{D}}^{22}$: +11.676 (c=0.800, CHCl₃).

Synthesis of **18**

To a solution of **16** (1.178 g, 0.003570 mol) in CH₂Cl₂ (35 ml) DMAP (0.740 g, 0.006068 mol) is added. Boc-Phe-OH (**17**, 0.946 g, 0.003570 mol) and EDC·HCl (1.028 g, 0.005355 mol) are then added and the reaction mixture is stirred overnight at room temperature.

The solvent is then removed under reduced pressure and the crude residue is purified by flash chromatography (AcOEt:Hex from 1:2 to 2:1) affording **18** as a white solid (1.196 g, Yield: 62%).

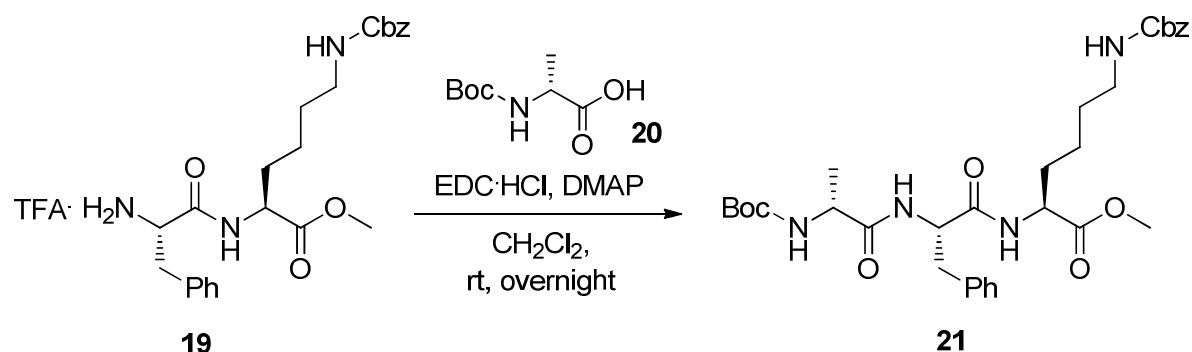
¹H-NMR (CD₃OD, 300 MHz): δ (ppm)= 7.13-7.33 (m, 10H); 6.69 (bs, 1H); 5.03-5.22 (m, 4H); 4.48-4.55 (m, 1H); 3.67 (s, 3H); 2.90-3.18 (m, 4H); 1.45-1.86 (m, 4H); 1.37 (s, 9H); 1.06-1.30 (m, 2H). **¹³C-NMR** (CD₃OD, 75 MHz): δ (ppm)= 172.2; 171.2; 156.5; 155.5; 136.6 (2C); 129.3 (3C); 128.6 (4C); 128.1 (2C); 126.9; 80.2; 66.7; 57.8; 52.4; 51.9; 40.5; 38.1; 31.9; 29.2; 28.3; 22.1. $[\alpha]_{D}^{33}$: -14.636 (c=0.450, CH₃OH).

Synthesis of **19**

To a solution of **18** (0.127 g, 0.000234 mol) in CH_2Cl_2 (2 ml) TFA (1.5 ml) is added and the reaction mixture is stirred at room temperature for 1h. The volatiles are then removed under reduced pressure, affording **19** as a white solid without any further purification (0.130 g, Yield: 99%).

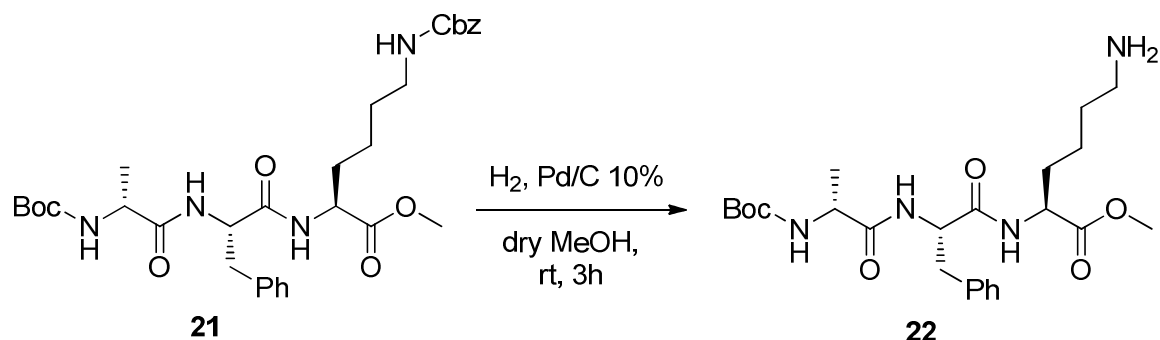
¹H-NMR (CD_3OD , 300 MHz): δ (ppm)= 8.20 (bs, 3H); 7.67 (bs, 1H); 7.11-7.42 (m, 10H); 5.15 (bs, 1H); 4.99 (s, 2H); 4.40 (bs, 1H); 4.29 (bs, 1H); 3.61 (s, 3H); 2.95-3.30 (m, 4H); 1.12-1.86 (m, 6H). **¹³C-NMR** (CD_3OD , 75 MHz): δ (ppm)= 173.7; 170.0; 159.3; 138.7; 135.8; 130.9 (2C); 130.4 (2C); 129.8; 129.2 (5H); 67.7; 55.8; 54.2; 53.1; 41.8; 38.8; 32.4; 30.7; 24.2. **ESI-MS**: 442 [M-TFA+1]⁺. $[\alpha]_{\text{D}}^{33}$: +0.958 (c=1.050, CH_3OH).

Synthesis of 21



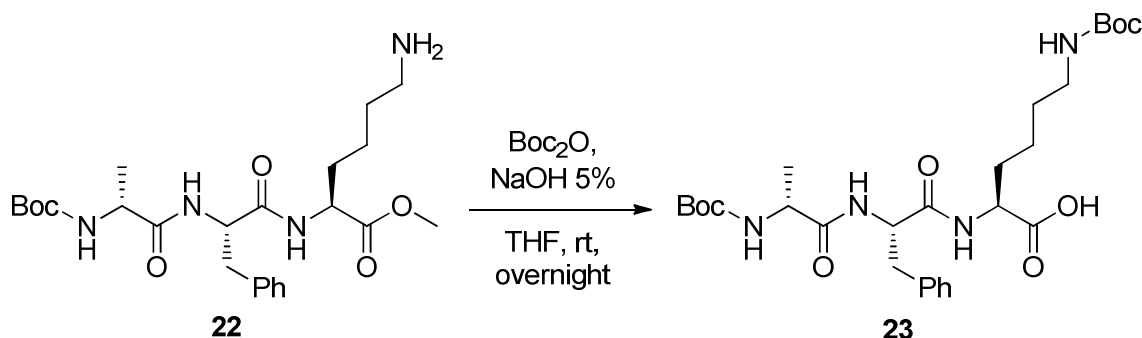
To a solution of **19** (0.525 g, 0.000946 mol) in CH₂Cl₂ (9 ml) DMAP (0.231 g, 0.001892 mol) is added. Boc-D-Ala-OH (**20**, 0.179 g, 0.000946 mol) and EDC·HCl (0.272 g, 0.001419 mol) are then added and the reaction mixture is stirred overnight at room temperature. The solvent is then removed under reduced pressure and the crude residue is purified by flash chromatography (AcOEt:Hex 1:2) affording **21** as a white solid (0.496 g, Yield: 85%).

¹H-NMR (CD₃OD, 300 MHz): δ (ppm)= 7.16-7.39 (m, 10H); 6.59-6.62 (m, 2H); 5.04-5.29 (m, 4H); 4.46-4.63 (m, 3H); 3.68 (s, 3H); 3.02-3.23 (m, 4H); 0.97-1.84 (m, 18H). **¹³C-NMR** (CD₃OD, 75 MHz): δ (ppm)= 173.1; 172.2; 170.7; 156.6; 155.7; 136.6 (2C); 129.3 (2C); 128.6 (3C); 128.1 (3C); 126.9; 80.2; 66.7; 54.3; 52.3; 52.0; 50.1; 40.4; 37.3; 31.2; 29.0; 28.3 (3C); 22.2; 17.9. **ESI-MS**: 636 [M+Na]⁺. **[α]_D²²**: -9.115 (c=1.000, CH₃OH).

Synthesis of **22**

To a solution of **21** (1.125 g, 0.001835 mol) in dry MeOH (28 ml) Pd/C 10% (0.195 g, 0.000183 mol) is added and the reaction mixture is stirred under H₂ pressure at room temperature for 3 hours. After filtration over celite and evaporation of the solvent under reduced pressure, the desired **22** is obtained as a white solid without any further purification (0.866 g, Yield: 98%).

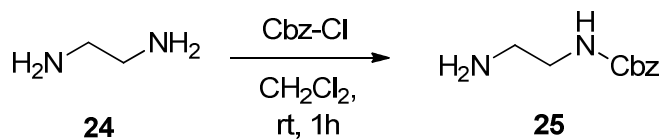
¹H-NMR (CD₃OD, 300 MHz): δ (ppm)= 7.18-7.32 (m, 5H); 4.62-4.66 (m, 1H); 4.37-4.48 (m, 1H); 3.90-3.97 (m, 1H); 3.68 (s, 3H); 3.30 (bs, 2H); 2.88 (dd, J = 13.9 Hz, J = 9.8 Hz, 1H); 2.66 (t, J = 6.5 Hz, 2H); 1.76-1.88 (m, 2H); 1.48-1.50 (m, 2H); 1.41 (s, 9H); 1.06 (d, J = 7.0 Hz, 3H). **¹³C-NMR** (CD₃OD, 75 MHz): δ (ppm)= 176.2; 174.0; 173.9 (2C); 138.8; 130.6 (2C); 129.7 (2C); 128.0; 80.9; 55.8; 54.0; 53.0; 52.2; 42.4; 38.6; 32.3; 31.6; 29.0 (3C); 24.3; 18.2. **ESI-MS**: 479 [M + 1]⁺. [α]_D²²: -8.646 (c=1.000, CH₃OH).

Synthesis of **23**

To a solution of **22** (1.853 g, 0.003868 mol) in THF (35 ml) NaOH 5% (10 ml) and Boc_2O (1.265 g, 0.005803 mol) are added and the reaction mixture is stirred overnight at room temperature. The solvent is removed under reduced pressure, H_2O (40 ml) is added and the pH value is adjusted to 5 with HCl 0.1M. The precipitate is recovered by filtration and washed with H_2O , obtaining the desired product **23** without any further purification (1.831 g, Yield: 84%).

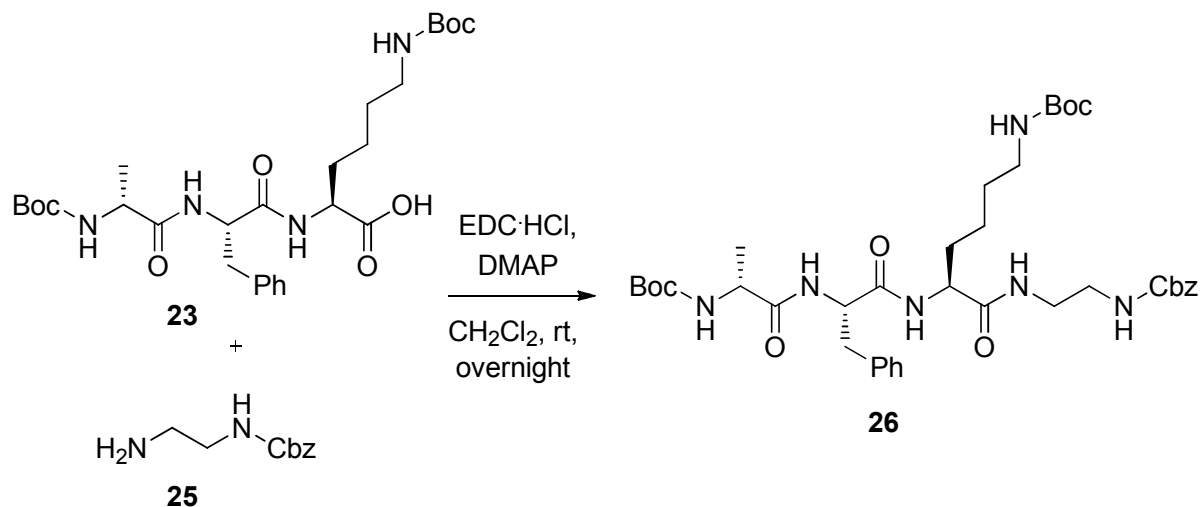
$^1\text{H-NMR}$ (CD_3OD , 300 MHz): δ (ppm)= 7.19-7.30 (m, 5H); 4.66-4.70 (m, 1H); 4.38 (dd, $J = 9.0$ Hz, $J = 4.9$ Hz, 1H); 3.99 (q, $J = 7.2$ Hz, 1H); 3.27-3.31 (m, 1H); 3.06 (t, $J = 6.3$ Hz, 2H); 2.92 (dd, $J = 14.0$ Hz, $J = 9.8$ Hz, 1H); 1.89-1.94 (m, 1H); 1.79-1.84 (m, 1H); 1.42-1.56 (m, 22H); 1.10 (d, $J = 7.2$ Hz). **$^{13}\text{C-NMR}$** (CD_3OD , 75 MHz): δ (ppm)= 174.4; 173.8; 172.0; 157.1; 156.2; 137.1; 129.0 (2C); 128.0 (2C); 126.3; 79.3; 78.5; 54.0; 52.5; 50.4; 39.8; 36.9; 30.9; 29.1; 27.4 (6C); 22.8; 16.6. **ESI-MS**: 563 $[\text{M} - 1]^+$. $[\alpha]_{\text{D}}^{22}$: -1.168 ($c=1.000$, CH_3OH).

Synthesis of 25



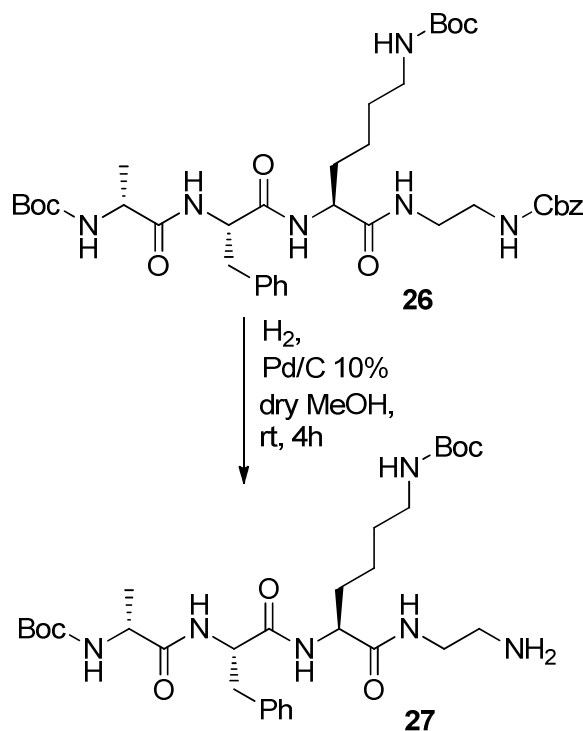
A solution of Cbz-Cl (1.000 g, 0.005848 mol) in CH₂Cl₂ (90 ml) is added dropwise over 1.5 hours to a solution of ethylenediamine (**24**, 2.342 ml, 0.035088 mol) in CH₂Cl₂ (10 ml) and stirred at room temperature for 1 h. Then the solvent is removed under reduced pressure, a saturated solution of K₂CO₃ (140 ml) is added and extracted with AcOEt (3x30 ml). The organic layers are dried over Na₂SO₄ and evaporated under reduced pressure, affording **25** as a pale yellow oil without any further purification (1.049 g, Yield: 92%).

¹H-NMR (CDCl₃, 300 MHz): δ (ppm)= 7.29-7.32 (m, 5H); 5.31 (bs, 1H); 5.08 (s, 2H); 3.18-3.23 (m, 2H); 2.76-2.80 (m, 2H); 1.32 (bs, 2H). **¹³C-NMR** (CDCl₃, 75 MHz): δ (ppm)= 156.7; 136.6; 128.6; 128.2; 66.8; 43.8; 41.8.

Synthesis of **26**

To a solution of **23** (0.900 g, 0.001593 mol) in CH₂Cl₂ (15 ml) EDC·HCl (0.459 g, 0.002389 mol), DMAP (0.136 g, 0.001115 mol) and finally **25** (0.309 g, 0.001593 mol) are added and the reaction mixture is stirred overnight at room temperature. Then the solvent is removed under reduced pressure and the crude material is purified by flash chromatography (AcOEt 100%), affording **26** as a white solid (0.430 g, Yield: 36%).

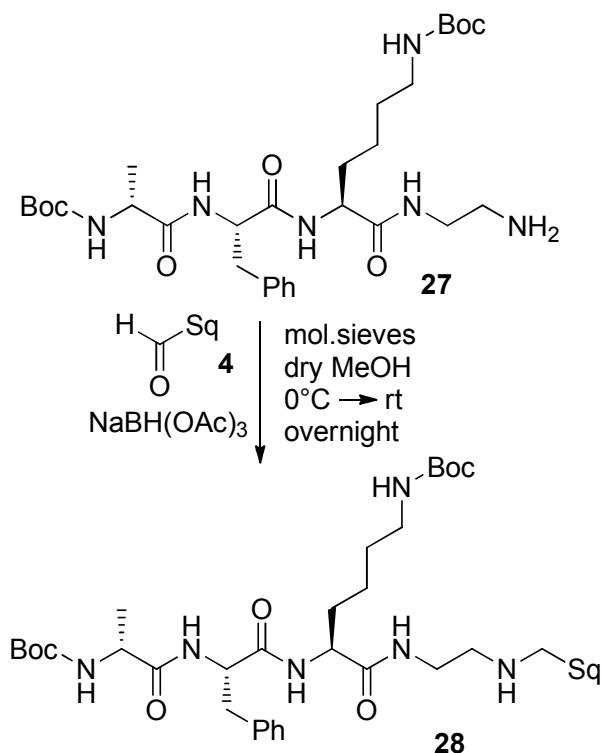
¹H-NMR (CD₃OD, 300 MHz): δ (ppm)= 7.13-7.34 (m, 10H); 5.07 (s, 2H); 4.53-4.58 (m, 1H); 4.19-4.24 (m, 1H); 3.94 (q, J = 9.1 Hz, 1H); 3.17-3.25 (m, 4H); 3.02 (t, J = 6.2 Hz, 2H); 2.90 (dd, J = 14.2 Hz, J = 10.1 Hz, 1H); 1.62-1.97 (m, 2H); 1.28-1.56 (m, 22H); 1.07 (d, J = 7.0 Hz, 3H). **¹³C-NMR** (CD₃OD, 75 MHz): δ (ppm)= 177.1; 174.7; 174.0; 159.2; 158.9; 158.3; 138.8 (2C); 130.5 (3C); 129.8 (3C); 129.3 (2C); 128.1; 81.0 (2C); 67.8; 56.6; 55.6; 52.1; 41.5 (2C); 40.9; 38.1; 32.4; 30.8; 29.1 (6C); 24.8; 17.9. **ESI-MS**: 764 [M+Na]⁺. [α]_D³³: +8.3265 (c=0.8300, CH₃OH).

Synthesis of **27**

To a solution of **26** (0.067 g, 0.000090 mol) in dry MeOH (1.5 ml) Pd/C 10% (0.010 g, 0.000009 mol) is added and the reaction mixture is stirred under H₂ pressure at room temperature for 4 hours. After filtration over celite and evaporation of the solvent under reduced pressure, the desired **27** is obtained as a white solid without any further purification (0.053 g, Yield: 97%).

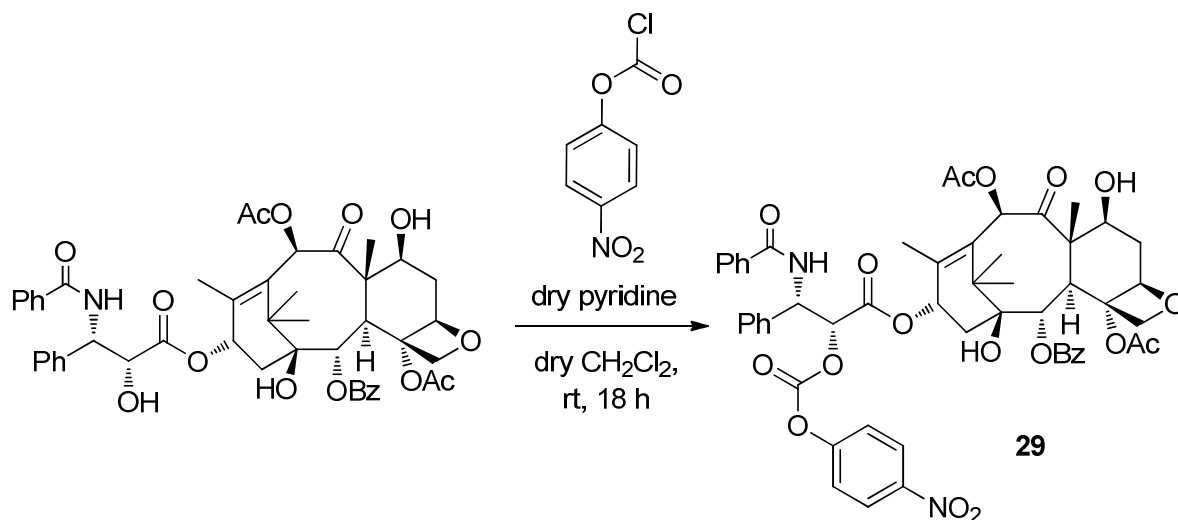
¹H-NMR (CD₃OD, 400 MHz): δ (ppm)= 7.22-7.33 (m, 5H); 4.55-4.57 (m, 1H); 4.24 (dd, J = 9.7 Hz, J = 4.7 Hz, 1H); 3.98 (q, J = 7.1 Hz, 1H); 3.20-3.30 (m, 3H); 3.05 (t, J = 6.7 Hz, 2H); 2.95 (dd, J = 14.2 Hz, J = 9.8 Hz, 1H); 2.75 (t, J = 6.1 Hz, 2H); 1.91 (bs, 1H); 1.78 (bs, 1H); 1.45 (bs, 13H); 1.42 (s, 9H); 1.13 (d, J = 7.1 Hz, 3H). **¹³C-NMR** (CD₃OD, 100 MHz): δ (ppm)= 176.2; 173.8; 173.0; 157.8; 157.2; 137.7 (2C); 129.5 (2C); 128.8 (2C); 127.1; 80.0; 79.1; 55.7; 54.7; 51.1; 42.4; 41.0; 40.4; 37.0; 31.3; 29.8; 28.1 (6C); 23.9; 16.8. **ESI-MS**: 630 [M+Na]⁺. [α]_D³³: +0.6926 (c=0.6050, CH₃OH).

Synthesis of **28**



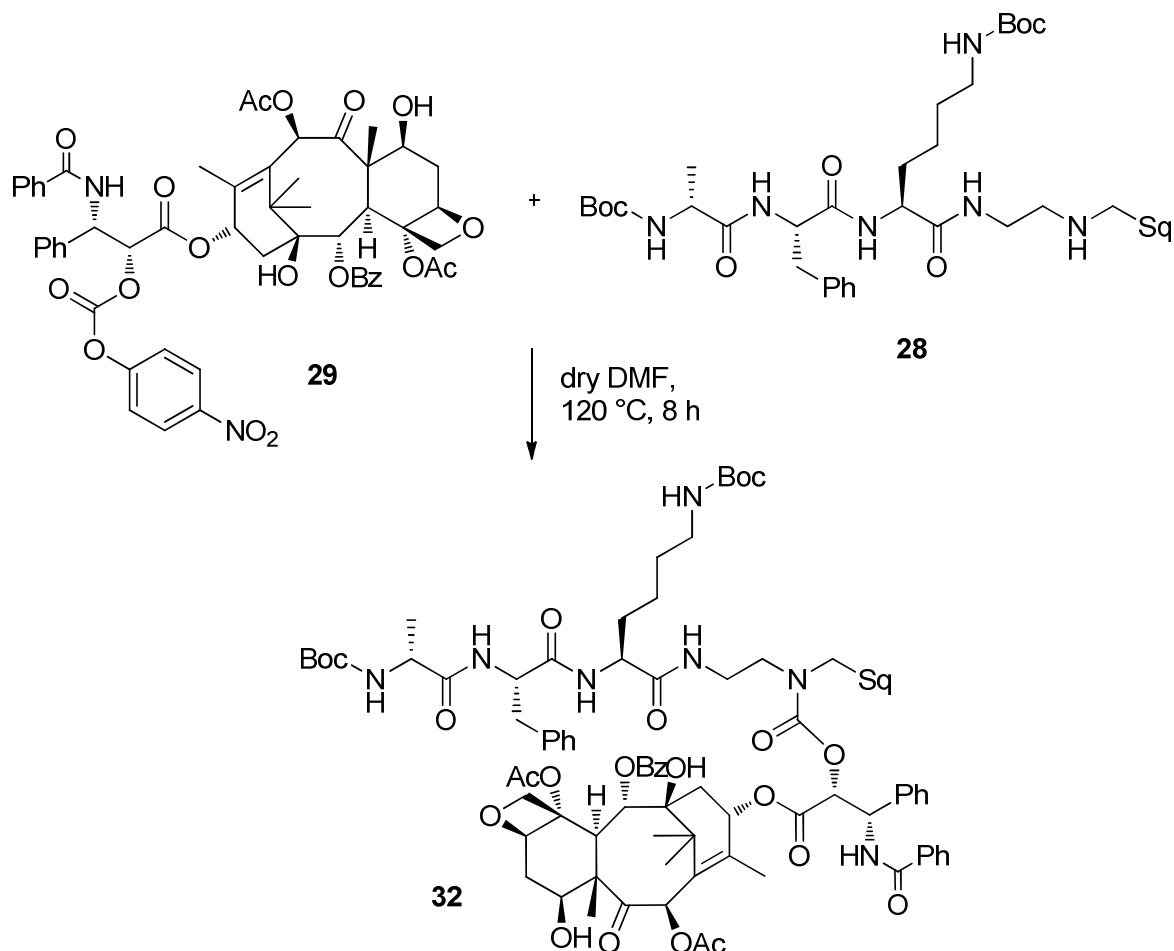
27 (0.236 g, 0.000390 mol) and 4Å molecular sieves are added at 0 °C to a solution of **4** (0.060 g, 0.000156 mol) in dry MeOH (2 ml). The reaction mixture is stirred for 1 h, $\text{NaBH}(\text{OAc})_3$ (0.046 g, 0.000218 mol) is added and then warmed up to room temperature and stirred overnight. The solvent is then evaporated and the crude material is purified by flash chromatography ($\text{CH}_2\text{Cl}_2/\text{MeOH}$ from 10:1 to 7:3), affording **28** as a pale yellow solid (0.088 g, Yield: 58%).

$^1\text{H-NMR}$ (CD_3OD , 400 MHz): δ (ppm)= 7.22-7.34 (m, 5H); 5.10-5.24 (m, 5H); 4.44-4.56 (m, 1H); 4.08-4.20 (m, 1H); 3.97-4.02 (m, 1H); 2.82-3.59 (m, 10H); 1.96-2.17 (m, 24H); 1.73-1.86 (m, 2H); 1.69 (s, 3H); 1.65 (s, 3H); 1.61 (bs, 9H); 1.46 (bs, 18H); 1.42 (s, 3H); 1.12 (d, $J = 7.1$ Hz, 3H).
 $^{13}\text{C-NMR}$ (CD_3OD , 100 MHz, detected signals): δ (ppm)= 175.1; 173.8; 173.7; 172.9; 157.1; 137.0; 134.6; 134.5; 133.1; 130.7; 129.0; 128.8; 128.2; 126.6; 126.5; 125.3; 124.7; 124.2; 124.1; 79.4; 78.5; 55.2; 54.4; 50.6; 39.5; 36.8; 36.4; 30.4; 29.1; 27.8; 27.4; 26.4; 26.2; 25.1; 23.1; 14.8.
ESI-MS: m/z 998.2 $[\text{M}+\text{Na}]^+$. $[\alpha]_{\text{D}}^{31}$: +9.3570 ($c=1.0000$, CH_3OH).

Synthesis of **29**

To a solution of paclitaxel (0.060 g, 0.000070 mol) in dry CH_2Cl_2 (1 ml) dry pyridine (0.017 g, 0.000211 mol) and *p*-nitrophenyl-chloroformate (0.028 g, 0.000141 mol) were added and the reaction mixture was stirred at room temperature for 18 h. Then the volatiles were removed under reduced pressure and the crude material was purified by flash chromatography (AcOEt/Hex 4:5) affording **29** as a white solid (0.042 g, Yield: 59%).

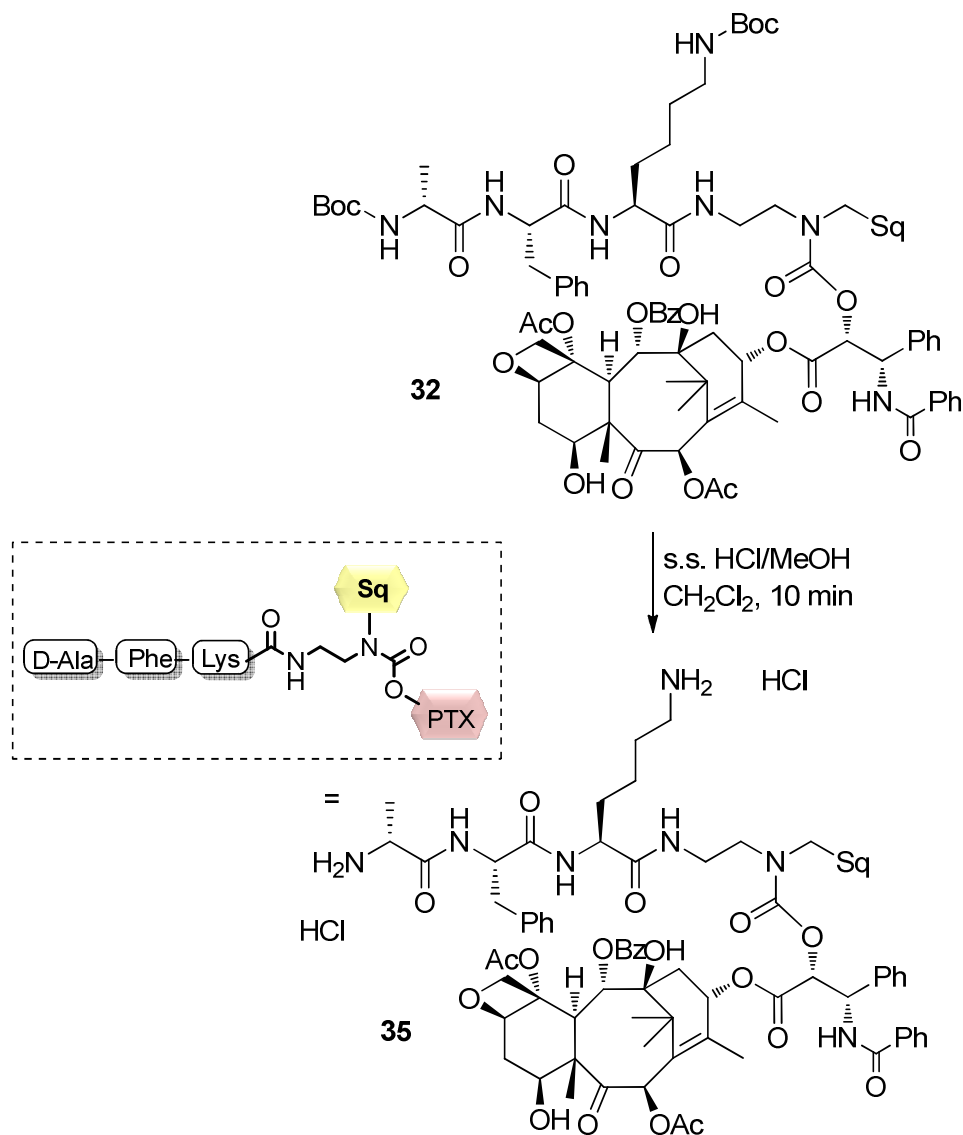
$^1\text{H-NMR}$ (CDCl_3 , 300 MHz): δ (ppm)= 8.24 (d, $J = 7.2$ Hz, 2H); 8.13 (d, $J = 7.6$ Hz, 2H); 7.75 (d, $J = 7.6$ Hz, 2H); 7.62 (t, $J = 7.2$ Hz, 1H); 7.39-7.53 (m, 10H); 7.32 (d, $J = 9.2$ Hz, 2H); 6.89 (d, $J = 9.3$ Hz, 1H); 6.37 (bs, 1H); 6.31 (t, $J = 8.9$ Hz, 1H); 6.07 (d, $J = 9.3$ Hz, 1H); 5.72 (d, $J = 6.8$ Hz, 1H); 5.51-5.58 (m, 2H); 4.99 (d, $J = 8.8$ Hz, 1H); 4.36 (d, $J = 8.5$ Hz, 1H); 4.20 (d, $J = 8.5$ Hz, 1H); 3.98 (d, $J = 6.8$ Hz, 1H); 2.66-2.76 (m, 1H); 2.39-2.48 (m, 4H); 2.24-2.32 (m, 1H); 2.18 (s, 3H); 1.97-2.09 (m, 4H); 1.86 (s, 3H); 1.24 (s, 3H); 1.18 (s, 3H). **FAB-MS**: m/z 1042.2 $[\text{M}+\text{Na}]^+$.

Synthesis of **32**

To a solution of **29** (0.035 g, 0.000034 mol) in dry DMF (1.5 ml) **28** (0.035 g, 0.000068 mol) was added and the reaction mixture was stirred at 120°C for 8 h. The solvent was removed under reduced pressure and the crude material was purified by flash chromatography (AcOEt/Hex 1:1) affording **32** as a white solid (0.014 g, Yield: 22%).

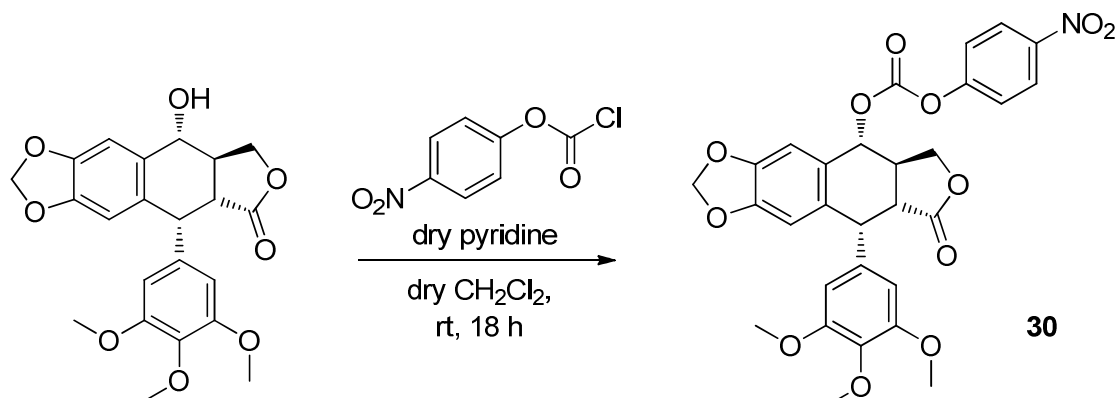
¹H-NMR (CDCl₃, 400 MHz): δ (ppm)= 8.11 (d, J = 7.0 Hz, 2H); 7.73 (d, J = 8.1 Hz, 2H); 7.62-7.68 (m, 1H); 7.17-7.48 (m, 10H); 6.89-6.98 (m, 1H); 6.16-6.45 (m, 4H); 5.70-5.79 (m, 2H); 5.08-5.19 (m, 5H); 4.81-5.02 (m, 1H); 4.53-4.68 (m, 1H); 3.95-4.37 (m, 4H); 2.54-3.65 (m, 10H); 1.10-2.35 (m, 93H). **ESI-MS**: 1854.3 [M-1]⁺ [α]_D³³: -19.4500 (c=0.2000, CH₃OH).

Synthesis of 35



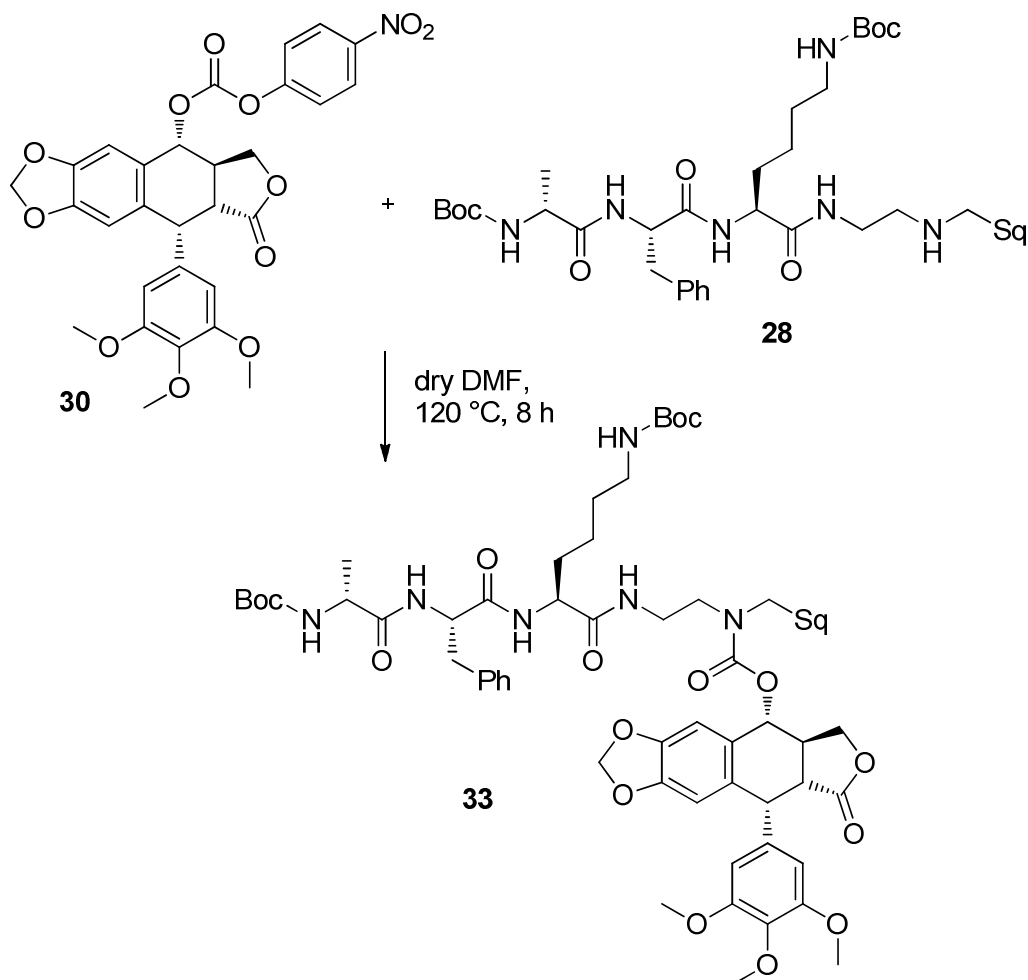
To a solution of **32** (0.014 g, 0.000007 mol) in CH_2Cl_2 (1.0 ml) a drop of a saturated solution of HCl in MeOH was added and the reaction mixture was stirred at room temperature for 10 min. The volatiles were then evaporated under reduced pressure affording **35** (0.012 g, Yield: 95%) without any further purification.

$^1\text{H-NMR}$ (CDCl_3 , 300 MHz): δ (ppm)= 7.11-8.28 (m, 16 H); 6.23-6.55 (m, 2H); 5.51-6.03 (m, 4H); 5.09-5.18 (m, 5H); 4.60-4.98 (m, 2H); 4.05-4.52 (m, 4H); 2.48-3.75 (m, 10H); 0.79-2.48 (m, 75H). **ESI-MS**: 1773.9 $[\text{M}+2\text{Na}]^{++}$ $[\alpha]_{\text{D}}^{25}$: -20.4734 ($c=0.6400$, CH_3OH).

Synthesis of **30**^[163]

To a solution of podophyllotoxin (0.100 g, 0.000242 mol) in dry CH_2Cl_2 (2 ml) dry pyridine (0.035 g, 0.000430 mol) and *p*-nitrophenylchloroformate (0.097 g, 0.000483 mol) were added and the reaction mixture was stirred at room temperature for 18 h. Then the volatiles were removed under reduced pressure and the crude material was purified by flash chromatography (AcOEt/Hex 1:1) affording **30** as a pale yellow solid (0.105 g, Yield: 75%).

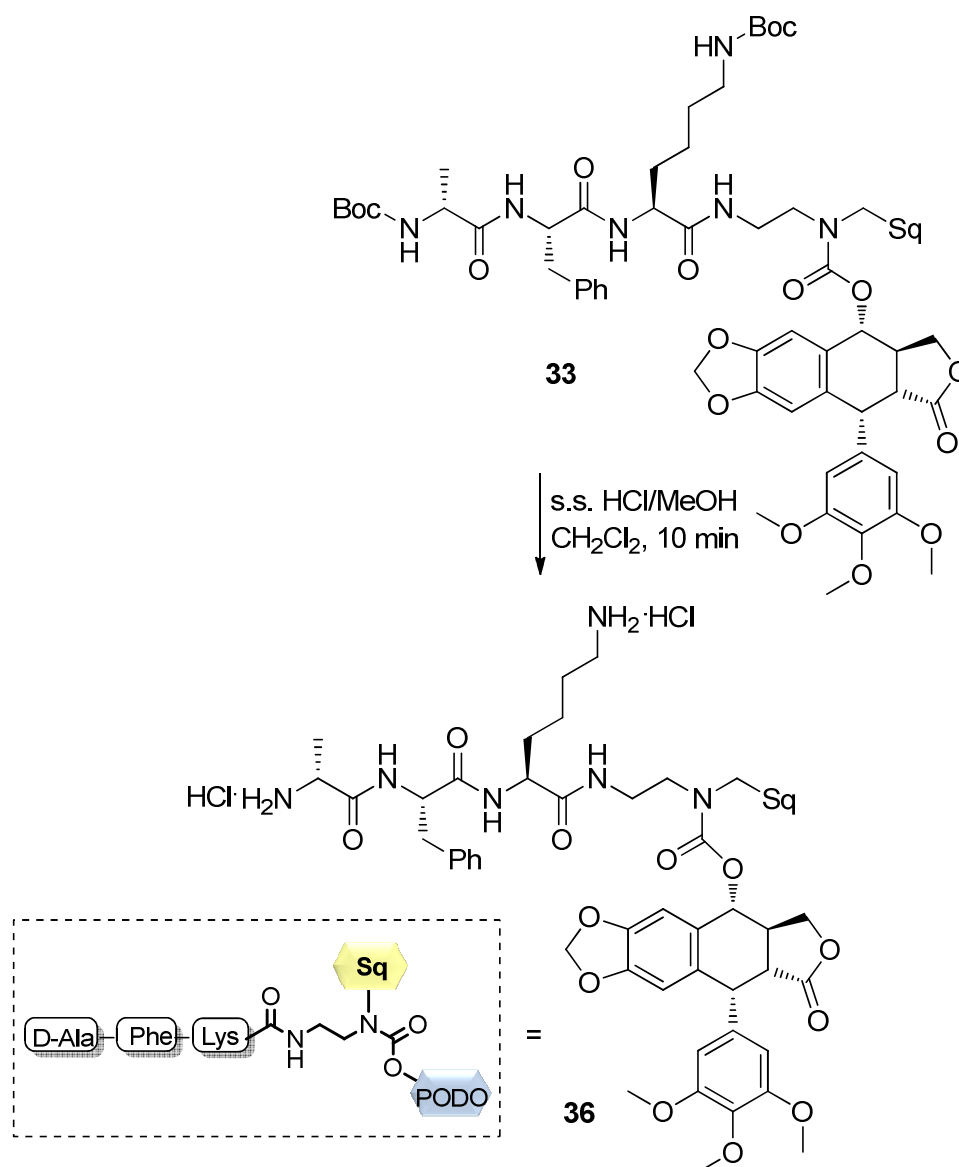
$^1\text{H-NMR}$ (CDCl_3 , 300 MHz): δ (ppm)= 8.32 (d, $J = 7.5$ Hz, 2H); 7.43 (d, $J = 7.5$ Hz, 2H); 6.94 (s, 1H); 6.58 (s, 1H); 6.40 (s, 2H); 6.01 (bs, 2H); 5.88 (d, $J = 9.0$ Hz, 1H); 4.64 (d, $J = 6.0$ Hz, 1H); 4.51 (dd, $J = 8.9$ Hz, $J = 6.7$ Hz, 1H); 4.25 (t, $J = 9.6$ Hz, 1H); 3.81 (s, 3H); 3.76 (bs, 6H); 2.92-3.06 (m, 2H). **$^{13}\text{C-NMR}$** (CDCl_3 , 75 MHz): δ (ppm)= 173.7; 155.2; 152.8; 149.6; 148.5; 147.6; 145.6; 134.3; 133.4; 126.3; 125.4; 121.6; 110.5; 109.6; 108.5; 101.9; 74.2; 66.9; 60.7; 56.3; 43.9; 43.8; 41.2; 36.8. **FAB-MS**: 580.6 $[\text{M}+1]^+$. $[\alpha]_{\text{D}}^{25}$: -122.1000 ($c=1.0000$, CHCl_3).

Synthesis of **33**

To a solution of **30** (0.037 g, 0.000064 mol) in dry DMF (1.2 ml) **28** (0.062 g, 0.000064 mol) was added and the reaction mixture was stirred at 120°C for 8 h. The solvent was removed under reduced pressure and the crude material was purified by flash chromatography (AcOEt/Hex 1:1) affording **33** as a white solid (0.044 g, Yield: 49%).

¹H-NMR (CD₃OD, 300 MHz): δ (ppm)= 7.18-7.31 (m, 5H); 6.96 (s, 1H); 6.52 (s, 1H); 6.41-6.48 (m, 2H); 5.83-5.91 (m, 3H); 5.05-5.19 (m, 5H); 3.90-4.64 (m, 6H); 3.71 (bs, 9H); 2.83-3.59 (m, 12H); 1.91-2.25 (24H); 1.55-1.80 (m, 20H); 1.41 (bs, 18H); 1.09 (d, J = 6.9 Hz, 3H). **ESI-MS**: 1438.5 [M+Na]⁺. [α]_D³³: -158.0660 (c=0.0667, CH₃OH).

Synthesis of 36



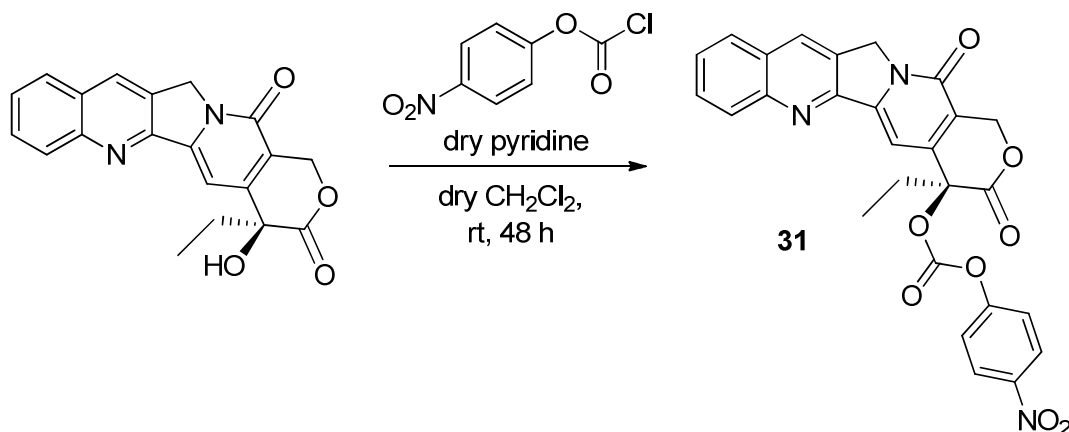
To a solution of **33** (0.010 g, 0.000007 mol) in CH_2Cl_2 (0.5 ml) a drop of a saturated solution of HCl in MeOH was added and the reaction mixture was stirred at room temperature for 10 min. The volatiles were then evaporated under reduced pressure affording **36** (0.008 g, Yield: 90%) without any further purification.

$^1\text{H-NMR}$ (CD_3OD , 400 MHz): δ (ppm)= 7.21-7.38 (m, 5H); 6.95 (s, 1H); 6.56 (s, 1H); 6.47-6.50 (m, 2H); 5.90-5.98 (m, 3H); 5.12-5.25 (m, 5H); 4.45-4.73 (m, 3H); 4.07-4.38 (m, 2H); 3.83-3.89 (m, 1H); 3.74 (bs, 9H);

194

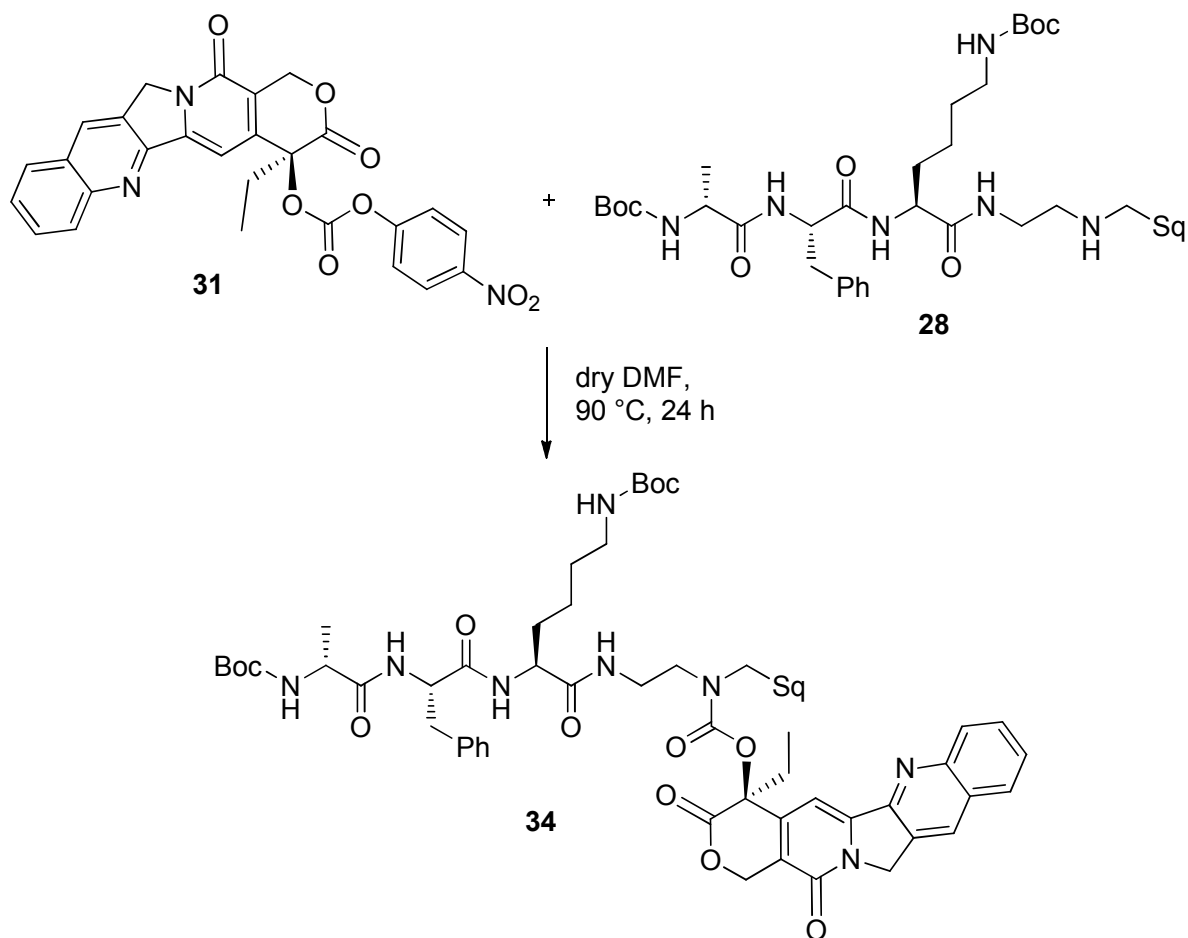
2.81-3.70 (m, 12H); 1.11-2.16 (m, 47H). **¹³C-NMR** (CD₃OD, 100 MHz, detected signals): δ (ppm)= 148.2; 129.1; 129.0; 128.2; 126.6; 126.5; 124.3; 124.2; 108.4; 55.3; 39.4; 39.1; 37.1; 36.5; 35.9; 29.3; 27.8; 26.6; 26.4; 26.3; 26.2; 22.0; 14.8. **ESI-MS**: 1239.1 [M-2HCl+Na]⁺. **[α]_D²⁵**: -141.0000 (c=0.1000, CH₃OH).

Synthesis of 31



To a solution of camptothecin (0.060 g, 0.000172 mol) in dry CH₂Cl₂ (1.5 ml) dry pyridine (0.054 g, 0.000690 mol) and *p*-nitrophenylchloroformate (0.104 g, 0.000517 mol) were added and the reaction mixture was stirred at room temperature for 48 h. Then the volatiles were removed under reduced pressure and the crude material was purified by flash chromatography (CH₂Cl₂/MeOH 80:1) affording **31** as a yellow solid (0.035 g, Yield: 40%).

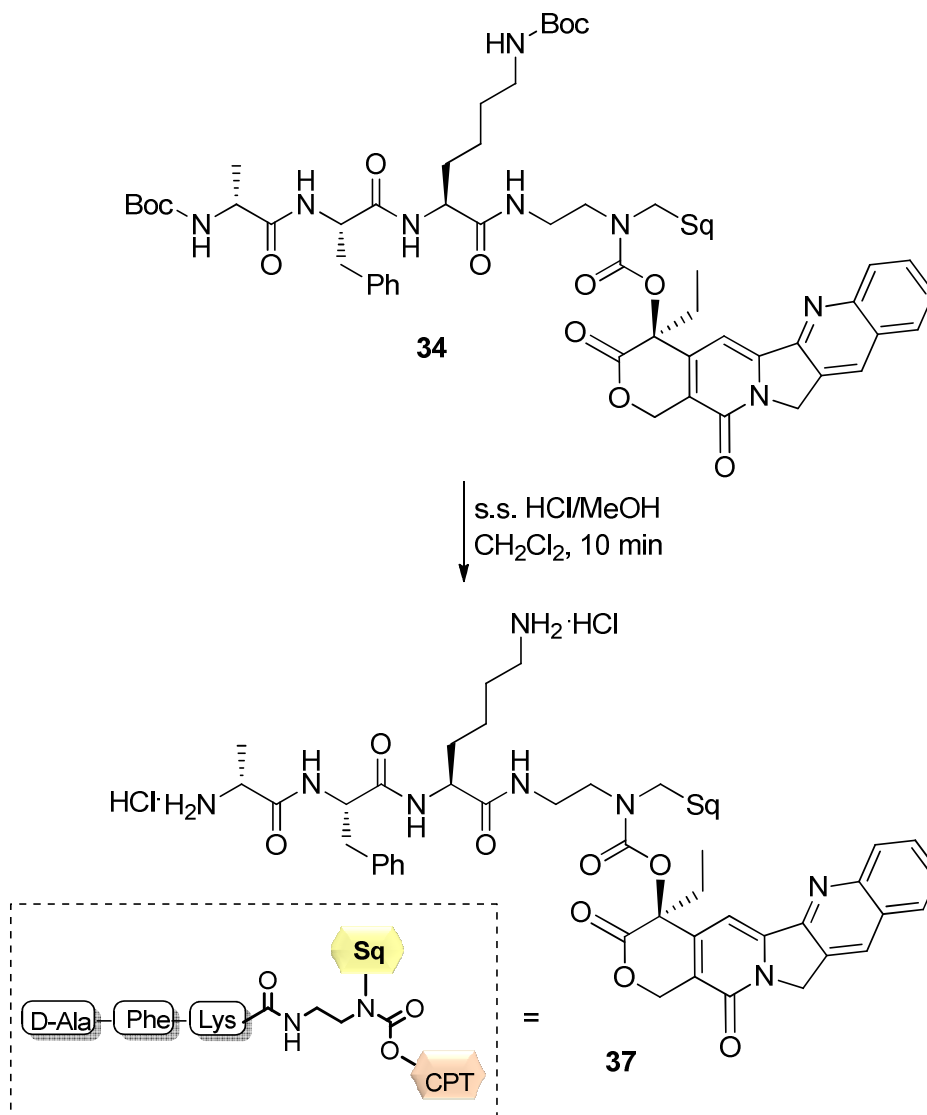
¹H-NMR (CDCl₃, 300 MHz): δ (ppm)= 8.42 (s, 1H); 8.15-8.23 (m, 3H); 7.95 (d, *J* = 7.6 Hz, 1H); 7.86 (t, *J* = 7.6 Hz, 1H); 7.68 (t, *J* = 7.6 Hz, 1H); 7.36-7.42 (m, 3H); 5.71 (d, *J* = 17.5 Hz, 1H); 5.40 (d, *J* = 17.5 Hz, 1H); 5.30 (bs, 2H); 2.17-2.42 (m, 2H); 1.06 (t, *J* = 7.6 Hz, 3H). **ESI-MS**: 536.2 [M+Na]⁺. [α]_D²⁵: +20.5700 (c=1.0000, CHCl₃).

Synthesis of **34**

To a solution of **31** (0.035 g, 0.000068 mol) in dry DMF (1.5 ml) **28** (0.066 g, 0.000068 mol) was added and the reaction mixture was stirred at 90°C for 24 h. The solvent was removed under reduced pressure and the crude material was purified by flash chromatography (CH₂Cl₂/MeOH 30:1) affording **34** as a yellow solid (0.016 g, Yield: 17%).

¹H-NMR (CD₃OD, 300 MHz): δ (ppm)= 8.70 (bs, 1H); 8.11-8.20 (m, 1H); 8.00-8.09 (m, 1H); 7.79-7.90 (m, 1H); 7.62-7.73 (m, 1H); 7.38-7.47 (m, 1H); 7.11-7.29 (m, 5H); 5.54-5.60 (m, 1H); 5.47-5.51 (m, 1H); 5.30 (bs, 2H); 5.01-5.19 (m, 5H); 4.49-4.68 (m, 1H); 4.10-4.38 (m, 1H); 3.88-4.00 (m, 1H); 2.74-3.61 (m, 10H); 1.82-2.29 (m, 26H); 1.21-1.74 (m, 38H); 1.05-1.12 (m, 6H). **ESI-MS**: 1372.3 [M+Na]⁺. [α]_D²⁵: -48.7706 (c=0.0667, CH₃OH).

Synthesis of 37



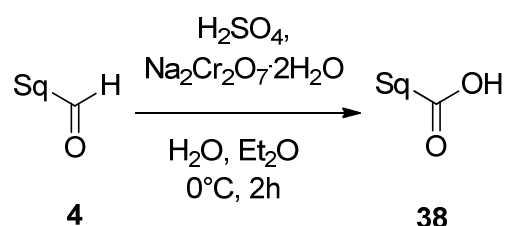
To a solution of **34** (0.009 g, 0.000007 mol) in CH₂Cl₂ (0.5 ml) a drop of a saturated solution of HCl in MeOH was added and the reaction mixture was stirred at room temperature for 10 min. The volatiles were then evaporated under reduced pressure affording **37** (0.008 g, Yield: 98%) without any further purification.

¹H-NMR (CD₃OD, 400 MHz): δ (ppm)= 8.38-8.50 (m, 1H); 8.30-8.37 (m, 1H); 8.18-8.29 (m, 1H); 7.96-8.10 (m, 1H); 7.77-7.93 (m, 2H); 7.08-7.33 (m, 5H); 5.61-5.70 (m, 1H); 5.48-5.56 (m, 1H); 5.42 (bs, 2H); 5.08-5.21 (m, 5H); 4.50-4.58 (m, 1H); 4.37-4.48 (m, 1H); 4.19-4.26 (m, 1H); 2.82-

198

3.94 (m, 10H); 1.07-2.31 (m, 52H). **¹³C-NMR** (CD₃OD, 100 MHz, detected signals): δ (ppm)= 136.8; 129.0; 128.7; 128.1; 127.9; 126.5; 76.4; 66.3; 54.8; 53.5; 50.5; 43.7; 39.1; 37.4; 31.5; 30.9; 29.3; 26.7; 22.6; 22.3; 16.1; 7.1. **ESI-MS**: 1223.9 [M+Na]⁺. [α]_D²⁵: -31.7100 (c=0.1000, CH₃OH).

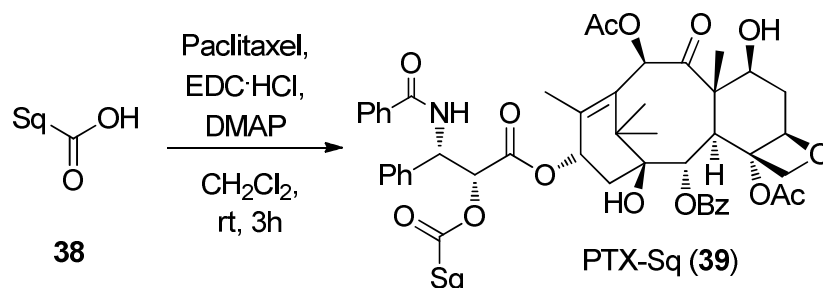
Synthesis of 38



Sodium dichromate dihydrate (6.350 g, 0.021780 mol) was slowly added at 0°C to a solution of sulfuric acid (11.600 ml, 0.217796 mol) in H₂O (110 ml). The resulting solution was then added to a solution of **4** (7.940 g, 0.021778 mol) in Et₂O (160 ml) and stirred at 0 °C for 2 h. The reaction mixture was washed with brine (3 x 1000 ml) until neutral pH, then dried over Na₂SO₄ and evaporated under reduced pressure. The crude material was purified by flash chromatography (petroleum ether/Et₂O 95:5) obtaining **38** as a colorless oil (2.862 g, Yield: 35%).

¹H-NMR (Acetone-*d*₆, 300 MHz): δ (ppm) = 5.11 (m, 5H), 2.38 (t, J = 7.1 Hz, 2H), 2.26 (t, J = 7.1 Hz, 2H), 2.13-1.86 (m, 16H), 1.65-1.59 (m, 15H), 1.26 (s, 3H). **EI-MS**: m/z 400 [M]⁺.

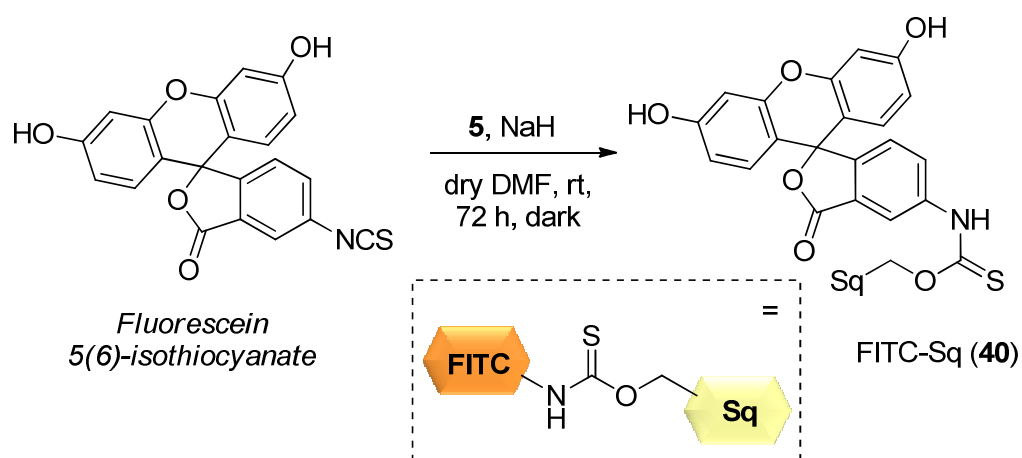
Synthesis of PTX-Sq (39)



To a solution of paclitaxel (1.200 g, 0.001405 mol) in CH_2Cl_2 (30 ml) EDC·HCl (0.270 g, 0.001405 mol), DMAP (0.120 g, 0.000983 mol) and **38** (0.562 g, 0.001405 mol) were added and the reaction mixture was stirred at room temperature for 3 h. The reaction mixture was then extracted with HCl 0.1 M (3 x 15 ml), the organic layers were dried over Na_2SO_4 and evaporated under reduced pressure. The crude material was then purified by flash chromatography ($\text{CH}_2\text{Cl}_2/\text{AcOEt}$ from 95:5 to 80:20) affording PTX-SQ (**39**) as a white solid (1.128 g, Yield: 65%).

$^1\text{H NMR}$ (CDCl_3 , 300 MHz): δ (ppm) = 8.13 (d, $J = 7.3$ Hz, 2H); 7.75 (d, $J = 6.9$ Hz, 2H); 7.62 (t, $J = 7.1$ Hz, 1H); 7.53-7.49 (m, 3H); 7.43-7.35 (m, 7H); 6.91 (d, 1H); 6.35 (s, 1H); 6.24 (m, 1H); 5.99 (m, 1H); 5.69 (d, 1H); 5.53 (d, 1H); 5.20 (m, 5H); 4.97 (d, 1H); 4.44 (m, 1H); 4.33 (d, 1H); 4.20 (d, 1H); 3.85 (d, 1H); 2.55 (m, 1H); 2.49 (s, 3H); 2.45 (m, 2H); 2.30 (t, 2H); 2.23 (s, 3H); 2.09 (s, 3H); 2.00 (m, 16H); 1.97 (m, 1H); 1.70 (m, 1H); 1.67 (s, 3H); 1.61 (m, 18H); 1.25 (m, 1H); 1.21 (s, 3H); 1.13 (s, 3H). **ESI-MS**: m/z 1237.2 $[\text{M}+\text{H}]^+$.

Synthesis of FITC-Sq (40)



To a solution of **5** (0.040 g, 0.000103 mol) in dry DMF (2 ml) NaH (0.003 g, 0.000103 mol) was added and stirred at room temperature for 3 h. Then FITC (0.041 g, 0.000103 mol) was added and the reaction was stirred in the dark at room temperature for 72 h. Then the volatiles were removed under reduced pressure affording **40** without any further purification

¹H-NMR: (CDCl₃, 300 MHz): δ(ppm)= 6.50-7.20 (m, 9H); 5.00-5.23 (m, 5H); 4.55 (bs, 1H); 4.10 (t, J=7.1 Hz, 2H); 1.72-2.19 (m, 20H); 1.65 (s, 3H); 1.57 (bs, 15H). **ESI-MS:** m/z 775.7 [M-2]⁺.

Biology

Stability of conjugates 8-11a in serum

Incubation in human serum was performed at 37°C with a final concentration of NAs of 0.33 mg/mL. Aliquots (60-80 µL) were removed after 48 h of incubation. After addition of 0.8 mL of acetonitrile, the aliquots were centrifuged and the solution was analyzed. All the tests were repeated thrice.

The chemical stability of our conjugates was determined by HPLC analysis: samples in a range of 5-15 µg of the compounds were injected into a LiChrospher 100 RP 18e (4.6 × 250 mm, 5 µm) equipped with a C18 guard column. The column was eluted with acetonitrile / water (40:60 and, after 5 min, a linear gradient to 100% acetonitrile, 35 min) at flow rate of 1 ml/min, and the column effluent was detected at $\lambda = 227$ nm for compounds **8a** and **10a** and at $\lambda = 217$ nm for **9a** and **10a**. The assay was linear over the tested concentration range (1-50 µg as paclitaxel, podophyllotoxin, camptothecin and epothilone A). Eluted peaks were also characterized using a Waters HPLC-MS Micromass ZQ with ESI detector, eluting the column with methanol and 0.05% trifluoroacetic acid in water, with the same gradient as described above.

Cell culture and fluorescence microscopy

Human lung carcinoma cell line A549 (CCL-185; American Type Culture Collection, Rockville, MD, USA) was grown in minimal essential medium with Earle's (E-MEM), supplemented with 10% fetal bovine serum (Hyclone Europe, Oud-Beijerland, Holland), 2 mM L-glutamine, 100 U/mL penicillin, and non-essential amino acids. Cells were maintained at 37°C in a humidified atmosphere at 5% CO₂. To test the ability of squalene bioconjugated to affect microtubule cytoskeleton, A549 cells (50000 cell/ml) were seeded on glass coverslips and grown in control medium. After 24 h, cells were incubated for 1 h with 200 µg/ml of the squalene bioconjugated, or with equal concentration of the parent compounds (paclitaxel, epothilone-A, podophyllotoxin). Cells were fixed and permeabilized for 6 min with methanol at -20°C, washed with PBS, and blocked in PBS+5% bovine serum albumin (BSA) for 15 min at room temperature. To localize tubulin, the cells were incubated with monoclonal anti- α -tubulin antibody (clone B-5-1-2, Sigma-Aldrich, St. Louis, MO) 1:500 in PBS for 1 h at 37°C. We used goat anti-mouse Alexa Fluor568 (Molecular Probes, Eugene, OR) 1:1000 in PBS+1% BSA for 45 min at 37°C as secondary antibodies. Nuclei staining was performed by incubation with DAPI (0.25 µg/mL in PBS) for 15 minutes at room temperature. The coverslips were mounted in Mowiol (Calbiochem, San Diego, CA)-DABCO (Sigma-Aldrich) and examined with a Zeiss Axiovert 200 microscope equipped with a 63x Neofluor lens (Zeiss, Oberkochen, Germany).

Cytotoxicity assay (MCF-7 cell line)

Cytotoxicity was evaluated by incubating the cells with different concentrations of nanoassemblies for 48 h at 37 °C/5% CO₂. To evaluate the activity of nanosuspensions after reduction of disulfide bonds, dithiothreitol was added to reach a 10 mM concentration and samples (at a 1 mM concentration) were incubated for 1h at 37°C. For comparison purposes, Paclitaxel, Podophyllotoxin , Camptothecin and Epothilone A were used as a control.

MCF-7 cells (25000/well) were cultured in RPMI 1640 supplemented with 10% fetal calf serum, 50 U/mL penicillin, 50 µg/mL streptomycin and 2 mM L-glutamine. The cytotoxicity of drugs and drug-squalene NAs was determined using sulforhodamine B (SRB) assay essentially as described by Voigt^[164]. MCF-7 cells were seeded at a density of 25×10³ cells/well in a 96 well plate and incubated for 24 h. Then various concentrations of drug-squalene NAs were added to the medium. After 48 h, the cell viability was determined by the SRB assay: the medium was removed and cells were fixed with trichloroacetic acid, washed and stained with SRB (100 µl/well SRB 0,057% w/v in acetic acid 1% v/v). After the washings, 200 µl/well of 10 mM Tris base (pH 10.5) were added and, after 30 min, the absorbance was measured ($\lambda = 492$ nm) using a 96-well plate reader (Titertek Multiskan PLUS MKII). The survival percentages were calculated using the following formula: Survival % = (A_{492 nm} for the treated cells/A_{492 nm} for the control cells) ×100%. The experiment was repeated thrice in triplicate for each concentration of the tested compounds.

Cytotoxicity assay (A549 cell line)

A549 cell line was maintained in RPMI1640 (Lonza) with the addition of 10% FBS (fetal bovine *serum*) and 2 mM L-Glutamine (Lonza) in a Heraeus CO₂ Auto-Zero incubator at 37°C in a humidified atmosphere of 5% (v/v) CO₂ in air.

Cytotoxic assays on A549 cells were performed in tissue-treated 96 well plates (Falcon). In particular, cells were trypsinized, washed with PBS (Lonza) and plated in 96 well plates at a concentration of 15,000 cells/ml in a total volume of 100 µl. 72 h later cells were treated with 100 µl of different chemical compounds (2X solutions were prepared) at various concentrations, diluted in culture medium. Cell survival was assessed 96 h after treatment by MTS assay. MTS (3-(4,5-dimethylthiazol-2-yl)-5-(3-carboxymethoxyphenyl)-2-(4-sulphophenyl)-2H-tetrazolium) in the presence of phenazinemethosulfate (PMS), produces a formazan product that has an absorbance (Abs) maximum at 490-500 nm in phosphate-buffered saline. The reading of absorbance at 540 nm was performed by using a reader plate (TECAN).

The “% Ctr” was calculated for each dose as:

$$\% \text{Ctr} = \frac{\text{Abs in "x" dose treated sample}}{\text{Abs in Ctr sample}} * 100$$

For each dose 5 replicates were performed and dose/response curves were plotted as mean ± standard deviation for each dose. IC₅₀ values were extrapolated from the dose-response curves.

Cell cultures and live cell imaging

Human lung carcinoma cell line A549 (CCL-185; American Type Culture Collection, Rockville, MD, USA) was grown in minimal essential medium with Earle's (E-MEM), supplemented with 10% fetal bovine serum (Hyclone Europe, Oud-Beijerland, Holland), 2 mM l-glutamine, 100 U/ml penicillin, and non-essential amino acids. Cells were maintained at 37 °C in a humidified atmosphere at 5% CO₂.

For the internalization assay, A549 cells (50000 cell/well) were seeded onto glass coverslips in 6-well tissue culture plates, and the day after cells were incubated for different time with mixture of PTX-Sq and FITC-Sq at two different molar ratios:

- ✚ Mixture B (PTX-Sq/FITC-Sq 10:1): 13.8 μM
- ✚ Mixture D (PTX-Sq/FITC-Sq 30:1): 4.6 μM

After defined times (10, 30 and 60 minutes), cells were washed in PBS and some random images per plate were captured, in both phase contrast and fluorescence, using an Axiovert 200M microscope (Zeiss, Oberkochen, Germany). Immediately after, cells were fixed with 4% paraformaldehyde, and then cells were incubated with phalloidin-tetramethylrhodamine B isothiocyanate and 4',6-diamidino-2-phenylindole dihydrochloride (Sigma-Aldrich). The coverslips were mounted in Mowiol[®] (Calbiochem, San Diego, CA)–DABCO (Sigma-Aldrich) and examined with the Axiovert 200M microscope (Zeiss).

Cultures were washed once in PBS and transferred to a live cell imaging workstation composed of an inverted microscope (Axiovert 200, Carl Zeiss) equipped with a Plan neofluar 63x/1.25 NA oil objective, and images were collected every minute with a cooled camera (AxioCam HRM Rev. 2, Carl Zeiss), for a total time of 20 minutes.

Bibliography

- [1] S.D. Steichen, M. Caldorera-Moore, N.A. Peppas "A review of current nanoparticle and targeting moieties for the delivery of cancer therapeutics" *Eur. J. Pharm. Sci.* **2013**, *48*, 416-427.
- [2] P. Vieghe, M. Khrestchatsky "Medicinal chemistry based approaches and nanotechnology-based systems to improve CNS drug targeting and delivery" *Med. Res. Rev.* **2013**, *33*, 457.
- [3] J-Y. Fang, S.A. Al-Suwayeh "Nanoparticles as delivery carriers for anticancer prodrugs" *Expert Opin. Drug Deliv.* **2012**, *9*, 657-669.
- [4] A.D. MacNaught, A.R. Wilkinson "Compendium of chemical terminology: IUPAC recommendations" 2nd ed. (1997), Blackwell Science.
- [5] A.H. Faraji, P. Wipf "Nanoparticles in cellular drug delivery" *Bioorg. Med. Chem.* **2009**, *17*, 2950-2962.
- [6] H. Otsuka, Y. Nagasaki, K. Kataoka "PEGylated nanoparticles for biological and pharmaceutical applications" *Adv. Drug Del. Rev.* **2012**, *64*, 246-255.
- [7] R. Cheng, F. Meng, C. Deng, H-A Klok, Z. Zhong "Dual and multi-stimuli responsive polymeric nanoparticles for programmed site-specific drug delivery" *Biomaterials* **2013**, *34*, 3647-3657.
- [8] H. Ding, X. Wang, S. Zhang, X. Liu "Application of polymeric micelles with tumor targeted in chemotherapy" *J. Nanopart. Res.* **2012**, *14*, 1254-1266.
- [9] M. Talekar, J. Kendall, W. Denny, S. Garg "Targeting of nanoparticles in cancer: drug delivery and diagnostics" *Anti-cancer Drugs* **2011**, *22*, 949.
- [10] Y. H. Bae "Drug targeting and tumor heterogeneity" *J. Control. Release* **2009**, *133*, 2-3.
- [11] A.J. Simnick, M. Amiram, W. Liu, G. Hanna, M.W. Dewhirst, C.D. Kontos, A. Chilkoti "In vivo tumor targeting by NGR-decorated micelles of a recombinant diblock copolypeptide" *J. Control. Release* **2011**, *155*, 144-151.
- [12] J.A. Flygare, T.H. Pillow, P. Aristoff "Antibody-drug conjugates for the treatment of cancer" *Chem. Biol. Drug Des.* **2013**, *81*, 113-121.
- [13] L. Treuel, X. Jiang, G.U. Nienhaus "New views on cellular uptake and trafficking on manufactured nanoparticles" *J. R. Soc. Interface* **2013**, *10*, 1-25.
- [14] H. Hillaireu, P. Couvreur "Nanocarriers' entry into the cell: relevance to drug delivery" *Cell. Mol. Life Sci.* **2009**, *66*, 2873-2896.
- [15] R.H. Müller, K.H. Wallis, S.D. Tröster, J. Kreuter "In vitro characterization of poly(methyl methacrylate) nanoparticles and correlation to their in vivo fate" *J. Control. Release* **1992**, *20*, 237-246.
- [16] S.I. Jean, J.H. Lee, J.D. Andrade, P.G. De Gennes "Protein-surface interactions in the presence of poly-ethylene oxide: I. Simplified theory" *J. Colloid Interface Sci.* **1991**, *142*, 149-158.

-
- [17] N. Bege, T. Renette, M. Jansch, R. Reul, O. Merkel, H. Petersen, C. Curdy, R.H. Müller, T. Kissel **"Biodegradable poly(ethylene carbonate) nanoparticles as a promising drug delivery system with "stealth" potential"** *Macromol. Biosci.* **2011**, *11*, 897-904.
- [18] R. Gref, Y. Minamitake, M.T. Peracchia, V. Trubetskoy, V. Torchilin, R. Langer **"Biodegradable long-circulating polymeric nanospheres"** *Science* **1994**, *263*, 1600-1603.
- [19] R. Pignatello, A. Leonardi, R. Pellitteri, C. Carbone, S. Caggia, A.C.E. Graziano, V. Cardile **"Evaluation of new amphiphilic PEG derivatives for preparing stealth lipid nanoparticles"** *Colloids and Surfaces A: Physicochem. Eng. Aspects* **2013**, *434*, 136-144.
- [20] Z. Amoozgar, J. Park, Q. Lin, Y. Yeo **"Low molecular-weight chitosan as a pH-sensitive stealth coating for tumor-specific drug delivery"** *Mol. Pharmaceutics* **2012**, *9*, 1262-1270.
- [21] J. Ernst, W.S. Sheldrick, J.H. Fuhrhop **"The crystal structure of squalene"** *Angew. Chem. Int. Ed.* **1976**, *15*, 778.
- [22] E.E. van Tamelen **"Bioorganic chemistry: sterol and acyclic terpene terminal epoxides"** *Acc. Chem. Res.* **1968**, 111-120.
- [23] L. Pogliani, M. Ceruti, G. Ricchiardi, D. Viterbo **"An NMR and molecular mechanics study of squalene and squalene derivatives"** *Chem. Phys. Lipids* **1994**, *70*, 21-34.
- [24] L. Pogliani, M. Milanesio, M. Ceruti, D. Viterbo **"Conformational and dynamical study of squalene derivatives.III: Azasqualenes and solvated squalenes"** *Chem. Phys. Lipids* **1999**, *103*, 81-93.
- [25] T. Tadrosa, P. Izquierdob, J. Esquenab, C. Solans **"Formation and stability of nanoemulsions"** *Adv. Colloid Interface Sci.* **2004**, *108*, 303.
- [26] C.B. Fox, R.C. Anderson, T.S. Dutil, Y. Goto, S.G. Reed, T.S. Vedvick **"Monitoring the effects of component structure and source on formulation stability and adjuvant activity of oil-in-water emulsions"** *Colloid Surf. B Biointerfaces* **2008**, *65*, 98-105.
- [27] C. Mesa, L.E. Fernandez **"Challenges facing adjuvants for cancer immunotherapy"** *Immunol. Cell Biol.* **2004**, *82*, 644-650.
- [28] T.J. Smith **"Squalene: potential chemopreventive agent"** *Expert Opinion on Investigational Drugs* **2000**, *9*, 1841-1848.
- [29] H.L. Newmark **"Squalene, olive oil, and cancer risk: review and hypothesis"** *Annals of the New York Academy of Sciences* **1999**, *889*, 193-203.
- [30] E. Yarkoni, H.J. Rapp **"Tumor regression after intralesional injection of mycobacterial components emulsified in 2,6,10,15,19,23-hexamethyl-2,6,10,14,18,22-tetracosahexaene (squalene), 2,6,10,15,19,23-hexamethyltetracosane (squalane), peanut oil, or mineral oil"** *Cancer Res.* **1979**, *39*, 1518-1520.
- [31] M. Nakagawa, T. Yamaguchi, H. Fukawa, J. Ogata, S. Komiyama, S. Akiyama, M. Kuwano **"Potentiation by squalene of the cyto-toxicity of anticancer**

agents against cultured mammalian-cells and murine tumor" *Jpn. J. Cancer Res* 1985, 76, 315-320.

[32] B. Das, H. Yeger, H. Baruchel, M.H. Freedman, G. Koren, S. Baruchel **"In vitro cytoprotective activity of squalene on a bone marrow versus neuroblastoma model of cisplatin-induced toxicity: implications in cancer chemotherapy" *Eur. J. Cancer* 2003, 39, 2556-2565.**

[33] R. Nowicki, W. Baranska-Rybak **"Shark liver oil as a supporting therapy in atopic dermatitis" *Pol. Merkur. Lekarski* 2007, 22, 312-313.**

[34] Y. Kohno, Y. Egawa, S. Itoh, S. Nagaoka, M. Takahashi, K. Mukai **"Kinetic study of quenching reaction of singlet oxygen and scavenging reaction of free radical by squalene in n-butanol" *Biochimica et Biophysica Acta (BBA) - Lipids and Lipid Metabolism* 1995, 1256, 52-56.**

[35] R.W. Owen, A. Giacosa, W.E. Hull, R. Haubner, G. Würtele, B. Spiegelhalder, H. Bartsch **"Olive-oil consumption and health: the possible role of antioxidants" *The Lancet Oncology* 2000, 1, 107-112.**

[36] K.S. Soppimath, T.M. Aminabhavi, A.R. Kulkarni, W.E. Rudzinski **"Biodegradable polymeric nanoparticles as drug delivery device" *J. Control. Release* 2001, 70, 1-20.**

[37] P. Couvreur, C. Vauthier **"Nanotechnology: intelligent design to treat complex disease" *Pharmaceutical Research* 2006, 23, 1417-1450.**

[38] J.J. Wang, K.C. Sung, C.H. Yeh, J.Y. Fang **"The delivery and antinociceptive effects of morphine and its ester prodrugs from lipid emulsions" *Int. J. Pharm.* 2008, 353, 95-104.**

[39] J.J. Wang, K.C. Sung, O.Y. Hu, C.H. Yeh, J.Y. Fang **"Submicron lipid emulsions as a drug delivery system for nalbuphine and its prodrugs" *J. Control. Release* 2006, 115, 140-149.**

[40] R.L. Alexander, G.L. Kucera **"Lipid nucleoside conjugates for the treatment of cancer" *Curr. Pharm. Des.* 2005, 11, 1079-1089.**

[41] S.M. Ali, A.R. Khan, M.U. Ahmad, P. Chen, S. Sheikh, I. Ahmad **"Synthesis and biological evaluation of gemcitabine-lipid conjugate (NEO6002)" *Bioorg. Med. Chem. Lett.* 2005, 15, 2571-2574.**

[42] M. Payne, P. Ellis, D. Dunlop, M. Ranson, S. Danson, L. Schacter, D. Talbot **"DHApaclitaxel (Taxoprexin) as first-line treatment in patients with stage IIIB or IV non-small cell lung cancer: report of a phase II open-label multicenter trial" *J. Thorac. Oncol.* 2006, 1, 984-990.**

[43] S. Dueland, S. Aamdal, M.J. Lind, H. Thomas, M.L. Sandvold, J.M. Gaullier, W. Rasch **"Intravenous administration of CP-4055 (ELACYT) in patients with solid tumors. A phase I study" *Acta Oncol.* 2009, 48, 137-145.**

[44] P.Chen, P.Y. Chien, A.R. Khan, S. Sheikh, S.M. Ali, M.U. Ahmad, I. Ahmad **"In-vitro and in-vivo anticancer activity of a novel gemcitabine-cardiolipin conjugate" *Anticancer Drugs* 2006, 17, 53-61.**

[45] P. Couvreur, B. Stella, L.H. Reddy, S. Mangenot, J.H. Poupaert, D. Desmaele, S. Lepetre-Mouelhi, F. Rocco, N. Dereuddre-Bosquet, P. Clayette, V. Rosilio, V.

Marsaud, J.M. Renoir, L. Cattel "Squalenoyl nanomedicines as potential therapeutics" *Nano Lett.* **2006**, *6*, 2544-2548.

[46] D. Desmaële, R. Gref, P. Couvreur "Squalenoylation: a generic platform for nanoparticulate drug delivery" *J. Control. Release* **2012**, *161*, 609-618.

[47] V. Heinemann, Y.Z. Xu, S. Chubb, A. Sen, L.W. Hertel G.B. Grindey, W. Plunkett "Cellular Elimination of 2',2'-Difluorodeoxycytidine 5'-Triphosphate: A Mechanism of Self-Potentialiation" *Cancer Res.* **1992**, *52*, 533-539.

[48] M. Gilbert-Sirieix, H. Ripoché, C. Malvy, L. Massaad-Massade "Effects of silencing RET/PTC1 junction oncogene in human papillary thyroid carcinoma cells" *Thyroid* **2010**, *20*, 1053-1065.

[49] W.M. Bertling, M. Gareis, V. Paspaleeva, A. Zimmer, J. Kreuter, E. Nurnberg, P. Harrer "Use of liposomes, viral capsids and nanoparticles as DNA carriers" *Biotechnol. Appl. Biochem.* **1991**, *13*, 390-405.

[50] M. Raouane, D. Desmaele, M. Gilbert-Sirieix, C. Gueutin, F. Zouhiri, C. Bourgaux, E. Lepeltier, R. Gref, R. B. Salah, G. Clayman, L. Massaad-Massade P. Couvreur "Synthesis, characterization, and in vivo delivery of siRNA-squalene nanoparticles targeting fusion oncogene in papillary thyroid carcinoma" *J. Med. Chem.* **2011**, *54*, 4067-4076.

[51] H. Pinto-Alphandary, A. Andremont, P. Couvreur "Targeted delivery of antibiotics using liposomes and nanoparticles: research and applications" *Int. J. Antimicrob. Agents* **2000**, *13*, 155-168.

[52] Z. Drulis-Kawa, A. Dorotkiewicz-Jach "Liposomes as delivery systems for antibiotics" *Int. J. Pharm.* **2010**, *387*, 187-198.

[53] F. Forestier, P. Gerrier, C. Chaurmand, A.M. Quero, P. Couvreur, C. Labarre "Effect of nanoparticle-bound ampicillin on the survival of *Listeria Monocytogenes* in mouse peritoneal macrophages" *J. Antimicrob. Chemother.* **1992**, *30*, 173-179.

[54] N. Sémiramoth, C. Di Meo, F. Zouhiri, F. Saïd-Hassane, S. Valetti, R. Gorges, V. Nicolas, J.H. Poupaert, S. Chollet-Martin, D. Desmaële, R. Gref, P. Couvreur "Self-assembled squalenoylated penicillin bioconjugates: an original approach for the treatment of intracellular infections" *ACS Nano* **2012**, *6*, 3820-3831.

[55] F. Dosio, L.H. Reddy, A. Ferrero, B. Stella, L. Cattel, P. Couvreur "Novel nanoassemblies composed of squalenoyl-paclitaxel derivatives: synthesis, characterization and biological evaluation" *Bioconjugate Chem.* **2010**, *21*, 1349-1361.

[56] M.G. Sarpietro, S. Ottimo, D. Paolino, A. Ferrero, F. Dosio, F. Castelli "Squalenoyl prodrug of paclitaxel: synthesis and evaluation of its incorporation in phospholipid bilayers" *In. J. Pharmaceutics* **2012**, *436*, 135-140.

[57] J. Caron, A. Maksimenko, S. Wack, E. Lepeltier, C. Bourgaux, E. Morvan, K. Leblanc, P. Couvreur, D. Desmaële "Improving the antitumor activity of squalenoyl-paclitaxel conjugate nanoassemblies by manipulating the

linker between paclitaxel and squalene" *Adv. Healthcare Mater.* **2013**, *2*, 172-185.

[58] C.A. Blencowe, A.T. Russel, F. Greco, W. Hayes, D.W. Thorthwaite **"Self-immolative linkers in polymeric delivery systems"** *Polym. Chem.* **2011**, *2*, 773-790.

[59] F. Kratz, I.A. Müller, C. Ryppa, A. Warnecke **"Prodrug Strategies in Anticancer Chemotherapy"** *ChemMedChem* **2008**, *3*, 20-53

[60] A. Furlan, F. Colombo, A. Kover, N. Issaly, C. Tintori, L. Angeli, V. Leroux, S. Letard, M. Amat, Y. Asses, B. Maigret, P. Dubreuil, M. Botta, R. Dono, J. Bosch, O. Piccolo, D. Passarella, F. Maina **"Identification of new aminoacid amides containing the imidazo[2,1-b]benzotriazol-2-ylphenyl moiety as inhibitors of tumorigenesis by oncogenic Met signaling"** *Eur. J. Med. Chem.* **2012**, *47*, 239-254.

[61] F. Calogero, S. Borrelli, G. Speciale, M.S. Christodoulou, D. cartelli, D. Ballinari, F. Sola, C. Albanese, A. Ciavolella, D. Passarella, G. Cappelletti, S. Pieraccini, M. Sironi **"9-Fluorenone-2-carboxylic acid as a scaffold for tubulin- interacting compounds"** *ChemPlusChem* **2013**, *78*, 663-669.

[62] M.S. Christodoulou, F. Zunino, V. Zuco, S. Borrelli, D. Comi, G. Fontana, M. Martinelli, J.B. Lorens, L. Evensen, M. Sironi, S. Pieraccini, L. Dalla Via, O.M. Gia, D. Passarella **"Camptothecin-7-yl-methanethiole: semisynthesis and biological evaluation"** *ChemMedChem* **2012**, *7*, 2134-2143.

[63] M.S. Christodoulou, A. Sacchetti, V. Ronchetti, S. Caufin, A. Silvani, G. Lesma, G. Fontana, F. Minicone, B. Riva, M. Ventura, M. Lahtela-Kakkonen, E. Jarho, V. Zuco, F. Zunino, N. Martinet, F. Dappiaggi, S. Pieraccini, M. Sironi, L. Dalla Via, O.M. Gia, D. Passarella **"Quinazolinecarboline alkaloid evodiamine as scaffold for targeting topoisomerase I and sirtuins"** *Bioorg. Med. Chem.* **2013**, *21*, 6920-6928.

[64] F. Arioli, S. Borrelli, F. Colombo, F. Falchi, I. Filippi, E. Crespan, A. Naldini, G. Scalia, A. Silvani, G. Maga, F. Carraro, M. Botta, D. Passarella **"N-[2-methyl-5-(triazol-1-yl)phenyl]pyrimidine-2-amine as scaffold for the synthesis of inhibitors of Bcr-Abl"** *ChemMedChem* **2011**, *6*, 2009-2018.

[65] F. Colombo, C. Tintori, A. Furla, S. Borrelli, M.S. Christodoulou, R. Dono, F. Maina, M. Botta, M. Amat, J. Bosch, D. Passarella **" 'Click' synthesis of a triazole-based inhibitor of Met functions in cancer cells"** *Bioorg. Med. Chem. Lett.* **2012**, *22*, 4693-4696.

[66] C. Peruzzotti, S. Borrelli, M. Ventura, R. Pantano, G. Fumagalli, M.S. Christodoulou, D. Monticelli, M. Luzzani, A.L. Fallacara, C. Tintori, M. Botta, D. Passarella **"Probing the binding site of Abl tyrosine kinase using in situ click chemistry"** *ACS Med. Chem. Lett.* **2013**, *4*, 274-277.

[67] D. Passarella, D. Comi, G. Cappelletti, D. Cartelli, J. Gertsch, A.R. Quesada, J. Borlak, K-H. Altmann **"Synthesis and biological evaluation of epothilone A dimeric compounds"** *Bioorg. Med. Chem.* **2009**, *17*, 7435-7440.

-
- [68] D. Passarella, D. Comi, A. Vanossi, G. Paganini, F. Colombo, L. Ferrante, V. Zuco, B. Danieli, F. Zunino **"Histone deacetylase and microtubules as targets for the synthesis of releasable conjugate compounds"** *Bioorg. Med. Chem. Lett.* **2009**, *19*, 6358-6363.
- [69] D. Passarella, B. Peretto, R. Blasco y Yepes, G. Cappelletti, D. Cartelli, C. Ronchi, J. Snaith, G. Fontana, B. Danieli, J. Borlak **"Synthesis and biological evaluation of novel thiocolchicine-podophyllotoxin conjugates"** *Eur. J. Med. Chem.* **2010**, *45*, 219-226.
- [70] E. Riva, D. Comi, S. Borrelli, F. Colombo, B. Danieli, J. Borlak, L. Evensen, J.B. Lorens, G. Fontana, O.M. Gia, L. Dalla Via, D. Passarella **"Synthesis and biological evaluation of new camptothecin derivatives obtained by modification of position 20"** *Bioorg. Med. Chem.* **2010**, *18*, 8660-8668.
- [71] G. Cappelletti, D. Cartelli, B. Peretto, M. Ventura, M. Riccioli, F. Colombo, J.S. Snaith, S. Borrelli, D. Passarella **"Tubulin-guided dynamic combinatorial library of thiocolchicine-podophyllotoxin conjugates"** *Tetrahedron* **2011**, *67*, 7354-7357.
- [72] M.C. Wani, H.L. Taylor, M.E. Wall, P. Coggon, A.T. McPhail **"Plant antitumor agents. VI. The isolation and structure of Taxol, a novel antileukemic and antitumor agent from *Taxus Brevifolia*"** *J. Am. Chem. Soc.* **1971**, *93*, 2325-2327.
- [73] T.H. Wang, H.S. Wang, Y.K. Soong **"Paclitaxel-induced cell death: where the cell cycle and apoptosis come together"** *Cancer* **2000**, *88*, 2619-2628.
- [74] H. Gelderblom, J. Verweij, K. Nooter, A. Sparreboom **"Cremophor EL: the drawbacks and advantages of vehicle selection for drug formulation"** *Eur. J. Cancer* **2001**, *37*, 1590-1598.
- [75] M. Skwarczynski, Y. Hayashi, Y. Kiso **"Paclitaxel prodrugs: toward smarter delivery of anticancer agents"** *J. Med. Chem.* **2012**, *49*, 7253-7269.
- [76] R.B. Greenwald, A. Pendri, D. Bolikal **"Highly water soluble taxol derivatives: 7-polyethylene glycol carmabates and carbonates"** *J. Org. Chem.* **1995**, *60*, 331-336.
- [77] R.B. Greenwald, C.W. Gilbert, A. Pendri, C.D. Conover, J. Xia, A. Martinez **"Drug delivery systems: water soluble taxol 2'-poly(ethylene glycol) ester prodrugs- design and in vivo effectiveness"** *J. Med. Chem.* **1996**, *39*, 424-431.
- [78] K.C. Nicolaou, C. Riemer, M.A. Kerr, D. Rideout, W. Wrasidlo **"Design, synthesis and biological activity of protaxols"** *Nature* **1993**, *364*, 464-466.
- [79] V.M. Vrudhula, J.F. MacMaster, Z. Li, D.E. Kerr, P.D. Senter **"Reductively activated disulfide prodrugs of paclitaxel"** *Bioorg. Med. Chem. Lett.* **2002**, *12*, 3591-3594.
- [80] S. Arpicco, F. Dosio, B. Stella, L. Cattel **"Anticancer prodrugs: an overview of major strategies and recent development"** *Curr. Top. Med. Chem.* **2011**, *11*, 2346-2381.
- [81] Z. Zhang, L. Mei, S-S. Feng **"Paclitaxel drug delivery systems"** *Expert Opin. Drug Deliv.* **2013**, *10*, 325-340.

-
- [82] C.D. Scripture, W.D. Figg, A. Sparreboom "Paclitaxel chemotherapy: from empiricism to a mechanism-based formulation strategy" *Ther. Clin. Risk Manag.* **2005**, *1*, 107-114.
- [83] P.K. Paik, L.P. James, G.J. Riely, C.G. Azzoli, V.A. Miller, K.K. Ng, C.S. Sima, R.T. Heelan, M.G. Kris, E. Moore, N.A. Rizvi "A phase 2 study of weekly albumin-bound paclitaxel (Abraxane) given as a two-hour infusion" *Cancer Chemother. Pharmacol.* **2011**, *68*, 1331-1337.
- [84] N.K. Inbrahim, N. Desai, S. Legha, P. Soon-Shiong, R.L. Theriault, E. Rivera, B. Esmaeli, S.E. Ring, A. Bedikian, G.N. Hortobagyi, J.A. Ellerhrst "Phase I and pharmacokinetic study of ABI-007, a cremophor-free protein-stabilized, nanoparticle formulation of paclitaxel" *Clin. Cancer Res.* **2002**, *8*, 1038-1044.
- [85] G. Hofle, N. Bedorf, H. Seinmetz, D. Schomburg, K. Gerth, H. Reichenbach "Epothilone A and B - Novel 16-membered macrolides with cytotoxic activity: isolation, crystal structure, and conformation in solution" *Angew. Chem. Int. Ed. Engl.* **1996**, *35*, 1567-1569.
- [86] K-H. Altmann, J. Gertsch "Anticancer drugs from nature - Natural products as a unique source of new microtubule-stabilizing agents" *Nat. Prod. Rep.* **2007**, *24*, 327-357.
- [87] C.J. Cowden, I. Paterson "Synthetic chemistry: cancer drugs better than Taxol?" *Nature* **1997**, *387*, 238-239.
- [88] K.C. Nicolaou, N. Winssinger, J. pastor, S. Nikovic, F. Sarabia, Y. He, D. Vourloumis, Z. Yang, T. Li, P. Giannakakou, E. Hamel "Synthesis of epothilones A and B in solid and solution phase" *Nature* **1997**, *387*, 268-272.
- [89] D.M. Bollag, P.A. McQueney, J. Zhu, O. Hensens, L. Koupal, J. Liesch, M. Goetz, E. Lazarides, C.M. Woods "Epothilones, a new class of microtubule-stabilizing agents with a taxol-like mechanism of action. *Cancer Res* **1995**, *55*, 2325-2333.
- [90] F.Y. F. Lee, R. Borzilleri, C.R. Fairchild, S-H. Kim, B.H. Long, C. Reventos-Suarez, G.D. Vite, W.C. Rose, R.A. Kramer "BMS-247550: a novel epothilone analog with a mode of action similar to paclitaxel but possessing superior antitumor efficacy" *Clin Cancer Res* **2001**, *7*, 1429-37.
- [91] M. Yousefzadi, M. Sharifi, M. Behmanesh, E. Moyano, M. Bonfill, R.M. Cusido, J. Palazon "Podophyllotoxin: current approaches to its biotechnological production and future challenges" *Eng. Life Sci.* **2010**, *10*, 281-292.
- [92] S. Anand, S. Penrhyn-Lowe, A.R. Venkitaraman "Aurora-a amplification overrides the mitotic spindle assembly checkpoint, inducing resistance to taxol" *Cancer Cell* **2003**, *3*, 51-62.
- [93] Y. Ma, S. Fang, H. Li, C. Han, Y. Lu, Y. Zhao, Y. Liu C. Zhao "Biological evaluation and molecular modelling study of podophyllotoxin derivatives as potent inhibitors of tubulin polymerization" *Chem Biol Drug Des* **2013**, *82*, 12-21.
- [94] D.S. Ettinger, D.M. Finkelstein, P.S. Ritch, S.T. Lincoln, R.H. Blum "Study of either ifosfamide or teniposide compared to a standard chemotherapy for

extensive disease small cell lung cancer: an Eastern Cooperative Oncology Group randomized study (E1588)" *Lung Cancer* 2002, 37, 311-318.

[95] S. Sharma, C. Lagisetti, B. Poliks, R.M. Coates, D.G.I. Kingston, S. Bane **"Dissecting paclitaxel-microtubule association: quantitative assessment of the 2'-OH group" *Biochem.* 2013, 52, 2328-2336.**

[96] J.J. Field, J.F. Diaz, J.H. Miller **"The binding sites of microtubule-stabilizing agents" *Chemistry&Biology* 2013, 20, 301-315.**

[97] J.H. Nettles, H. Li, B. Cornett, J.M. Krahn, J.P. Snyder, K.H. Downing **"The binding mode of Epothilone A on α,β -tubulin by electron crystallography" *Science* 2004, 305, 866-869.**

[98] S. Gupta, L. Das, A.B. Datta, A. Poddar, M.E. Janik, B. Bhattacharyya **"Oxalone and Lactone Moieties of Podophyllotoxin Exhibit Properties of Both the B and C Rings of Colchicine in Its Binding with Tubulin" *Biochemistry* 2006, 45, 6467-6475.**

[99] M.E. Wall, M.C. Wani, C.E. Cook, K.H. Palmer, A.T. MacPhail, G.A. Sim **"Plant antitumor agent. I. A novel alkaloidal leukemia and tumor inhibitor from *Camptotheca Acuminata*" *J. Am. Chem. Soc.* 1966, 88, 3888-3890.**

[100] G.J. Creemers, B. Lund, J Verweij **"Topoisomerase I inhibitors: topotecan and irinotecan" *Cancer Treatment Rev.* 1994, 20, 73-96.**

[101] R.M. Wadkins, D. Bearss, G. Manikumar, M. C. Wani, M.E. Wall, D.D. von Hoff **"Hydrophilic camptothecin analogs that form extremely stable cleavable complexes with DNA and Topoisomerase I" *Cancer Res.* 2004, 64, 6679-6683.**

[102] B. Vladu, J.M. Woynarowski, G. Manikumar, M.C. Wani, M.E. Wall, D.D. von Hoff, R.M. Wadkins **"7- and 10-substituted camptothecins: dependence of Topoisomerase I-DNA cleavable complex formation and stability on the 7- and 10-substituents" *Mol. Pharmacol.* 2000, 57, 243-251.**

[103] M. Watanabe, K. Kawano, M. Yokoyama, P. Opanasopit, T. Okano, Y. Maitani, **"Preparation of camptothecin-loaded polymeric micelles and evaluation of their incorporation and circulation stability" *Int. J. Pharm.* 2006, 308, 183-189.**

[104] D.L. Emerson, **"Liposomal delivery of camptothecins" *Pharm. Sci. Technol. Today* 2000, 3, 205-209.**

[105] K.H. Min, K. Park, Y-S. Kim, S.M. Bae, S. Lee, H.G. Jo, R.W. Park, I-S. Kim, S.Y. Jeong, K. Kim, I.C. Kwon **"Hydrophobically modified glycol chitosan nanoparticles-encapsulated camptothecin enhance the drug stability and tumor targeting in cancer therapy" *J. Controlled Release* 2008, 127, 208-218.**

[106] A. Chenite, C. Chaput, D. Wang, C. Combes, M. Buschmann, C.D. Hoemann, J.C. Leroux, B.L. Atkinson, F. Binette, A. Selmani, **"Novel injectable neutral solutions of chitosan from biodegradable gels in situ" *Biomaterials* 2000, 21, 2155-2161.**

[107] C. Jaxel, K.W. Kohn, M.C. Wani, M.E. Wall, Y. Pommier **"Structure-activity study of the actions of camptothecin derivatives on mammalian**

topoisomerase I: evidence for site specific receptor site and a relation to antitumor activity" *Cancer Res.* 1989, 49, 1465–1469.

[108] R.P. Hertzberg, M.J. Caranfa, S.M. Hecht, "On the mechanism of topoisomerase I inhibition by camptothecin evidence for binding to an enzyme-DNA complex" *Biochemistry* 1989, 28, 4629-4638.

[109] Y. Fan, J. N. Weinstein, K. W. Kohn, L. M. Shi, and Y. Pommier "Molecular Modeling Studies of the DNA-Topoisomerase I Ternary Cleavable Complex with Camptothecin" *J. Med. Chem.* 1998, 41, 2216-2226.

[110] B.L. Staker, M.D. Feese, M. Cushman, Y. Pommier, D. Zembower, L. Stewart, A.B. Burgin "Structures of Three Classes of Anticancer Agents Bound to the Human Topoisomerase I-DNA Covalent Complex" *J. Med. Chem.* 2005, 48, 2336-2345

[111] J.E. Kerrigan, D.S. Pilch "A structural model for the ternary cleavable complex formed between human topoisomerase I, DNA, and camptothecin" *Biochemistry* 2001, 40, 9792-9798.

[112] A. Satyam "Design and synthesis of releasable folate-drug conjugates using a novel heterobifunctional disulfide-containing linker" *Bioorg. Med. Chem. Letters.* 18, 3196-3209.

[113] L-Y. Qiu, L. Yan, L. Zhang, Y-M. Jin, Q-H. Zhao "Folate-modified poly(2-ethyl-2-oxazoline) as hydrophilic corona in polymeric micelles for enhanced intracellular doxorubicin delivery" *International Journal of Pharmaceutics* 2013, 456, 315– 324.

[114] G. Cappelletti, G. Tedeschi, M.G. Maggioni, A. Negri, S. Nonnis, R. Maci "The nitration of τ protein in neurone-like PC12 cells" *FEBBS* 2004, 562, 35-39.

[115] J.M. Ruch, E.J. Kim "Hedgehog signaling pathway and cancer therapeutics: progress to date" *Drugs* 2013, 73, 613-622.

[116] J.K. Chen, J. Taipale, M.K. Cooper, P.A. Beachy "Inhibition of Hedgehog signaling by direct binding of cyclopamine to Smoothed" *Genes Dev.* 2002, 16, 2743-2748.

[117] M.R. Tremblay, M. Nevalainen, S.J. Nair, J.R. Porter, A.C. Castro, M.L.Behnke, L-C. Yu, M. Hagel, K. White, K. Faia, L. Grenier, M.J. Campbell, J. Cushing, C.N. Woodward, J.Hoyt, M.A. Foley, M.A. Read, J.R. Sydor, J.K. Tong, V.J. Palombella, K. McGovern, J.Adams "Semisynthetic cyclopamine analogues as potent and orally bioavailable hedgehog pathway inhibitors" *J. Med. Chem.* 2008, 51, 6646-6649.

[118] A.K. Isaacs, C. Xiang, V. Baubet, N. Dahmane, J. Winkler "Studies directed toward the elucidation of the pharmacophore of steroid-based sonic hedgehog signaling inhibitors" *Org. Lett.* 2011, 13, 5140.

[119] B. Renoux, T. Legigan, S. Bensalma, C. Chadéneau, J-M Muller, S. Papot "A new cyclopamine glucuronide prodrug with improved kinetics of drug release" *Org. Biomol. Chem.* 2011, 9, 8459.

-
- [120] R.W. Gantt, P. Peltier-Pain, J.S. Thorson "Enzymatic methods for glyco(diversification/randomization) of drugs and small molecules" *Nat. Prod. Rep.* **2011**, *28*, 1811-1853.
- [121] J.S. Thorson, T.J. Hosted, J. Jiang, J.B. Biggins, J. Ahlert "Nature's carbohydrate chemists: the enzymatic glycosylation of bioactive bacterial metabolites" *Curr. Org. Chem.* **2001**, *5*, 139-167.
- [122] R.D. Goff, J.S. Thorson "Enhancing the divergent activities of betulinic acid via neoglycosylation" *Org. Lett.* **2009**, *11*, 461-464.
- [123] R.D. Goff, J.S. Thorson "Assessment of chemoselective neoglycosylation method using chloroambucil as a model" *J. Med. Chem.* **2010**, *53*, 8129-8139.
- [124] R.D. Goff, S. Singh, J.S. Thorson "Glycosyloxyamine neoglycosylation: a model study using calicheamicin" *ChemMedChem* **2011**, *6*, 774-776.
- [125] R.D. Goff, J.S. Thorson "Enhancement of cyclopamine via conjugation with nonmetabolic sugars" *Org. Lett.* **2012**, *14*, 2454-2457.
- [126] S.K. Kumar, I. Roy, R.K. Anchoori, S. Fazli, A. Maitra, P.A. Beachy, S.R. Khan "Targeted inhibition of hedgehog signaling by cyclopamine prodrugs for advanced prostate cancer" *Bioorg. Med. Chem.* **2008**, *16*, 2764-2768.
- [127] H. Cho, T.C. Lai, G.S. Kwon "Poly(ethylene glycol)-block-poly(ϵ -caprolactone) micelles for combination drug delivery: evaluation of paclitaxel, cyclopamine and gossypol in intraperitoneal xenograft models of ovarian cancer" *J. Controlled Release* **2013**, *166*, 1-9.
- [128] V.J. Stella, K.J. Himmelstein "Prodrugs and site-specific drug delivery" *J. Med. Chem.* **1980**, *23*, 1275-1282.
- [129] A. Trouet, A. Passioukov, K. Van derpoorten, A-M. Fernandez, J. Abarca-Quinones, R. Baurain, T.J. Lobl, C. Oliyai, D. Shochat, V. Dubois "Extracellularly Tumor-activated Prodrugs for the Selective Chemotherapy of Cancer: Application to Doxorubicin and Preliminary *in Vitro* and *in Vivo* Studies" *Cancer Res* **2001**, *61*, 2843-2846.
- [130] U. Ruening, V. Magdolen, O. Wilhem, K. Fischer, V. Lutz, H. Graeff, M. Schmitt "Multifunctional potential of the plasminogen activation system in tumor invasion and metastasis" *Int. J. Oncol.* **1998**, *13*, 893-906.
- [131] P.H.A. Quax, A.C.W. de Bart, J.A. Schalken, J.H. Verheijn "The plasminogen activator and matrix metalloproteinase production and extracellular matrix degradation by rat prostate cancer cells *in vitro*: correlation with metastatic behavior *in vivo*" *Prostate* **1997**, *32*, 196-204.
- [132] R. Hewitt, K. Dano "Stromal cell expression of components of matrix-degradating protease systems in human cancer" *Enzyme Protein* **1996**, *49*, 163-173.
- [133] P.H.A. Quax, R.T.J. Leeuwen, H.W. Verspaget, J.H. Verheijn "Protein and messenger RNA levels of plasminogen activators and inhibitors analyzed in 22 human tumor cell lines" *Cancer Res.* **1990**, *50*, 1488-1494.
- [134] S. Ganesh, C.F.M. Sier, G. Griffioen, H.J.M. Vloedgraven, A. de Boer, K. Welvaart, C.J.H. Vandavelde, H.W. Verspaget "Prognostic relevance of

plasminogen activators and their inhibitors in colorectal cancer" *Cancer Res.* **1994**, *54*, 4065-4071.

[135] P.L. Carl, P.K. Chakravarty, J.A. Katzenellenbogen, M.J. Weber "**Protease-activated "prodrugs" for cancer chemotherapy"** *Proc. Natl. Acad. Sci. USA* **1980**, *77*, 224-228.

[136] P.K. Chakravarty, P.L. Carl, M.J. Weber, J.A. Katzenellenbogen "**Plasmin-activated prodrugs for cancer chemotherapy. 1. Synthesis and biological activity of peptidylacivicin and peptidyl-phenylenediamine mustard"** *J. Med. Chem.* **1983**, *26*, 633-638.

[137] P.K. Chakravarty, P.L. Carl, M.J. Weber, J.A. Katzenellenbogen "**Plasmin-activated prodrugs for cancer chemotherapy. 2. Synthesis and biological activity of peptidyl derivatives of doxorubicin"** *J. Med. Chem.* **1983**, *26*, 638-644.

[138] F.M.H. de Groot, W.J. Loos, R. Koekkoek, L.W.A. van Berkom, G.F. Busscher, A.E. Seelen, C. Albrecht, P. de Bruijn, H.W. Scheeren "**Elongated multiple electronic cascade and cyclization spacer systems in activable anticancer prodrugs for enhanced drug release"** *J. Org. Chem.* **2001**, *66*, 8815-8830.

[139] L. Devy, F.M.H. de Groot, S. Blacher, A. Hajitou, P.H. Beusker, H.W. Scheeren, J.-M. Foidart, A. Noël "**Plasmin-activated doxorubicin prodrugs containing a spacer reduce tumor growth and angiogenesis without systemic toxicity"** *The FASEB Journal* **2004**, *18*, 565-575.

[140] F.M.H. de Groot, A.C.W. de Bart, J.H. Verheijn, H.W. Scheeren "**Synthesis and biological evaluation of novel prodrugs of anthracyclines for selective activation by the tumor-associated protease plasmin"** *J. Med. Chem.* **1999**, *42*, 5277-5283.

[141] F.M.H. de Groot, L.W.A. van Berkom, H.W. Scheeren "**Synthesis and biological evaluation of 2'-carbamate-linked and 2'-carbonate-linked prodrugs of paclitaxel: selective activation, by the tumor-associated protease plasmin"** *J. Med. Chem.* **2000**, *43*, 3093-3102.

[142] F.M.H. de Groot, G.F. Busscher, R.W.M. Aben, H.W. Scheeren "**Novel 20-carbonate linked prodrugs of camptothecin and 9-aminocamptothecin designed for activation by tumor-associated plasmin"** *Bioorg. Med. Chem. Lett.* **2002**, *12*, 2371-2376.

[143] Y. Fukumori, H. Ichikawa "**Nanoparticles for cancer therapy and diagnosis"** *Adv. Powder Technol.* **2006**, *17*, 1-28.

[144] S. Lee, J. Xie, X. Y. Chen "**Peptide-Based Probes for Targeted Molecular Imaging"** *Biochemistry* **2010**, *49*, 1364-1376.

[145] M. Liong, J. Lu, M. Kovichich, T. Xia, S. G. Ruehm, A. E. Nel, F. Tamanoi, J. I. Zink "**Multifunctional Inorganic Nanoparticles for Imaging, Targeting, and Drug Delivery"** *ACS Nano* **2008**, *2*, 889-896.

-
- [146] D. W. Holdsworth, M. M. Thornton "Micro-CT in small animal and specimen imaging" *Trends Biotechnol.* **2002**, *20*, S34 –S39.
- [147] M. Mahmoudi, H. Hosseinkhani, M. Hosseinkhani, S. Boutry, A. Simchi, W. S. Journey, K. Subramani, S. Laurent "Magnetic Resonance Imaging Tracking of Stem Cells in Vivo Using Iron Oxide Nanoparticles as a Tool for the Advancement of Clinical Regenerative Medicine" *Chem. Rev.* **2011**, *111*, 253–280.
- [148] H. Amiri, M. Mahmoudi, A. Lascialfariabd "Superparamagnetic colloidal nanocrystal clusters coated with polyethylene glycol fumarate: a possible novel theranostic agent" *Nanoscale* **2011**, *3*, 1022 –1030.
- [149] R. Weissleder "A clearer vision for *in vivo* imaging" *Nat. Biotechnol.* **2001**, *19*, 316 –317.
- [150] R.C. Somers, M.G. Bawendi, D.G. Nocera "CdSe nanocrystal based chem-/bio- sensors" *Chem. Soc. Rev.* **2007**, *36*, 579–591.
- [151] D. Margulies, G. Melman, A. Shanzer "A Molecular Full-Adder and Full-Subtractor, an Additional Step toward a Moleculator" *J. Am. Chem. Soc.* **2006**, *128*, 4865 –4871.
- [152] J.I. Clark, D. Garland "Fluorescein colchicine. Synthesis, purification and biological activity" *J. Cell. Biol.* **1978**, *76*, 619-627.
- [153] G. Jones II, X. Qian "Emission quenching via intramolecular electron transfer for fluorescein conjugates. Dependence on driving force and medium" *J. Photochem. Photobiol A: Chemistry* **1998**, *113*, 125-134.
- [154] E. Riva, M. Mattarella, S. Borrelli, M.S. Christodoulou, D. Cartelli, M. Main, S. Faulkner, D. Sykes, G. Cappelletti, J.S. Snaith, D. Passarella "Preparation of Fluorescent Tubulin Binders" *ChemPlusChem* **2013**, *78*, 222 – 226.
- [155] M.J. Ruedas-Rama, J.D. Walters, A. Orte, E.A.H. Hall "Fluorescent nanoparticles for intracellular sensing: A review" *Analytica Chimica Acta* **2012**, *751*, 1– 23.
- [156] H. Goesmann, C. Feldmann "Nanoparticulate Functional Materials" *Angew. Chem. Int. Ed.* **2010**, *49*, 1362–1395.
- [157] F. Chen, D. Gerion "Fluorescent CdSe/ZnS Nanocrystal–Peptide Conjugates for Long-term, Nontoxic Imaging and Nuclear Targeting in Living Cells" *Nano Lett.* **2004**, *4*, 1827–1832.
- [158] X. Wu, H. Liu, J. Liu, K.N. Haley, J.A. Treadway, J.P. Larson, N. Ge, F. Peale, M.P. Bruchez "Immunofluorescent labeling of cancer marker Her2 and other cellular targets with semiconductor quantum dots" *Nat. Biotechnol.* **2003**, *21*, 41–46.
- [159] S. Seo, H.Y. Lee, M. Park, J.M. Lim, D. Kang, J. Yoon, J.H. Jung "Fluorescein-Functionalized Silica Nanoparticles as a Selective Fluorogenic Chemosensor for Cu²⁺ in Living Cells" *Eur. J. Inorg. Chem.* **2010**, *2010*, 843–847.
- [160] P.J. Patel, N.S. Acharya, S.R. Acharya "Development and characterization of glutathione-conjugated albumin nanoparticles for improved brain

delivery of hydrophilic fluorescent marker" *Drug Delivery*, 2013, 20, 143-155.

[161] L. Yuan, W. Chen, J. Hu, J.Z. Zhang D. Yang "**Mechanistic Study of the Covalent Loading of Paclitaxel via Disulfide Linkers for Controlled Drug Release" *Langmuir* 2013, 29, 734-743.**

[162] F. Dosio, B. Stella, A. Ferrero, C. Garino, D. Zonari, S. Arpicco, L. Cattel, S. Giordano, R. Gobetto "**Ruthenium polypyridyl squalene derivative: a novel self-assembling lipophilic probe for cellular imaging" *Int. J. Pharm.* 2013, 440, 221-228.**

[163] A. Kamal, B.A. Kumar, P. Suresh, A. Juvekar, S. Zingde "**Synthesis of 4 β -carbamoyl epipodophyllotoxins as potential antitumor agents" *Bioorg. Med. Chem.* 2011, 19, 2975-2979.**

[164] W. Voigt W "Sulforhodamine B assay and chemosensitivity" *Methods in molecular medicine* 2005, 110, 39-48.